Transactions

of the

ASME

NOVEMBER, 1949

VOL. 71, No. 8

Transactions

of The American Society of Mechanical Engineers

Published on the tenth of every month, except March, June, September, and December

---

Published monthly by The American Society of Mechanical Engineers. Publication office at 20th and Northampton Streets, Easton, Pa. The editorial department is located at the headquarters of the Society, 29 West Thirty-Ninth Street, New York 18, N. Y. Cable address, "Dynamic," New York. Price $1.50 a copy, $12.00 a year for Transactions and the *Journal of Applied Mechanics;* to members and affiliates, $1.00 a copy, $6.00 a year. Changes of address must be received at Society headquarters three weeks before they are to be effective on the mailing list. Please send old as well as new address.... By-Law: The Society shall not be responsible for statements or opinions advanced in papers or...printed in its publications (B13, Par. 4)....Entered as second-class matter March 2, 1928, at the Post Office at Easton, Pa., under the Act of August 24, 1912....

Thermodynamic Properties of Oxygen, Nitrogen, and Air at Low Temperatures

By L. C. CLAITOR[1] and D. B. CRAWFORD[2]

The proper engineering design of modern low-pressure tonnage oxygen plants requires data on the thermodynamic properties of oxygen, nitrogen, and air that are more accurate than those previously available from charts. In this paper, new temperature-entropy diagrams of suitable scale are presented for these materials over a range of temperatures and pressures adequate for the purpose. These diagrams are calculated from literature data on zero-pressure heat capacity and latent heats of vaporization, and from a reduced equation of state which was obtained from a correlation of literature data on volumes, Joule-Thomson coefficients, and velocity-of-sound measurements.

Introduction

THE engineering design of low-pressure air-separation plants, which are currently of great interest in the United States, requires accurate thermodynamic data on the atmospheric gases at low temperatures and at pressures below 10 atm. These data are particularly important for estimating temperature differences in heat exchangers or regenerators and refrigeration produced by expansion engines.

The literature contains many thermodynamic charts, most of which were made while high-pressure plants were of major importance. The need to cover a large pressure range has caused the methods of preparing these charts to suffer several handicaps such as scale factor and limitations in the analysis of the fundamental data.

The charts on the properties of air, prepared by Hausen (8, 9, 10)[3] from his differential Joule-Thomson measurements, have been criticized by Williams (36) who presented new charts for air, computed from the Joule-Thomson measurements of Roebuck (30, 31). The M. W. Kellogg Company prepared a chart for air which was published by Rushton (34). An examination of the Williams and the Kellogg charts showed variations of about 5 per cent in isentropic work, in the usual low-temperature expansion-turbine range, from the work obtained from volumes calculated by the use of generalized compressibility factors along the temperature path of the charts. This is serious disagreement when it is considered that the generalized relation, which should be roughly correct for air, shows twice as great deviation from the ideal gas law as does the Williams chart. Thus it seemed necessary to secure a new correlation for the properties of air of sufficient accuracy for engineering use in the design of oxygen plants and expansion turbines.

Keesom and Houtoff (18) presented charts for nitrogen at low temperatures. The properties of oxygen and nitrogen were calculated by Millar and Sullivan (26) at pressures up to 60 atm. None of these charts will pass the isentropic work test which was applied to the Williams chart for air. The thermodynamic properties of oxygen and nitrogen are also important in engineering design, so they were included in this paper.

Limiting the maximum pressure to 15 atm allowed the use of an algebraic equation of state in the vapor region for computation of the new charts, instead of the graphical or stepwise methods employed by previous investigators. The advantages gained by this procedure were the ability to consider more than one form of data and the assurance of an internally consistent chart.

A survey of the published equations of state showed that none was available whose constants were determined at the low temperatures needed. The first problem, then, was finding a suitable equation of state.

Theory

The most common algebraic equations of state in present-day use are of the virial type; such as the Beattie-Bridgeman equation (3). It was found that, for our problem, a satisfactory equation having three coefficients, R, B, and C, could be written as follows

$$PV = RT(1 + B\rho + C\rho^2) \quad [1]$$

where P is absolute pressure, V is molal volume, R is the universal-gas-law constant, T is absolute temperature, B is the second virial coefficient, ρ is density, and C is the third virial coefficient. The virial coefficients are functions of temperature only.

The virial coefficients, while they are volumetric quantities, are closely related to other available thermodynamic data.

Corresponding States. The equation of state can be put in reduced form as follows

$$PV = RT(1 + B_r\rho_r + C_r\rho_r^2) \quad [2]$$

where $\rho_r = \rho/\rho_c$, $B_r = B/V_c$, $C_r = C/V_c^2$. For all gases obeying the law of corresponding states, the reduced virial coefficients, B_r and C_r, will be functions only of reduced temperature, $T_r = T/T_c$. As will be shown, the gases, oxygen, nitrogen, and air can be compared very well on the reduced basis. This is fortunate, since there are not enough good data on the individual gases from which to prepare reliable correlations of each gas separately.

Second Virial Coefficient. The second virial coefficient can be calculated from low-pressure data on volume, Joule-Thomson effect, velocity of sound, and theoretically, at least, from other data.

1 Calculation from volumetric data. The equation of state can be arranged to give

$$-B_r - C_r\rho_r = \frac{RT - PV}{\rho_r RT} \quad [3]$$

The right-hand term can be computed from volumetric data as they are usually reported (Amagat compressibilities). A plot of

---

[1] Research and Development Department, Elliott Company, Jeannette, Pa.

[2] American Machine and Foundry Company, Brooklyn, N. Y. Formerly Elliott Company, Jeannette, Pa.

[3] Numbers in parentheses refer to the Bibliography at the end of the paper.

Contributed by the Research Committee on Properties of Gases and Gas Mixtures, the Applied Mechanics Division, and the Heat Transfer Division, and Section M of the American Association for the Advancement of Science, and presented at the Annual Meeting, New York, N. Y., November 28–December 3, 1948, of The American Society of Mechanical Engineers.

Note: Statements and opinions advanced in papers are to be understood as individual expressions of their authors and not those of the Society. Paper No. 48—A-75.

these values versus reduced density ρ_r, will give a straight line in the region where the three-term equation is adequate. The intercept of the line at zero density is the second virial coefficient and the slope of the line is the third virial coefficient. This method will be illustrated later.

2 Calculation from Joule-Thomson data. The Joule-Thomson coefficient at zero pressure is closely related to the second virial coefficient. At very low pressures the equation of state can be written

$$V = RT/P + B \quad [4]$$

The Joule-Thomson coefficient is obtained from the exact relation

$$\mu C_p = -V + T(\partial V/\partial T)_p \quad [5]$$

which, upon substituting the previous equation becomes

$$\mu C_p = -B + TdB/dT = -B + B'T \quad [6]$$

This can be put in reduced form

$$\mu C_p/V_c = -B_r + B_r'T_r \quad [7]$$

3 Calculation from velocity-of-sound data. The pressure coefficient of the velocity of sound at zero pressure is related to the second virial coefficient in the following way (15)

$$sRT = S = B + \frac{B'RT}{C_v^0} + \frac{B''(RT)^2}{2C_p^0C_v^0} \quad [8]$$

where

$$s = \left[\frac{\partial(W/W_0)}{\partial P}\right]_{T,\,P=0}$$

s = pressure coefficient of velocity of sound
W = velocity of sound
W_0 = velocity of sound, ideal value
C_p^0 = zero-pressure heat capacity at constant pressure
C_v^0 = zero-pressure heat capacity at constant volume

This equation in reduced form becomes

$$S_r = S/V_c = B_r + \frac{RB_r'T_r}{C_v^0} + \frac{R^2B_r''T_r^2}{2C_p^0C_v^0} \quad [9]$$

For oxygen and nitrogen we can use

$$C_p^0/R = 7/2$$

and

$$C_v^0/R = 5/2$$

Substituting these equations gives

$$S_r = B_r + \frac{2B_r'T_r}{5} + \frac{2B_r''T_r^2}{35} \quad [10]$$

Third Virial Coefficient. The third virial coefficient can be obtained most easily from the plots described in the calculation of second virial coefficients from volumetric data.

Derivation of Working Equations. The following equations for the reduced virial coefficients proved to be satisfactory for this correlation

$$B_r = a + b/T_r + c/T_r^3 + d/T_r^5 \quad [11]$$

$$C_r = \alpha + \beta/T_r + \gamma/T_r^3 \quad [12]$$

The derivatives which will be needed are as follows

$$B_r'T_r = -b/T_r - 3c/T_r^3 - 5d/T_r^5 \quad [13]$$

$$B_r''T_r^2 = 2b/T_r + 12c/T_r^3 + 30\,d/T_r^5 \quad [14]$$

The reduced Joule-Thomson coefficient then becomes

$$\mu C_p/V_c = -a - 2b/T_r - 4c/T_r^3 - 6d/T_r^5 \quad [15]$$

and the reduced pressure coefficient of the velocity of sound becomes

$$S_r = a + 5b/7T_r + 17c/35T_r^3 + 5d/7T_r^5 \quad [16]$$

Data

Data for Second Virial Coefficients. A literature search for data on the properties of oxygen, nitrogen, and air revealed a considerable amount of data for temperatures above 0 deg C; however, reliable data for low temperatures are relatively meager. The best available second virial-coefficient equation for any of these gases, that of Keyes for nitrogen (19), was calculated to a large extent from Joule-Thomson data of Roebuck and Osterberg (33) at the lowest temperatures. These data will be shown to disagree with most other data. The volumetric data which proved useful in this work were those of Nijhoff and Keesom (27) on oxygen, Onnes and Kuypers (28) on oxygen, Onnes and Urk (29) on nitrogen, and Hölborn and Otto (11, 12) on nitrogen. Second and third virial coefficients for nitrogen have been computed from these data by Urk (35) and Holborn and Otto (13), and appear here in Tables 1 and 2, respectively. Second virial coefficients for oxygen were presented by Nijhoff and Keesom (27) and are given in Table 3.

TABLE 1 VIRIAL COEFFICIENTS FOR NITROGEN[a]

Temp., Deg.C	Reduced Temp., $T_r=T/T_c$	Second Virial Coeff., -10^3B, Amagat Vol. Units	Reduced Second Virial Coeff., $-B_r=-B/V_c$	Third Virial Coeff., 10^6C, Amagat Vol. Units	Reduced Third Virial Coeff., $C_r=C/V_c^2$
20.00	2.327	0.2445	0.0608	2.328	0.144
0.00	2.167	0.410	0.102	2.0656	0.128
-23.62	1.980	0.7465	0.1860	3.057	0.189
-50.26	1.770	1.1063	0.275	2.680	0.166
-81.10	1.524	1.7459	0.4345	3.513	0.217
-102.25	1.356	2.3445	0.584	4.167	0.258
-121.19	1.207	3.1169	0.775	5.367	0.332
-131.27	1.125	3.6003	0.896	5.725	0.354
-141.53	1.044	4.2168	1.050	6.455	0.399
-144.46	1.020	4.3863	1.091	6.911	0.427
-146.32	1.007	4.5417	1.129	6.664	0.410

[a] Data of Onnes and Urk.

TABLE 2 VIRIAL COEFFICIENTS FOR NITROGEN[a]

Temp., Deg.C	Reduced Temp., $T_r=T/T_c$	Second Virial Coeff., -10^3B, Amagat Vol. Units	Reduced Second Virial Coeff., $-B_r=-B/V_c$	Third Virial Coeff., 10^6C, Amagat Vol. Units	Reduced Third Virial Coeff., $C_r=C/V_c^2$
50	2.565	0.0115	0.0286	2.60	0.161
0	2.165	0.4614	0.1145	3.34	0.206
-50	1.770	1.1773	0.292	4.08	0.252
-100	1.376	2.3146	0.575	4.24	0.262
-130	1.138	3.5608	0.8845	5.27	0.326

[a] Data of Holborn and Otto.

The data of Onnes and Kuypers appear in Table 4 and are analyzed graphically in Fig. 1. The resulting values of B_r and C_r are shown in Table 5.

Joule-Thomson measurements on air have been reported by Hausen (7, 8, 9) and by Roebuck (30, 31). These data are presented in Tables 6 and 7. Table 8 contains Joule-Thomson coefficients for nitrogen as determined by Roebuck and Osterberg (33). The Roebuck data were extrapolated linearly from 1 atm to zero pressure, using the 20-atm point to determine slope. Further, the pressure correction (32), necessary to Roebuck's work prior to 1941, was applied.

Data on velocity of sound are quite limited, but, fortunately, are available at very low temperatures. In fact, it is the utilization of these data that makes possible the extension of the second virial-coefficient equation to the normal boiling point. The most reliable data on the velocity of sound are those of Itterbeek and

TABLE 3 SECOND VIRIAL COEFFICIENTS FOR OXYGEN[a]

Temperature, Deg. C	Reduced Temperature, $T_r=T/T_c$	Second Virial Coefficient, -10^3B, Amagat Volume Units	Reduced Second Virial Coefficient, $-B_r=-B/V_c$
20.00	1.8998	0.748	0.225
0.00	1.7702	0.957	0.288
-40.07	1.5109	1.473	0.444
-80.00	1.2516	2.288	0.690
-102.49	1.1058	3.014	0.908
-109.99	1.0572	3.291	0.991
-113.94	1.0316	3.494	1.051
-116.01	1.0182	3.562	1.072
-117.01	1.0117	3.634	1.093
-118.58	1.0016	3.690	1.111
-124.95	0.9603	4.037	1.216
-135.29	0.8932	4.663	1.403
-145.39	0.8298	5.437	1.638
-152.56	0.7813	6.021	1.811

[a] Data of Nijhoff and Keesom.

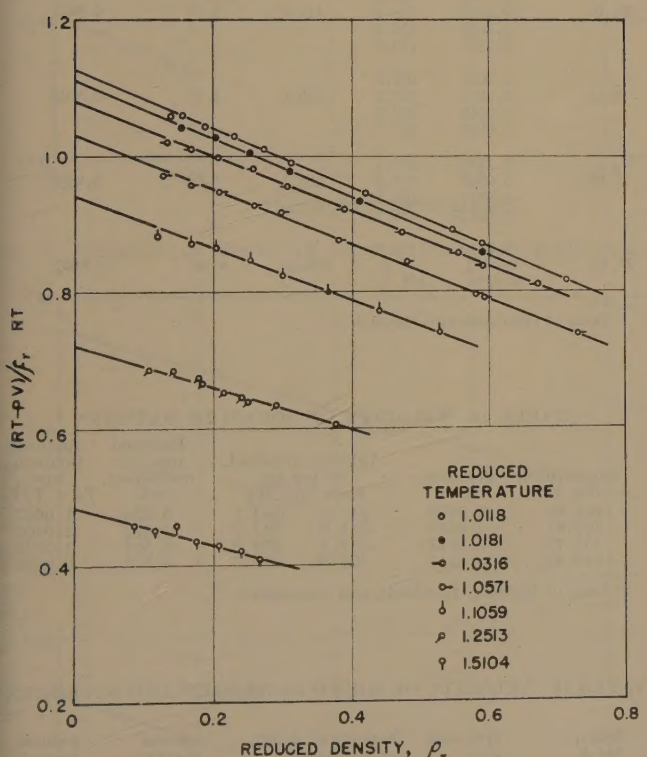

FIG. 1 VOLUMETRIC DATA OF ONNES AND KUYPERS FOR OXYGEN

TABLE 5 SECOND VIRIAL COEFFICIENTS FOR OXYGEN[a]

Reduced temperature, $T_r = T/T_c$	Reduced second virial coefficient, $-B_r = -B/V_c$	Reduced third virial coefficient, $C_r = C/V_c^2$
1.0118	1.125	0.432
1.0181	1.110	0.429
1.0316	1.079	0.407
1.0571	1.029	0.400
1.1059	0.939	0.380
1.2513	0.719	0.303
1.5104	0.483	0.284

[a] Calculated from data of Onnes and Kuypers.

TABLE 4 OXYGEN-VOLUMETRIC DATA OF ONNES AND KUYPERS

Pressure, Atmospheres	PV, Relative	ρr, Reduced Density	$\frac{RT-PV}{\rho_r RT}$
-40.050C.;	233.11°K.;	RT = 0.8542;	T_r = 1.5104
21,142	0.8218	0.0855	0.458
28.034	0.8112	0.1150	0.451
34.744	0.7992	0.145	0.458
41.818	0.7898	0.1738	0.434
49.255	0.7806	0.207	0.428
55.425	0.7713	0.2385	0.419
61.030	0.7642	0.266	0.408
-80.04°C.;	193.12°K.;	RT = 0.7076;	T_r = 1.2513
21.010	0.6550	0.1064	0.685
27.295	0.6388	0.1420	0.683
33.475	0.6221	0.1780	0.674
34.178	0.6213	0.1827	0.666
39.240	0.6086	0.214	0.652
43.247	0.5976	0.2405	0.645
44.613	0.5949	0.2490	0.639
50.430	0.5772	0.2900	0.635
61.880	0.5464	0.376	0.605
-102.47°C.;	170.69°K.;	RT = 0.6254;	T_r = 1.1059
20.118	0.5594	0.1196	0.881
26.932	0.5344	0.1672	0.869
31.601	0.5155	0.2035	0.864
37.564	0.4910	0.2535	0.846
42.513	0.4710	0.300	0.824
48.720	0.4420	0.366	0.800
54.588	0.4127	0.440	0.772
60.474	0.3811	0.528	0.740
-109.98°C.;	163.18°K.;	RT = 0.5979;	T_r = 1.0571
20.010	0.5244	0.127	0.970
25.330	0.5022	0.1674	0.957
29.977	0.4804	0.208	0.947
35.427	0.4544	0.259	0.926
38.979	0.4346	0.298	0.916
45.687	0.3989	0.3805	0.875
51.130	0.3618	0.480	0.844
56.200	0.3220	0.580	0.795
56.655	0.3174	0.593	0.791
-113.98°C.;	159.14°K.;	RT = 0.5831;	T_r = 1.0316
20.149	0.5044	0.1329	1.018
24.462	0.4847	0.1677	1.009
28,893	0.4624	0.208	0.997
33.731	0.4370	0.256	0.979
33.758	0.4369	0.256	0.979
37.979	0.4133	0.306	0.953
43.890	0.3739	0.389	0.921
48,304	0.3385	0.474	0.887
51.059	0.3061	0.555	0.857
52.543	0.2951	0.591	0.836
54.066	0.2672	0.671	0.809
-116.02°C.;	157.14°K.;	RT = 0.5758;	T_r = 1.0181
22.300	0.4835	0.154	1.041
27.849	0.4560	0.203	1.026
32.648	0.4297	0.252	1.003
37.468	0.4012	0.310	0.976
43.947	0.3541	0.412	0.931
50.445	0.2836	0.591	0.857
-117.00oC.;	156.16°K.;	RT = 0.5722;	T_r = 1.0118
20.264	0.4891	0.1375	1.057
22.298	0.4783	0.1551	1.058
26.413	0.4579	0.1880	1.042
30.248	0.4371	0.230	1.027
34.117	0.4144	0.273	1.009
37.210	0.3958	0.312	0.989
43.662	0.3458	0.420	0.945
48.344	0.2936	0.547	0.890
49.507	0.2790	0.590	0.870
51.297	0.2388	0.714	0.817

TABLE 6 JOULE-THOMSON COEFFICIENTS FOR AIR[a]

Temperature, Deg. K	Reduced Temperature, T_r	Joule-Thomson Coefficient, Deg.K/Atm.	Reduced Joule-Thomson Coefficient, $\mu c_p/v_c$
120	0.9064	1.221	4.12
125	0.9441	1.135	3.84
130	0.9818	1.053	3.56
140	1.0574	0.912	3.08
150	1.1329	0.805	2.72
160	1.2084	0.716	2.42
170	1.2850	0.640	2.16
180	1.3595	0.582	1.97
190	1.4350	0.530	1.79
200	1.5105	0.484	1.63
210	1.5861	0.445	1.50
220	1.6616	0.410	1.386
230	1.7372	0.380	1.283
240	1.8126	0.350	1.182
250	1.8882	0.323	1.091
260	1.9638	0.300	1.013
270	2.0394	0.275	0.930
280	2.1150	0.258	0.872
290	2.1906	0.240	0.810

[a] Data of Hausen.

TABLE 7 JOULE-THOMSON COEFFICIENTS FOR AIR[a]

Temperature, deg.K	Reduced Temperature, T_r	Joule-Thomson Coefficient, degrees K. per atmosphere 19.7 atm.	0.968 atm.	0.00 atm.	Reduced Joule-Thomson Coeff., $\mu c_p/v_c$
123.16	0.9285	1.240	1.138	1.133	3.82
133.16	1.0060	1.000	0.968	0.966	3.22
143.16	1.0815	0.846	0.834	0.833	2.805
153.16	1.1571	0.734	0.734	0.734	2.47
163.16	1.2326	0.648	0.658	0.659	2.22
173.16	1.3082	0.581	0.596	0.597	2.015
198.16	1.4970	0.456	0.478	0.479	1.680
223.16	1.6858	0.370	0.391	0.392	1.322
248.16	1.8746	0.307	0.327	0.328	1.108
273.16	2.0634	0.258	0.275	0.276	0.931
333.16	2.5165	0.184	0.195	0.196	0.661

[a] Data of Roebuck.

TABLE 8 JOULE-THOMSON COEFFICIENTS FOR NITROGEN[a]

Temperature, deg. K.	Joule-Thomson Coefficient, degrees K. Per atmosphere 19.7 atm.	0.968 atm.	0.00 atm.	Reduced Joule-Thomson Coeff., $\mu c_p/v_c$	Reduced Temperature, T_r
373.16	0.1179	0.1292	0.1298	0.414	2.9619
348.16	0.1428	0.1558	0.1564	0.495	2.7635
323.16	0.1716	0.1856	0.1863	0.595	2.5651
298.16	0.2065	0.2220	0.223	0.711	2.3667
273.16	0.2600	0.2655	0.266	0.848	2.1682
248.16	0.3025	0.3230	0.324	1.090	1.9698
223.16	0.3750	0.3970	0.398	1.270	1.7614
198.16	0.468	0.5030	0.505	1.610	1.5730
185.66	0.526	0.5710	0.573	1.829	1.4738
173.16	0.598	0.649	0.652	2.080	1.3746
160.66	0.686	0.743	0.746	2.380	1.2754
148.66	0.798	0.856	0.859	2.740	1.1762
135.66	0.941	0.998	1.001	3.195	1.0770
123.16	1.132	1.268	1.275	4.06	0.9778
113.16		1.633	1.641*	5.235	0.8984
103.16		2.01	2.02*	6.44	0.8190
93.16		2.39	2.40 *	7.65	0.7397

* Extrapolated by comparison with values above.

[a] Data of Roebuck and Osterberg.

TABLE 9 VELOCITY OF SOUND IN OXYGEN[a]

Temp., deg.K	Pressure, Atm.	Velocity of Sound, Meters/Sec. W_{obs}	W_o	Reduced Pressure Coefficient, $-S_r$	Reduced Temperature, $T_r = T/T_c$
92.03	0.9815	179.6			
	0.8355	179.9			
	0.6770	180.5	183.0	2.05	0.5968
	0.5145	180.9			
	0.3500	181.5			
	0.2026	181.9			
86.92	0.6250	174.9			
	0.3007	176.2			
	0.1108	177.1	177.8	2.50	0.5636
	0.5164	175.5			
	0.4115	175.9			
	0.2007	176.6			
88.72	0.7242	176.7			
	0.5974	177.3			
	0.4723	177.6	179.6	2.20	0.5752
	0.3408	178.0			
	0.2024	178.6			
84.95	0.4776	173.5			
	0.3454	173.9	175.8	2.68	0.5508
	0.2276	174.5			
	0.1203	175.1			
83.05	0.4226	171.3			
	0.3111	172.0	173.8	3.08	0.5385
	0.1889	172.5			
	0.0842	173.3			
80.60	0.2624	169.5			
	0.2526	169.8			
	0.1803	169.9	171.2	3.30	0.5227
	0.1091	170.4			
	0.0566	170.9			
78.15	0.2061	167.2			
	0.1470	167.7	168.6	3.36	0.5068
	0.0968	167.9			
	0.0451	168.5			
76.00	0.1329	165.3			
	0.0892	165.8	166.3	3.65	0.4939
	0.0517	166.1			
	0.01139	165.3			
74.12	0.1032	163.3			
	0.0703	163.6	164.2	4.20	0.4807
	0.0358	164.3			

[a] Data of Itterbeek and Paemel.

TABLE 10 VELOCITY OF SOUND IN OXYGEN[a]

Temperature, deg K	Pressure, atm	Velocity of sound, m per sec W_{obs}	W_o	Reduced pressure coefficient, $-S_r$	Reduced temperature, $T_r = T/T_c$
164.63	0.9075	244.3	244.7	0.326	1.0667
160.61	0.8930	241.0	241.7	0.572	1.0406
155.79	0.8747	237.4	238.0	0.527	1.0094
144.84	0.8311	229.0	229.5	0.418	0.9384

[a] Data of Keesom, Itterbeek, and Lammeren.

TABLE 11 VELOCITY OF SOUND IN OXYGEN AND NITROGEN[a]

Temp., deg.K	Pressure, Atm.	Velocity of Sound, Meters/Second W_{obs}	W_o	Reduced Pressure Coefficient, $-S_r$	Reduced Temperature, $T_r = T/T_c$
90.23 (Oxygen)	0.947	178.0			
	0.596	179.2	181.16	1.84	0.5851
	0.339	180.3			
	0.093	180.8			
90.19 (Oxygen)	0.784	178.4			
	0.566	179.1	181.1		
	0.319	179.8			
	0.117	180.6			
90.14 (Nitrogen)	0.946	190.7			
	0.636	191.7	193.5	1.29	0.7154
	0.343	192.5			
	0.123	193.1			

[a] Data of Itterbeek and Mariens.

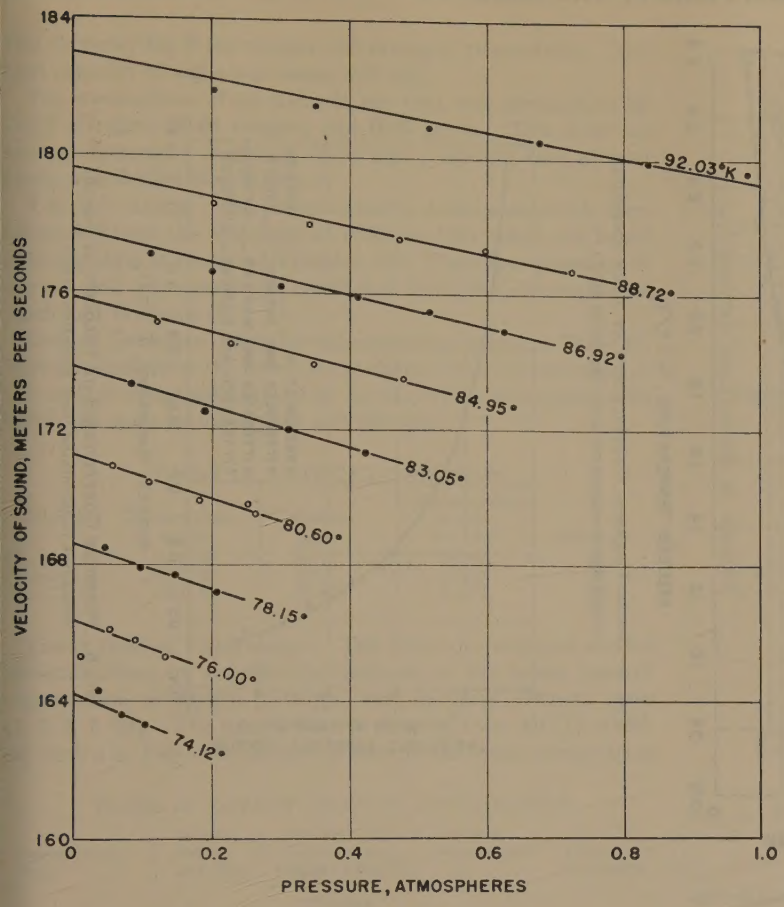

FIG. 2 VELOCITY OF SOUND IN OXYGEN FROM VAN ITTERBEEK AND PAEMEL

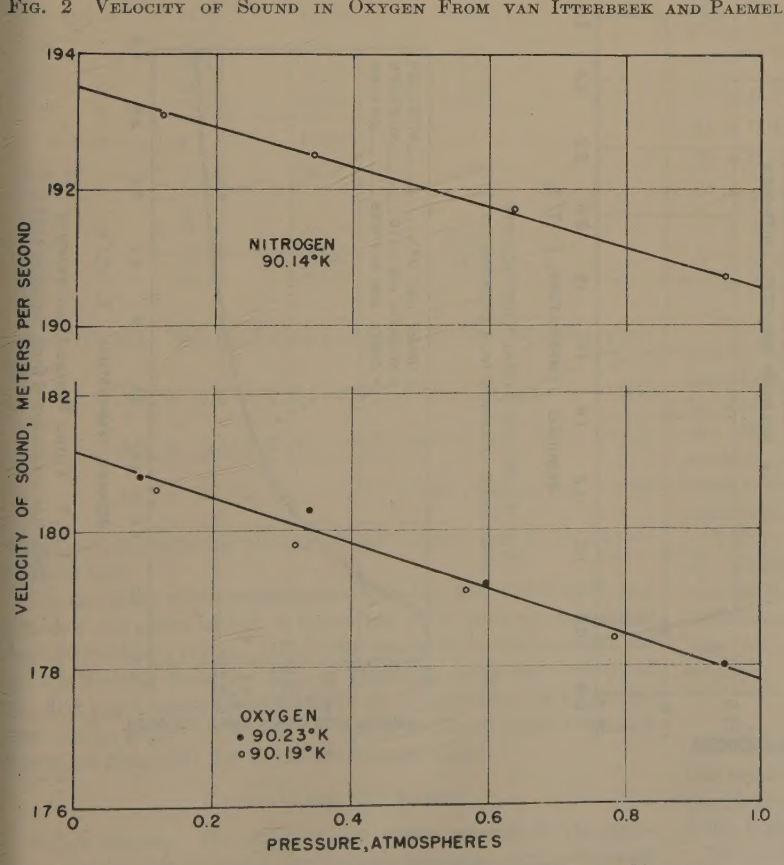

FIG. 3 VELOCITY OF SOUND FROM VAN ITTERBEEK AND MARIENS

Paemel (15) on oxygen. These data and the results from the graphical analysis of them in Fig. 2 are given in Table 9. A few measurements by Keesom, Itterbeek, and Lammeren (21) on oxygen are analyzed in Table 10. The determinations of Itterbeek and Mariens (14) on oxygen and nitrogen are presented in Table 11, and analyzed in Fig. 3.

The velocity of sound at zero pressure which was used in the analysis was the theoretical value calculated with a ratio of heat capacities of 1.400. This is in contrast with the purpose of the Leiden workers in performing the experiments, namely, to determine the heat capacities at zero pressure. At the present time more confidence can be placed in statistical calculations, and, considering the precision of the Leiden temperature measurements, the calculated velocity at zero pressure should be quite accurate.

The data were correlated by fitting the constants of the chosen virial coefficient Equations [11] and [12], to the experimental data. The fitting was done by a trial-and-error process to obtain a satisfactory agreement with the data. The following constants were obtained for Equation [11]

$$a = 0.539$$
$$b = -1.382$$
$$c = -0.201$$
$$d = -0.0566$$

The proposed correlation is shown as the solid line in Figs. 4, 5, and 6, where it is compared graphically with the volumetric, Joule-Thomson, and velocity-of-sound data, respectively.

As can be seen from the curves, the correlation is good, in general, although the Joule-Thomson coefficients for nitrogen in the region of the critical temperature deviate rather widely. The excellent agreement of volumetric data for oxygen and nitrogen in this region, and of Joule-Thomson coefficients themselves at higher temperatures, makes a true deviation in Joule-Thomson coefficients appear doubtful.

Third Virial Coefficients. Data applicable to the calculation of third virial coefficients are quite limited. Tables 1, 2, and 5 show the data on oxygen and nitrogen which were used in this work. As can be observed in the tables, no data were included below the critical temperature. The contribution of the third virial term is not very important in the pressure range studied, however, and the necessary extrapolation was made. The constants for Equation [12] determined by trial and error, are as follows

$$\alpha = 0.126$$
$$\beta = 0.059$$
$$\gamma = 0.252$$

The data are compared graphically with Equation [12] (solid line) in Fig. 7.

Zero-Pressure Heat Capacity. The heat capacity at zero pressure was calculated by Johnston and his associates for both oxygen (17) and nitrogen (16). From ordinary temperatures downward the values were taken to be constant at 6.962 and 6.955

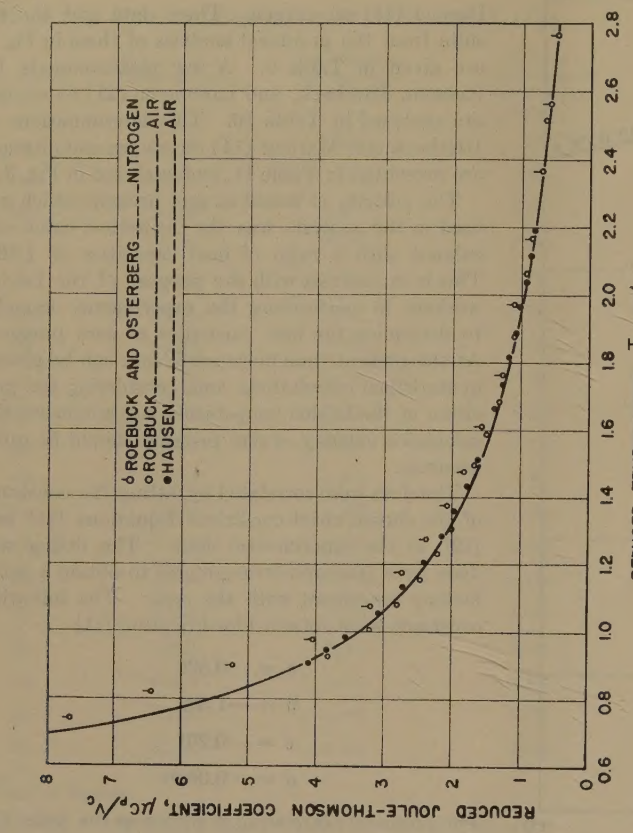

FIG. 5 JOULE-THOMSON COEFFICIENTS AT ZERO PRESSURE
(Solid line is calculated from Equation [15].)

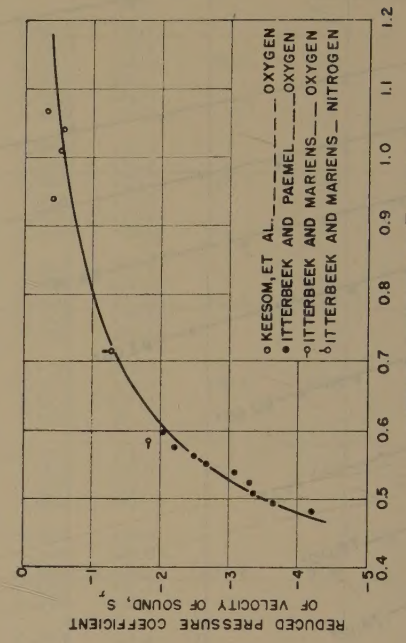

FIG. 6 PRESSURE COEFFICIENTS OF VELOCITY OF SOUND
(Solid line is calculated from Equation [16].)

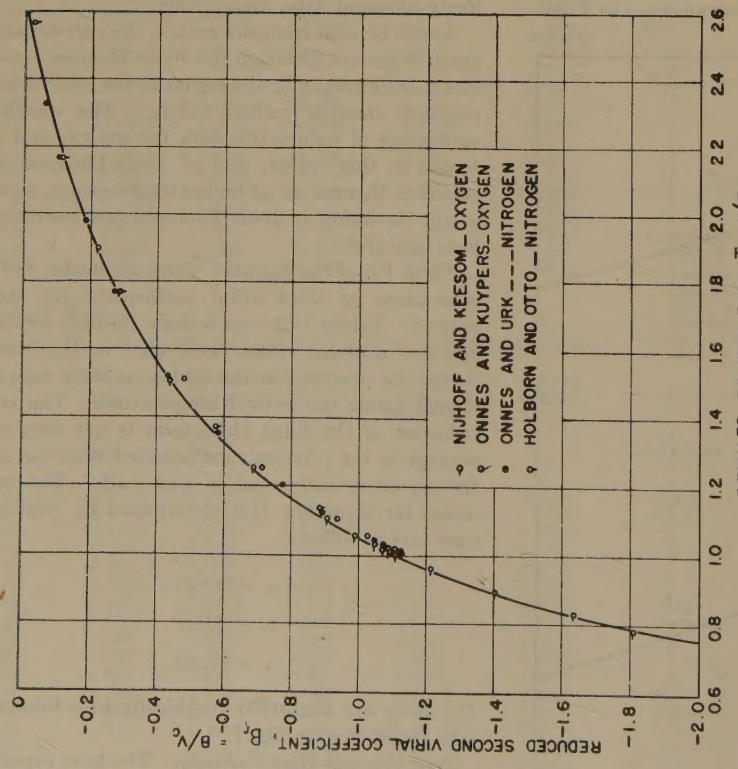

FIG. 4 SECOND VIRIAL COEFFICIENTS
(Solid line is calculated from Equation [11].)

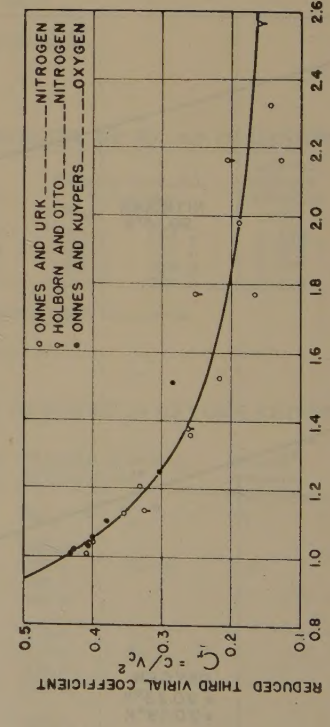

FIG. 7 THIRD VIRIAL COEICFFIENTS
(Solid line is calculated from Equation [12].)

Btu/lb mole/deg F for oxygen and nitrogen, respectively. The heat capacity of argon was taken as 4.962.

The composition of air in mole per cent was assumed to be 78.12 nitrogen, 20.95 oxygen, and 0.93 argon. This gives an average molecular weight of 28.96 and a specific heat at zero pressure of 0.2396 Btu/lb/deg F.

Vapor Pressures. The bubble point and dew point of air were calculated from the equations of Williams (36), which are based upon the data of Dodge and Dunbar (6). The vapor pressures of oxygen and nitrogen were calculated from the correlation of Koch and Williams (22).

Critical Constants. The critical constants, shown in Table 12, were obtained from the literature as shown, with the exception of the critical compressibility factor for air, which was taken to be 0.292, the same as for oxygen and nitrogen.

TABLE 12 CRITICAL CONSTANTS

Material	Temperature, deg K	Pressure, atm	Compressibility factor, PV/RT	Reference
Oxygen.....	154.34	49.7	0.292	24
Nitrogen....	126.00	33.5	0.292	25
Air.....	132.40	37.25	0.292	36

Latent Heat of Vaporization. The literature contains several determinations by calorimetric methods of the latent heat of vaporization of oxygen, nitrogen, and mixtures of these gases (1, 2, 5, 7, 20). The most extensive data are from Alt (1), which are shown in Table 13, along with some of the latest comparative

TABLE 13 LATENT HEAT OF VAPORIZATION

Temperature, deg.C	Latent Heat, Cal./gm.	Entropy of Vaporization, Cal/gm. Mole/°K	Reduced Temperature, T_r	Literature Reference
		NITROGEN		
-195.55	47.65	17.18	0.6160	1
-195.55	47.74			5
-198	48.32	17.99	0.5965	1
-202	49.42	19.44	0.5648	1
-206	50.51	21.05	0.5330	1
-210	51.61	22.88	0.5013	1
		OXYGEN		
-182.93	50.92	18.05	0.5850	1
-182.93	51.01			5
-182.93	50.8			20
-188	51.98	19.54	0.5519	1
-194	53.23	21.51	0.5130	1
-200	54.48	23.84	0.4741	1
-205	55.52	26.06	0.4417	1

values (5, 20). The data were correlated by the following qeuations

$$\Delta S_v = (14.14/T_r)(1 - T_r)^{0.392} \text{ for nitrogen} \quad [17]$$

$$\Delta S_v = (14.08/T_r)(1 - T_r)^{0.392} \text{ for air} \quad [18]$$

$$\Delta S_v = (13.73/T_r)(1 - T_r)^{0.392} \text{ for oxygen} \quad [19]$$

where ΔS_v is the molal entropy of vaporization and T_r is reduced temperature.

Comparisons of the correlations with the data for oxygen and nitrogen are given in Fig. 8 where the solid lines are calculated from Equations [17] and [19]. The constant for the equation for air was derived from the data of Dana (5) using the average of the dew point and bubble point for the temperature of vaporization, and a slight correction for the presence of argon from the literature data (23), for the latent heat of argon.

Calculation of Charts

Vapor Region. The superheated vapor regions of the temperature-entropy diagrams, for oxygen, nitrogen, and air were all

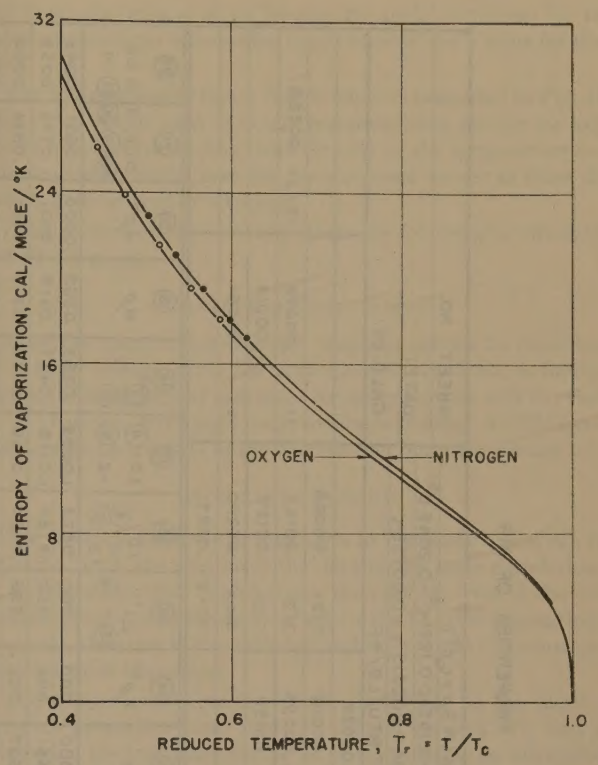

FIG. 8 ENTROPY OF VAPORIZATION OF OXYGEN AND NITROGEN (Solid lines are calculated from Equations [17] and [19].)

calculated from the same reduced equation of state, Equations [2], [11], and [12]. The manner of performing the calculations will be described for air. The following equation of state was used for superheated air vapor

$$P = 0.370\, T\rho(1 + B\rho + C\rho^2)$$

$$B = 0.0254 - 0.1551\tau - 0.1281\tau^3 - 0.2048\tau^5$$

$$C = 0.00028 + 0.000313\tau + 0.00759\tau^3$$

P = psia

$\tau = 100/T$

T = deg R

ρ = density, lb per cu ft

Fig. 9 is a copy of the calculation sheet used for calculating the deviations from ideal-gas-law values of the thermodynamic functions. From this figure the exact manner of calculation may be observed. In the left-hand corner at the top, the temperature of —260 F was selected. Below and to the right of this are various quantities which are required for calculating the deviations. Then several constants, B, C, D, E, F, G, H, and J, were calculated as shown.

Arbitrary values were chosen for ρ in column 1. Column 2 is ρ^2. Columns 3 through 7 are straightforward and show the calculations for the compressibility factor and the pressure.

Columns 8 through 12 show the calculation of entropy deviation $\Delta S'$ with which the entropy can be computed from the relation

$$S = C_p^0 \ln T - R \ln P - \Delta S' \quad [20]$$

The deviation is measured from an ideal gas, so the entropy from this equation is for a gas of constant heat capacity measured above the ideal state at 1 deg abs and one unit of pressure. This basis, 1 deg R and 1 psia, was used for the charts.

The enthalpy deviation $\Delta i'$, is calculated in columns 13 through

THERMODYNAMIC PROPERTIES OF AIR

t= −260 °F	$\tau = 100/T$ = .50078		Log T = 2.300356		$P = 0.370T\rho(1 + B\rho + C\rho^2)$																		
T = 459.69 − t = 199.69 °R	τ^2 = .25078		.5516 Log T = 1.26888		$B = 0.0254 - 0.1551\tau - 0.1281\tau^3 - 0.2048\tau^5$																		
.370 T = 73.885	τ^3 = .12558		.2396 T = 47.846		$C = 0.00028 + 0.000313\tau + 0.00759\tau$																		
.068617 T = 13.702	τ^5 = .03149				$R = 0.068617$ BTU/LB/°F																		
.1551τ = .07767	·1 = .07767				.00028																		
.1281τ^3 = .01609	·3 = .04826	·2 = .03217	·6 = .09652		.000313τ = .00016	·1/2 = .00008																	
.2048τ^5 = .00645	·5 = .03225	·4 = .02580	·20 = .12900		.00759τ^3 = .00095	·3/2 = .00143																	
Sum = .10021	−B = −.07481	+ .02540	H = .22552		C = .00139	C = .00139																	
−0.02540	Sum = .23299	F = .08337				Sum = .00290																	
−B = .07481	·RT = D = 3.1924					·RT = E = .0397																	

SHEET NO.
DATE:
CALC. BY

·1 = .00095 ·3 = J = .00286
−.00014
G = .00081

(1) ρ lb/ft.^{3}	(2) ρ^2	(3) .37Tρ	(4) −Bρ	(5) Cρ^2	(6) Z 1−(4)+(5)	(7) P (6)·(3)	(8) Fρ	(9) Gρ^2	(10) −Ln Z	(11) $\Delta S'/R$ (8)+(9)+(10)	(12) $\Delta S'$ (11)·R	(13) Dρ	(14) Eρ^2	(15) $\Delta i'$ (13)−(14)	(16) 1.0 −2·(4) +3·(5)	(17) 1.0+(8) −2·(9)	(18) $\frac{(17)^2}{(16)} - 1$	(19) Hρ	(20) Jρ^2	(21) $\Delta C'p/R$ (18)+(19)+(20)	(22) $\Delta C'p$ (21)·R
.1189	.0141	8.79	.0089	.0000	.9911	8.71	.0099	.0000	.0089	.0188	.00129	.380	.000	.380	.9823	1.0099	.0383	.0268	.0000	.0651	.0045
.1414	.0200	10.45	.0106	.0000	.9894	10.34	.0118	.0000	.0106	.0224	.00154	.451	.001	.450	.9789	1.0118	.0457	.0319	.0001	.0775	.0053
.1682	.0283	12.43	.0126	.0000	.9874	12.27	.0140	.0000	.0126	.0266	.00183	.537	.001	.536	.9750	1.0140	.0546	.0379	.0001	.0924	.0063
.2000	.0400	14.78	.0150	.0001	.9851	14.56	.0167	.0000	.0150	.0316	.00217	.638	.002	.636	.9703	1.0166	.0652	.0451	.0001	.1102	.0076
.2378	.0566	17.57	.0178	.0001	.9823	17.26	.0198	.0000	.0179	.0376	.00258	.759	.002	.757	.9647	1.0198	.0780	.0536	.0002	.1315	.0090
.2828	.0800	20.90	.0212	.0001	.9789	20.46	.0236	.0001	.0213	.0448	.00307	.903	.003	.899	.9580	1.0235	.0934	.0638	.0002	.1569	.0108
.3364	.1131	24.85	.0252	.0002	.9750	24.23	.0280	.0001	.0253	.0533	.00365	1.074	.004	1.070	.9502	1.0279	.1119	.0759	.0003	.1874	.0129
.4000	.1600	29.55	.0299	.0002	.9703	28.68	.0336	.0001	.0301	.0634	.00435	1.277	.006	1.271	.9408	1.0331	.1344	.0902	.0005	.2242	.0154
.4757	.2263	35.14	.0356	.0003	.9647	33.90	.0397	.0002	.0359	.0754	.00517	1.519	.009	1.510	.9298	1.0393	.1617	.1073	.0006	.2684	.0184
.5657	.3200	41.80	.0423	.0004	.9581	40.05	.0472	.0003	.0428	.0897	.00615	1.806	.013	1.793	.9167	1.0466	.1950	.1276	.0009	.3217	.0221
.6727	.4525	49.70	.0503	.0006	.9503	47.23	.0561	.0004	.0510	.1067	.00732	2.148	.018	2.130	.9012	1.0554	.2358	.1517	.0013	.3862	.0265
.8000	.6400	59.11	.0598	.0009	.9410	55.62	.0667	.0005	.0608	.1270	.00871	2.554	.025	2.529	.8830	1.0657	.2862	.1804	.0018	.4647	.0319
.9514	.9051	70.29	.0712	.0013	.9301	65.37	.0793	.0007	.0725	.1511	.01036	3.037	.036	3.001	.8614	1.0778	.3486	.2146	.0026	.5606	.0385
1.1314	1.2800	83.59	.0846	.0018	.9172	76.67	.0943	.0010	.0865	.1798	.01233	3.612	.051	3.561	.8361	1.0922	.4269	.2552	.0037	.6784	.0466
1.3454	1.8102	99.41	.1006	.0025	.9019	89.65	.1122	.0015	.1033	.2140	.01468	4.295	.072	4.223	.8063	1.1092	.5260	.3034	.0052	.8243	.0566
1.6000	2.5600	118.22	.1197	.0036	.8839	104.49	.1334	.0021	.1234	.2548	.01748	5.108	.102	5.006	.7713	1.1292	.6533	.3608	.0073	1.0068	.0691
1.9027	3.6204	140.58	.1423	.0050	.8627	121.27	.1586	.0030	.1477	.3034	.02082	6.074	.144	5.933	.7304	1.1527	.8193	.4291	.0104	1.2380	.0850
2.2627	5.1200	167.18	.1693	.0071	.8378	140.07	.1887	.0042	.1769	.3614	.02480	7.224	.203	7.021	.6828	1.1803	1.0404	.5103	.0146	1.5360	.1054
2.6909	7.2407	198.82	.2013	.0101	.8088	160.80	.2244	.0059	.2122	.4307	.02955	8.590	.287	8.303	.6275	1.2126	1.3431	.6068	.0207	1.9292	.1324
3.200	10.240	236.43	.2394	.0142	.7748	183.20	.2668	.0083	.2551	.5136	.03524	10.216	.406	9.810	.5639	1.2502	1.7715	.7217	.0293	2.4639	.1691

Fig. 9 Calculation Sheet

15. The enthalpy, measured above 0 deg abs for a gas of constant heat capacity, can be obtained from

$$i = C_p{}^0T - \Delta i' \quad [21]$$

This basis for enthalpy was used in the charts.

The deviation in heat capacity $\Delta Cp'$, was calculated in the remainder of the columns. The heat-capacity deviation is added to the zero-pressure heat capacity to give the true value.

The derivations of the equations for the foregoing deviations in terms of the virial coefficients are simple and well known and are not included here. The calculation sheet shows how the operations were performed.

After the calculations were completed, the deviations of entropy, enthalpy, and heat capacity were plotted versus pressure. From these plots values of the deviations were read and used to calculate the functions at desired pressures.

The deviations were calculated for each temperature at 5-deg intervals below —260 F and at 10-deg intervals above this temperature. The corresponding entropy, enthalpy, and heat capacity were calculated for the desired pressures at each temperature by the procedure just outlined. The temperature at which the enthalpy was an integral value at the desired pressure was obtained by interpolating with the aid of heat capacity. This completed the data required for the superheated-vapor region of the temperature-entropy diagrams.

Liquid Region. After the vapor region had been calculated and plotted on a temperature-entropy chart, the dew point of the fluid was then plotted at the corresponding pressures. The dew-point line gave entropy and enthalpy of the saturated vapor. With these values of entropy and enthalpy, and with the latent heat of vaporization, the liquid region was calculated. The latent heat of vaporization was calculated from the equation shown in the previous section. For air, the average temperature between the bubble point and dew point was again used as the temperature for determining the relation between entropy of vaporization and latent heat of vaporization.

Charts

The heat capacity of air vapor from the foregoing calculations is given in Fig. 10. This curve can also be used to determine the heat capacity of oxygen or nitrogen. The temperature and pressure for air are calculated which give the same reduced values as those desired for the oxygen or nitrogen. The heat capacity for air is found at these conditions, and the zero-pressure value is deducted to give the deviation. This deviation is multiplied by the molecular weight of air to give the molal deviation for the oxygen or nitrogen to be added to the zero-pressure value for that gas.

The compressibility factor for air vapor is presented in Fig. 11. This chart can be used to obtain compressibility factors for oxygen or nitrogen by reading them directly at the temperature and pressure for air which give the same reduced values as those desired for the oxygen or nitrogen.

Finally, temperature-entropy diagrams for oxygen, nitrogen, and air are given.

Charts for Computation

Since the temperature-entropy diagrams cannot be published at a large enough scale for accurate computations, a limited number of lithographed charts for oxygen, nitrogen, and air, each 11 × 17 inches, have been made available through ASME headquarters and are on file in the Engineering Societies Library.

Accuracy of Charts

The probable accuracy of the charts in the vapor region can be estimated from the scatter of the data in the basic correlations. In the compressibility-factor chart, the possible error in the calculated volume is of interest; while in the temperature-entropy diagrams, the error in the enthalpy and the error in the isentropic work are most important.

The greatest contributions of the deviations to the thermodynamic properties occur near the critical temperature, and in this region the maximum scatter of the data from the correlation is about 5 per cent for second virial coefficients in Fig. 4, and about 10 per cent for Joule-Thomson coefficients for nitrogen in Fig. 5. These divergences in this temperature region at the maximum pressure of the charts could cause an error of 1 per cent in volume and isentropic work, and an error of 0.8 Btu per lb in enthalpy.

The Joule-Thomson data for nitrogen are apparently not as reliable, however, as are the three sets of volumetric data from high-pressure measurements in Fig. 4. Another equation for second virial coefficient developed more recently and including data on argon has been computed (4), which represents these volumetric high-pressure measurements very closely. Calculations with this alternate second-virial-coefficient equation showed maximum differences from the proposed correlation of 1 per cent in volume and isentropic work and less than 0.5 Btu per lb in enthalpy.

The total contribution of the third virial term is never more

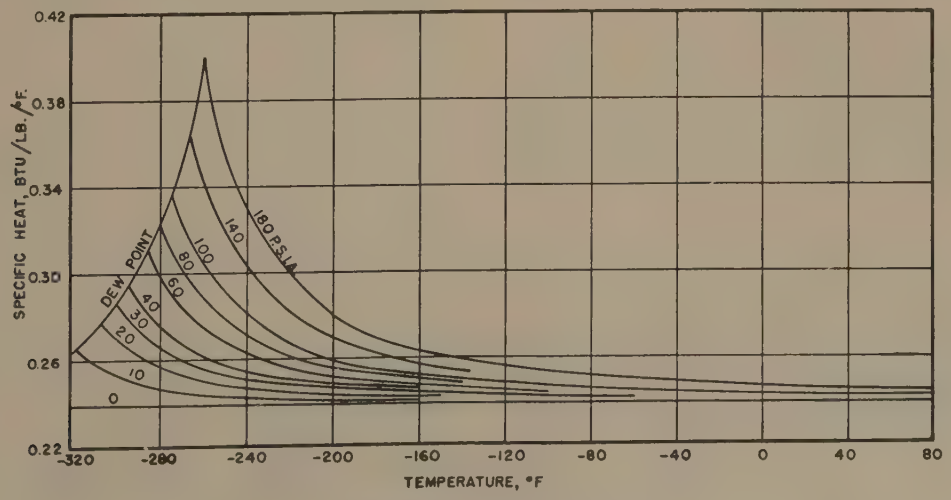

Fig. 10 Specific Heat of Air

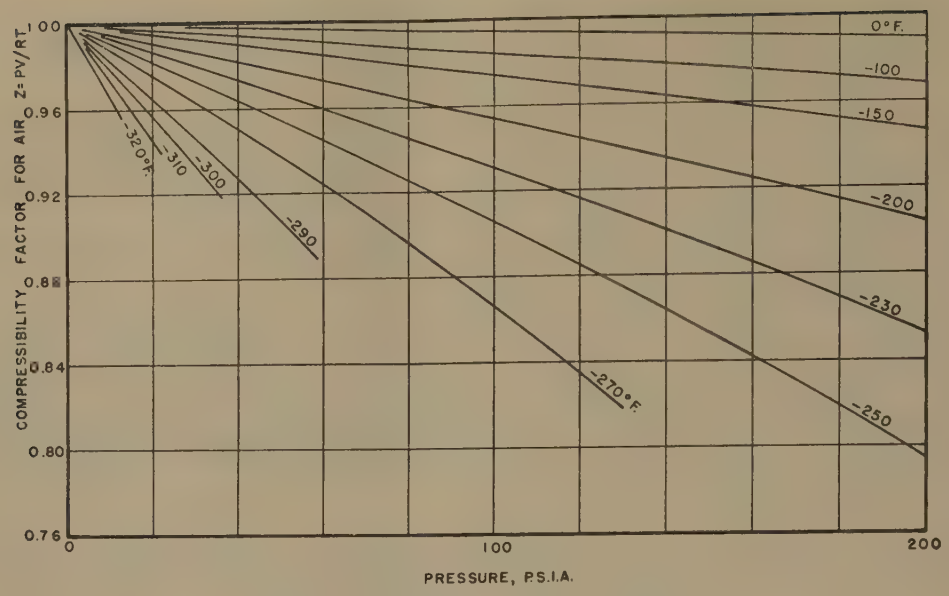

FIG. 11 COMPRESSIBILITY FACTORS FOR AIR

than 1.3 per cent in volume nor more than 0.4 Btu per lb in enthalpy. Thus the probable error in this term is negligible compared with that of the second virial coefficient in the range of the charts.

It is believed that the charts as presented are correct in the vapor region within 1 per cent in volume and isentropic work, and within 0.5 Btu per lb in enthalpy at the maximum pressure given. This error decreases as the pressure decreases in an approximately linear manner.

CONCLUSIONS

A new reduced equation of state has been developed for oxygen, nitrogen, and air, based upon volumetric, Joule-Thomson, and velocity-of-sound data. From this equation there have been prepared compressibility-factor charts, specific-heat charts, and temperature-entropy diagrams for temperatures below 160 F and pressures below 200 psia. The accuracy of the charts in the vapor region at 100 psia is believed to be of the order of 0.5 per cent in volume and isentropic work, and 0.25 Btu per lb in enthalpy, which is adequate for the engineering design of low-pressure oxygen plants.

ACKNOWLEDGMENT

The authors wish to acknowledge the valuable assistance of Ann Kindelan and Jean Minster, who performed most of the calculations; Jack Barth who drafted the diagrams; Dr. I. Roberts, under whose direction the work was done; and our thanks to the Elliott Company for permission to publish the work.

BIBLIOGRAPHY

1 "Über die Verdampfungswärme des flüssigen Sauerstoffs und flüssigen Stickstoffs und deren Änderung mit der Temperatur," by H. Alt, *Annalen der Physik*, vol. 19, 1906, pp. 739–782.

2 "Über die Verdampfungswärme des Sauerstoffs," by H. Barschall, *Zeitschrift für Elektrochemie und angewandte physikalische Chemie*, vol. 17, 1911, pp. 345–348.

3 "A New Equation of State for Fluids," by J. A. Beattie and O. C. Bridgeman, *Journal of the American Chemical Society*, vol. 50, 1928, pp. 3133–3138.

4 "The Second Virial Coefficient of the Major Atmospheric Gases at Low Temperatures," by L. C. Claitor, thesis, Agricultural and Mechanical College of Texas, 1948.

5 "The Latent Heat of Vaporization of Liquid Oxygen-Nitrogen Mixtures," by L. I. Dana, Proceedings of the American Academ of Arts and Sciences, vol. 60, 1925, pp. 241–267.

6 "An Investigation of the Coexisting Liquid and Vapor Phas of Solutions of Oxygen and Nitrogen" by B. F. Dodge and A. F Dunbar, *Journal of the American Chemical Society*, vol. 49, 192 pp. 591–610.

7 "Über das Thermische Verhalten einiger Komprimierter un Kondensierter Gase bei tiefen Temperaturen," by A. Eucken, *Ve handlungen der deutschen Physikalischen Gesellschaft*, vol. 18, 191 pp. 4–17.

8 "Über die Temperaturänderung von Gasen bei der Entspan nung durch Drosselung und durch äusere Arbeitsleistung," by H Hausen, *Zeitschrift für technische Physik*, vol. 7, 1926, pp. 371–377.

9 Ibid., vol. 7, 1926, pp. 444–452.

10 "Der Thomson-Joule Effekt," by H. Hausen, *Forschung au em Gebiete des Ingenieurwesens*, vol. 274, 1926, pp. 3–48.

11 "Über die Isothermen von Stickstoff, Sauerstoff, und Helium, by L. Holborn and J. Otto, *Zeitschrift für Physik*, vol. 10, 1922, pp 367–376.

12 "Über die Isothermen von Helium, Stickstoff, und Argon un terhalb 0°," by L. Holborn and J. Otto, *Zeitschrift für Physik*, vol. 30 1924, pp. 320–328.

13 "Über die Isothermen einiger Gase Zwischen +400° an —183°," by L. Holborn and J. Otto, *Zeitschrift für Physik*, vol. 33 1925, pp. 1–11.

14 "Measurements With Ultra-Sonics on the Velocity and Ab sorption of Sound at Ordinary and Low Temperatures," by A. va Itterbeek and P. Mariens, *Physica*, vol. 4, 1937, pp. 207–215.

15 "Measurements on the Velocity of Sound as a Function o Pressure in Oxygen Gas at Liquid Oxygen Temperatures," by A van Itterbeek and O. van Paemel, *Physica*, vol. 5, 1938, pp. 593–603

16 "Heat Capacity of the Simpler Gases, IV. Extension of th 'Free Energy' Formula of Giauque and Overstreet to Yield Reliabl Approximation Formulas for the Calculation of Entropy and o Heat Capacity from Spectroscopic Data. Entropy and Heat Capacit of Carbon Monoxide and of Nitrogen From Near Zero Absolute t 5000°K," by H. L. Johnston and C. O. Davis, *Journal of the Americ Chemical Society*, vol. 56, 1934, pp. 271–276.

17 "Heat Capacity of the Simpler Gases, II. Heat Capacity Entropy and Free Energy of Gaseous Oxygen From Near Zero Abso lute to 5000°K," by H. L. Johnston and M. K. Walker, *Journal o the American Chemical Society*, vol. 55, 1933, pp. 172–193.

18 "Diagrammes entropique et Mollier de l'azote," by W. H Keesom and D. J. Houtoff, Communications from the Physica Laboratory of the University of Leiden, Holland, Supplement no. 65 to nos. 181–192, 1927, pp. 15–24.

19 "Gas Thermometer Scale Corrections Based on an Objectiv Correlation of Available Data for Hydrogen, Helium and Nitro gen," by F. G. Keyes, *Temperature*, Reinhold Publishing Corporation New York, N. Y., 1941, pp. 45–59.

20 "The Heat of Vaporization of Hydrogen," by W. H. Keesom

Communications from the Physical Laboratory of the University of Leiden, Holland, no. 137e, 1911, p. 49.

21 "Measurements About the Velocity of Sound in Oxygen Gas," by W. H. Keesom, A. van Itterbeek, and J. A. van Lammeren, Communications from the Physical Laboratory of the University of Leiden, Holland, no. 216d, 1931, pp. 28–38.

22 "Graphical Residual. Its Application to Phase Relations of Oxygen and Nitrogen," by H. A. Koch, Jr., and V. C. Williams, *Chemical Engineering Progress*, vol. 43, 1947, pp. 623–632.

23 "La Chaleur de Vaporisation et la difference des chaleurs specifiques a l'etat de saturation pour le neon," by E. Mathias, C. A. Crommelin, and H. K. Onnes, Comptes Rendus Hebdomadaires Des Seances de L'Academie des Sciences, vol. 176, 1923, pp. 939–940.

24 "The Rectilinear Diameter of Oxygen," by E. Mathias and H. K. Onnes, Communications from the Physical Laboratory of the University of Leiden, Holland, no. 117, 1911.

25 "The Rectilinear Diameter of Nitrogen," by E. Mathias, H. K. Onnes, and C. A. Crommelin, Communications from the Physical Laboratory of the University of Leiden, Holland, no. 145c, 1924.

26 "Thermodynamic Properties of Oxygen and Nitrogen," by R. W. Millar and J. D. Sullivan, U. S. Department of Commerce, Bureau of Mines Technical Paper no. 424, 1928, U. S. Government Printing Office, Washington, D. C.

27 "Isotherms of Oxygen Between —40°C and —152.5°C and Pressures From 3 to 9 Atmospheres," by G. P. Nijhoff and W. H. Keesom, Communications from the Physical Laboratory of the University of Leiden, Holland, no. 179b, 1925, pp. 10–19.

28 "On the Isotherms of Oxygen at Low Temperatures," by H. K. Onnes and H. A. Kuypers, Communications from the Physical Laboratory of the University of Leiden, Holland, no. 169a, 1924, pp. 3–9.

29 "On the Isotherms of Nitrogen at Low Temperatures," by H. K. Onnes and A. Th. van Urk, Communications from the Physical Laboratory of the University of Leiden, Holland, no. 169d, 1924.

30 "The Joule-Thomson Effect in Air," by J. R. Roebuck, Proceedings of the American Academy of Arts and Sciences, vol. 60, 1925, pp. 537–596.

31 Ibid., vol. 64, 1930, pp. 287–334.

32 "The Kelvin Scale From the Gas Scales by Use of Joule-Thomson Data," by J. R. Roebuck and T. A. Murrell, *Temperature*, Reinhold Publishing Corporation, New York, N. Y., 1941, p. 61.

33 "The Joule-Thomson Effect in Nitrogen," by J. R. Roebuck and H. Osterberg, *Physical Review*, vol. 48, 1935, pp. 450–457.

34 "The Low Pressure Liquefaction of Air," by J. H. Rushton, *Refrigerating Engineering*, vol. 53, 1947, p. 28.

35 "On the Behavior of Nitrogen According to the Law of Corresponding States," by A. Th. van Urk, Communications from the Physical Laboratory of the University of Leiden, Holland, no. 169e, 1924, pp. 47–60.

36 "The Thermodynamic Properties of Air at Low Temperatures," by V. C. Williams, Trans. AIChE, vol. 39, 1943, pp. 93111.

Zero-Pressure Thermodynamic Properties of Carbon Dioxide

By SERGE GRATCH,[1] PHILADELPHIA, PA.

In this report are presented tables of the principal thermodynamic properties of carbon dioxide along the zero-pressure isobar in the range 100 to 5000 deg R at the intervals indicated by the numbers in parentheses as follows: 100(5)130(10)240(20)500(50)1000(100)2000(200)5000. The data have been computed by the methods of quantum statistical mechanics from best available information regarding (*a*) the general physical constants, (*b*) the spectroscopic constants for carbon dioxide, (*c*) the isotopic weights of carbon and oxygen, (*d*) the relevant abundance ratios. The computations were carried out in the University of Pennsylvania Thermodynamics Research Laboratory under Project G-12. Computational accuracy well beyond present physical accuracy has been maintained for practical reasons. It is believed that the tables given herein should supersede all previous ones. Although the estimated uncertainties of the values tabulated are still somewhat larger than those for some of the simpler molecules, they are probably small enough for most engineering applications. The calculated values are in fair agreement with those obtained from calorimetric and acoustic-velocity measurements.

Introduction

ONE of the most important accomplishments of the steam research program, conducted by the ASME Special Research Committee on Thermal Properties of Steam during the 1920's and 1930's, was to impress the engineer with the powerfulness of modern theory as an aid in formulating the thermodynamic properties of gases and vapors. In particular, it focused the engineer's attention on the zero-pressure isobar as the line along which he could expect his knowledge of the thermodynamic properties of a given gas or vapor to be most complete and most accurate, thanks to developments in the science of interpreting atomic and molecular spectra. Thus the formulations on which all modern steam tables are based rest firmly on the zero-pressure values of the product pv, of the enthalpy h, and of the reduced entropy $s + R \log_e p$ as calculated from spectroscopic data by the methods of statistical mechanics; direct experimental measurements are used only to extend these values to higher pressures.

The usefulness of spectroscopic data as the source of information regarding the zero-pressure thermodynamic properties of gases was again impressed upon the engineer by Justi (21),[2] who explained the method involved and collected the values published by various authors into a very valuable set of tables. Heck (16) further emphasized the importance of the information obtainable by this method by interpolating the tables previously published to intervals of temperature sufficiently close for convenient practical application. Although Heck's treatment of the data was not at all critical, and, although his method of interpolation was not entirely reliable, nevertheless, his 1940 paper performed a valuable service to the engineer by calling his attention again to the powerfulness of this new theoretical tool.

The general principles of the method of calculating the zero-pressure thermodynamic properties of a gas from its spectroscopic data have been summarized by Herzberg (18, 19), who also has reviewed the present state of our knowledge of such data for various common gases. This knowledge is usually expressed by an equation giving wave number E (cm^{-1}) as a function of certain quantum numbers which independently can take on all nonnegative integral values within prescribed limits; the constants appearing in this equation are called spectroscopic constants. To each wave number E_i there is assigned a definite energy $\epsilon_i = hcE_i$, where h denotes Planck's constant, and c the velocity of light in vacuo. To each set of values of the various quantum numbers there corresponds a distinct quantum state; but there may be more than one, say p_i, distinct quantum states having the same energy ϵ_i in the absence of an external electric or magnetic field.

The first step in the calculations is to form the state sum or partition function Q defined by

$$Q = \Sigma p_i e^{-\epsilon_i/kT} = \Sigma p_i e^{-c_2 \tau E_i} \quad [1]$$

where k is Boltzmann's constant, c_2 is the so-called second radiation constant hc/k, and τ denotes reciprocal absolute temperature T^{-1}. The summation is to be extended over all accessible energy levels ϵ_i. Values of the product pv, of the enthalpy h, and of the reduced entropy $s + R \log_e p$ are readily derivable from a knowledge of Q as a function of pressure p and temperature T. If the energy levels ϵ_i are those characterizing the various modes of molecular and intramolecular motion without correction for the effects of intermolecular forces, the properties, derived in the foregoing, apply strictly to the limiting case of zero pressure only, where the effects of intermolecular forces vanish.

From the previous discussion it is clear that once the energy levels of a given molecule are known it is a straightforward though sometimes long and laborious task to compute the zero-pressure thermodynamic properties of the corresponding gas. At not too-low temperatures the effects of intermolecular forces remain small until fairly high pressures are reached; therefore the zero-pressure properties can be used without correction in ordinary engineering calculations not involving too-high pressures.

The only extensive, original tabulation of the zero-pressure thermodynamic properties of carbon dioxide, besides the one here presented, is that of Kassel (23) for the range 300 to 3500 deg K. Less complete calculations have been carried out by Badger and Woo (3), by Gordon (12), and by Giauque and Egan (11). Wagman, et al (28), have corrected Kassel's tables

---

[1] Assistant Professor of Mechanical Engineering, Towne Scientific School, University of Pennsylvania; Project Leader, University of Pennsylvania Thermodynamics Research Laboratory. Jun. ASME.

[2] Numbers in parentheses refer to the Bibliography at the end of the paper.

Contributed by the Research Committee on Properties of Gases and Gas Mixtures, the Applied Mechanics Division and the Heat Transfer Division, and Section M of the American Association for the Advancement of Science, and presented at the Annual Meeting, New York, N. Y., November 28–December 3, 1948, of The American Society of Mechanical Engineers.

Note: Statements and opinions advanced in papers are to be understood as individual expressions of their authors and not those of the Society. Paper No. 48—A-150.

for recent changes in the accepted values of the general physical constants and atomic weights. Michels and deGroot (25) have calculated the zero-pressure isobaric specific heat of carbon dioxide for the range 25 to 150 C, but by means of oversimplified formulas so that their results can hardly be accepted. All of these previously published tables have been based on the spectroscopic data of Adel and Dennison published in 1933, or on older data; hence they are in need of replacement by new tables based upon more recent and reliable spectroscopic data.

In 1940 Dennison (7) published new spectroscopic data for carbon dioxide. Some additions and corrections thereto have been proposed by Herzberg (17, 20), by A. H. Nielsen and Yao (26), and by others. An excellent summary of the present state of our knowledge of the CO_2 spectrum has been given by Herzberg (18) and on it are mainly based the calculations reported in this paper.

Unfortunately, the values of some of the spectroscopic constants for carbon dioxide are still to be regarded as somewhat uncertain; hence the results presented here cannot be considered definitive. They are, nevertheless, believed to be sufficiently accurate for all ordinary engineering applications. As has been mentioned previously, they are characterized by computational accuracy well beyond present physical accuracy in order to facilitate possible future revision.

Theory

The energy levels ϵ_i for translation are specified by the quantum numbers n_x, n_y, n_z and are not affected by internal motions (rotation, vibration, etc.), to which belongs a completely independent set of energy levels to be specified by additional quantum numbers. For translation

$$\epsilon_i = (h^2/8\pi mV^{2/3})(n_x^2 + n_y^2 + n_z^2)$$

the corresponding contribution to the state sum Q being

$$Q_{\text{trans}} = (2\pi mkT/h^2)^{3/2} \cdot V$$

where m denotes the mass of the molecule in question and V, the volume of the N-molecules composing the gas in question. The two sets of energy levels, one for translation and the other for internal motions, being independent, each makes its own separate contribution to the state sum Q as follows

$$Q = Q_{\text{trans}} \cdot Q_{\text{int}}$$

Now the specific free enthalpy g of the gas in question is given by

$$g = -RT \log_e (Q/n N_0)$$

where n is the number of mols of gas within the volume V and N_0 is Avogadro's number. This is subject to augmentation by an arbitrary constant $\bar{u}$, which can be identified as the null-point ($p = 0$, $T = 0$) energy of the gas in question, since the numerical value to be assigned to the energy ϵ_0 of the lowest level is arbitrary.[3] Replacing the mass m by the ratio M/N_0, where M denotes the molecular weight of the gas in question, it is easy to derive

$$(\log_e p - g/RT)_{p=0} = \frac{5}{2} \log_e T + \log_e [(2\pi Mk/h^2)^{3/2}(R/N_0^{5/2}) + \log_e Q_{\text{int}} \quad \ldots\ldots [2]$$

where the R on the right is to be expressed in cm^3 atm/$g_{p=0}$ mol deg K if pressure is to be expressed in atmospheres. The subscript $p = 0$ is affixed to the quantity on the left to emphasize that Equation [2] is valid only in the absence of intermolecular forces, that is, it is valid only in the limiting case of zero pressure. Since free enthalpy g is a characteristic function of pressure p and temperature T, the enthalpy h and reduced entropy $s + R \log_e p$ can be derived from it in a simple manner by application of well-known identical relations of thermodynamics, namely, $h = \partial(\tau g)/\partial\tau$ and $s = -\partial g/\partial T$. From the first of these relations it is to be noticed that enthalpy h, like free enthalpy g, is subject to augmentation by a constant amount $\bar{u}$ called the null-point energy of the gas in question; the second shows that such augmentation does not affect the entropy s.

Internal State Sum

From Equation [2] it appears that practically all of the experimental, analytical, and computational difficulties to be encountered in the determination of zero-pressure thermodynamic properties from spectroscopic data are associated with the evaluation of the internal state sum Q_{int}. The energy levels ϵ_i entering this sum are those which characterize the rotational, vibrational, electronic, and nuclear motions of the molecule in question. It has been shown that the contribution to Q_{int} from nuclear spin may be disregarded if the resulting properties are to be used only in the analysis of processes which involve no transmutation of atomic species, provided of course that the practice is followed consistently for all molecules.

In the case of carbon dioxide, the energy levels ϵ_i, which characterize the electronic motions of the molecule, as well as the interaction effects between these and the other levels, make altogether negligible contributions to the state sum Q_{int} in the temperature range here considered. In this range, therefore, it is only necessary to take account of the rotational-vibrational energy levels for the ground electronic state.

To a first approximation the rotational-vibrational energy levels for the CO_2 molecule can be expressed by the following equation for the corresponding wave numbers E_i^0 measured from the lowest level

$$E_i^0 = \omega_1^0 v_1 + \omega_2^0 v_2 + \omega_3^0 v_3 + x_{11}v_2^2 + x_{22}v_2^2 + x_{33}v_3^2 + x_{12}v_1v_2 + x_{13}v_1v_3 + x_{23}v_2v_3 + g_{22}l_2^2 + B_{[v]}J(J+1) - D_0J^2(J+1)^2 \quad \ldots\ldots [3]$$

with

$$B_{[v]} = B_0 - \alpha_1 v_1 - \alpha_2 v_2 - \alpha_3 v_3 \quad \ldots\ldots [3a]$$

$$\omega_1^0 = \omega_1 + x_{11} + x_{12} + {}^1/_2 x_{13} \quad \ldots\ldots [3b]$$

$$\omega_2^0 = \omega_2 + 2x_{22} + {}^1/_2 x_{12} + {}^1/_2 x_{23} \quad \ldots\ldots [3c]$$

$$\omega_3^0 = \omega_3 + x_{33} + {}^1/_2 x_{13} + x_{23} \quad \ldots\ldots [3d]$$

$$B_0 = Be - {}^1/_{12}\alpha_1 - \alpha_2 - {}^1/_2\alpha_3 \quad \ldots\ldots [3e]$$

where

$\omega_1, \omega_2, \omega_3$ = zero-order vibrational frequencies
$x_{11}, x_{22}, x_{33}, x_{12}, x_{13}, x_{23}, g_{22}$ = anharmonicity constants
B_0 = rotational constant[4]
D_0 = rotational stretching constant
$\alpha_1, \alpha_2, \alpha_3$ = rotation-vibration coupling constants
v_1, v_2, v_3, l_2, J = quantum numbers

In applying Equation [3] it is to be understood: (*a*) that each vibrational quantum number v_1, v_2, v_3 can independently assume any nonnegative integral value up to its respective dissociation limit; (*b*) that the quantum number l_2 can assume any nonnegative integral value belonging to the set $v_2, v_2 - 2, v_2 - 4,$

[3] Not completely arbitrary, because the null-point energy of a molecular gas is definitely related to the null-point energies of the associated monatomic gases.

[4] B_0 is inversely proportional to the average principal moment of inertia $I_{[0]}$ in the ground state, $J = v_1 = v_2 = v_3 = 0$, that is, $B_0 = h/8\pi^2 c \cdot I_{[0]}$.

etc., independently of the values assumed by the other vibrational quantum numbers v_1, v_3; (*c*) that the rotational quantum number J must be larger or at least equal to l_2 so that it can assume only those values belonging to the set l_2, $l_2 + 1$, $l_2 + 2$, etc.

For any particular set of permitted values of the quantum numbers v_1, v_2, v_3, Equation [3] assigns only one wave number E_i^0 to each permitted pair of values of the quantum numbers l_2 and J. A more precise equation would assign two distinct wave numbers to each such pair for which l_2 is different from zero. This so-called *l*-type doubling has been studied by Herzberg (17); fortunately, it turns out that the two distinct wave numbers referred to differ so slightly in numerical value as to make it unnecessary to take account of the difference in evaluating the state sum Q_{int} over the temperature range here considered.

Quantum mechanics predicts that for each value of the rotational quantum number J there are $2J + 1$ distinct quantum states having the same energy in the absence of an external electric or magnetic field. Accordingly, for the set of energy levels given by Equation [3] we must take $p_i = 2J + 1$ for $l_2 = 0$, but $p_i = 2(2J + 1)$ for $l_2 \neq 0$.

Mathematical Rearrangement

The first step in the evaluation of the internal state sum Q_{int} for the set of energy levels given by Equation [3] is to evaluate it for arbitrarily fixed values of the vibrational quantum numbers v_1, v_2, v_3. This can easily be done by application of the Euler-McLaurin summation formula (sometimes called the Mulholland formula when used in this connection) after expanding the exponential $e^{-c_2\tau g_{22} l_2^2}$ in a Taylor series. The result is

$$2b_1 Q^0_{\text{int}} = \Sigma y_{ijk}(v_2 + 1)v_1^i v_2^j v_3^k e^{-c_2\tau F_i^0} \quad \ldots\ldots [4]$$

where the y_{ijk} are simple functions of $b_1 = c_2\tau B_0$, $b_2 = c_2\tau D_0$, $c_2\tau g_{22}$, α_1/B_0, α_2/B_0, and α_3/B_0 which need not be listed in detail. The F_i^0 are the subset of wave numbers E_i^0 for $l_2 = J = 0$. A detailed explanation of this rearrangement has been published by Kassel (22) and by others also. The summation in Equation [4] is to extend over all values of the vibrational quantum numbers v_1, v_2, v_3 and over all values of their indices i, j, k.

The contribution to the exponential $e^{-c_2\tau F_i^0}$ from the quadratic terms (fourth to ninth, inclusive) in Equation [3] can be reduced, by expansion in a Taylor series, to the sum

$$\Sigma C_{\alpha\beta\gamma} v_1^\alpha v_2^\beta v_3^\gamma$$

where the coefficients $C_{\alpha\beta\gamma}$ are obvious combinations of the $c_2\tau x_{11}$, $c_2\tau x_{12}$, etc. This reduction facilitates evaluation of the quantities Y_{ijk} defined by

$$Y_{ijk} = (1 - x_1)(1 - x_2)^2(1 - x_3)\Sigma(v_2 + 1)v_1^i v_2^j v_3^k e^{-c_2\tau F_i^0}$$

where

$$x_1 = e^{-c_2\tau\omega_1^0}, \quad x_2 = e^{-c_2\tau\omega_2^0}, \text{ and } x_3 = e^{-c_2\tau\omega_3^0}$$

Each Y_{ijk} is a combination of sums of the forms

$$A_n = (1 - x)\sum_{v=0}^{\infty} v^n x^v, \text{ and } B_n = (1 - x)^2 \sum_{v=0}^{\infty}(v + 1)v^n x^v$$

The sums A_n can be expressed as simple functions of $y = x/(1 - x)$; thus

$$A_0 = 1,\ A_1 = y,\ A_2 = y + 2y^2,\ A_3 = y + 6y^2 + 6y^3, \text{ etc.}$$

The sums B_n are also simple functions of y given by $B_n = (A_{n+1} + A_n)/(1 + y)$. Recursion formulas for the A_n's, as well as some approximate formulas useful for large values of n or of y, have been given in a previous report from the University of Pennsylvania Thermodynamics Research Laboratory (13); similar formulas for the B_n's can be obtained easily by the methods outlined in this same report. Strictly speaking, the sums wanted for the evaluation of the Y_{ijk} are not the infinite sums A_n and B_n but analogous finite sums. The substitution produces a negligible error in the final results, however, in the temperature range here considered.

After having evaluated the y_{ijk} and the Y_{ijk}, it is a straightforward matter to calculate Q_{int}^0 from

$$2b_1(1 - x_1)(1 - x_2)^2(1 - x_3)Q_{\text{int}}^0 = \Sigma y_{ijk} Y_{ijk} = \alpha^0 \ldots [5]$$

Fermi Resonance

Equation [3] is a somewhat oversimplified expression for the rotational-vibrational energy levels of the CO_2 molecule because it fails to take account of a phenomenon first recognized by Fermi (9) by which some of the levels are perturbed. The theory of this so-called Fermi resonance phenomenon has been discussed in detail by several authors, a very elegant treatment having been given recently by H. H. Nielsen (27). The discussion cannot be repeated here but it can be briefly stated that some of the levels, which Equation [3] would place very close together, are in fact separated appreciably as a result of Fermi resonance. The actual positions of the perturbed levels can be calculated from the constants in Equation [3] and an additional constant related to the anharmonicity constants which Dennison (7) has designated by the letter *b*. Nielsen's equations have to be modified slightly in the case of CO_2 to take account of anharmonicity. The effect of Fermi resonance on the rotational constants has been treated by Herzberg (17, 18).

The corrections for Fermi resonance can be lumped into an additive correction $\Delta\alpha$ to the sum α^0 in Equation [5]. They are of two kinds, namely, those accounting for the perturbation of the vibrational levels themselves, and those accounting for the alteration of the rotational constants produced thereby. Corrections of the latter kind are almost negligible; those of the former kind can be calculated in a straightforward manner especially if the terms in the corrected sum $\alpha = \alpha^0 + \Delta\alpha$ be first paired with those in the uncorrected sum α^0 in such a way as to make the component corrections for each group of perturbed levels cancel to the first order. Although straightforward, this calculation involves algebraic operations which cannot be given in concise form, hence the details will be omitted here.

Zero-Pressure Properties

Having evaluated the sum α^0 in Equation [5] and then corrected it for the effects of Fermi resonance to obtain α, we are now in a position to write down convenient expressions for the various zero-pressure thermodynamic properties of carbon dioxide of particular interest. In the first place

$$[\log_e p - g/RT]_{p=0} = \frac{7}{2}\log_e T - \log_e [(1 - e^{-\theta_1\tau})(1 - e^{-\theta_2\tau})^2 \cdot (1 - e^{-\theta_3\tau})] + \log_e \alpha + \log_e [(2\pi Mk/h^2)^{3/2}(R/2c_2B_0N_0^{5/2})] \ldots [6]$$

where again it is to be noted (*a*) that the free enthalpy g is subject to augmentation by a constant amount $\bar{u}$ representing the null-point energy, and (*b*) that the R in the last term to the right must be expressed in cm atm/gmol deg K if pressure is to be expressed in atmospheres. The quantities, $\theta_1 = c_2\omega_1^0$, $\theta_2 = c_2\omega_2^0$, and $\theta_3 = c_2\omega_3^0$ are the so-called characteristic temperatures for carbon dioxide.

From Equation [6] it is easy to derive expressions for the zero-pressure values of mean isobaric specific heat $\tau(h - \bar{u})$, reduced entropy $s + R\log_e p$, and isobaric specific heat c_p by application of well-known identical relations of thermodynamics. In the following expressions these quantities have been divided by the universal gas constant R in order to render them dimensionless

$$[(h-\bar{u})/RT]_{p=0} = \frac{7}{2} + \frac{\theta_1\tau}{e^{\theta_1\tau}-1} + \frac{2\theta_2\tau}{e^{\theta_2\tau}-1} + \frac{\theta_3\tau}{e^{\theta_3\tau}-1} + \frac{T\,d\log_e\alpha}{dT} \quad [6a]$$

$$(s/R + \log_e p)_{p=0} = (\log_e p - g/RT)_{p=0} + (h/RT)_{p=0} \quad [6b]$$

$$(c/R)_{p=0} = \frac{7}{2} + \frac{(\theta_1\tau)^2 e^{\theta_1\tau}}{(e^{\theta_1\tau}-1)^2} + \frac{2(\theta_2\tau)^2 e^{\theta_2\tau}}{(e^{\theta_2\tau}-1)^2} + \frac{(\theta_3\tau)e^{\theta_3\tau}}{(e^{\theta_3\tau}-1)^2} + \frac{Td^2(T\log_e\alpha)}{dT^2} \quad [6c]$$

The terms containing $\log_e \alpha$ essentially represent the combined corrections for anharmonicity, rotational stretching, Fermi resonance, etc. They are relatively small so that it is possible to obtain sufficient accuracy in the derivatives of $\log_e \alpha$ by numerical differentiation.

Physical Constants and Conversion Factors

In conformity with the practice of the author's laboratory, the 1941 Birge (6) values of the general physical constants have been used consistently. While the present calculations were in progress, DuMond and Cohen (8) published a revision of some of the Birge values which, however, leaves the quantities hcN_0 and hc/k practically unchanged in value. Therefore adoption of the DuMond and Cohen revisions would involve nothing more than the addition of a very small constant amount to each of the values of reduced entropy tabulated herein. A comparison of the two sets of constants is shown in Table 1.

TABLE 1 GENERAL PHYSICAL CONSTANTS

Constant	Symbol	Units	Value: 1941 Birge (6)	Value: 1948 DuMond and Cohen (8)
Velocity of light	c	cm sec^{-1}	$(2.99776 \pm 0.00004) \times 10^{10}$	$(2.99776 \pm 0.00004) \times 10^{10}$
Standard atmosphere, (0 deg C)	A_0	dyne cm^{-2} atm^{-1}	$(1.013246 \pm 0.000004) \times 10^{6}$	.....
Ice-point	T_0	deg K	273.16 ± 0.01	.....
Avogadro's number (chem. scale)	N_0	g mol^{-1}	$(6.0228_3 \pm 0.0011) \times 10^{23}$	$(6.0235 \pm 0.0004) \times 10^{23}$
Int. joule ($= pq^2$ abs joules)	pq^2	(abs joule)(int. joule)$^{-1}$	$1.00020 \pm 0.0000_{45}$	.....
Planck's constant	h	erg sec	$(6.624_2 \pm 0.002_4) \times 10^{-27}$	$(6.6234 \pm 0.0011) \times 10^{-27}$
Boltzmann's constant	k	erg deg K^{-1}	$(1.38047_4 \pm 0.00026) \times 10^{-16}$	$(1.38032 \pm 0.00011) \times 10^{-16}$
Second radiation constant	c_2	cm deg K	$1.4384_3 \pm 0.0003_4$	1.43847 ± 0.00019
Universal gas constant	R	erg deg K^{-1} g mol^{-1}	$(8.31436 \pm 0.00038) \times 10^{7}$	$(8.31436 \pm 0.00038) \times 10^{7}$
Ratio physical to chemical atomic weights scale	r	.....	1.000272 ± 0.000005	.....

Note: The 1941 Birge values have been used in the present calculations.

Following usual steam-tables practice, the Btu has been used as unit of energy in preparing the tables presented in this report. The particular Btu used is defined by the following conversion factors: 1.8 Btu·g/IT cal·lb and 860/1.00019 IT cal/abs kwhr. Temperature on the Rankine scale (deg R) is used as independent argument, and the pound-mol (mol) is used as unit of weight in order to simplify the analysis of problems involving gas mixtures. In the case of reduced entropy $s + R \log_e p$ it is to be understood that pressure is expressed in international atmospheres (atm).

Molecular and Spectroscopic Constants

The values used in the present calculations for the atomic weights of the carbon and oxygen isotopes are those recommended by Birge (6) in 1941. Almost no new experimental data have been published since that time although the then existing data have been re-examined by a number of physicists, the most recent and probably the most significant review being that of Bainbridge (4). The differences between the recommendations of the various authorities are too slight to affect the thermodynamic properties appreciably, hence the Birge values have been retained for the sake of consistency with other tables (13, 14, 15) previously prepared in the author's laboratory. The adopted values of isotopic weights and of the relevant abundance ratios are listed in Table 2.

TABLE 2 ISOTOPIC WEIGHTS OF CARBON AND OXYGEN (PHYSICAL SCALE)

Isotope	Weight	Abundance
C^{12}	12.00386	92
C^{13}	13.00761	1
O^{16}	16.0000	506
O^{17}	17.0045	0.204
O^{18}	18.0049	1

The molecular weights of the various possible CO_2 molecules can be computed directly from the data in Table 2. The following are of particular interest

$$C^{12}O_2^{16}: M = 43.9919 \text{ (chemical scale)}$$

$$CO_2: M = 44.01139 \text{ (normal isotopic mixture, chemical scale)}$$

The latter value is in excellent agreement with the value 44.010 adopted by the Committee on Atomic Weights of the International Union of Chemistry (5).

The first thorough analysis of the CO_2 spectrum was carried out by Adel and Dennison (1, 2) after some anomalies in it had been explained by Fermi (9), as mentioned previously. A revision of this analysis was published by Dennison (7) and, although some bands have since been measured more accurately, it remains the most recent complete analysis available. The accuracy of Dennison's vibrational constants, especially that of his anharmonicity constants, is not as high as desired, but it will probably not be improved significantly within the near future; therefore his values have been adopted for the present calculations.

The most recent complete set of rotational constants has been obtained by Herzberg (17, 19, 20) whose values have been adopted for the present calculations. Slightly different values for B_0 and α_3 have been obtained by A. H. Nielsen and Yao (26), which, if they had been adopted instead, would have decreased the calculated values of reduced entropy by about 0.003 Btu/mol deg R without producing any other significant changes in the final tables.

The spectroscopic constants adopted for the present calculations are summarized in Table 3. No uncertainties are given since, for most of the constants, no probable errors are listed in the original references. It is believed, however, that the uncertainty of the vibrational constants is of the order of 1 cm^{-1}, that the uncertainty of B_0 is less than 0.0004 cm^{-1}, that the uncertainty of the α's is of the order of 0.0001 to 0.0002 cm^{-1}.

Isotope Effects

The zero-pressure properties presented in this paper apply strictly to the most abundant isotope of carbon dioxide, namely, $C^{12}O_2^{16}$. This molecule is symmetrical with respect to the interchange of its oxygen atoms, and quantum mechanics predicts that only one half of the possible rotational levels represent

TABLE 3 SPECTROSCOPIC CONSTANTS FOR CARBON DIOXIDE, $C^{12}O_2^{16}$

Constant	Value, cm^{-1}	Source, Bibliography	Constant	Value, cm^{-1}	Source, Bibliography
ω_1	1351.2	(7)	x_{13}	—21.9	(7)
ω_2	672.2	(7)	x_{23}	—11.0	(7)
ω_3	2396.4	(7)	b^2	5081	(7)
x_{11}	—0.3	(7)	B_e	0.3904	(20)
x_{22}	—1.3	(7)	D_e	1.8×10^{-7}	(20)
x_{33}	—12.5	(7)	α_1	0.00056	(18)
g_{22}	1.7	(7)	α_2	—0.00062	(18)
x_{12}	5.7	(7)	α_3	0.0029	(18)

distinct quantum states to be included in the state sum Q_{int}. For the ground vibrational state the rotational levels for odd J are missing; the rules for determining what rotational levels are missing for higher vibrational states are discussed in detail in several references, e.g., (18). These remarks apply also to the other symmetrical molecules, $C^{13}O_2^{16}$ and $C^{12}O_2^{18}$. The symmetry is removed in the case of $C^{12}O^{16}O^{18}$, for instance, whose state sum Q_{int} is therefore very nearly double that for the most abundant isotope $C^{12}O_2^{16}$.

To double the state sum Q_{int} is to add the quantity $R \log_e 2$ to the reduced entropy without affecting the enthalpy or isobaric specific heat. It appears that previous authors have neglected to make this necessary addition in calculating the entropies of nonsymmetrical CO_2 molecules. There are of course some additional, temperature-dependent corrections to account for the isotope effects on the rotational and vibrational constants, but the changes in the thermodynamic properties produced thereby appear to be well within the uncertainties of the most accurate values of these properties that can be obtained at present, hence it has not seemed worth while to tabulate them.

Regarding the thermodynamic properties of the normal isotopic mixture of carbon dioxide (CO_2), the following statements may be made: Its enthalpy and isobaric specific heat are almost identical with those of the most abundant isotope $C^{12}O_2^{16}$; its reduced entropy exceeds that of $C^{12}O_2^{16}$ by about 0.00132 Btu/mol deg R because it contains some isotopes of higher molecular weight M than that of $C^{12}O_2^{16}$ (each individual state sum Q is proportional to $M^{3/2}$), by about 0.0066 Btu/mol deg R because the statistical weights p_i for some of these isotopes differ from those for $C^{12}O^{16}$ (the state sum for a nonsymmetrical molecule is very nearly double that for a symmetrical one), and by a mixing entropy of about 0.18 Btu/mol deg R. The mixing entropy has been estimated on the assumption that the mixture contains only the following isotopes: $C^{12}O_2^{16}$, $C^{13}O_2^{16}$, $C^{12}O^{16}O^{17}$, and $C^{12}O^{16}O^{18}$. In order to refine this estimate it would be necessary to assume that $C^{12}O_2^{17}$, $C^{13}O_2^{13}$, etc., are also present in appreciable concentrations. The refinement has not been attempted because of the computational labor involved and because it is not known that all necessary data regarding dissociation energies are available. In addition to the foregoing corrections, there are, strictly speaking, some temperature-dependent corrections to account for the fact that the rotational and vibrational constants differ slightly from isotope to isotope. These, however, reasonably can be expected not to exceed the uncertainties in the calculated properties of $C^{12}O_2^{16}$ and therefore may be ignored.

Comparison With Other Data

The results of the present calculations are compared with those of previous authors in Table 4, the comparison being based on the isobaric specific heat $c_{p=0}$. In the second column are listed the original Kassel (23) values converted to Btu/mol deg R by multiplication by 1.98581/1.9869 = 0.99945. In the third volumn are listed the Wagman, et al (28) revisions of the original Kassel values converted to Btu/mol deg R by multiplication by 1.98581/1.98718 = 0.99931. In the fourth column are listed values interpolated from the final tables presented in this report rounded off to the number of figures used by Kassel.

TABLE 4 ZERO-PRESSURE ISOBARIC SPECIFIC HEAT OF CARBON DIOXIDE (Btu/mol deg R)

T(deg R)	Kassel	Wagman	Gratch
540	8 903	8.888	8.865
720	9.880	9.864	9.845
900	10.670	10.655	10.629
1080	11.318	11.303	11.271
1260	11.855	11.841	11.803
1440	12.305	12.292	12.249
1620	12.682	12.669	12.622
1800	12.998	12.966	12.934
1980	13.26	13.25	13.20
2160	13.49	13.48	13.42
2250	13.59	13.58	13.52
2340	13.68	13.67	13.61
2520	13.85	13.84	13.77
2700	13.99	13.98	13.90
3150	14.3	14.3	14.2
3600	14.5	14.5	14 4
4500	14.8	14.8	14.6

The present calculations give consistently lower values of isobaric specific heat than those of Wagman, et al. At the lower temperatures the differences are mainly due to the use of more accurate data on the vibrational constants; at the higher temperatures they are due in part also to the fact that Kassel obtained his values above 1800 deg R by applying an estimated correction for anharmonicity to the rigid-rotator harmonic-vibrator approximation.

Several comparisons of the thermodynamic properties of carbon dioxide, as calculated from spectroscopic data, with those obtained by other methods have been published. Of particular interest are the comparison with the calorimetric determinations of Henry, as given by Fowler and Guggenheim (10), and that with acoustic-velocity determinations as given by Katz (24). These comparisons are improved somewhat by the results of the present calculations though the discrepancies are still left somewhat larger than those for most other simple molecules. It is believed that the remaining discrepancies in the case of carbon dioxide are mainly due to errors in the calorimetric and acoustic-velocity determinations on the ground that they are larger than the estimated probable errors in the calculated values presented here.

Final Results

The final results of the present calculations are given in Table 5. It might be well to repeat that the data listed in this table are characterized by computational accuracy well beyond present physical accuracy. The unit of energy used is the (International Steam Tables) Btu in terms of which the universal gas constant R has the value 1.98581 Btu/mol deg R. The usual practice of excluding the contribution to the reduced entropy from nuclear spin has been followed.

Acknowledgment

The author is greatly indebted to Dr. John A. Goff, Dean of the Towne Scientific School and Director of the Thermodynamics Research Laboratory of the University of Pennsylvania, for the guidance and encouragement generously given during the course of this work; to Dr. G. Herzberg of the National Research Council of Canada for extremely valuable advice and suggestions; to Miss Eleanor Smith and other members of the computational staff of the Thermodynamics Research Laboratory for their painstaking care in carrying out the very laborious and tedious calculations involved in the preparation of this paper. It is, of course, a pleasure to acknowledge the substantial co-operation of the Navy Department Bureau of Ships, and Office of Naval Research, under contract with whom the Thermodynamics Research Laboratory has been operated.

BIBLIOGRAPHY

1 "The Infrared Spectrum of Carbon Dioxide. Part I," by A. Adel and D. M. Dennison, *Physical Review*, vol. 43, 1933, pp. 716–723.

TABLE 5 ZERO-PRESSURE PROPERTIES OF CARBON DIOXIDE, $C^{12}O_2^{16}$

Temp T, deg R	Reduced entropy $(s + R\log_e p)_{p=0}$, Btu/mol deg R	Average specific heat $[(h - \bar{u})/T]_{p=0}$, Btu/mol deg R	Enthalpy $(h - \bar{u})_{p=0}$, Btu/mol	Specific heat $c_{p=0}$, Btu/mol deg R
100	38.63668	6.94383	694.38	6.95074
105	38.97581	6.94416	729.14	6.95079
110	39.29916	6.94446	763.89	6.95087
115	39.60814	6.94474	798.65	6.95100
120	39.90398	6.94501	833.40	6.95119
125	40.18775	6.94526	868.16	6.95147
130	40.46040	6.94550	902.92	6.95190
140	40.97563	6.94600	972.44	6.95326
150	41.45543	6.94656	1041.98	6.95571
160	41.90446	6.94725	1111.56	6.95968
170	42.32656	6.94815	1181.18	6.96568
180	42.72493	6.94934	1250.88	6.97421
190	43.10230	6.95094	1320.68	6.98573
200	43.46099	6.95304	1390.61	7.00062
210	43.80298	6.95573	1460.70	7.01918
220	44.13002	6.95911	1531.00	7.04163
230	44.44360	6.96326	1601.55	7.06808
240	44.74504	6.96825	1672.38	7.09855
260	45.31600	6.98097	1815.05	7.17124
280	45.85055	6.99759	1959.33	7.25844
300	46.35467	7.01824	2105.47	7.35820
320	46.83302	7.04288	2253.72	7.46826
340	47.28929	7.07134	2404.26	7.58633
360	47.72640	7.10338	2557.22	7.71027
380	48.14669	7.13867	2712.69	7.83820
400	48.55204	7.17690	2870.76	7.96850
420	48.94400	7.21772	3031.44	8.09986
440	49.32384	7.26080	3194.75	8.23120
460	49.69261	7.30584	3360.68	8.36172
480	50.05122	7.35253	3529.21	8.49077
500	50.40041	7.40061	3700.30	8.61791
550	51.23633	7.52537	4138.95	8.92538
600	52.02553	7.65427	4592.56	9.21610
650	52.77413	7.78504	5060.27	9.48954
700	53.48687	7.91605	5541.24	9.74626
750	54.16760	8.04619	6034.64	9.98736
800	54.81949	8.17467	6539.73	10.21410
850	55.44518	8.30098	7055.83	10.42774
900	56.04698	8.42479	7582.31	10.62941
950	56.62684	8.54588	8118.59	10.82013
1000	57.18647	8.66415	8664.15	11.00078
1100	58.25091	8.89202	9781.2	11.3349
1200	59.25032	9.10837	10930.0	11.6365
1300	60.19269	9.31351	12107.6	11.9093
1400	61.08446	9.50790	13311.1	12.1564
1500	61.93093	9.69205	14538.1	12.3803
1600	62.73652	9.86651	15786.4	12.5833
1700	63.50500	10.03183	17054.1	12.7674
1800	64.23956	10.18851	18339.3	12.9344
1900	64.94302	10.33709	19640.5	13.0861
2000	65.6178	10.4780	20956.1	13.2240
2200	66.8898	10.7389	23625.6	13.4640
2400	68.0701	10.9746	26339.0	13.6639
2600	69.1706	11.1881	29089.0	13.8314
2800	70.2010	11.3821	31869.8	13.9725
3000	71.1692	11.5589	34676.6	14.0920
3200	72.0820	11.7204	37505.4	14.1934
3400	72.9451	11.8685	40352.9	14.2797
3600	73.7634	12.0046	43216.4	14.3530
3800	74.5412	12.1298	46093.4	14.4148
4000	75.2819	12.2454	48981.6	14.4665
4200	75.9888	12.3522	51879.3	14.509
4400	76.6646	12.4511	54784.6	14.543
4600	77.3116	12.5426	57695.7	14.568
4800	77.9319	12.6273	60610.9	14.584
5000	78.5274	12.7057	63528.4	14.590

2 "The Infrared Spectrum of Carbon Dioxide. Part II," by A. Adel and D. M. Dennison, *Physical Review*, vol. 44, 1933, pp. 99–104.

3 "The Entropies of Some Simple Polyatomic Gases Calculated From Spectral Data," by R. M. Badger and S. C. Woo, *Journal of the American Chemical Society*, vol. 54, 1932, pp. 3523–3529.

4 "Isotopic Weights of the Fundamental Isotopes," by K. T. Bainbridge, Preliminary Report no. 1, Nuclear Science Series, National Research Council, Washington, D. C., 1948.

5 "Thirteenth Report of the Committee on Atomic Weights of the International Union of Chemistry," by G. P. Baxter, M. Guichard, and R. Whytlaw-Gray, *Journal of the American Chemical Society*, vol. 69, 1947, pp. 731–736.

6 "A New Table of Values of the General Physical Constants," by R. T. Birge, *Reviews of Modern Physics*, vol. 13, 1941, pp. 233–239.

7 "The Infra-Red Spectra of Polyatomic Molecules. Part II," by D. M. Dennison, *Reviews of Modern Physics*, vol. 12, 1940, pp. 175–214.

8 "Our Knowledge of the Atomic Constants F, N, m, and h in 1947, and of Other Constants Derivable Therefrom," by J. W. M. DuMond and E. R. Cohen, *Reviews of Modern Physics*, vol. 20, 1948, pp. 82–108.

9 "Über den Ramaneffekt des Kohlendioxyds," by E. Fermi, *Zeitschrift für Physik*, vol. 71, 1931, pp. 250–259.

10 "Statistical Thermodynamics," by R. H. Fowler and E. A. Guggenheim, Cambridge University Press, London, Eng., 1939, p. 115.

11 "Carbon Dioxide. The Heat Capacity and Vapor Pressure of the Solid. The Heat of Sublimation. Thermodynamic and Spectroscopic Values of the Entropy," by W. F. Giauque and C. J. Egan, *Journal of Chemical Physics*, vol. 5, 1937, pp. 45–54.

12 "The Free Energy of Steam and Carbon Dioxide," by A. R. Gordon, *Journal of Chemical Physics*, vol. 1, 1933, pp. 308–312.

13 "Zero-Pressure Properties of Diatomic Gases. I. Nitrogen," by S. Gratch, Annual Report from the Thermodynamics Research Laboratory, University of Pennsylvania, July, 1946, Project G-3.

14 "Zero-Pressure Properties of Diatomic Gases. II. Carbon Monoxide," by S. Gratch, Annual Report from the Thermodynamics Research Laboratory, University of Pennsylvania, July, 1947, Project G-3.

15 "Zero-Pressure Properties of Monatomic Gases. I. Hydrogen, Helium, Carbon, Nitrogen, Oxygen, Fluorine, Sulfur, Chlorine, Argon, Bromine, Iodine, Mercury," by S. Gratch and S. W. Van Voorhis, Annual Report from the Thermodynamics Research Laboratory, University of Pennsylvania, July, 1947, Project G-1.

16 "The New Specific Heats," by R. C. H. Heck, *Mechanical Engineering*, vol. 62, 1940, pp. 9–12.

17 "1-Type Doubling in Linear Polyatomic Molecules," by G. Herzberg, *Reviews of Modern Physics*, vol. 14, 1942, pp. 219–223.

18 "Infrared and Raman Spectra of Polyatomic Molecules," by G. Herzberg, D. Van Nostrand Company, Inc., New York, N. Y., 1945.

19 "Molecular Constants From Spectroscopic Data," by G. Herzberg, Trans. ASME, vol. 70, 1948, pp. 623–624.

20 Private Communication from G. Herzberg, unpublished.

21 "Spezifische Wärme, Enthalpie, Entropie und Dissoziation technischer Gase," by E. Justi, Julius Springer, Berlin, Germany, 1938.

22 "Mathematical Methods for Computing Thermodynamic Functions From Spectroscopic Data," by L. S. Kassel, *Journal of Chemical Physics*, vol. 1, 1933, pp. 576–585.

23 "Thermodynamic Functions of Nitrous Oxide and Carbon Dioxide," by L. S. Kassel, *Journal of the American Chemical Society*, vol. 56, 1934, pp. 1838–1842.

24 "Specific Heat Ratios in CO_2," by L. Katz, *Journal of Chemical Physics*, vol. 11, 1943, pp. 496–497.

25 "Thermodynamical Properties of Carbon Dioxide as Function of Density and Temperature," by A. Michels and S. R. deGroot, *Applied Scientific Research*, vol. A 1, 1948, pp. 94–102.

26 "The Analysis of the Vibration-Rotation Band ω_3 for $C^{12}O_2^{16}$ and for $C^{13}O_2^{16}$," by A. H. Nielsen and Y. T. Yao, *Physical Review*, vol. 68, 1945, pp. 173–180; ibid, vol. 71, 1947, p. 825.

27 "The Vibration-Rotation Energies of Polyatomic Molecules. Part II. Accidental Degeneracies," by H. H. Nielsen, *Physical Review*, vol. 68, 1945, pp. 181–191.

28 "Heats, Free Energies, and Equilibrium Constants of Some Reactions Involving O_2, H_2, H_2O, C, CO, CO_2, and CH_4," by D. D. Wagman, J. E. Kilpatrick, W. J. Taylor, K. S. Pitzer, and F. D. Rossini, *Journal of Research*, National Bureau of Standards, vol. 34, 1945, pp. 143–161, Research Paper RP 1634.

Final Report of the Working Subcommittee of the International Joint Committee on Psychrometric Data

By JOHN A. GOFF,[1] PHILADELPHIA, PA.

Introduction

THE inaugural meeting of the International Joint Committee on Psychrometric Data (IJCPD) was held in Boston, Mass., on January 23, 1945, in connection with the 51st annual meeting of the American Society of Heating and Ventilating Engineers. In November, 1945, the late J. H. Walker, temporary chairman, appointed a Working Subcommittee, of which the author was privileged to be chairman, to assist in the drafting of an agenda for the next meeting of his committee.

The Working Subcommittee met first in Philadelphia on February 16, 1946. The minutes of this first meeting were used as an agenda for the second meeting held in Washington, D. C., on November 26, 1946, and attended by a number of interested nonmembers, including representatives of the British Meteorological Office, the British Commonwealth Scientific Office, and the National Bureau of Standards. The minutes of this second meeting contain an item instructing the chairman to prepare a report of the Working Subcommittee's deliberations.

A preliminary draft of the report mentioned was submitted, under date of April 14, 1947, to Mr. Walker who offered several valuable criticisms and suggestions for incorporation in the final draft. Not until now, however, has the author found it possible to prepare this final draft. Meantime the preliminary draft has served a very useful purpose as will be noted later.

At the first full session of the Aerological Commission of the International Meteorological Organization (IMO) which met in Toronto, Canada, during August, 1947, there was appointed a Subcommission I on Functions and Tables under the chairmanship of Prof. P. A. Sheppard, Department of Meteorology, Imperial College of Science and Technology, University of London. By its terms of reference this subcommission was charged with the task of recommending a set of self-consistent internationally acceptable values of physical functions and constants of common use in meteorological practice. It is exceedingly gratifying to note the extent to which those recommendations of the Subcommission having to do with the thermodynamic properties of moist air agree with the recommendations of the Working Subcommittee as set forth in the preliminary draft referred to in the preceding paragraph. The former were adopted officially by the Twelfth Conference of Directors of the International Meteorological Organization sitting in Washington, D. C., September, 1947.

The report of Professor Sheppard's subcommission is soon to be printed and widely distributed by the International Meteorological Organization as Document No. 71 of its Aerological Commission. It seems especially appropriate, therefore, to publish the final report of the Working Subcommittee of the International Joint Committee on Psychrometric Data more or less simultaneously. There is ample justification for the ASME Special Research Committee on Properties of Gases and Gas Mixtures to sponsor the presentation and publication of this final report in the fact that it deals with the thermodynamic properties of one of the most common and technically important gas mixtures, namely, moist air.

It is deeply to be regretted that this report must record the death late in 1947, of J. H. Walker, temporary chairman, International Joint Committee on Psychrometric Data. It was upon his recommendation that Council of the American Society of Heating and Ventilating Engineers invited "all organizations likely to be interested in the problem of the properties of mixtures of air and water vapor to appoint a representative on a joint Inter-Society Committee to consider the adoption, when available, of basic equations and tables of such properties" (1).[2] Mr. Walker's untimely death leaves the status of his Committee somewhat indefinite. It is hoped that the publication of this report will serve to reactivate the committee, especially since by disposing of one part of the committee's over-all problem, it prepares the way for consideration of other important parts.

Problem

The problem before the International Joint Committee on Psychrometric Data may be regarded as consisting of three parts: (*a*) To obtain information regarding the thermodynamic properties of moist air which can claim general acceptance as standard on the ground that it is thermodynamically consistent within the accuracy of existing knowledge; (*b*) to develop specifications of standard instruments for the practical realization of these properties in the field; (*c*) to recommend standard symbols, terminology, and charts calculated to promote a better understanding of underlying theory in its application to practical problems involving moist air. This report sets forth the recommendations of the Working Subcommittee on part (*a*) of the over-all problem and explains the reasoning on which these recommendations are based.

Criterion

The Working Subcommittee agreed from the start to try to recommend a formulation, rather than discrete tables, of the thermodynamic properties of moist air, valid over the widest practicable ranges of pressure and temperature. While for the majority of present-day applications in the field of air conditioning it might suffice to recommend a table of properties at stand-

---

[1] Dean, Towne Scientific School, University of Pennsylvania, Mem. ASME; Chairman of the Working Subcommittee, composed of C. S. Cragoe, National Bureau of Standards; L. P. Harrison, U. S. Weather Bureau; F. G. Keyes, Massachusetts Institute of Technology. S. Gratch, Towne Scientific School, University of Pennsylvania, rendered invaluable aid to the Working Subcommittee as technical adviser.

Contributed by the Research Committee on Properties of Gases and Gas Mixtures, the Applied Mechanics Division and the Heat Transfer Division, and Section M of the American Association for the Advancement of Science, and presented at the Annual Meeting, New York, N. Y., November 28—December 3, 1948, of The American Society of Mechanical Engineers

Note: Statements and opinions advanced in papers are to be understood as individual expressions of their authors and not those of the Society. Paper No. 48—A-151.

[2] Numbers in parentheses refer to the Bibliography at the end of the paper.

ard atmospheric pressure, such a table would by no means satisfy the needs of the meteorologist or the aerodynamic engineer; moreover, it would be shortsighted to assume that, even in the field of air-conditioning engineering, the number of applications in which accurate properties at other pressures are needed will not increase substantially as time goes on. Fortunately, the pressure range of principal interest now and probably for some time in the future is the low-pressure range where well-tested theory is able to make reliable predictions regarding the effect of pressure on the various thermodynamic properties of moist air.

The Working Subcommittee found no difficulty in adopting "thermodynamic consistency within the accuracy of existing knowledge" as the principal criterion by which to judge the validity of its recommendations. The adoption of this criterion at once implies the abrogation of Dalton's law on which most predictions of the thermodynamic properties of moist air heretofore have been based. By present-day standards Dalton's law must be regarded as an inaccurate conjecture based upon an unwarranted faith in the "ultimate simplicity of Nature." Granted that the law and the consequences inferred more or less intuitively from it are extremely useful as rough and sometimes even close approximations to the truth, their use as a basis for standardization is now completely out of the question.

Dalton's Law

Dalton's law is a difficult matter to discuss in any clear and unequivocal manner because such a variety of interpretations have come to be placed upon it. If the statement of it given by Preston (2) be accepted, it would appear that the pressure is the only property of a gas mixture which the law attempts to predict; and this, it says, is the sum of the pressures which the constituents would individually exert if each occupied separately the volume of the mixture at the temperature of the mixture. Now statistical mechanics predicts that the law would hold identically if each constituent were a hypothetically perfect gas showing no effects of intermolecular forces, whereupon (*a*) the individual pressures would be the individual mol-fractions times the pressure of the mixture, (*b*) the sum of the individual enthalpies would equal the enthalpy of the mixture, and (*c*) the sum of the individual entropies would equal the entropy of the mixture.

Unfortunately, predictions (*a*), (*b*), and (*c*), which are strictly valid only in the case of a hypothetical mixture of perfect gases, have been used as vehicles for the introduction of various concepts which cannot be applied without ambiguity or thermodynamic inconsistency to mixtures of actual imperfect gases. It may be stated that Dalton's law, regarding the additivity of individual pressures and its alleged consequences regarding the additivity of individual enthalpies and entropies, fails mainly, if not entirely, because of the effects of intermolecular forces between "unlike" molecules, while the alleged consequence that the individual pressures are the individual mol-fractions times the pressure of the mixture fails because of the effects of forces between "like" molecules also.

Various modifications of Dalton's law have been proposed from time to time, including the so-called Gibbs-Dalton, Amagat, and Lewis-Randall rules. None of these, however, offers any substantial improvement over Dalton's law itself; all of them must now be regarded as conjectures based pretty much on wishful thinking.

Statistical Mechanics

Developments in statistical mechanics have given us a well-tested theory of the thermodynamic properties of gas mixtures which is entirely workable in the range of sufficiently low pressures. This theory can be expressed succinctly in the following form

$$\mu_i = g_i^0(T) + R\,T\log_e(x_i p) + p\left[\sum_{ik} x_i x_k A_{ik}(T) - 2\sum_k x_k A_{ik}(T)\right] + \ldots\ldots\ldots\ldots \quad [1]$$

where $g_i^0(T)$ are pure temperature functions called "zero-pressure reduced free enthalpies" which are directly calculable from a knowledge of the spectroscopic constants of the atomic or molecular species in question; the x_i and x_k are mol-fractions; $A_{ik}(T) = A_{ki}(T)$ are pure temperature functions called "second virial coefficients" ($i = k$), or "interaction coefficients" ($i \neq k$) in terms of which the effects of intermolecular forces are expressed. The "chemical potentials" μ_i, when expressed as functions of temperature, pressure, and the various mol-fractions, are characteristic functions in the sense that from a knowledge of them can be derived all thermodynamic properties of the homogeneous phase to which they belong by application of such identical relations as the following

$$g = \Sigma x_i \mu_i;\quad v = \partial g/\partial p;\quad s = -\partial g/\partial T;\quad h = \partial(\tau g)/\partial\tau \ldots [2]$$

where g, v, s, h denote specific free enthalpy, specific volume, specific entropy, specific enthalpy, respectively; and where τ denotes reciprocal absolute temperature.

Dry Air

Atmospheric air is a mixture of at least a dozen different gases including: oxygen (O_2), nitrogen (N_2), argon (A), carbon dioxide (CO_2)—neon (Ne), helium (He), krypton (Kr), hydrogen (H_2), xenon (Xe), ozone (O_3), radon (Rn)—water vapor (H_2O). Those in the middle group comprise what is commonly referred to as the residual part of atmospheric air. Paneth (3) finds their individual concentrations to be about as follows:

	Per cent
Neon	0.0018
Helium	0.00053
Krypton	0.00010
Hydrogen	0.00005
Xenon	0.000008
Ozone	0.000001 (increasing with altitude)
Radon	0.6×10^{-18} (decreasing with altitude)

Accordingly, the total concentration of the residual part of atmospheric air should be expected not to exceed 0.0025 per cent.

The gases in the first group compose what is commonly called "dry air." It is true that the relative composition of this group is subject to secular variations and variations with location, meteorological conditions, and season, but these variations are produced mainly, if not entirely, by variations in the concentration of carbon dioxide. All evidence indicates that the average concentration of carbon dioxide in dry air in the troposphere is very close to 0.03 per cent. Carpenter (4) recommends the value 0.031 per cent.

For the purpose of standardization the composition of dry air can be defined more or less arbitrarily. It would seem desirable, however, to base the definition on available information regarding the average composition of atmospheric air in the troposphere. Carpenter (4) finds that dry air contains 20.939 per cent oxygen and 0.031 per cent carbon dioxide. Paneth (3) accepts the value 20.95 per cent oxygen in dry air containing carbon dioxide, recommended by Benedict (5). The National Bureau of Standards has come to prefer the values, 20.94 per cent oxygen and 0.03 per cent carbon dioxide, which are the values originally agreed upon by the Working Subcommittee. It later developed, however, that the International Meteorological Organization holds a strong preference for the Paneth (3) values just quoted. Hence, and particularly in view of the fact that the definition of what is to be referred to as dry air must be decided upon more or less arbitrarily, the author agreed on behalf of his Working Subcom-

mittee to accept the values, 20.95 per cent oxygen and 0.03 per cent carbon dioxide.

Cady and Cady (6) find that dry, CO_2—free air contains 0.93 per cent argon by volume. This figure would not have to be modified appreciably to apply to dry air containing 0.03 per cent carbon dioxide; hence it was accepted by the Working Subcommittee.

The (revised) recommendation of the Working Subcommittee regarding the composition of dry air is as follows:

Oxygen (O_2)	0.2095
Nitrogen (N_2)	0.7809
Argon (A)	0.0093
Carbon dioxide (CO_2)	0.0003
	1.0000

This is a "fixed", "mol-fraction" composition which the Subcommittee intends should be regarded as exact by definition. The fact that these figures were derived from experimental determinations made with an Orsat-like apparatus which does not yield information regarding the mol-fractions directly was disregarded, because it is almost certain that the experimental data themselves are not sufficiently precise to justify any attempt at refinement; moreover, as has been stated previously, any definition of what is to be called dry air necessarily involves some exercise of arbitrariness.

The definition of dry air adopted by the International Meteorological Organization differs slightly from that just recommended, by including the Paneth (3) values of the concentrations (converted to mol-fractions) of the residual gases. This slight difference will not affect the calculated values of the various thermodynamic properties of dry air, at any rate not within the accuracy of existing knowledge.

The Working Subcommittee recommends adoption of the International Committee on Atomic Weights (1947), values of the relevant molecular weights (7), namely

Oxygen (O_2)	32.0000
Nitrogen (N_2)	28.016
Argon (A)	39.944
Carbon dioxide (CO_2)	44.01
Water (H_2O)	18.016

These yield the value, 28.966, for the apparent molecular weight of dry air.

Physical Constants and Conversion Factors

The Working Subcommittee recommends that each individual zero-pressure reduced free enthalpy $g_i^0(T)$, appearing in Equation [1], be computed from best available spectroscopic data on the energy levels of the molecule in question, by the methods of statistical mechanics. Certain fundamental physical constants which have to be determined experimentally and which therefore are subject to experimental error enter these computations. These include: Planck's constant h, Boltzmann's constant k, speed of light c, Avogadro's number N_0, and the relevant molecular weights M_i. For the first four of these the Subcommittee recommends adoption of the Birge (1941), values as follows (8):

$h = (6.6242 \pm 0.0024).10^{-27}$	erg-sec
$k = (1.380474 \pm 0.00026).10^{-16}$	erg/deg K
$c = (2.99776 \pm 0.00004).10^{10}$	cm/sec
$N_0 = (6.02283 \pm 0.0011).10^{23}$	g mol^{-1}

DuMond and Cohen (9) have treated the various input data from which the values of the foregoing constants have to be computed, in a more impartial manner than Birge was able to employ in 1941. Theirs may shortly come to supersede the Birge (1941) values. Fortunately, they leave the combinations kN_0, hcN_0, and hc/k unchanged in value. This means that the only effects of using the DuMond-Cohen (1948) instead of the Birge (1941) values in calculating the thermodynamic properties of moist air would be (*a*) to reduce the estimated uncertainties of the results, and (*b*) to shift by a constant amount the so-called "absolute" entropy of each constituent. At present, however, the air-conditioning engineer, the meteorologist, and the aerodynamicist are interested in "relative" values only of enthalpy and entropy; hence effect (*b*) is of no practical consequence at present.

The Working Subcommittee also recommends adoption of the following conversion factors:

1.8	deg R/deg K
30.48	cm/ft
453.5924	g/lb
1	Btu kg deg K/kcal lb deg R
860/1.00019	kcal/abs kwhr
1,013,250	dyne/cm^2 atm

The last two of these will bear some explanation. The symbol kcal is intended to designate the so-called "steam tables kilocalorie" defined in the report of the First International Steam Tables Conference (10) as 1/860 (mean) international kwhr. Birge (1941) recommends the conversion factor 1.00020 ± 0.000045 (mean) international kwhr per abs kwhr. The International Committee of Weights and Measures, at its meetings in October, 1946, revised the value of this factor downward to 1.00019. This revision should of course be accepted, especially since none of the other fundamental constants or conversion factors listed is affected thereby.

According to Birge (1941), the mean density of the mercury in a column 76 cm high at 0 deg C and 980.665 cm/sec^2 is 13.59504 ± 0.000057 g/cm^3. If the standard atmosphere be defined as the pressure exerted by such a column it would be equal to 1,013,246 ± 4 dyne/cm^2. This is the definition adopted by the International Meteorological Organization. Alternatively, the standard atmosphere is defined in some quarters as equal to 1,013,250 dyne/cm^2, exactly. This is the definition recommended by the Working Subcommittee. The difference between the two atmospheres is exceedingly small but is mentioned here for the sake of definiteness.

Zero-Pressure Reduced Free Enthalpies

By way of introduction it may be well to mention that, in accordance with relations, Equations [2], zero-pressure enthalpy h^0 and zero-pressure reduced entropy s^0 (by reduced entropy is meant the sum, $s + R \ln p$) are derivable from zero-pressure reduced free enthalpy g^0 (by reduced free enthalpy is meant the difference, $g - R\,T \ln p$) as follows

$$h^0 = d(\tau g^0)/d\tau; \quad s^0 = -dg^0/dT$$

Oxygen. Gratch has reduced the recently computed data of Woolley (11) to the following semirational equation

$$g^0/RT = (7/2)\ln\tau + \ln(1 - e^{-\theta\tau}) - A\tau - B\tau^2 - D/\tau - F/(e^{\theta\tau} - 1) - 1.2164$$

with

$$\theta = 2235.4 \text{ deg K}$$
$$A = 1.073 \text{ deg K}$$
$$B = 0$$
$$D = 3.30 \times 10^{-6} \text{ deg K}^{-1}$$
$$F = 0.0111$$

Values of zero-pressure enthalpy h^0, derived from this equation, agree with the Woolley data to within a maximum deviation of 0.010 per cent and a root-mean-square deviation of 0.005 per cent in the range 100 to 600 deg K. Values of zero-pressure reduced free enthalpy g^0 and zero-pressure reduced entropy s^0 show maximum deviations of 0.002 per cent and root-mean-square

deviations of 0.001 per cent from the Woolley data in this range. These data themselves are probably accurate to within 0.015 per cent in the range 100 to 600 deg K so that a conservative estimate of the probable error of the foregoing equation in this range is 0.02 per cent in h^0, g^0, and s^0.

Nitrogen. Gratch (12) has reduced his own calculations of the zero-pressure properties of nitrogen to the following semirational equation

$$g^0/RT = (7/2)\ln\tau + \ln(1 - e^{-\theta\tau}) - A\tau - B\tau^2 - D/\tau - F/(e^{\theta\tau} - 1) + 0.414686$$

with

$$\theta = 3352.69 \text{ deg K}$$
$$A = 0.9580 \text{ deg K}$$
$$B = 0.09 \text{ deg K}^2$$
$$D = 2.023 \times 10^{-6} \text{ deg K}^{-1}$$
$$F = 0.009009$$

The estimated uncertainty in values of g^0 calculated from this equation is 0.011 per cent in the range 50 to 800 deg K.

Argon. Gratch and Van Voorhis (13) give the following equation valid in the range 50 to 2000 deg K with a probable error in g^0 itself of about 0.02 per cent

$$g^0/RT = (5/2)\ln\tau - 1.867$$

Carbon Dioxide. Gratch has reduced the tabulated data of Wagman, et al, (14) to the following semirational equation

$$g^0/RT = (7/2)\ln\tau + 2\ln(1 - e^{-\theta_1\tau}) + \ln(1 - e^{-\theta_2\tau}) + \ln(1 - e^{-\theta_3\tau}) - 1.8945$$

with

$$\theta_1 = 960 \text{ deg K}$$
$$\theta_2 = 1944 \text{ deg K}$$
$$\theta_3 = 3379 \text{ deg K}$$

In the range 300 to 600 deg K, values of h^0 and s^0 derived from this equation agree with the Wagman data within 0.05 per cent and 0.005 per cent, respectively. The probable error of the equation itself is thought to be less than 0.1 per cent in this range.

Water Vapor. Goff and Gratch (15) give what amounts to the following semirational equation

$$g^0/RT = 4\ln\tau + \ln(1 - e^{-\theta_1\tau}) + \ln(1 - e^{-\theta_2\tau}) + \ln(1 - e^{-\theta_3\tau}) - a_1e^{-\theta_1\tau} - a_2e^{-\theta_2\tau} - a_3e^{-\theta_3\tau} - A\tau - D/\tau + \text{const}$$

with

$$\theta_1 = 2291.16 \text{ deg K}$$
$$\theta_2 = 5176.37 \text{ deg K}$$
$$\theta_3 = 5445.59 \text{ deg K}$$
$$a_1 = -0.03958$$
$$a_2 = +0.05353$$
$$a_3 = +0.04000$$
$$A = 5.011 \text{ deg K}$$
$$D = 2.32 \times 10^{-5} \text{ deg K}^{-1}$$

Gratch has subsequently adjusted the constant by comparison with the Wagman (14) data as follows

$$\text{const} = 4.1083$$

The probable error of values of g^0 calculated from the foregoing equation is 0.015 per cent in the range —90 to +90 deg C.

Zero-Pressure Properties of Dry Air

All necessary data are now at hand to compute values of the zero-pressure enthalpy h_a^0 and zero-pressure reduced entropy s_a^0 for dry air in accordance with the relations

$$h_a^0 = \Sigma x_i h_i^0, \quad \text{and} \quad s_a^0 = \Sigma x_i s_i^0 \ldots\ldots [3]$$

The numerical value of the gas constant R is obtained by multiplying Boltzmann's constant k into Avogadro's number N_0 and applying appropriate conversion factors from the approved list given earlier in this report; the result is

$$R = 1.98581 \pm 0.00022 \text{ kcal/kmol deg K}$$

The apparent molecular weight of dry air is

$$M_a = 28.966 \pm 0.0016 \text{ kg/kmol}$$

the indicated uncertainty arising solely from uncertainties in the molecular weights of its several constituents.

In Table 1 are listed the values so computed, at 10-deg intervals of centigrade temperature t(deg C) defined in terms of absolute temperature T(deg K) by the relation

$$T(\text{deg K}) = t(\text{deg C}) + 273.16 \ldots\ldots [4]$$

Recommended tolerances set at 0.04 per cent of the values to which they apply are also listed in this table.

Zero-Pressure Properties of Water Vapor

The necessary data are also at hand to compute the zero-pressure enthalpy h_w^0 and zero-pressure reduced entropy s_w^0 of water vapor. The present best value of the molecular weight of water is

$$M_w = 18.016 \pm 0.0002 \text{ kg/kmol}$$

Values of these two properties are listed in Table 2, together with recommended tolerances set at 0.03 per cent.

TABLE 1 ZERO-PRESSURE PROPERTIES OF DRY AIR

t °C	h_a^0 (kcal/kg)	Tol. ±	s_a^0 (kcal/kg°K)	Tol. ±
-90	43.771	18	1.52160	61
-80	46.165	18	1.53431	61
-70	48.560	19	1.54640	62
-60	50.953	20	1.55791	62
-50	53.348	21	1.56889	63
-40	55.743	22	1.57938	63
-30	58.138	23	1.58944	64
-20	60.533	24	1.59910	64
-10	62.929	25	1.60838	64
0	65.326	26	1.61732	65
10	67.724	27	1.62594	65
20	70.122	28	1.63427	65
30	72.523	29	1.64231	66
40	74.924	30	1.65010	66
50	77.326	31	1.65765	66
60	79.730	32	1.66498	67
70	82.135	33	1.67210	67
80	84.542	34	1.67901	67
90	86.952	35	1.68574	67

TABLE 2 ZERO-PRESSURE PROPERTIES OF WATER VAPOR

t °C	h_w^0 (kcal/kg)	Tol. ±	s_w^0 (kcal/kg°K)	Tol. ±
-90	80.290	24	2.28627	69
-80	84.709	25	2.30975	69
-70	89.130	27	2.33207	70
-60	93.552	28	2.35331	71
-50	97.975	29	2.37359	71
-40	102.400	31	2.39299	72
-30	106.828	32	2.41158	72
-20	111.259	33	2.42945	73
-10	115.693	35	2.44661	73
0	120.130	36	2.46317	74
10	124.573	37	2.47914	74
20	129.020	39	2.49457	75
30	133.473	40	2.50951	75
40	137.932	41	2.52399	76
50	142.399	43	2.53803	76
60	146.873	44	2.55166	77
70	151.355	45	2.56492	77
80	155.845	47	2.57780	77
90	160.345	48	2.59037	78

Virial Coefficients of Dry Air

The temperature function $A_{aa}(T)$ is called the "second virial coefficient" of dry air. From Bridgeman's (16) adjustment of constants in the well-known Beattie-Bridgeman equation of state, its dependence upon absolute temperature T(deg K) is given by

$$A_{aa} = -40.70 + 13116\tau + 12 \times 10^{7}\tau^{3}\text{cm}^3/\text{gmol}$$

Table 3 lists values of A_{aa} and of the derived coefficients

$$B_{aa} = d(\tau A_{aa})/d\tau \quad \text{and} \quad C_{aa} = dA_{aa}/dT$$

together with recommended tolerances obtained by comparison with other formulations.

Strictly speaking, the values listed in Table 3 apply to dry, CO_2-free air. The Subcommittee, however, recommends them

TABLE 3 SECOND VIRIAL COEFFICIENTS OF DRY AIR

t °C	A_{aa} (cm³/gmol)	Tol. ±	B_{aa} (cm³/gmol)	Tol. ±	C_{aa} (cm³/gmol °K)	Tol. ±
-90	50.4	39	180.6	195	-0.711	107
-80	43.9	33	161.7	167	-0.610	86
-70	38.2	29	145.7	143	-0.529	71
-60	33.2	25	131.9	124	-0.463	58
-50	28.9	22	120.0	108	-0.409	48
-40	25.0	19	109.7	95	-0.363	41
-30	21.6	17	100.6	83	-0.325	34
-20	18.5	15	92.5	74	-0.292	29
-10	15.7	13	85.3	66	-0.265	25
0	13.2	12	78.9	59	-0.240	22
10	10.9	11	73.1	53	-0.220	19
20	8.81	95	67.8	48	-0.201	16
30	6.87	86	63.1	43	-0.1853	142
40	5.09	78	58.7	39	-0.1712	125
50	3.44	71	54.7	36	-0.1586	110
60	1.91	65	51.0	32	-0.1474	98
70	0.49	59	47.6	30	-0.1373	87
80	-0.84	54	44.5	27	-0.1283	77
90	-2.07	54	41.6	25	-0.1201	69

as applying to dry air, as defined in this report, because it estimates that the corrections necessary to achieve complete consistency would be well within the probable error of the values themselves.

Following the rightmost term in Equation [1] comes a term proportional to the square of the pressure (p^2), in which the so-called "third virial coefficients" $A_{ijk}(T)$ appear. By analogy, this term is

$$+ \tfrac{1}{2}p^2[2\Sigma x_i x_j x_k A_{ijk} - 3\Sigma x_j x_k A_{ijk}]$$

the value of A_{ijk} being unchanged by permutation of the indexes i, j, k. The third virial coefficient of dry air $A_{aaa}(T)$ is entirely negligible in the range 150 to 400 deg K, 0 to 10 atm.

Virial Coefficients of Water Vapor

Goff and Gratch (17) have formulated the data on the second and third virial coefficients of water vapor as follows

$$A_{ww} = -33.97 + 55306\tau \times 10^{7200\tau^2}, \text{ cm}^3/\text{gmol}$$

$$A_{www} = 0.0348\tau^2 A^3_{ww}, \text{ cm}^3/\text{gmol} \cdot \text{atm}$$

Values of these and the corresponding derived coefficients, $B = d(\tau A)/d\tau$ and $C = dA/dT$, are listed in Table 4 and Table 5, together with tolerances set at twice the probable error of the values themselves as inferred from the deviations in the experimental data upon which they are based. Higher virial coefficients make negligible contributions at pressures below the saturation pressure up to at least 400 deg K.

Interaction Coefficients of Moist Air

For the purpose of thermodynamic analysis, moist air may be regarded as a binary mixture of dry air and water vapor. By

TABLE 4 SECOND VIRIAL COEFFICIENTS OF WATER VAPOR

t °C	A_{ww} (cm³/gmol)	Tol. ±	B_{ww} (cm³/gmol)	Tol. ±	C_{ww} (cm³/gmol °K)	Tol. ±
-90	-	-	-	-	-	-
-80	-	-	-	-	-	-
-70	-	-	-	-	-	-
-60	-	-	-	-	-	-
-50	-	-	-	-	-	-
-40	-	-	-	-	-	-
-30	-	-	29000	26000	-100	110
-20	-	-	20800	9500	- 71	38
-10	2300	1900	15600	3800	- 51	14
0	1830	800	12000	1600	- 37.2	59
10	1510	400	9440	800	- 28.0	20
20	1260	210	7570	420	- 21.5	14
30	1074	116	6180	230	- 16.84	76
40	924	66	5120	130	- 13.40	42
50	803	40	4298	80	- 10.81	25
60	705	25	3653	49	- 8.85	15
70	625	16	3138	31	- 7.324	20
80	558	10	2722	21	- 6.129	59
90	501	7	2382	14	- 5.179	39

TABLE 5 THIRD VIRIAL COEFFICIENTS OF WATER VAPOR

t °C	A_{www} (cm³/gmol atm)	Tol. ±	B_{www} (cm³/gmol atm)	Tol. ±	C_{www} (cm³/gmol atm°K)	Tol. ±
0	-	-	-	-	-	-
10	-	-	-	-	-	-
20	-	-	15000	18000	-47	61
30	-	-	8100	5300	-25	17
40	-	-	4600	1800	-14.0	58
50	-	-	2770	640	- 8.0	20
60	110	120	1710	240	- 4.80	72
70	72	50	1090	100	- 2.97	29
80	48	21	709	43	- 1.87	12
90	33	10	474	20	- 1.21	6

this simplification the number of chemical potentials μ_i is reduced to two, namely, μ_a and μ_w. Each of these is given by an expression of form, Equation [1]; each contains, besides the second virial coefficients A_{aa} and A_{ww}, an interaction coefficient A_{aw}. Goff and Gratch (15) have formulated data obtained under a co-operative investigation between the Towne Scientific School, University of Pennsylvania, and the American Society of Heating and Ventilating Engineers into the following semi-rational equation

$$A_{aw} = -29.53 + 0.00669T(1 - e^{-\theta\tau}) + A\tau + B\tau^2 + D\tau^3, \text{ cm}^3/\text{gmol}$$

with

$$\theta = 4416.5 \text{ deg K}$$
$$A = 17546 \text{ cm}^3 \text{ deg K/gmol}$$
$$B = 95300 \text{ cm}^3 \text{ deg K}^2/\text{gmol}$$
$$D = 8.515 \times 10^7 \text{ cm}^3 \text{ deg K}^3/\text{gmol}$$

Values of A_{aw} and of the corresponding derived coefficients, B_{aw} and C_{aw}, are listed in Table 6, together with tolerances set at thrice the estimated probable errors of the values to which they refer. These probable errors are difficult to estimate reliably because of the meagerness of experimental data; hence they are multiplied by three instead of two to get the corresponding tolerances.

Each chemical potential also contains, besides the third virial coefficients A_{aaa} and A_{www}, the higher-order interaction coefficients A_{aaw} and A_{aww}. Pending further research it is necessary to assume that of these four coefficients only A_{www} makes any appreciable contribution to the thermodynamic properties of moist air, at any rate in the range 150 to 400 deg K and 0 to 3 atm.

Saturation Pressure of Water

Goff and Gratch (17) have calculated the saturation pressure of pure water from other relevant data by means of the identical relations of thermodynamics. Their calculations involve an in-

TABLE 6 INTERACTION COEFFICIENTS OF MOIST AIR

t °C	A_{aw} (cm^3/gmol)	Tol. ±	B_{aw} (cm^3/gmol)	Tol. ±	C_{aw} (cm^3/gmol °K)	Tol. ±
-90	84.2	86	226	17	-0.774	93
-80	77.0	82	207	16	-0.674	81
-70	70.7	78	191	15	-0.591	71
-60	65.1	75	177	14	-0.523	63
-50	60.2	72	164	13	-0.466	56
-40	55.8	70	153	13	-0.418	50
-30	51.8	67	143	12	-0.376	45
-20	48.2	65	135	12	-0.341	41
-10	45.0	63	126.6	112	-0.310	37
0	42.0	61	119.5	108	-0.284	34
10	39.3	60	113.0	104	-0.260	31
20	36.8	58	107.0	100	-0.240	29
30	34.5	57	101.6	97	-0.221	27
40	32.3	55	96.5	94	-0.205	25
50	30.4	54	91.9	91	-0.190	23
60	28.5	53	87.6	89	-0.177	21
70	26.8	52	83.6	86	-0.165	20
80	25.2	51	79.9	84	-0.155	19
90	23.7	50	76.4	82	-0.145	17

tegration, over the logarithm of absolute temperature, of an integrand which varies only slowly with temperature. Therefore their results may be regarded as determining the function $p_s(T)$ or the function $p_s(t)$, where t is the centigrade temperature defined by Equation [4].

(*a*) *Saturation Pressure of Ice:* —100 to 0 deg C. Values of the saturation pressure of pure ordinary water ice are to be computed from the Goff-Gratch formula

$$\log_{10}p_{si} = -9.09718(T_0/T - 1) - 3.56654\log_{10}(T_0/T) + 0.876793(1 - T/T_0) + \log_{10}p_{si}(T_0) \quad [5]$$

with T_0 = 273.16 deg K = 491.688 deg R and with $p_{si}(T_0)$ = 0.0060273 atm, a constant of integration which has been adjusted so as to make p_{si} equal to p_{sf} (see the following) at T = 273.17 deg K, the triple point of water.

The formula as published (loc. cit.) gives the logarithm of the saturation pressure as the sum of three terms, only one of which is explicit in temperature, the other two having been left in the form of definite integrals, over the logarithm of absolute temperature, whose integrands contain both temperature and saturation pressure. In computing numerical values it is easy to evaluate these integrals by the method of successive approximations. For the greater convenience of the user, however, Gratch (18), has replaced these integrals by empirical expressions whose constants he has then adjusted by the method of least squares to make the formula as just given yield values of $\log_{10}[p_s/p_{si}(T_0)]$ showing an average deviation of 0.002 per cent and a maximum deviation of 0.015 per cent from those given by the formula as previously published.

(*b*) *Saturation Pressure of Liquid Water:* —50 to 100 deg C. Values of the saturation pressure of pure ordinary liquid water are to be computed directly from the Goff-Gratch formula (17), namely

$$\log_{10}p_{sf} = -7.90298\,(T_s/T - 1) + 5.02808\log_{10}(T_s/T) - 1.3816 \times 10^{-7}[10^{11.344(1-T/T_s)} - 1] + 8.1328 \times 10^{-3}[10^{-3.49149(T_s/T-1)} - 1] + \log_{10}p_{sf}(T_s) \quad [6]$$

with T_s = 373.16 deg K = 671.688 deg R and with $p_{sf}(T_s)$ = 1 atm.

(*c*) *Undercooled Liquid.* At temperatures below 0 deg C it is not possible for the vapor and liquid phases of pure water to coexist in stable equilibrium; it is an experimental fact, however, that they can coexist in what is called "metastable" equilibrium, in which case the coexisting liquid phase is called "undercooled liquid."

Since reliable experimental data on the thermodynamic properties of undercooled liquid are not presently available, interim values can be obtained only by some sort of extrapolation. Washburn (19) has, in effect, extrapolated the specific-heat data of Barnes and Cooke (20) in the range, —5 to 5 deg C, to develop a formula for $\log_{10}(p_{sf}/p_{si})$ which has heretofore been widely used. This formula may now be corrected to make it consistent with the Osborne (21) value of the heat of fusion of ice at 0 deg C and with the Giauque and Stout (22) measurements of the specific heat of ice.

Gratch (23) has calculated values of the ratio p_{sf}/p_{si} from (*a*) the original Washburn formula; (*b*) the corrected Washburn formula; (*c*) the Osborne, Stimson, and Ginnings (24) formulation of the calorimetric quantity γ using the approximate relation $\gamma = RT^2d\ln p_{sf}/dT$; (*d*) the corrected Washburn formula adjusted to fit the Scheel and Heuse (25) experimental measurements of p_{sf} down to about —15 deg C after omitting the last term which is quite small in the experimental range but increases very rapidly as temperature decreases; and (*e*) the Goff-Gratch formulas previously quoted. The results of these calculations are compared as follows:

SATURATION PRESSURE OF UNDERCOOLED LIQUID

	(p_{sf}/p_{si})				
t(°C)	(*e*)	(*a*) — (*e*)	(*b*) — (*e*)	(*c*) — (*e*)	(*d*) — (*e*)
0	1.0001	—.0001	0.0000	0.0000	0.0000
—10	1.1023	—.0002	—.0001	+.0005	—.0014
—20	1.2154	—.0004	—.0003	+.0013	—.0018
—30	1.3395	—.0014	—.0009	+.0031	—.0033
—40	1.4738	—.0039	—.0031	+.0072	—.0020
—50	1.6151	—.0077	—.0098	+.0167	+.0044

Another comparison based on an extrapolation of the Smith and Keyes (26) data on the specific volume v_f of the saturated liquid is of interest. Using the Goff-Gratch values of p_{sf}, together with previously quoted information regarding zero-pressure enthalpy h_w^0, the virial coefficients A_{ww}, A_{www}, and the corresponding derived coefficients B_{ww}, B_{www}, we may compute values of the specific enthalpy h_f of the saturated liquid from the identical relation, $h_f = h_g - (v_g - v_f)(dp_{sf}/dT)$. It is safe to ignore the extremely small variation with temperature of the difference between h_f and the specific enthalpy h_w' of compressed liquid at atmospheric pressure, and regard values of the quantity dh_f/dT as values of the isobaric specific heat c_w' at atmospheric pressure. In the following table these are compared with (*a*) values obtained from extrapolation of the Osborne, Stimson, and Ginnings (24) formula, and (*b*) values obtained from extrapolation of the Washburn (19) formulation of the Barnes and Cooke (20) data:

SPECIFIC HEAT OF UNDERCOOLED LIQUID

t(°C)	Goff-Gratch	NBS	Barnes and Cooke
—10	1.018	1.022	1.023
—20	1.039	1.055	1.045
—30	1.075	1.130	1.074
—40	1.14	1.30	1.11
—50	1.27	1.70	1.15

The saturation pressure of undercooled liquid is of such great concern to the meteorologist, if not to the engineer, that it seems necessary to recommend one of the foregoing extrapolations pending further research. The International Meteorological Organization recommends extrapolation of the Goff-Gratch formula down to —50 deg C because it insures continuity of 0 deg C and minimizes the number of formulas that have to be quoted.

Table 7 lists values of saturation pressure calculated from the Goff-Gratch formulas. Recently Keyes (27) has reviewed and reformulated existing data on this important property in the range 0 to 150 deg C in the light of the findings of Blaisdell and Kaye (28), regarding the relation between the absolute and the international Centigrade temperature scales. His results are in

remarkably close agreement with the values listed in Table 7 for temperatures above 0 deg C.

Regarding the tolerances listed in Table 7, each of those below 0 deg C has been set at thrice the estimated probable error of the corresponding saturation pressure; those above 0 deg C are the ones recommended by the Third International Conference on Steam Tables (29); no attempt has been made to set tolerances on the recommended values of the saturation pressure of undercooled liquid.

TABLE 7 SATURATION PRESSURE OF PURE WATER IN MILLIBARS*

t °C	p_{sf}	Tol. ±	p_{si}	Tol. ±
-90	-	-	0.0000967	9
-80	-	-	0.0005472	44
-70	-	-	0.002615	19
-60	-	-	0.01080	7
-50	0.06355	-	0.03935	22
-40	0.18909	-	0.1283	6
-30	0.50888	-	0.3799	14
-20	1.2543	-	1.032	3
-10	2.863	-	2.597	5
0	6.1078	59	6.107	6
10	12.272	10	-	-
20	23.373	20	-	-
30	42.430	29	-	-
40	73.777	37	-	-
50	123.40	6	-	-
60	199.26	10	-	-
70	311.69	16	-	-
80	473.66	24	-	-
90	701.14	35	-	-

* 1 millibar = 1000 dyne/cm.²

Above 0 deg C the recommended values of saturation pressure differ slightly, but, nevertheless, significantly, from those previously recommended by the Third International Conference on Steam Tables (29) if the difference between the absolute and the international Centigrade temperature scales be ignored in making the comparison. The analysis of Keyes (27) may be taken to show, however, that the two sets are brought into remarkably close agreement by transferring the latter from the international Centigrade to the absolute scale by means of the Blaisdell and Kaye (28) findings regarding the relation between the two scales. It seems clear, therefore, that the tolerances recommended by the Third International Conference on Steam Tables could stand substantial reduction.

Saturation in the Case of Moist Air

Moist air is said to be saturated when its condition is such that it can coexist in neutral equilibrium with an associated condensed phase presenting a flat surface to it. Strictly speaking, the associated condensed phase is not pure water, but water containing small concentrations of dissolved gases. The relative concentrations of these dissolved gases are not the same as those of the same gases in the vapor phase, but we are practically compelled to ignore the very slight differences and to regard the condensed phase as an ideal mixture of pure water and dry air having but two component chemical potentials, μ_w' and μ_a'.

In line with this simplification we can say that moist air is saturated when it has the same values of temperature, pressure, and its two component chemical potentials as does the associated condensed phase. There are thus four relations to be satisfied at saturation. These four relations involve, however, six independent variables, namely, the two temperatures, the two pressures, and the two mol-fractions; hence the two-phase system has two degrees of freedom at saturation. This means that such quantities as the weight of water, the volume, the enthalpy, and the entropy—all per unit weight of dry air—must be regarded as functions of two independent variables which are usually chosen to be pressure p and temperature T.

Humidity Ratio at Saturation

The weight of water vapor per unit weight of dry air is called "humidity ratio" or "mixing ratio." It is denoted by the letter W to which may be affixed the subscript s to specify its value at saturation. It is convenient to introduce a coefficient $f_s(p,T)$ defined by the equation

$$W_s = 0.62197 \frac{f_s p_s/p}{1 - f_s p_s/p} \quad \ldots\ldots\ldots\ldots [7]$$

where p_s is the saturation pressure of pure water, a function of temperature only, and 0.62197 = 18.0160/28.966.

Goff and Gratch (30, 31) have reduced the conditions for saturation in the case of moist air to the following equation

$$\log_e f_s = \alpha(1 - p_s/p) + \beta(p/p_s - 1) \quad \ldots\ldots\ldots [8]$$

with

$$\alpha = (A_{aa} - 2A_{aw} + A_{ww})p_s/RT + A_{www}p_s^2/RT$$
$$\beta = -k'p_s + v_w'p_s/RT + (A_{aa} + 2A_{aw})p_s/RT$$

where

k' = solubility coefficient of air in water

v_w' = specific volume of (liquid or solid) water

Table 8 gives an idea of how the coefficient $f_s(p, T)$ varies with pressure and temperature. In computing the data listed in Table 8, values of k' for liquid water above 0 deg C have been taken from the International Critical Tables (32); k' has been assumed to be zero for undercooled liquid and ice. Values of v_w' for liquid water above 0 deg C have been taken from Osborne, Stimson, and Ginnings (33); a constant value of 18.0 cm³/gmol has been assumed for undercooled liquid; values for ice have been taken from Jakob and Erk (34) and from Keenan and Keyes (35).

TABLE 8 THE COEFFICIENT $f_s(p,T)$

t	p = 300 mb.*		p = 700 mb.		p = 1100 mb.	
°C	f_{sf}	f_{si}	f_{sf}	f_{si}	f_{sf}	f_{si}
-90	-	1.0027	-	-	-	-
-80	-	1.0024	-	1.0057	-	1.0089
-70	-	1.0022	-	1.0051	-	1.0080
-60	-	1.0020	-	1.0046	-	1.0073
-50	1.0018	1.0018	1.0042	1.0042	1.0065	1.0066
-40	1.0017	1.0017	1.0038	1.0039	1.0060	1.0061
-30	1.0016	1.0016	1.0036	1.0036	1.0055	1.0056
-20	1.0015	1.0015	1.0034	1.0034	1.0052	1.0052
-10	1.0015	1.0015	1.0032	1.0033	1.0049	1.0050
0	1.0016	1.0016	1.0032	1.0032	1.0047	1.0048
10	1.0018	-	1.0032	-	1.0047	-
20	1.0020	-	1.0034	-	1.0048	-
30	1.0023	-	1.0037	-	1.0050	-
40	1.0026	-	1.0041	-	1.0054	-
50	-	-	1.0045	-	1.0059	-
60	-	-	1.0048	-	1.0064	-

* 1 millibar = 1000 dyne/cm.²

Rather than list the values of k' and v_w', used in calculating values of the coefficient $f_s(p, T)$, it seems better to list, as is done in Table 9, values of the coefficients α and β, in which they appear along with other properties discussed previously. In Table 9 the tolerances given are based on the previously stated tolerances for A_{aa}, A_{aw}, etc., on an arbitrarily chosen tolerance of 10 per cent in k', and on zero tolerance in v_w'.

Table 10 lists values of humidity ratio at saturation at standard atmospheric pressure, together with tolerances at least twice estimated probable error.

Volume

The correct expression for the specific volume of moist air can be derived from Equations [1] for the chemical potentials by

TABLE 9 COEFFICIENTS IN THE EXPRESSION FOR SATURATION

t °C	α_f	Tol. ±	α_i	Tol. ±	β_f	Tol. ±	β_i	Tol. ±
-90	-	-	0.0000	4	-	-	0.87x10-9	13
-80	-	-	0.0000	4	-	-	0.44x10-8	7
-70	-	-	0.0000	4	-	-	1.90x10-8	29
-60	-	-	0.0000	4	-	-	0.71x10-7	11
-50	0.0000	-	0.0000	4	3.7 x10-7	-	2.35x10-7	35
-40	0.0000	-	0.0000	4	1.02x10-6	-	0.70x10-6	11
-30	0.0001	-	0.0001	4	2.52x10-6	-	1.91x10-6	29
-20	0.0002	-	0.0001	4	0.57x10-5	-	0.48x10-5	7
-10	0.0003	-	0.0003	4	1.21x10-5	-	1.11x10-5	17
0	0.00048	42	0.0005	4	2.37x10-5	36	2.43x10-5	-
10	0.00076	41	-	-	4.44x10-5	67	-	-
20	0.00117	41	-	-	0.79x10-4	12	-	-
30	0.00174	41	-	-	1.34x10-4	20	-	-
40	0.00251	41	-	-	2.19x10-4	33	-	-
50	0.00352	42	-	-	3.46x10-4	52	-	-
60	0.00483	44	-	-	5.26x10-4	79	-	-
70	0.00649	46	-	-	0.78x10-3	12	-	-
80	0.00854	49	-	-	1.12x10-3	17	-	-
90	0.01103	56	-	-	1.58x10-3	24	-	-

TABLE 10 HUMIDITY RATIO AT SATURATION

Standard Atmospheric Pressure

t °C	W_{sf}	Tol. ±	W_{si}	Tol. ±
-90	-	-	0.5991x10-7	66
-80	-	-	0.3336x10-6	34
-70	-	-	0.1617x10-5	14
-60	-	-	0.6677x10-5	53
-50	0.3924 x10-4	-	0.2430x10-4	17
-40	1.168 x10-4	-	0.7923x10-4	47
-30	0.3141 x10-3	-	0.2345x10-3	11
-20	0.7744 x10-3	-	0.6370x10-3	26
-10	1.7688 x10-3	-	1.6057x10-3	48
0	0.37886x10-2	80	3.7886x10-3	80
10	0.7659 x10-2	15	-	-
20	0.14754x10-1	28	-	-
30	0.27319x10-1	49	-	-
40	0.49114x10-1	79	-	-
50	0.8630 x10-1	13	-	-
60	0.15340	25	-	-
70	0.27884	47	-	-
80	0.55200	105	-	-
90	1.1160	38	-	-

TABLE 11 VOLUME OF MOIST AIR PER UNIT WEIGHT OF DRY AIR

Standard Atmospheric Pressure
(cm^3/g)

t °C	v_a	Tol. ±	v_{sf}	Tol. ±	v_{si}	Tol. ±
-90	517.13	25	-	-	517.13	25
-80	545.69	23	-	-	545.69	23
-70	574.20	22	-	-	574.20	22
-60	602.70	21	-	-	602.71	21
-50	631.18	20	631.22	-	631.20	20
-40	659.65	19	659.77	-	659.73	19
-30	688.09	18	688.44	-	688.35	18
-20	716.53	18	717.42	-	717.26	18
-10	744.96	17	747.06	-	746.88	18
0	773.36	17	778.06	18	778.06	18
10	801.77	17	811.61	19	-	-
20	830.18	17	849.80	21	-	-
30	858.57	18	896.13	25	-	-
40	886.96	18	956.67	29	-	-
50	915.35	19	1042.38	38	-	-
60	943.73	19	1174.90	56	-	-
70	972.10	20	1404.25	93	-	-
80	1000.48	20	1879.2	19	-	-
90	1028.85	21	3341.2	64	-	-

forming the specific free enthalpy g, according to the identical relation, $g = \Sigma x_i \mu_i$, and differentiating this according to the identical relation, $v = \partial g/\partial p$. The volume of moist air per unit weight of dry air is obtained from its specific volume in an obvious manner. Table 11 lists values of the volume of moist air per unit weight of dry air at standard atmospheric pressure, together with tolerances at least twice the estimated probable error.

Enthalpy

The correct expression for the specific enthalpy of moist air can be derived from Equations [1] for the chemical potentials by forming the specific free enthalpy g, according to the identical relation, $g = \Sigma x_i \mu_i$, and differentiating this according to the identical relation, $h = \partial(\tau g)/\partial \tau$, where τ denotes reciprocal absolute temperature. The enthalpy of moist air per unit weight of dry air is obtained from its specific enthalpy in an obvious manner.

The enthalpy of moist air per unit weight of dry air is subject to augmentation by amount $\bar{h}_a + W\bar{h}_w$, where $\bar{h}_a$ and $\bar{h}_w$ are arbitrary constants. In Table 12 the constant $\bar{h}_a$ has been adjusted so as to make the specific enthalpy of dry air zero at 0 deg C and standard atmospheric pressure; the constant $\bar{h}_w$ has been adjusted so as to make the specific enthalpy of saturated liquid water zero at 0 deg C in conformity with the usual steam-table practice.

TABLE 12 ENTHALPY OF MOIST AIR PER UNIT WEIGHT OF DRY AIR

Standard Atmospheric Pressure
(kcal/kg)

t °C	h_a	Tol. ±	h_{sf}	Tol. ±	h_{si}	Tol. ±
-90	-21.641	20	-	-	-21.641	20
-80	-19.230	17	-	-	-19.230	17
-70	-16.823	14	-	-	-16.822	14
-60	-14.418	11	-	-	-14.414	11
-50	-12.0132	89	-11.9897	-	-11.9992	90
-40	- 9.6093	68	- 9.5410	-	- 9.5634	71
-30	- 7.2065	49	- 7.0226	-	- 7.0696	55
-20	- 4.8046	31	- 4.3487	-	- 4.4298	46
-10	- 2.4027	16	- 1.3540	-	- 1.4510	45
0	0.0000	0	+ 2.2622	45	+ 2.2622	45
10	2.4021	15	7.0091	105	-	-
20	4.8052	28	13.744	20	-	-
30	7.2096	42	23.880	34	-	-
40	9.6140	55	39.796	54	-	-
50	12.0195	67	65.731	87	-	-
60	14.4264	80	110.00	16	-	-
70	16.8348	91	191.71	31	-	-
80	19.2447	104	367.68	67	-	-
90	21.657	12	921.1	24	-	-

Entropy

The correct expression for the specific entropy of moist air can be derived from Equations [1], for the chemical potentials, by forming the specific free enthalpy g according to the identical relation, $g = \Sigma x_i \mu_i$, and differentiating this according to the identical relation, $s = -\partial g/\partial T$. The entropy of moist air per unit weight of dry air is obtained from its specific entropy in an obvious manner.

The entropy of moist air per unit weight of dry air is subject to augmentation by amounts $\bar{s}_a + W\bar{s}_w$, where $\bar{s}_a$ and $\bar{s}_w$ are arbitrary constants. In Table 13, the constant $\bar{s}_a$ has been adjusted so as to make the specific entropy of dry air zero at 0 deg C and atmospheric pressure; the constant $\bar{s}_w$ has been adjusted so as to

TABLE 13 ENTROPY OF MOIST AIR PER UNIT WEIGHT OF DRY AIR

Standard Atmospheric Pressure
(kcal/kg degK)

t °C	s_a	Tol. ±	s_{sf}	Tol. ±	s_{si}	Tol. ±
-90	-0.09611	11	-	-	-0.09611	11
-80	-0.08332	9	-	-	-0.08332	9
-70	-0.07116	7	-	-	-0.07116	7
-60	-0.05960	5	-	-	-0.05958	5
-50	-0.04957	4	-0.04846	-	-0.04850	4
-40	-0.03804	3	-0.03774	-	-0.03783	3
-30	-0.02795	2	-0.02716	-	-0.02735	2
-20	-0.01826	1	-0.01638	-	-0.01670	2
-10	-0.00896	1	-0.00478	-	-0.00514	2
0	0.00000	0	+0.00870	2	+0.00870	2
10	+0.00864	1	0.02574	4	-	-
20	0.01698	1	0.04911	7	-	-
30	0.02504	2	0.08312	12	-	-
40	0.03284	2	0.13485	18	-	-
50	0.04040	2	0.21669	29	-	-
60	0.04774	3	0.35246	52	-	-
70	0.05486	3	0.59601	95	-	-
80	0.06178	4	1.11236	203	-	-
90	0.06852	4	2.67830	71	-	-

make the specific entropy of saturated liquid water zero at 0 deg C in conformity with the usual steam-table practice.

Condensed Water

In the definition on thermodynamic wet-bulb temperature to be given later there appears the specific enthalpy h_w' of pure (air-free) compressed liquid (or solid) water. Values of h_w' and of the corresponding specific entropy s_w' are listed in Table 14 for standard atmospheric pressure. The reference point at which both enthalpy and entropy are assigned the value zero is saturated liquid at 0 deg C in conformity with usual steam-table practice.

TABLE 14 PROPERTIES OF CONDENSED WATER
Standard Atmospheric Pressure

t	Enthalpy, h_w' (kcal/kg)		Entropy, s_w' (kcal/kg°K)	
°C	liquid	solid	liquid	solid
-90	-	-117.79	-	-0.4590
-80	-	-114.25	-	-0.4402
-70	-	-110.54	-	-0.4214
-60	-	-106.64	-	-0.4028
-50	-53.97	-102.58	-0.2192	-0.3841
-40	-42.00	- 98.34	-0.1666	-0.3655
-30	-30.96	- 93.92	-0.1201	-0.3470
-20	-20.40	- 89.34	-0.0776	-0.3285
-10	-10.14	- 84.57	-0.0378	-0.3101
0	+ 0.02	- 79.64	0.0000	-0.2916
10	10.06	-	+0.0361	-
20	20.06	-	0.0708	-
30	30.04	-	0.1043	-
40	40.03	-	0.1367	-
50	50.01	-	0.1681	-
60	60.00	-	0.1985	-
70	69.99	-	0.2281	-
80	80.01	-	0.2568	-
90	90.05	-	0.2848	-

The values for undercooled liquid are based in part on an extrapolation of the Smith and Keyes (26) volume data, in part on the recommended extrapolation of the Goff-Gratch Equation [6] for the saturation pressure p_{sf}, and in part on other data previously quoted. Since the first extrapolation is a fairly safe one, inasmuch as the final results depend only slightly upon the liquid volume, these values should be recommended for adoption, pending further research, if for no other reason than that they are consistent with previous recommendations.

Reference Points

The Working Subcommittee discussed the question of reference points at some length. Moist air, as defined in this report, is a mixture of five constituent gases: oxygen (O_2), nitrogen (N_2), argon (A), carbon dioxide (CO_2), and water vapor (H_2O). The enthalpy of each of these constituent gases i is subject to augmentation by a constant amount $\bar{h}_i$, called its null-point ($p = 0$, $T = 0$) enthalpy; the entropy of each constituent is subject to augmentation by a constant amount $\bar{s}_i$, called its null-point reduced entropy (by reduced entropy is meant the sum, $s + R \ln p$, with pressure expressed in standard atmospheres). It follows that the enthalpy and entropy of dry air are subject to augmentation by constant amounts, $\bar{h}_a = \Sigma x_i \bar{h}_i$ and $\bar{s}_a = \Sigma x_i \bar{s}_i$, respectively; similarly, the enthalpy and entropy of water are subject to augmentation by constant amounts, $\bar{h}_w$ and $\bar{s}_w$, respectively.

Tables 1 and 2 of this report are based on the arbitrary assignments

$$\bar{h}_a = \bar{s}_a = \bar{h}_w = \bar{s}_w = 0$$

Tables 12, 13, 14 are based on the following assignments: For dry air, both enthalpy and entropy are assigned the value zero at 0 deg C, atmospheric pressure; for water, both enthalpy and entropy are assigned the value zero at 0 deg C, saturated liquid. Using the data previously quoted in this report, it is easy to compute that these assignments are to be implemented by making: $\bar{h}_a = -65.260$ kcal/kg, $\bar{s}_a = -1.61712$ kcal/kg deg K, $\bar{h}_w = +477.277$ kcal/kg, $\bar{s}_w = -0.83960$ kcal/kg deg K.

The Goff-Gratch tables (15, 17) are based on the following assignments: For dry air, both enthalpy and entropy are assigned the value zero at 0 deg F, atmospheric pressure; for water, both enthalpy and entropy are assigned the value zero at 32 deg F, saturated liquid. Using the data previously quoted in this report, it is easy to compute that these assignments are to be implemented by making: $\bar{h}_a = -109.782$ Btu/lb, $\bar{s}_a = -1.60096$ Btu/lb deg R, $\bar{h}_w = +859.099$ Btu/lb, $\bar{s}_w = -0.83960$ Btu/lb deg R. The tables referred to have been published (37) and widely distributed by the American Society of Heating and Ventilating Engineers. Using the same assignments, additional tables, giving the thermodynamic properties of moist air for six different pressures above atmospheric and up to 150 psi, have been compiled in the University of Pennsylvania Thermodynamics Research Laboratory (36) under Project G-8. It is clear, therefore, that the assignments of this paragraph are destined to be used rather widely in engineering circles.

On the other hand, the tables being compiled in the University of Pennsylvania Thermodynamics Research Laboratory for publication in Smithsonian Meteorological tables (31) are based on the following assignments: For dry air, both enthalpy and reduced entropy (by reduced entropy is here meant the sum, $s + R \ln p$, with pressure expressed in millibars) are assigned the value zero at 0 deg C, zero pressure; for water, both enthalpy and entropy are assigned the value zero at 0 deg C, saturated liquid. Using the data previously quoted in this report, it is easy to compute that these assignments are to be implemented by making $\bar{h}_a = -65.326$ kcal/kg, $\bar{s}_a = -2.09179$ kcal/kg deg K, $\bar{h}_w = +477.277$ kcal/kg, $\bar{s}_w = -0.83960$ kcal/kg deg K.

In most, if not all, tables giving the thermodynamic properties of moist air, the usual steam-tables practice of assigning the value zero to both the enthalpy and the entropy of water at 0 deg C, saturated liquid is followed. There is, however, no unanimity in the choice of reference point for dry air. Perhaps this lack of unanimity is of little practical importance because it is so easy to convert from one choice to another. The Working Subcommittee decided not to indicate a preference.

Recent developments in the science of interpreting atomic and molecular spectra have focused attention upon the zero-pressure isobar as the line along which the thermodynamic properties of gases and gas mixtures generally can at any time be known with greatest accuracy. This is certainly true in the case of moist air; hence the relative permanence of the numerical values assigned to the null-point enthalpies and reduced entropies of dry air and water would be enhanced by placing both reference points on the zero-pressure isobar at some stated value (s) of absolute temperature. The obvious location would be the null-point ($p = 0$, $T = 0$) itself; indeed the null-point suggests itself as the logical reference point for all gases.

Even if the null-point were to be adopted as the common reference point, it would still be necessary to decide what are the best values to assign to the enthalpy and reduced entropy there for each gas under consideration. Tables 1 and 2 of this report are based on the assignments, $\bar{h}_a = \bar{s}_a = \bar{h}_w = \bar{s}_w = 0$, as is the following skeleton table

THERMODYNAMIC PROPERTIES OF MOIST AIR
(Standard Atmospheric Pressure)

t(°C)	h_a	h_s	s_a	s_s	h_w'	s_w'
—90	43.619	43.619	1.52101	1.52101	—595.07	0.3806
0	65.260	65.714	1.61712	1.62030	—477.26	0.8396
90	86.917	310.54	1.68564	2.87451	—387.23	1.1244

In this table the unit of enthalpy is the kcal/kg, that of en-

tropy, the kcal/kg deg K. At —90 deg C the values given for h_s and s_s are for saturation with respect to ice; those for h_w' and s_w' at this temperature are for ice also. The data in this table should be compared with those in Tables 12, 13, and 14.

According to the so-called "third law of thermodynamics" the assignments, $\bar{s}_i = 0$, are always permissible if nuclear changes are ruled out of consideration, provided that, in computing values of $s_i^0 - \bar{s}_i$, possible contributions from nuclear spin and other nuclear motions are consistently included or excluded (it has become common practice to exclude). But the assignments, $\bar{h}_i = 0$, are in general not permitted if ordinary chemical changes are not to be ruled out of consideration. In this case only as many of the $\bar{h}_i$ can be disposed of arbitrarily as there are distinct atomic species. Therefore it would seem logical to exercise this permitted arbitrariness on the null-point enthalpies of the monatomic gases themselves. Undoubtedly, there will be a move in this direction as the accuracy and completeness of our knowledge of the dissociation energies of molecular gases, by which their null-point enthalpies are related to those of the associated monatomic gases, become more satisfactory.

Thermodynamic Dew-Point Temperature

A derived thermodynamic property of moist air of great importance in hygrometry is the so-called thermodynamic dew-point temperature T_d. The Working Subcommittee recommends that this important property be defined as the solution $T_d(p, W)$ of the equation

$$W_s(p, T_d) = W \quad \ldots\ldots\ldots\ldots\ldots\ldots [9]$$

The definition is given in mathematical form to avoid ambiguity. It is a problem belonging properly to practical hygrometry to design and construct dew-point hygrometers capable of reading values of thermodynamic dew-point temperature as defined by Equation [9] after suitable calibration. The International Meteorological Organization has concurred in the foregoing definition.

Thermodynamic Wet-Bulb Temperature

Another derived thermodynamic property of moist air of great importance in psychrometry is the so-called thermodynamic wet-bulb temperature T_w. The Working Subcommittee recommends that this important property be defined as the solution $T_w(p,T,W)$ of the equation

$$h(p,T,W) - W \cdot h_w'(p,T_w) = h_s(p,T_w) - W_s(p,T_w) \cdot h_w'(p,T_w) \quad \ldots\ldots\ldots [10]$$

where it is to be understood that h_w' denotes the specific enthalpy of pure compressed liquid (or solid) water. This definition is also given in mathematical form to avoid ambiguity. It is a problem belonging properly to practical psychrometry to design and construct psychrometers capable of reading values of thermodynamic wet-bulb temperature as defined by Equation [10] after suitable calibration. It seems likely that the International Meteorological Organization will concur in the foregoing definition.

In justification of the the definition it may be said that it combines the correct energy and weight accountings for the steady-flow process of injecting pure compressed liquid (or solid) water at pressure p and temperature T_w into a stream of moist air at pressure p, temperature T, and humidity ratio W to bring the air adiabatically to saturation at pressure p and temperature T_w. This is to be regarded as the appropriate idealization of the actual process by which the thin film of water on a wet-bulb thermometer immersed in a stream of moist air maintains, at any rate for a time, a steady value below that of the air itself.

Tables

In Tables 1 through 14, referred to previously, where tolerances are given, it is to be understood that the rightmost digit of the tolerance is to be placed directly underneath the rightmost digit of the value to which it applies regardless of the location of the decimal point.

Acknowledgment

It is a pleasure to acknowledge the substantial co-operation of the Navy Department, Bureau of Ships, in the preparation of this report. It was under the sponsorship of the Bureau that the University of Pennsylvania Thermodynamics Research Laboratory was operated from July 1, 1945, until June 30, 1948, when cognizance was transferred to the Office of Naval Research. The invaluable aid of Mr. S. Gratch, assistant professor of mechanical engineering, Towne Scientific School, University of Pennsylvania, and project leader in charge of gas-properties research in the University of Pennsylvania Thermodynamics Research Laboratory, is also gratefully acknowledged.

BIBLIOGRAPHY

1 "51st Annual Meeting Proceedings," Trans. American Society of Heating and Ventilating Engineers, vol. 51, 1945, p. 27.

2 "The Theory of Heat," by Thomas Preston, Macmillan & Company, London, England, 1894, p. 350.

3 "The Chemical Composition of the Atmosphere," by F. A. Paneth, *Quarterly Journal of the Royal Meteorological Society*, vol. 63, 1937, pp. 433–438.

4 "The Constancy of the Atmosphere With Respect to Carbon Dioxide and Oxygen Content," by T. M. Carpenter, *Journal of the American Chemical Society*, vol. 59, 1937, p. 358.

5 "The Composition of the Atmosphere With Special Reference to Its Oxygen Content," by F. G. Benedict, Washington, D. C., 1912.

6 "Determination of the Helium Group Gases in Natural Gases and in the Atmosphere," by G. H. Cady and H. P. Cady, *Industrial and Engineering Chemistry*, Analytical edition, vol. 17, 1945, pp. 760–766.

7 "Thirteenth Report of the Committee on Atomic Weights of the International Union of Chemistry," by G. P. Baxter, M. Guichard, and F. Whytlaw-Gray, *Journal of the American Chemical Society*, vol. 69, 1947, pp. 731–736.

8 "A New Table of Values of the General Physical Constants," by R. T. Birge, *Review of Modern Physics*, vol. 13, 1941, pp. 233–239.

9 "Our Knowledge of the Atomic Constants, F, N, m, and h in 1947 and of Other Constants Derivable Therefrom," by J. W. M. DuMond and E. R. Cohen, *Review of Modern Physics*, vol. 20, 1948, pp. 82–108.

10 "International Steam-Table Conference—Skeleton Steam Tables," *Mechanical Engineering*, vol. 52, 1930, pp. 120–122.

11 "Thermodynamic Functions for Molecular Oxygen in the Ideal Gas State," by H. W. Woolley, *Journal of Research*, National Bureau of Standards, RP1864, vol. 40, 1948, pp. 163–168.

12 "Zero-Pressure Properties of Diatomic Gases," by S. Gratch, Summary Report of Project G-3, University of Pennsylvania Thermodynamics Research Laboratory, April, 1946.

13 "Zero-Pressure Properties of Monatomic Gases," by S. Gratch and S. W. Van Voorhis, Final Report of Project G-1, University of Pennsylvania Thermodynamics Research Laboratory, April, 1947.

14 "Heats, Free Energies, and Equilibrium Constants of Some Reactions Involving, O_2, H_2, H_2O, C, CO, CO_2, and CH_4," by D. D. Wagman, J. E. Kilpatrick, W. J. Taylor, K. S. Pitzer, and F. D. Rossini, *Journal of Research*, National Bureau of Standards, RP1634, vol. 34, 1945, pp. 143–161.

15 "Thermodynamic Properties of Moist Air," by J. A. Goff and S. Gratch, Trans. American Society of Heating and Ventilating Engineers, vol. 51, 1945, pp. 125–158.

16 "The Joule-Thomson Effect and Heat Capacity at Constant Pressure for Air," by O. C. Bridgeman, *Physical Review*, vol. 34, 1929, pp. 527–533.

17 "Low Pressure Properties of Water From —160 to 212 F," by J. A. Goff and S. Gratch, Trans. American Society of Heating and Ventilating Engineers, vol. 52, 1946, pp. 95-121.

18 "The Saturation Pressure of Water Below 60°C," by J. A. Goff and S. Gratch, Special Report, University of Pennsylvania Thermodynamics Research Laboratory, January, 1948.

19 "Vapor Pressure of Ice and of Water Below the Freezing

Point," by E. W. Washburn, *Monthly Weather Review*, vol. 52, 1924, pp. 488–490.

20 "On the Specific Heat of Supercooled Water," by H. T. Barnes and H. L. Cooke, *Physical Review*, vol. 15, 1902, pp. 65–72.

21 "Heat of Fusion of Ice. A Revision," by N. S. Osborne, *Journal of Research*, National Bureau of Standards, RP1260, vol. 23, 1939, pp. 643–646.

22 "The Entropy of Water and the Third Law of Thermodynamics. The Heat Capacity of Ice From 15 to 273°K," by W. F. Giauque and J. W. Stout, *Journal of the American Chemical Society*, vol. 58, 1936, pp. 1144–1150.

23 "Vapor Pressure of Subcooled Liquid Water to —50°C," by S. Gratch, Special Report, University of Pennsylvania Thermodynamics Research Laboratory, August, 1947.

24 "Measurements of Heat Capacity and Heat of Vaporization of Water in the Range 0° to 100°C," by N. S. Osborne, H. F. Stimson, and D. C. Ginnings, *Journal of Research*, National Bureau of Standards, RP1228, vol. 23, 1939, pp. 197–260.

25 "Bestimmung des Sättigungsdruckes von Wasserdampf unter 0°," by K. Scheel and W. Heuse, *Annalen der Physik*, vol. 29, 1909, pp. 723–737.

26 "The Volumes of Unit Mass of Liquid Water and Their Correlation as a Function of Pressure and Temperature," by L. B. Smith and F. G. Keyes, Proceedings of the American Academy of Arts and Sciences, vol. 69, 1934, p. 285.

27 "The Thermodynamic Properties of Water Substance 0° to 150°C," by F. G. Keyes, *Journal of Chemical Physics*, vol. 15, 1947, pp. 602–612.

28 "The Location of the Normal Sulfur and Mercury Boiling Points on the Thermodynamic Temperature Scale," by B. E. Blaisdell and J. Kaye, in "Temperature, Its Measurement and Control in Science and Industry," Reinhold Publishing Corporation, New York, N. Y. 1941, pp. 127–140.

29 "The Third International Conference on Steam Tables," *Mechanical Engineering*, vol. 57, 1935, pp. 710–713.

30 "The Humidity Ratio (Mixing Ratio) of Moist Air at Saturation," by J. A. Goff and S. Gratch, Special Report, University of Pennsylvania Thermodynamics Research Laboratory, March, 1948.

31 "Compilation of Properties of Moist Air for the Smithsonian Meteorological Tables," by S. Gratch, Progress Report, University of Pennsylvania Thermodynamics Research Laboratory, August, 1948.

32 "International Critical Tables," published for the National Research Council, McGraw-Hill Book Company, Inc., New York, N. Y., vol. 3, 1928, p.257.

33 "Thermal Properties of Saturated Water and Steam," by N. S. Osborne, H. F. Stimson, and D. C. Ginnings, *Journal of Research*, National Bureau of Standards, RP1229, vol. 23, 1939, pp. 261–270.

34 "Wärmedehnung des Eises Zwischen 0 und —253°," by M. Jakob and S. Erk, *Wissenschaftliche Abhandlungen der physikalisch-technischen Reichsanstalt*, vol. 12, 1929, pp. 301–316.

35 "Thermodynamic Properties of Steam," by J. H. Keenan and F. G. Keyes, John Wiley & Son, Inc., New York, N. Y., 1936.

36 "Goff Chart for Moist Air," by S. Gratch, Summary Report of Project G-8, University of Pennsylvania Thermodynamics Research Laboratory, April, 1946, 1947, 1948.

37 "Heating, Ventilating, Air Conditioning Guide," published by the American Society of Heating and Ventilating Engineers, New York, N. Y , 1948.

The Physical Properties of Air With Reference to Meteorological Practice and the Air-Conditioning Engineer

By P. A. SHEPPARD,[1] LONDON, ENGLAND

The paper summarizes numerical values of physical functions and constants, relating to dry and moist air, of common use in meteorology and of interest to the air-conditioning engineer, and definitions and specifications of water vapor in the atmosphere.

Introduction

AT THE sixteenth session of the Aerological Commission of the International Meteorological Organization (IMO) held under the presidency of Dr. Sverre Petterssen (Norway) in Toronto, August 4 to 16, 1947, a Subcommission was appointed to recommend a set of self-consistent, internationally acceptable values of physical functions and constants of common use in meteorological practice. This Subcommission was further charged to recommend to the Commission acceptable definitions and specifications of water vapor in the atmosphere so as to remove the confusion which had for long existed in such definitions and specifications.

The Subcommission was assisted by representatives from the Commission on Instruments and Methods of Observation of IMO and from the Working Subcommittee of the International Joint Committee on Psychrometric Data (IJCPD). The latter representation was especially acceptable in view of the existence of many problems of common interest to the Aerological Commission and the Working Subcommittee, and because the Working Subcommittee had already prepared some of the ground to be covered by the Subcommission. Moreover this representation helped to insure the widest possible agreement among physicists, engineers, and meteorologists concerned with the subjects under discussion.

The author was privileged to be chairman of the Subcommission and is pleased to be able to state that its two reports, "The Values of Some Physical Functions and Constants Used in Meteorology" and "Definitions and Specifications of Water Vapour in the Atmosphere," hereinafter referred to as Report A and Report B, respectively, were adopted by the Aerological Commission, and later by the Conference of Directors of the International Meteorological Organization sitting in Washington, D. C., September, 1947. Both reports are to be printed and widely distributed by the International Meteorological Organization. Their contents are thought to be of interest to all concerned with the physical properties of the atmosphere, in particular to the air-conditioning engineer to whom this note on the Subcommission's activities is especially directed.

[1] Assistant Professor of Meteorology, Imperial College of Science and Technology, University of London.

Contributed by the Research Committee on Properties of Gases and Gas Mixtures, the Applied Mechanics Division and the Heat Transfer Division, and Section M of the American Association for the Advancement of Science, and presented at the Annual Meeting, New York, N. Y., November 28–December 3, 1948, of THE AMERICAN SOCIETY OF MECHANICAL ENGINEERS.

NOTE: Statements and opinions advanced in papers are to be understood as individual expressions of their authors and not those of the Society. Paper No. 48—A-152.

The Subcommission also produced a Report C on "Aerological Functions and Tables" which, while of less likely interest to the air-conditioning engineer, is thought to merit reference here because it provides definitions of certain thermodynamic functions of common interest and makes recommendations as to the required tabulation of these functions.

Principles

In selecting values of physical constants and in formulating definitions and specifications to be recommended for adoption, the Subcommission was guided by the following principles: The set of constants and specifications selected should (*a*) be thermodynamically consistent, (*b*) take full account of modern laboratory techniques and data as well as of modern physical theory, (*c*) be consistent with the theoretical and practical requirements of meteorology, (*d*) agree as far as possible with the magnitudes and specifications of physical quantities adopted by physicists and engineers, in particular with the recommendations of the Working Subcommittee of the International Joint Committee on Psychrometric Data.

No serious incompatibility of our recommendations with the foregoing principles is thought to be involved. In Report A, values of some quantities, mainly enthalpy-derived quantities, could be recommended as tentative values only, pending completion of further work calculated to improve the accuracy of the then existing information, or to put it in a form more adaptable to meteorological and engineering application. The Subcommission is charged to report on definitive values as soon as the necessary work can be completed.

In regard to Report B, it is only by fairly strict adherence to the principles (*a*) to (*c*) mentioned, that more or less serious ambiguities in the existing specifications of water vapor in the atmosphere may be removed. The specifications which have been adopted are therefore to be regarded as a self-consistent whole.

Values of Physical Functions and Constants (Report A)

This section contains a summary of the adopted values of constants and functions thought to be of interest to the air-conditioning engineer.

Temperature Scales. It was concluded that, in the range of interest to both the air-conditioning engineer and the meteorologist, the relation between the international and the thermodynamic centigrade scales of temperature is known with sufficient accuracy to justify adoption of the latter which is therefore the one intended when the symbol $t(°C)$ is used. The corresponding absolute temperature is: $T(°K) = t(°C) + T_0(°K)$. Conversion from thermodynamic centigrade to thermodynamic Fahrenheit temperature $t(°F)$ is to be made by means of the relation: $t(°F) = 1.8\ t(°C) + 32$. The corresponding absolute temperature (Rankine scale) is: $T(°R) = t(°F) + T_0(°R) - 32$. The recommended best value of the absolute ice-point temperature is

$$T_0 = 273.16 \pm 0.01\,°K = 491.688 \pm 0.018\,°R$$

Atmosphere. The Subcommission favored the following

definition of the standard atmosphere, namely, the pressure exerted by a column of mercury 76 cm high at 0°C and under a gravitational acceleration of 980.665 cm/sec². According to Birge[2] (1941) the best value of the density of mercury in such a column is 13.59504 g/cm³ which makes the atmosphere equal to 1,013,246 dyne/cm² or 1,013.246 millibars.

Dry Air. Table 1 gives the mol-fraction composition of dry air recommended by the Subcommission as valid from ground level up to about 25 km; it also gives the recommended values of the relevant molecular weights.

TABLE 1 DRY AIR

Constituent gas	Mol-fraction, per cent	Molecular weight (O = 16.0000)
Nitrogen (N_2)	78.09	28.016
Oxygen (O_2)	20.95	32.0000
Argon (A)	0.93	39.944
Carbon dioxide (CO_2)	0.03	44.010
Neon (Ne)	1.8×10^{-3}	20.183
Helium (He)	5.24×10^{-4}	4.003
Krypton (Kr)	1.0×10^{-4}	83.7
Hydrogen (H_2)	5.0×10^{-5}	2.0160
Xenon (Xe)	8.0×10^{-6}	131.3
Ozone (O_3)	1.0×10^{-6}	48.0000
Radon (Rn)	6.0×10^{-18}	222

There are quite wide fluctuations in the carbon-dioxide content of dry air near the earth's surface, but 0.03 per cent is a representative mean value for its mol-fraction. There are also variations in time and place of the ozone and radon contents of dry air, but these variations and those of carbon dioxide are of no direct thermodynamical significance, though they may be important in other (e.g., radiative) considerations. From the data listed in Table 1 it is easy to compute the apparent molecular weight of dry air, namely

$$M = 28.966.$$

To within the accuracy given, this figure would remain unchanged if only the first four constituent gases were included in the definition of dry air.

International Steam Tables Calorie. The Subcommission recommends that, when it is desired to express quantities of energy in calories rather than in ergs, preference be given to the International Steam Tables Calorie (IT cal) defined as $^1/_{860,000}$ mean international kilowatthour (kwhr). With the adopted conversion, 1 mean international kwhr = 1.00019 abs kwhr, it follows that

$$1 \text{ IT cal} = 4.18684 \times 10^7 \text{ erg}$$

$$1 \text{ erg} = 2.38844 \times 10^{-8} \text{ IT cal}$$

The 15° C water calorie is rendered redundant by the definition just given and is replaced by a specific heat of water to be determined experimentally in terms of the IT cal/g° K. Where, however, it is required to convert a quantity of energy which has been expressed in terms of the 15° C water calorie (cal_{15}), the following is the adopted conversion

$$1 \text{ IT cal} = 1.00032 \text{ cal}_{15}$$

The adoption of the IT cal will insure that meteorological and engineering specifications will in the future be identical.

Gas Constant. The recommended value of the "universal" gas constant is

$$R^* = 8.31436 \times 10^7 \text{ erg/mol° K} = 1.98583 \text{ IT cal/mol° K}$$

The corresponding value of the gas constant for "dry air" is

$$R = 2.8704 \times 10^6 \text{ erg/g° K} = 6.8557 \times 10^{-2} \text{ IT cal/g° K}$$

and that for "water vapor" is

$$R_v = 4.6150 \times 10^6 \text{ erg/g° K} = 1.10226 \times 10^{-1} \text{ IT cal/g° K}$$

since the molecular weight of water is

$$M_v = 18.0160 \text{ g/mol}$$

Compressibility Factor, Enthalpy, and Entropy of Dry Air. The compressibility factor $C_a(p, T)$ for dry air is defined by

$$p = C_a R \rho T$$

where ρ is the density of dry air at pressure p and temperature T.

The enthalpy residual Δh_a for dry air is defined by

$$h_a = \frac{7}{2} R(T - T_0) + \Delta h_a$$

where h_a is the specific enthalpy of dry air to which is arbitrarily assigned the value zero at 0° C and zero pressure.

The entropy residual Δs_a for dry air is defined by

$$s_a = \frac{7}{2} R \log_e (T/T_0) - R \log_e p + \Delta s_a$$

where s_a is the specific entropy of dry air. To the sum $s_a + R \log_e p$ (with pressure p expressed in millibars) is arbitrarily assigned the value zero at 0° C and zero pressure.

In the range, —100 to 60° C by 0 to 1100 millibars, the values of the compressibility factor C_a lies between 0.9956 and 1.0000; the enthalpy residual Δh_a lies between —0.14 and +0.05 IT cal/g; the entropy residual Δs_a lies between —0.00053 and +0.00023 IT cal/g° K. The Subcommission expects that these corrections may be disregarded in rough calculations.

Compressibility Factor, Enthalpy, and Entropy of Water Vapor. The compressibility factor $C_v(e, T)$ for water vapor is defined by

$$e = C_v R_v \rho_v T$$

where ρ_v is the density of water vapor at pressure e and temperature T.

The enthalpy residual Δh_v for water vapor is defined by

$$h_v = L_v(0) + 4R_v(T - T_0) + \Delta h_v$$

where h_v is the specific enthalpy of water vapor and $L_v(0)$, its latent heat of vaporization at 0° C (= 597.31 IT cal/g). The enthalpy residual Δh_v is arbitrarily assigned the value zero at 0° C and e = 6.1078 millibars, the saturation pressure of pure water at 0° C, in conformity with usual steam tables practice.

The entropy residual Δs_v for water vapor is defined by

$$s_v = L_v(0)/T_0 + 4R_v \log_e (T/T_0) - R_v \log_e [e/e_w(0)] + \Delta s_v$$

where s_v is the specific entropy of water vapor and $e_w(0)$ = 6.1078 millibars is its saturation pressure at 0° C. The entropy residual Δs_v is arbitrarily assigned the value zero at 0° C, and $e = e_w(0)$ in conformity with usual steam tables practice.

In the range, —100 to 60° C by 0 to 199.26 millibars (the saturation pressure at 60° C), the compressibility factor C_v lies between 0.9948 and 1.0000; the enthalpy residual Δh_v lies between —0.6 and +0.4 It cal/g; the entropy residual Δs_v lies between —0.0013 and +0.0013 IT cal/g° K. Again the Subcommission expects that these corrections may be disregarded in rough calculations.

Compressibility Factor, Enthalpy, and Entropy of Moist Air. The compressibility factor $C(p, T, r)$ for moist air at pressure p, temperature T, and mixing ratio r (mass of water vapor per unit mass of dry air) is defined by

$$p = C R \rho T_v$$

[2] "A New Table of Values of the General Physical Constants," by R. T. Birge, *Review of Modern Physics*, vol. 13, 1941, pp. 233–239.

where ρ is the density of moist air and T_v is its "virtual temperature" defined by

$$T_v = T\left(1 + 0.60779\,\frac{r}{1+r}\right)$$

where T is the humidity mixing rates, for whose definition see below.

The enthalpy residual Δh for moist air is defined by

$$h = r\,L_v(0) + \left(\frac{7}{2}\,R + 4r\,R_v\right)(T - T_0) + \Delta h$$

where h is the enthalpy of moist air "per unit mass of dry air."

The entropy residual Δs for moist air is defined by

$$s = r[Lv(0)/T_0 + R_v \log_e e_w(0)] + \left(\frac{7}{2}\,R + 4r\,R_v\right)\log_e (T/T_0) - (R + r\,R_v)\log_e p + s_m + \Delta s$$

where s is the entropy of moist air "per unit mass of dry air" and s_m is its mixing entropy (per unit mass of dry air) defined by

$$s_m = R[(r/\epsilon\,(\log_e (r/\epsilon) - (1 + r/\epsilon)\log_e (1 + r/\epsilon)]$$

with

$$\epsilon = 18.0160/28.966 = 0.62197$$

Saturation Vapor Pressure of Water Substance. (*a*) *Over water* (e_w) *from —50° C to 100° C* (vapor in pure phase over a plane surface of pure water): The adopted saturation vapor pressures are those given by the Goff-Gratch (1946) formula[3]

$$\log_{10} e_w = -7.90298\,(T_s/T - 1) + 5.02808\log_{10}(T_s/T) - 1.3816 \times 10^{-7}[10^{11.344\,(1-T/T_s)} - 1] + 8.1328 \times 10^{-3}[10^{-3.49149\,(T_s/T-1)} - 1] + \log_{10} e_{ws}$$

where T_s(steam-point absolute temperature) = 373.16° K = 671.688° R and e_{ws} = 1013.246 millibars (1 standard atmosphere). A tabulation of five-figure values of e_w in millibars (four-figure values for e_w less than 1 millibar) has been prepared from this formula for every 0.5° C between —50 and +60° C, and for every 1° F between —60 and +140° F. Both tabulations will be included in Report A.

It is to be noted that the use of the Goff-Gratch formula[3] at temperatures below 0° C represents an extrapolation outside the stated range of its validity. But the saturation vapor pressure of supercooled water is of great concern to the meteorologist, if not to the engineer, and in the absence of satisfactory experimental values the Goff-Gratch formula seemed to the Subcommission the best basis for computation. The adoption of —50° C as the lowest temperature for tabulation does not imply that an opinion is expressed on the lowest temperature at which supercooling may occur in the atmosphere.

(*b*) *Over Ice* (e_i) *From 0° C to — 100° C* (vapor in pure phase over plane surface of pure ice): The adopted saturation vapor pressures are those provided by the formula

$$\log_{10} e_i = -0.09718\,(T_0/T - 1) - 3.56654\log_{10}(T_0/T) + 0.876793\,(1 - T/T_0) + \log_{10} e_{i0}$$

where e_{i0} = 6.1071 millibars (0.0060273 standard atmospheres). This formula is an empirical re-expression of the Goff-Gratch (1946) formula for the saturation vapor pressure over ice and gives an average deviation of 0.002 per cent and a maximum deviation of 0.015 per cent from the Goff-Gratch values, deviations which are well within the estimated uncertainty of the values themselves. The merit of the foregoing empirical formula is that it is adapted for direct computation. A tabulation of four-figure values of e_i in millibars has been prepared from this formula for every 0.5° C between —100 and 0° C, and for every 1° F between —150 and 32° F. Both tabulations will be included in Report *A*.

Moist Air at Saturation. The partial pressure e of water vapor in a mixture of dry air and water vapor (moist air) is defined as equal to the product of the mol-fraction N_v and the observed pressure p of the mixture. It follows that

$$e = \frac{r}{0.62197 + r}\,p$$

For moist air at saturation the partial pressure e takes on the value e_w' (or e_i') which exceeds the saturation vapor pressure e_w (or e_i) of pure water (or ice) by the factor f_w (or f_i). Thus the mixing ratio of moist air at saturation is given by one or other of the following expressions

$$r_w = 0.62197\,\frac{f_w e_w}{p - f_w e_w};\quad r_i = 0.62197\,\frac{f_i e_i}{p - f_i e_i}$$

In the range, —50 to +60° C by 5 to 1100 millibars, the factor f_w lies between 1.0000 and 1.0065. In the range, —100 to 0° C by 5 to 1100 millibars, the factor f_i lies between 1.0000 and 1.0089. The Subcommission expects, therefore, that the actual departures from unity of these factors may be disregarded in rough calculations.

Definitions and Specifications of Water Vapor in the Atmosphere (Report B)

In this section are given the adopted specifications of water vapor in the atmosphere which are likely to be of interest to the air-conditioning engineer. They are in agreement with the recommendations of the Working Subcommittee of the International Joint Committee on Psychrometric Data, apart from the specification of thermodynamic wet-bulb temperature.

The Subcommission found it desirable to recommend that certain specifications which have been used in the past be discontinued on account of their ambiguity. These are *"absolute humidity"* and *"vapor density."* Supporting arguments for the adopted specifications are given in Report B. They are not reproduced in full here, but notes are added where desirable.

Humidity Mixing Ratio (*Mixing Ratio or Humidity Ratio*). The mixing ratio r of moist air is the ratio of the mass m_v of water vapor to the mass m_a of dry air with which the water vapor is associated, that is, $r = m_v/m_a$.

Vapor Concentration. The vapor concentration d_v of moist air is the ratio of the mass m_v of water vapor to the volume V occupied by the mixture, that is, $d_v = m_v/V$. This quantity has commonly been called absolute humidity or vapor density, but these terms should be discontinued as inappropriate methods of referring to the quantity in question.

Mol-Fraction of Water Vapor. The mol-fraction N_v of water vapor in moist air is the ratio of the number of mols of water vapor m_v/M_v to the total number, $m_a/M + m_v/M_v$, of mols of the mixture; it follows that

$$N_v = \frac{r}{0.62197 + r}$$

with $M_v/M = 18.0160/28.966 = 0.62197$.

Partial Pressure of Water Vapor. The partial pressure e of water vapor in moist air is the product of the mol-fraction N_v into the total pressure p; it follows that

[3] "Low Pressure Properties of Water From —160 to 212 F," by J. A. Goff and S. Gratch, Trans. American Society of Heating and Ventilating Engineers, vol. 52, 1946, pp. 95–121.

$$e = \frac{r}{0.62197 + r}\, p$$

Saturation and Saturation Mixing Ratio. Moist air at a given temperature T and total pressure p is said to be saturated if its composition is such that it can coexist in neutral equilibrium with a plane surface of pure condensed liquid (or solid) water[4] at the same temperature T and pressure p. The symbol r_w denotes saturation mixing ratio of moist air with respect to a plane surface of pure (liquid) water; the symbol r_i denotes saturation mixing ratio of moist air with respect to a plane surface of pure ice.

Saturation Vapor Pressure in Moist Air. The saturation vapor pressure with respect to water e_w' of moist air at pressure p and temperature T is

$$e_w' = \frac{r_w}{0.62197 + r_w}\, p = f_w e_w$$

Similarly, the saturation vapor pressure with respect to ice e_i' of moist air at pressure p and temperature T is

$$e_i' = \frac{r_i}{0.62197 + r_i}\, p = f_i e_i$$

Note that e_w' and e_i' differ by very small percentages in the meteorological range from the saturation vapor pressures e_w and e_i, respectively, in pure phase.

Thermodynamic Dew-Point and Frost-Point Temperatures. The thermodynamic dew-point temperature T_d of moist air at temperature T, pressure p, and mixing ratio r is the temperature to which the air must be cooled in order that it shall be saturated with respect to (liquid) water at the initial pressure p and mixing ratio r.

The thermodynamic frost-point temperature T_f of moist air at temperature T, pressure p, and mixing ratio r is the temperature to which the air must be cooled in order that it shall be saturated with respect to ice at the initial pressure p and mixing ratio r.

The dew-point and frost-point temperatures so defined are related to the mixing ratio r and the total pressure p by the respective equations

$$\left.\begin{array}{l} f_w(T_d,p) \cdot e_w(T_d) \\ \text{or} \\ f_i(T_f,p) \cdot e_i(T_f) \end{array}\right\} = \frac{r}{0.62197 + r}\, p$$

For most meteorological purposes adequate accuracy is obtained if the correction factors f_w and f_i are taken to have the value unity.

Relative Humidity. The relative humidity U (in per cent) of moist air is defined by

$$U = 100\,(r/r_w)$$

This definition makes relative humidity synonymous with "degree of saturation," the corresponding specification familiar to the air-conditioning engineer. It represents a distinct break with former practice in which it has been customary to define relative humidity in terms either of vapor pressure or vapor density. A number of cogent reasons for redefining relative humidity in terms of mixing ratio as noted are given in Report B.

The Subcommission recommends that relative humidity be evaluated with respect to supercooled water at temperatures below 0° C. The relative humidity with respect to ice of a given sample of air would of course be greater than this figure and would frequently exceed 100 per cent by a substantial amount, whereas appreciable supersaturation with respect to (supercooled) water is probably a rare event in the atmosphere. Further most instruments which are essentially responsive to relativ humidity, e.g., hair and goldbeaters' skin hygrometers, indicat relative humidity with respect to water below as well as abov 0°C. There are further reasons of a quite practical kind whic make the convention very desirable (c.f. Report B).

Thermodynamic Wet-Bulb Temperature. The thermodynami wet-bulb temperature T_w of moist air at pressure p, temperatur T, and mixing ratio r is the temperature which this air assume when water is introduced gradually by infinitesimal amounts a the current temperature T, and evaporated into the air by a adiabatic process at constant pressure until saturation is reached An approximate formula from which to calculate values of th thermodynamic wet-bulb temperature so defined is

$$\log \frac{L_v(T_w)}{L_v(T)} = \frac{c_{pv} - c_w}{c_{pv}} \log \frac{c_p + c_{pv}}{c_p + c_{pv} r_w(T_w)}$$

This in turn can be approximated by

$$(c_p + c_{pv} r)(T - T_w) = [r_w(T_w) - r]\, L_v(T_w)$$

In these approximate formulas, L_v is the latent heat of vaporization of water; c_p, c_{pv}, and c_w are the isobaric specific heats, assumed to be independent of temperature, of dry air, water vapor and liquid water, respectively.

The relationship between thermodynamic wet-bulb temperature T_w and the wet-bulb temperature indicated by a particular psychrometer is a matter to be determined by carefully controlled experiment, taking account of the various parameters concerned e.g., ventilation, size of thermometer bulb, radiation, etc.

In formulating the foregoing definition of thermodynamic wet-bulb temperature, the Subcommission realized that there might be grounds for preferring a definition which involved introducing the water into the system at a temperature other than the current temperature T, e.g., at T_w itself, as, it is now understood, is to be the recommendation of the Working Subcommittee of the International Joint Committee on Psychrometric Data. Possibly this one point of difference between the two bodies can be resolved at a later time.

Virtual Temperature. The virtual temperature T_v of moist air at temperature T, pressure p, and mixing ratio r, is the temperature which dry air[5] must have at pressure p in order to be of the same density as the moist air.[5] According to this definition, the virtual temperature increment for moist air at saturation is given by

$$(T_v - T)_w = 0.60779\, T\, \frac{r_w}{1 + r_w}$$

At relative humidity U (in per cent), but at the same temperature T and pressure p, the virtual temperature increment would be given by

$$T_v - T = (U/100)(T_v - T)_w + \frac{(U/100)(1 - U/100) r_w}{1 + (U/100) r_w} (T_v - T)_w$$

The Subcommission expects that the rightmost term in the equation immediately preceding may be disregarded in rough calculations. In the first of these equations, 0.60779 is written for the quantity, $M/M_v - 1$.

Aerological Functions and Tables (Report C)

It is not proposed to make a résumé here of the Subcommission's "Report on Aerological Functions and Tables." Functions

[4] Strictly speaking, pure water containing a small quantity of dissolved air.

[5] Assuming its compressibility factor C to be identically unity.

of the water-vapor content of the air, of interest to the air-conditioning engineer, have been dealt with in the previous sections and the existence of the report is thought to be sufficient notification in regard to the definition of other thermodynamic functions.

The tabulations of thermodynamic functions required by the meteorologist, and possibly of interest in the present context, have been specified in detail (ranges, intervals, etc.), in the original report; and the Conference of Directors of IMO has resolved that these tabulations, using the numerical values of physical functions and constants summarized in the section of this paper, "Values of Physical Functions and Constants," shall be prepared.

Acknowledgment

On behalf of the Aerological Commission of the International Meteorological Organization, the author takes this opportunity of expressing its gratitude to the University of Pennsylvania Thermodynamics Research Laboratory, and in particular to Dean John A. Goff and Mr. Serge Gratch of that institution, for the tremendous assistance which they have rendered the International Meteorological Organization and therefore meteorologists generally, in providing tabulations of some of the physical functions which have been dealt with, though not tabulated, in this paper. Most notably is gratitude due to the most complete and reliable tabulation of the saturation vapor pressures of water and ice which exists in meteorological literature.

Viscosity and Other Physical Properties of Gases and Gas Mixtures[1]

By J. O. HIRSCHFELDER,[2] R. B. BIRD,[2] AND ELLEN L. SPOTZ,[2] MADISON, WIS.

This paper is of special importance to the engineer because it is perhaps the first attempt to present directly a comprehensive review of the theoretical tools available for the calculation of the thermodynamic properties of gases and gas mixtures at finite, if only moderate pressures. The paper reviews a mass of information collected during the past two decades and shows the extent to which it can be correlated and systematized by means of molecular theory. The paper goes further to outline a new and apparently very successful method of formulating and predicting the viscosity and other transport properties of gases and gas mixtures at sufficiently low pressures. The method is the first significant practical improvement over the relatively crude one developed by Sutherland, and it is almost certain that engineers will find it extremely useful once they come to understand it. The extensive tables which are vital to the paper not only illustrate the method but implement it as well so that the user is enabled to calculate the viscosity and other transport properties of a large class of technically important gases and gas mixtures with very little labor.

THE viscosity, coefficients of diffusion, equation of state, and other physical properties of gases are intimately connected with the law of force between the individual molecules. By making the relationship between the physical properties and the intermolecular forces explicit, we can predict all sorts of phenomena under conditions where no experimental data exist. The power of this method depends upon the fact that the potential energy of interaction between molecules is independent of temperature. Furthermore, only two parameters, ϵ_m, the maximum energy of attraction, and r_0, the low-velocity collision diameter, serve adequately to describe the potential for a collision between two nonpolar gases. These can be determined with precision from the knowledge of the viscosity or second virial coefficients at two temperatures. For gaseous mixtures, the additional parameters can be obtained from measurements of diffusion at two temperatures; or if sufficient experimental data are not available, any or all of these parameters can be estimated from such properties as the critical temperature and density, the volume of the liquid, boiling point, etc.

The energy of interaction $\epsilon(r)$ between two simple molecules can be expressed in the form

$$\epsilon(r) = 4\epsilon_m[(r_0/r)^{12} - (r_0/r)^6] \quad \ldots\ldots\ldots\ldots [1]$$

Here r is the separation between the molecules. The significance of the parameters ϵ_m and r_0 is shown in Fig. 1. The potential-energy curves for a number of actual molecular species are shown in Fig. 2. The inverse sixth-power energy of attraction, $-4\epsilon_m(r_0/r)^6$, can be justified rigorously on the basis of an instantaneous dipole moment in one molecule inducing a dipole in a

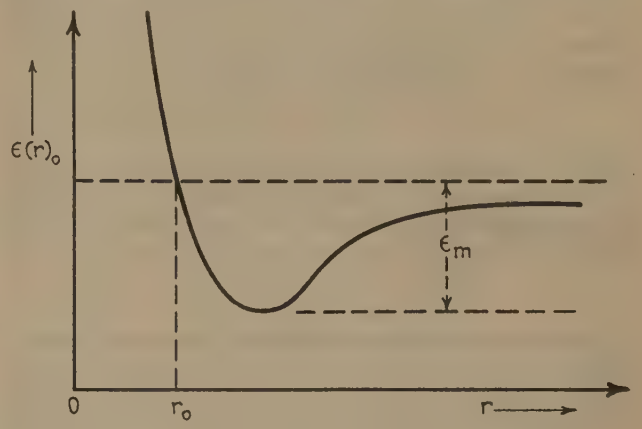

FIG. 1

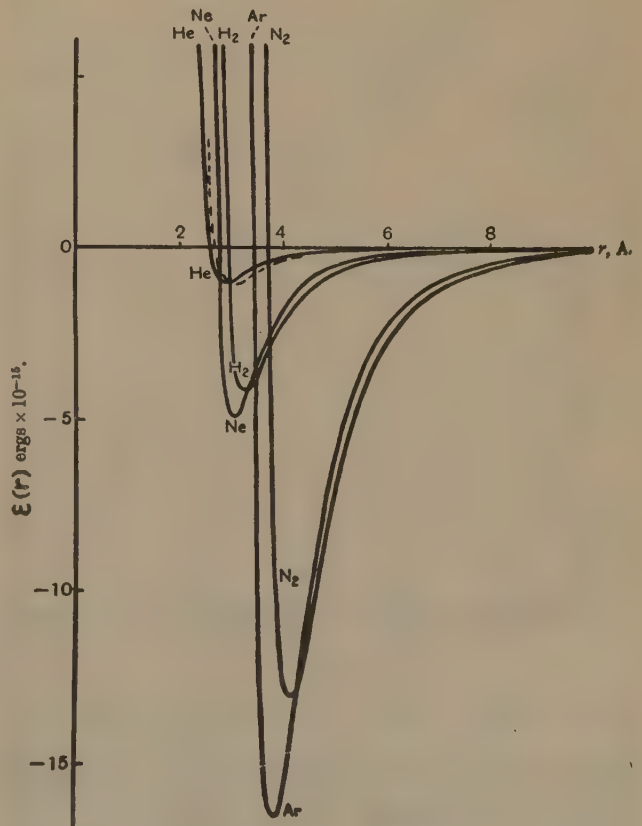

FIG. 2 POTENTIAL ENERGIES OF PAIRS OF INERT GAS ATOMS AS A FUNCTION OF THEIR DISTANCE APART

---

[1] This work was carried out under Contract NOrd 9938 with the Navy Bureau of Ordnance.

[2] University of Wisconsin, Naval Research Laboratory.

Contributed by the Research Committee on Properties of Gases and Gas Mixtures, the Applied Mechanics Division and the Heat Transfer Division, and Section M of the American Association for the Advancement of Science, and presented at the Annual Meeting, New York, N. Y., November 28–December 3, 1948, of THE AMERICAN SOCIETY OF MECHANICAL ENGINEERS.

NOTE: Statements and opinions advanced in papers are to be understood as individual expressions of their authors and not those of the Society. Paper No. 48—A-153.

second molecule and the two dipoles, the instantaneous and the induced, attracting one another. The inverse twelfth-power energy of repulsion, $4\epsilon_m(r_0/r)^{12}$, has no good theoretical foundation. Lennard-Jones (1)[3] and others have shown that it suffices to explain all of the available experimental second-virial-coefficient data. If the experimental data were accurate to 0.1 per cent rather than to 1 per cent, it is clear that a more accurate form for the energy of repulsion would be desired.

Second Virial Coefficients

The equation of state of gases at reasonably high temperatures or low pressure can always be written in the form

$$pV/RT = 1 + B(T)/V + C(T)/V^2 + \ldots\ldots\ldots [2]$$

Here $B(T)$, $C(T)$, etc., are functions of temperature but not of pressure or volume. From statistical mechanical considerations, Ursell (2) and Fowler (3) proved rigorously that

$$B(T) = 2\pi N \int^{\infty} r^2[1 - \exp(-\epsilon(r)/kT)]\,dr \ldots\ldots [3]$$

Here k is Boltzmann's constant and N is Avogadro's number. Substituting the potential energy of Equation [1] into Equation [3], Lennard-Jones (1) evaluated the integral explicitly in the form

$$B(T) = (2\pi/3)(Nr_0^3)F(\epsilon_m/kT)\ldots\ldots\ldots\ldots [4]$$

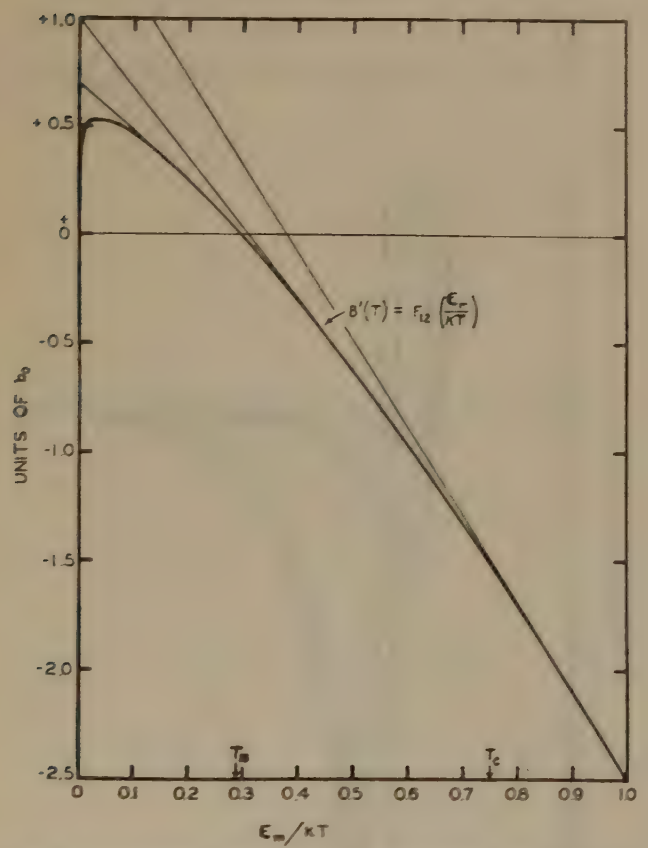

Fig. 3 Second Virial Coefficient as a Function of Temperature

The function $F(\epsilon_m/kT)$ is the function plotted (4) in Fig. 3, and presented (5) in Table 1. This table is very useful in predicting second virial coefficients once ϵ_m and r_0 are known.

[3] Numbers in parentheses refer to the Bibliography at the end of the paper.

It is interesting to examine $B(T)$ in terms of van der Waal a and b. First of all

$$b_0 = \left(\frac{2\pi N}{3}\right) r_0^3$$

is the van der Waal b for rigid molecules with a collision diameter, r_0. According to the van der Waal equation

$$B(T) = b - a/RT\ldots\ldots\ldots\ldots [5]$$

This would mean that $B(T)$ should be a straight line when plotted against $1/T$. The curvature of $B(T)$ indicates that a and b cannot be constants. Actually, they vary by as much as a factor of 2, depending on the exact temperature at which they are determined.

Stockmayer (6) showed that the energy of interaction between a pair of polar molecules can be expressed in the form

$$\epsilon(r) = 4\epsilon_m[(r_0/r)^{12} - (r_0/r)^6] - (p^2/r^3)[2\cos\theta_1\cos\theta_2 - \sin\theta_1\sin\theta_2\cos\omega]\ldots\ldots [6]$$

Here p is the dipole moment, while the θ's and ω describe the angles between the two dipoles. Using this potential, he integrated Equation [3], and letting $z = p^4/(\epsilon_m^2 r_0^6)$, he obtained

$$B(T) = b_0\{F(\epsilon_m/kT) + zH_{12}(\epsilon_m/kT) + z^2J_{12}(\epsilon_m/kT) + z^3K_{12}(\epsilon_m/kT) + z^4L_{12}(\epsilon_m/kT) + z^5M_{12}(\epsilon_m/kT) + z^6N_{12}(\epsilon_m/kT)\}\ldots\ldots [7]$$

The functions $H(\epsilon_m/kT)$, $J(\epsilon_m/kT)$, etc., are given in Table 2 (7). Fitting Equation [7] to experimental data gives the constants in Table 3.

For a gas mixture containing the mol-fractions x_i of the ith component

$$B(T) = \sum_{i,j} x_i x_j B_{ij}\ldots\ldots\ldots\ldots [8]$$

TABLE 1 SECOND VIRIAL COEFFICIENT

$$\frac{pV}{RT} = 1 + \frac{B}{V},\ B = b_0F,\ b_0 = \frac{2\pi}{3}Nr_0^3$$

$\frac{kT}{\epsilon}$	F	$\frac{kT}{\epsilon}$	F	$\frac{kT}{\epsilon}$	F
.30	-27.879	2.0	-.6277	5	.2435
.35	-18.754	2.1	-.5505	6	.3225
.40	-13.737	2.2	-.4820	7	.3764
.45	-10.756	2.3	-.4200	8	.4134
		2.4	-.3638	9	.4399
.50	- 8.7654				
.55	- 7.2743	2.5	-.3129	10	.4605
.60	- 6.1978	2.6	-.2664	20	.5254
.65	- 5.3677	2.7	-.2236	30	.5389
.70	- 4.7032	2.8	-.1845	40	.5186
.75	- 4.1796	2.9	-.1483	50	.5084
.80	- 3.7338			60	.4983
.85	- 3.3630	3.0	-.1150	70	.4887
.90	- 3.0474	3.1	-.0843	80	.4798
.95	- 2.7743	3.2	-.0559	90	.4716
		3.3	-.0298		
1.00	- 2.5386	3.4	-.0048	100	.4641
1.05	- 2.3300			200	.4114
1.10	- 2.1450	3.5	.0185	300	.3801
1.15	- 1.9812	3.6	.0403	400	.3647
1.20	- 1.8352	3.7	.0608		
1.25	- 1.7035	3.8	.0800		
1.30	- 1.5842	3.9	.0983		
1.35	- 1.4753				
1.40	- 1.3755	4.0	.1154		
1.45	- 1.2842	4.1	.1315		
		4.2	.1465		
1.50	- 1.2006	4.3	.1606		
1.55	- 1.1234	4.4	.1743		
1.60	- 1.0515				
1.65	- .9851	4.5	.1871		
1.70	- .9232	4.6	.1996		
1.75	- .8654	4.7	.2112		
1.80	- .8119	4.8	.2228		
1.85	- .7613	4.9	.2332		
1.90	- .7141				
1.95	- .6696				

TABLE 2

E_m/kT	$E_{12}(E_m/kT)$	$J_{12}(E_m/kT)$	$K_{12}(E_m/kT)$	$L_{12}(E_m/kT)$
.1225	-.0072	-.00001		
.1555	-.0113	-.00002		
.1936	-.0173	-.00004		
.2025	-.0189	-.00005		
.2500	-.0288	-.00011	$-.00 \times 10^{-4}$	$-.000 \times 10^{-5}$
.3025	-.0424	-.00023	$-.01 \times 10^{-4}$	$-.001 \times 10^{-5}$
.3600	-.0607	-.00045	$-.03 \times 10^{-4}$	$-.002 \times 10^{-5}$
.4900	-.1174	-.00152	$-.19 \times 10^{-4}$	$-.018 \times 10^{-5}$
.6400	-.2137	-.00453	$-.88 \times 10^{-4}$	$-.135 \times 10^{-5}$
.7225	-.2844	-.00758	-1.82×10^{-4}	$-.348 \times 10^{-5}$
.8100	-.3731	-.01237	-3.64×10^{-4}	$-.845 \times 10^{-5}$
1.0000	-.6324	-.03160	-13.85×10^{-4}	-4.698×10^{-5}

E_m/kT	$M_{12}(E_m/kT)$	$N_{12}(E_m/kT)$
.4900	$-.001 \times 10^{-6}$	
.6400	$-.017 \times 10^{-6}$	$-.02 \times 10^{-8}$
.7225	$-.052 \times 10^{-6}$	$-.06 \times 10^{-8}$
.8100	$-.151 \times 10^{-6}$	$-.22 \times 10^{-8}$
1.0000	-1.195×10^{-6}	-2.38×10^{-8}

TABLE 3 CONSTANTS FOR WATER AND AMMONIA

	ϵ_m/k	b_0(cm³/mole)	r_0(Å)	$z = \frac{p^4}{\epsilon_m^2 r_0^6}$
H_2O	363	23.62	2.655	12.74
NH_3	315	22.79	2.624	7.57

Here B_{ij} is the second virial coefficient which a gas would have if its energy of interaction were characteristic of the collisions between molecules of the ith and jth species. To a good approximation, and barring direct experimental evidence to the contrary, we can take for such a collision between unlike molecules the maximum energy of interaction equal to the geometrical mean of the pure components

$$(\epsilon_m)_{ij} = \sqrt{(\epsilon_m)_{ii}(\epsilon_m)_{jj}} \quad [9]$$

and the collision diameter is the arithmetical mean of the pure components

$$(r_0)_{ij} = [(r_0)_{ii} + (r_0)_{jj}]/2 \quad [10]$$

For the sake of simplicity, $(\epsilon_m)_{ij}$ and $(r_0)_{ij}$ will frequently appear as ϵ_{ij} and r_{ij}.

Often the mixture contains at least one polar component, and the question arises as to what to do about collisions between a polar molecule (designated by the subscript p) and a nonpolar molecule (designated by the subscript n). In this case, the energy of repulsion and the energy of attraction are of the normal nonpolar-nonpolar form except for a small angle dependent term in the energy of attraction due to the induction of a dipole in n by the permanent dipole in p

$$\frac{2\alpha_n p^2}{r^6}\sqrt{\frac{1+3\cos^2\theta}{4-3\cos^2\theta}} \quad [11]$$

Here α_n is the polarizability of n. London (8) has shown that this term is small compared to the normal energy of attraction, so that at all but the lowest temperatures, the orientational effect is small, i.e., the energy difference between different orientations is small compared with kT, so that we can make a spatial average of this extra term and obtain

$$1.75\alpha_n p^2/r^6 \quad [12]$$

The total energy of interaction between a polar and a nonpolar molecule has the same form as that between two nonpolar molecules as given in Equation [1]. The constants, $(\epsilon_m)_{np}$ and $(r_0)_{np}$, to be used in this equation can be determined from experimental diffusion or viscosity data for binary mixtures. However, if the experimental data are lacking, we would suggest using the following approximations (in keeping with the approximations of Equations [9] and [10] for nonpolar-nonpolar collisions)

$$(\epsilon_m)_{np} = \sqrt{(\epsilon_m)_{nn}(\epsilon_m)_{pp}}\left[1 + \frac{7}{16}\left(\frac{\alpha}{r_0^3}\right)_n\sqrt{\frac{z(\epsilon_m)_{pp}}{(\epsilon_m)_{nn}}}\right]^2 \quad [13]$$

$$(r_0)_{np} = \left[\frac{(r_0)_{nn} + (r_0)_{pp}}{2}\right]\left[1 + \frac{7}{16}\left(\frac{\alpha}{r_0^3}\right)_n\sqrt{\frac{z(\epsilon_m)_{pp}}{(\epsilon_m)_{nn}}}\right]^{-1/6} \quad [14]$$

Joule-Thomson Coefficient

The Joule-Thomson coefficient at low pressures μ_0, is simply related to the second virial coefficient

$$\mu_0 = \left[\frac{T^2}{R + C_v^0}\right]\frac{d}{dT}[B(T)/T] \quad [15]$$

Here R is the usual gas constant and C_v^0 is the specific heat at constant volume measured at low pressures. More conveniently

$$\mu_0 = \left[\frac{b_0}{R + C_v^0}\right]G(\epsilon_m/kT) \quad [16]$$

Here $G(\epsilon_m/kT)$ is a function given in Table 4. The accuracy of Equation [16] in predicting Joule-Thomson coefficients has been tested adequately for pure gases and mixtures (9) in much the same manner as has the second virial coefficient.

TABLE 4 JOULE-THOMSON FUNCTION, G

$$G = T^2\frac{d}{dT}(F/T) \text{ where } F = B/b_0$$

The Joule-Thomson coefficient, μ_0, at zero pressure is given by $\mu_0 = \left[\frac{b_0}{R + C_v^0}\right]G$

$$\mu = \frac{b_0 G}{C_p^0}$$

$\frac{kT}{\epsilon}$	G	$\frac{kT}{\epsilon}$	G	$\frac{kT}{\epsilon}$	G
.30	104.47	2.0	2.2572	5	.2489
.35	63.987	2.1	2.0781	6	.0610
.40	44.046	2.2	1.9180	7	-.0681
.45	32.758	2.3	1.7744	8	-.1614
		2.4	1.6450	9	-.2313
.50	25.637				
.55	20.848	2.5	1.5278	10	-.2852
.60	17.450	2.6	1.4211	20	-.4975
.65	14.911	2.7	1.3235	30	-.5444
.70	12.965	2.8	1.2339	40	-.5579
.75	11.434	2.9	1.1513	50	-.5600
.80	10.189			60	-.5576
.85	9.1668	3.0	1.0750	70	-.5532
.90	8.3100	3.1	1.0043	80	-.5479
.95	7.5897	3.2	.9387	90	-.5452
		3.3	.8776		
1.00	6.9663	3.4	.8207	100	-.5366
1.05	6.4268			200	-.4820
1.10	5.9555	3.5	.7674	300	-.4528
1.15	5.5408	3.6	.7176	400	-.4331
1.20	5.1728	3.7	.6707		
1.25	4.8440	3.8	.6267		
1.30	4.5476	3.9	.5852		
1.35	4.2802				
1.40	4.0420	4.0	.5461		
1.45	3.8166	4.1	.5089		
		4.2	.4738		
1.50	3.6146	4.3	.4405		
1.55	3.4291	4.4	.4089		
1.60	3.2577				
1.65	3.0992	4.5	.3788		
1.70	2.9523	4.6	.3503		
1.75	2.8158	4.7	.3232		
1.80	2.6887	4.8	.2972		
1.85	2.5701	4.9	.2725		
1.90	2.4591				
1.95	2.3550				

Outline of Derivation of Transport Properties

Viscosity, thermal conductivity, and diffusion are phenomena which represent transport of momentum, of energy, and of mass, respectively, and, accordingly, are called transport properties. Very simple relations may be obtained for these properties on the basis of elementary kinetic theory, but the results are untrustworthy because of the approximations used in the averaging processes.

Chapman and Cowling (10) have set forth a more rigorous treatment of the kinetic theory of gases, based on the work of Chapman, Enskog, Pidduck, and others. They have expressed the transport coefficients in terms of a set of collision integrals, which they call the $\Omega^{(l)}_{(r)}$. These integrals in turn are functions of the cross section. In simple kinetic theory, it is assumed that the cross sections are the same for all of the transport properties. But in Chapman and Cowling's fancy kinetic theory, there are different cross sections required for each of the different transport coefficients. When a law of force is assumed for the molecular interaction, it is possible to calculate the collision cross sections and all of the transport properties for gases and two-component mixtures from the collision integrals of Chapman and Cowling. In addition, these properties may be computed for multicomponent mixtures, using the recent formulations of Curtiss and Hirschfelder (11).

In the past the collision integrals have been evaluated only for several simple, nonrealistic laws of molecular interaction. We have succeeded in the difficult task of evaluating this set of integrals for the potential shown in Equation [1]. We shall discuss briefly the general mode of attack of the problem and mention some of the difficulties encountered. A comprehensive discussion of the detailed integrations and calculating methods employed is given in our recent publication on the transport properties (12).

The collision between two molecules is shown pictorially in Fig. 4. The only feature of the collision which affects the transport phenomena is the angle of deflection X. For the potential in Equation [1] it is not difficult to show that

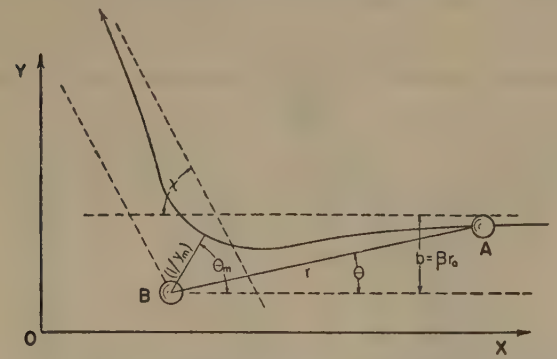

Fig. 4 Pictorial Representation of a Normal Molecular Encounter

$$X = \pi - 2\beta \int_0^{y_m} \frac{dy}{\sqrt{1 - \beta^2 y^2 + (4/K)(y^6 - y^{12})}} \quad [17]$$

in which K is the relative kinetic energy at large separation of the colliding molecules, along the line of centers, in units of ϵ; the other symbols are adequately described in Fig. 4. The evaluation of these angles of deflection for various values of K and β was made complicated by two facts, namely, (a) the integral in Equation [17] is an exceedingly complex hyperelliptic form and had to be tackled by numerical means, and (b) for certain low-energy collisions, orbiting of the two molecules about one another takes place as shown in Fig. 5. In spite of the apparent complexity of this problem, approximately 500 values of the angle of deflection were computed. These values were then used to get the several collision cross sections needed.

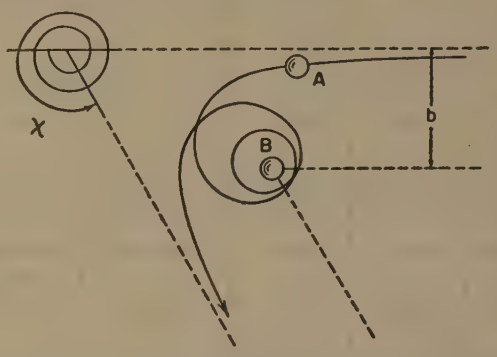

Fig. 5 Molecular Encounter Typical of Certain Low-Energy Collisions in Which Orbiting Takes Place at Distances of a Few Angstroms and Molecules Separate of Their Own Accord

The reduced collision cross sections, $S^{(l)}(K)$, were then determined by

$$S^{(l)}(K) = \frac{4}{\left[2 - \frac{1 + (-1)^l}{1 + l}\right]} \int_0^\infty [1 - \cos^{(l)} X]\beta d\beta \quad [18]$$

This integral was evaluated for $l = 1$, 2, and 4, the usual transport cross section corresponding to $l = 2$. For rigid spheres with collision diameter, r_0, the values of the cross sections would be unity.

Finally, the collision integrals, which we call $W^{(l)}(n; x)$ were evaluated. These are obtained from the expression

$$W^{(l)}(n; x) = \frac{1}{8}\left[2 - \frac{1 + (-1)^l}{1 + l}\right] x^{n+2} \int_0^\infty e^{-xK} K^{n+1} S^{(l)}(K) dK \quad [19]$$

in which

$$x = \epsilon/kT \quad [20]$$

k being Boltzmann's constant. The $W^{(l)}(n; x)$ are related to the $\Omega^{(l)}(n)$ of Chapman and Cowling by

$$\Omega^{(l)}(n) = r_0^2 \sqrt{\frac{2\pi kT}{\mu}}\, W^{(l)}(n; x) \quad [21]$$

The values of $W^{(l)}(n)$ for 84 values of kT/ϵ are presented in Table 5. In Equation [21], μ is the reduced mass of the colliding molecules

$$\mu = m_1 m_2/(m_1 + m_2) \quad [22]$$

Here the m_1 and the m_2 are the molecular weights of the colliding molecules divided by Avogadro's number.

The mechanical accuracy of the $W^{(l)}(n; x)$ is of the order of 1 part in 300, but there are certain physical limitations to their validity. Primarily, the calculations were made on the basis of classical mechanics; therefore it is to be expected that quantum corrections must be added at the lowest temperatures. Next, the form for the energy of interaction is substantially correct but not precisely accurate; for example, the energy of repulsion between helium atoms should increase less rapidly than the inverse twelfth power of the separation. Finally, all of the collisions are supposed to be elastic—an assumption which is valid for the noble gases but not altogether true for polyatomic molecules where the transfer of energy from translation to rotations and

TABLE 5 COLLISION INTEGRALS

$$\Omega^{(l)}(n) = r_0^2 \sqrt{\frac{2\pi kT}{\mu}}\, W^{(l)}(n), \quad \frac{kT}{\epsilon} = \frac{1}{x}$$

$\frac{kT}{\epsilon}$	$W^1(1)$	$W^1(2)$	$W^1(3)$	$W^2(2)$	$W^2(3)$	$W^2(4)$	$W^2(5)$	$W^2(6)$	$W^4(4)$
.3	1.331	3.384	11.77	2.785	10.14	46.66	258.3	1672.	61.36
.35	1.238	3.117	10.77	2.628	9.498	43.26	237.4	1528.	57.06
.4	1.159	2.896	9.976	2.492	8.927	40.32	220.0	1413.	53.36
.45	1.092	2.712	9.333	2.368	8.419	37.78	205.6	1322.	50.17
.5	1.033	2.557	8.809	2.257	7.968	35.62	193.7	1248.	47.41
.55	.9829	2.427	8.377	2.156	7.570	33.77	183.9	1189.	45.01
.6	.9383	2.315	8.016	2.065	7.222	32.19	175.6	1139.	42.92
.65	.8991	2.218	7.711	1.982	6.915	30.84	168.7	1098.	41.09
.7	.8644	2.135	7.452	1.908	6.645	29.67	162.9	1064.	39.49
.75	.8335	2.062	7.228	1.841	6.407	28.67	157.8	1034.	38.09
.8	.8058	1.998	7.033	1.780	6.195	27.78	153.4	1009.	36.83
.85	.7809	1.942	6.862	1.725	6.006	27.00	149.6	986.9	35.72
.9	.7585	1.892	6.711	1.675	5.838	26.32	146.3	967.5	34.73
.95	.7382	1.847	6.577	1.629	5.686	25.71	143.3	950.3	33.84
1.0	.7197	1.806	6.456	1.587	5.550	25.16	140.7	935.0	33.04
1.05	.7028	1.769	6.347	1.549	5.426	24.67	138.3	921.1	32.32
1.1	.6873	1.736	6.248	1.514	5.315	24.23	136.2	908.8	31.66
1.15	.6731	1.706	6.159	1.482	5.214	23.84	134.3	897.5	31.06
1.2	.6601	1.678	6.077	1.452	5.121	23.47	132.5	887.2	30.52
1.25	.6479	1.653	6.001	1.424	5.036	23.14	130.9	877.3	30.02
1.3	.6367	1.629	5.932	1.399	4.957	22.84	129.4	869.1	29.57
1.35	.6263	1.608	5.868	1.375	4.885	22.56	128.1	861.1	29.15
1.4	.6166	1.588	5.808	1.353	4.819	22.30	126.8	853.6	28.76
1.45	.6075	1.569	5.753	1.333	4.757	22.06	125.6	846.7	28.40
1.5	.5991	1.551	5.701	1.314	4.699	21.83	124.5	840.1	28.06
1.55	.5912	1.535	5.652	1.296	4.646	21.62	123.5	834.0	27.75
1.6	.5837	1.520	5.607	1.279	4.596	21.43	122.6	828.2	27.46
1.65	.5767	1.506	5.563	1.264	4.549	21.25	121.7	822.8	27.19
1.7	.5701	1.492	5.523	1.248	4.505	21.08	120.8	817.7	26.93
1.75	.5639	1.479	5.485	1.234	4.464	20.92	120.0	812.9	26.69
1.8	.5580	1.467	5.449	1.221	4.425	20.76	119.3	808.3	26.47
1.85	.5523	1.456	5.414	1.209	4.388	20.62	118.5	803.8	26.25
1.9	.5471	1.445	5.381	1.197	4.353	20.48	117.9	799.7	26.05
1.95	.5421	1.435	5.350	1.186	4.321	20.35	117.2	795.7	25.86
2.0	.5373	1.425	5.320	1.175	4.290	20.23	116.6	791.9	25.68
2.1	.5284	1.407	5.265	1.156	4.218	20.00	115.4	784.8	25.35
2.2	.5203	1.390	5.213	1.138	4.179	19.79	114.3	777.9	25.04
2.3	.5129	1.375	5.167	1.122	4.131	19.60	113.4	772.0	24.77
2.4	.5061	1.361	5.123	1.107	4.087	19.42	112.5	766.1	24.51
2.5	.4998	1.348	5.082	1.093	4.047	19.26	111.6	760.9	24.28
2.6	.4939	1.336	5.044	1.081	4.009	19.11	110.8	755.7	24.06
2.7	.4885	1.325	5.008	1.069	3.974	18.97	110.1	751.0	23.86
2.8	.4836	1.315	4.974	1.058	3.942	18.83	109.4	746.5	23.67
2.9	.4788	1.305	4.942	1.048	3.912	18.71	108.7	742.2	23.50
3.0	.4745	1.296	4.912	1.039	3.883	18.59	108.1	738.2	23.33
3.1	.4703	1.287	4.883	1.030	3.857	18.48	107.5	734.3	23.18
3.2	.4664	1.278	4.856	1.022	3.831	18.37	106.9	730.6	23.03
3.3	.4628	1.271	4.829	1.014	3.807	18.27	106.4	727.1	22.89
3.4	.4593	1.263	4.804	1.007	3.785	18.17	105.9	723.8	22.76
3.5	.4560	1.256	4.780	.9999	3.763	18.08	105.4	720.5	22.64
3.6	.4529	1.249	4.757	.9932	3.743	17.99	104.9	717.3	22.52
3.7	.4499	1.243	4.735	.9870	3.723	17.91	104.4	714.3	22.40
3.8	.4471	1.236	4.714	.9811	3.705	17.83	104.0	711.4	22.29
3.9	.4444	1.230	4.693	.9755	3.687	17.75	103.6	708.6	22.19
4.0	.4418	1.225	4.674	.9700	3.670	17.68	103.1	705.9	22.09
4.1	.4394	1.219	4.655	.9649	3.653	17.61	102.7	703.2	22.00
4.2	.4370	1.214	4.636	.9600	3.637	17.54	102.4	700.7	21.90
4.3	.4347	1.209	4.618	.9553	3.622	17.47	102.0	698.2	21.81
4.4	.4326	1.204	4.601	.9507	3.607	17.41	101.6	695.8	21.73
4.5	.4305	1.199	4.584	.9464	3.594	17.34	101.3	693.5	21.65
4.6	.4284	1.194	4.568	.9422	3.580	17.28	100.9	691.2	21.57
4.7	.4265	1.190	4.551	.9382	3.567	17.22	100.6	689.0	21.49
4.8	.4246	1.186	4.536	.9343	3.554	17.17	100.3	686.8	21.42
4.9	.4228	1.181	4.521	.9305	3.542	17.11	99.99	684.8	21.34
5.0	.4211	1.177	4.506	.9269	3.529	17.06	99.68	682.7	21.27
6	.4062	1.141	4.377	.8963	3.426	16.59	97.00	664.6	20.67
7	.3948	1.113	4.272	.8727	3.344	16.21	94.82	649.8	20.19
8	.3856	1.089	4.184	.8538	3.277	15.89	92.99	637.3	19.79
9	.3778	1.069	4.103	.8379	3.219	15.62	91.40	626.5	19.46
10	.3712	1.052	4.041	.8242	3.169	15.38	90.01	617.0	19.17
20	.3320	.9439	3.629	.7432	2.864	13.90	81.40	558.0	17.38
30	.3116	.8863	3.408	.7005	2.700	13.11	76.75	526.2	16.42
40	.2980	.8477	3.259	.6718	2.590	12.57	73.62	504.6	15.77
50	.2878	.8188	3.149	.6504	2.507	12.17	71.28	488.6	15.28
60	.2798	.7960	3.060	.6335	2.442	11.86	69.41	475.8	14.90
70	.2732	.7772	2.988	.6194	2.388	11.59	67.88	465.3	14.58
80	.2676	.7613	2.927	.6076	2.342	11.37	66.58	456.4	14.31
90	.2628	.7476	2.874	.5973	2.302	11.18	65.45	448.7	14.08
100	.2585	.7354	2.828	.5882	2.268	11.01	64.45	441.9	13.87
200	.2322	.6605	2.540	.5320	2.051	9.956	58.29	399.6	12.59
300	.2180	.6203	2.385	.5016	1.934	9.388	54.96	376.8	11.89
400	.2085	.5932	2.281	.4811	1.855	9.004	52.72	361.4	11.42

vibrations sometimes takes place. This latter effect is of considerable importance with respect to heat conductivity, but does not seem to affect viscosity.

There are several combinations of the various collision integrals which occur frequently enough to make it worth while to tabulate them for reference. In Table 6 are shown the viscosity correction factor V, and the thermal-conductivity correction factor H, which are complicated functions of the collision integrals. In

TABLE 6 VISCOSITY AND THERMAL-CONDUCTIVITY CORRECTION FACTORS

kT/	V	H
0.30	1.0014	1.0022
0.50	1.0002	1.0003
0.75	1.0000	1.0000
1.00	1.0000	1.0001
1.25	1.0001	1.0002
1.5	1.0004	1.0006
2.0	1.0014	1.0021
2.5	1.0025	1.0038
3.0	1.0034	1.0052
4.0	1.0049	1.0076
5.0	1.0058	1.0090
10.0	1.0075	1.0116
50.0	1.0079	1.0124
100.0	1.0080	1.0125
400.0	1.0080	1.0125

Table 7 are shown the three parameters, A, B, and C, which are quite useful in the study of mixtures; these are defined by

$$A = W^{(2)}(2)/[5W^{(1)}(1)] \quad [23]$$

$$B = [5W^{(1)}(2) - W^{(1)}(3)]/[5W^{(1)}(1)] \quad [24]$$

$$C = 2W^{(1)}(2)/[5W^{(1)}(1)] \quad [25]$$

All of the quantities necessary for the use of the equations for the transport coefficients are found in Tables 5, 6, and 7.

Determination of Intermolecular Force Constants

At the present time there is a decided dearth of accurate experimental data both for the transport properties and also for the determination of the second virial coefficients of simple gases and their mixtures. On this account, the values of ϵ and r_0 are by no means uniquely specified and must be altered as more precise experimental data become available. Not until more and better measurements have been obtained will it be reasonable to examine and interpret deviations of the actual energy of interaction from the form shown in Equation [1].

We have already discussed (12) the calculation of force constants between pairs of similar molecules from viscosity data for pure gases. In Table 8 are tabulated values of ϵ/k and r_0 so obtained. There are also shown some force constants which are estimated from critical and boiling-point data. These values were obtained using the approximate relations, which follow from the Lennard-Jones and Devonshire theory of gases and liquids (13)

$$\epsilon/k = 0.75\ T_c \quad [26]$$

$$\epsilon/k = 1.39\ T_b \quad [27]$$

$$r_0 = (8.33 \times 10^7)(V_c)^{1/3} \quad [28]$$

in which k is Boltzmann's constant; r_0 is the low-velocity collision diameter expressed in angstroms; T_c the critical temperature; V_c the critical volume in cubic centimeters; and T_b the boiling point. By means of these approximate relations it is possible to estimate the transport properties as well as the second virial coefficients without any direct experimental data.

TABLE 7 MIXTURES OF GASES

kT/ϵ	A	B	C
.3	.4185	.7739	1.017
.35	.4246	.7779	1.007
.4	.4300	.7772	.9995
.45	.4337	.7742	.9934
.5	.4370	.7698	.9901
.55	.4387	.765	.9877
.6	.4402	.759	.9869
.65	.4409	.752	.9868
.7	.4415	.746	.9880
.75	.4418	.740	.9896
.8	.4418	.734	.9918
.85	.4418	.729	.9947
.9	.4417	.725	.9978
.95	.4413	.720	1.001
1.00	.4410	.715	1.004
1.05	.4408	.711	1.007
1.10	.4406	.707	1.010
1.15	.4404	.705	1.014
1.20	.4399	.701	1.017
1.25	.4396	.696	1.021
1.30	.4395	.695	1.023
1.35	.4391	.694	1.027
1.40	.4389	.692	1.030
1.45	.4388	.689	1.033
1.50	.4387	.687	1.036
1.55	.4384	.684	1.039
1.60	.4382	.683	1.042
1.65	.4384	.682	1.045
1.70	.4378	.679	1.047
1.75	.4377	.677	1.049
1.80	.4376	.676	1.052
1.85	.4377	.676	1.054
1.90	.4376	.674	1.056
1.95	.4376	.673	1.059
2.00	.4374	.671	1.061
2.1	.4375	.670	1.065
2.2	.4374	.670	1.069
2.3	.4375	.666	1.072
2.4	.4375	.665	1.076
2.5	.4374	.664	1.079
2.6	.4377	.663	1.082
2.7	.4377	.662	1.085
2.8	.4376	.662	1.088
2.9	.4378	.661	1.090
3	.4379	.661	1.093
3.1	.4380	.660	1.095
3.2	.4383	.658	1.096
3.3	.4382	.659	1.099
3.4	.4385	.658	1.100
3.5	.4386	.658	1.102
3.6	.4386	.657	1.103
3.7	.4388	.658	1.105
3.8	.4389	.656	1.106
3.9	.4389	.656	1.107
4.0	.4391	.657	1.109
4.1	.4392	.655	1.110
4.2	.4393	.656	1.111
4.3	.4395	.656	1.112
4.4	.4395	.656	1.113
4.5	.4396	.656	1.114
4.6	.4398	.655	1.115
4.7	.4399	.656	1.116
4.8	.4400	.656	1.117
4.9	.4402	.655	1.117
5.0	.4402	.655	1.118
6	.4413	.656	1.125
7	.4421	.655	1.128
8	.4428	.657	1.131
9	.4435	.655	1.132
10	.4441	.657	1.134
20	.4477	.6569	1.137
30	.4496	.6569	1.138
40	.4508	.6574	1.138
50	.4520	.6567	1.138
60	.4528	.6569	1.138
70	.4535	.6574	1.138
80	.4540	.6573	1.138
90	.4546	.6575	1.138
100	.4551	.6569	1.138
200	.4582	.6568	1.138
300	.4602	.6573	1.138
400	.4615	.6571	1.138

The values given in Table 8, which are calculated from th viscosity data, should be quite good for those spherical nonpola gases whose interaction can be represented fairly well by th potential function mentioned. However, there are included i the table a number of gases which certainly do not meet thes qualifications. While we realize that the calculation of thes values is not strictly justified on the basis of the polarity and/o the nonspherical shape of many of the molecules listed, we hav set forth these force constants in the hope that they may be o some use in the estimation of the various transport propertie until the theory can be extended to include these special case Also, these figures give some qualitative ideas as to the size of th molecules and the strength of the interaction forces.

TABLE 8 FORCE CONSTANTS BETWEEN LIKE MOLECULES

Force Constants Determined from Viscosity Data			Reference for Viscosity Data	Force Constants Determined from 2nd Virial Coefficient		Reference for 2nd Virial Coefficient
Gas	ϵ/k (°K.)	r (Å)°		ϵ/k (°K.)	r (Å)°	
Air	97.0	3.617	a	99.2	3.522	c
H_2	33.3	2.968	a	37.02	2.92	d, e
N_2	91.46	3.681	a	95.9	3.72	f
CO_2	190.	3.996	a	185.	4.67	g
N_2O	220.	3.879	a	189.	4.59	g
NO	119.	3.470	a	131.	3.17	g
CH_4	136.5	3.882	a	142.7	3.81	g
O_2	113.2	3.433	a	117.5	3.58	f
CO	110.3	3.590	a	96.33	3.65	e
A	124.0	3.418	b	119.5	3.41	h
Ne	35.7	2.80	b	35.7	2.74	h
He	6.03	2.70	b	6.03	2.63	h

Notes to Table 8 (*left*)

(*a*) H. L. Johnston and K. E. McCloskey, *Journal of Physical Chemistry* vol. 44, 1939, p. 1038.
(*b*) H. L. Johnston and E. R. Grilly, *Journal of Physical Chemistry*, vol. 46, 1942, p. 948.
(*c*) L. Holborn and H. Schultze, *Annalen der Physik*, vol. 47, 1915, p. 1089.
(*d*) J. DeBoer and A. Michels, *Physica*, vol. 5, 1938, p. 945; vol. 6, 1939, p. 97.
(*e*) J. Corner, Proceedings of the Royal Society of London, vol. 58, 1946, p. 737.
(*f*) J. O. Hirschfelder and W. E. Roseveare, *Journal of Physical Chemistry*, vol. 43, 1939.
(*g*) J. O. Hirschfelder, F. T. McClure, C. F. Curtiss, and D. W. Osborne, NDRC-A116.
(*h*) R. A. Buckingham, Proceedings of the Royal Society of London, series A, vol. 168, 1938, p. 264.

TABLE 8(*a*) VISCOSITY, η
(In units 10^{-7} g/cm-sec)

T(°K)	Air ϵ/k=97.0 r_o=3.617		H_2 ϵ/k=33.3 r_o=2.968		N_2 ϵ/k=91.46 r_o=3.681		CO_2 ϵ/k=190 r_o=3.990		N_2O ϵ/k=220 r_o=3.879		NO ϵ/k=119 r_o=3.470	
	η_{exp}	η_{calc}	η_{exp}	η_{calc}	η_{exp}	η_{calc}	η_{exp}	η_{calc}	η_{exp}	η_{calc}	η_{exp}	η_{calc}
80												
100	713	702	421	416	698	687						
120	846	840	481	477	826	820					844	841
140	975	972	535	533	948	947					981	980
160	1101	1099	585	586	1068	1070					1115	1116
180	1221	1221	634	635	1183	1186			898	898	1245	1246
200	1336	1337	681	683	1295	1296	1015	1014	999	998	1371	1371
220	1448	1447	727	728	1403	1402	1112	1114	1099	1100	1493	1492
240	1556	1554	771	773	1505	1503	1209	1212	1198	1199	1610	1608
260	1659	1657	814	815	1603	1600	1303	1308	1296	1297	1711	1719
280	1756	1756	856	856	1696	1693	1400	1402	1393	1394	1838	1828
293.16	1819(b)	1819										
300	1851	1851	896	896	1786	1785	1495	1495	1489	1489	1934	1935
400	2294(d)	2290		1073		2202		1923				
500	2680(d)	2678		1237		2570		2309				
800	3613(d)	3680		1689	3493(d)	3528	3391(d)	3285				
1000	4165(d)	4257		1958	4011(d)	4068	3935(d)	3839				
1200	4631(d)	4761		2199	4452(d)	4554	4453(d)	4348				
1500	5262(d)	5494		2542	5050(d)	5268	5139(d)	5052				
5000		12080										
10000		18870										

T(°K)	CH_4 ϵ/k=136.5 r_o=3.822		O_2 ϵ/k=113.2 r_o=3.433		CO ϵ/k=110.3 r_o=3.590		Argon ϵ/k=124.0 r_o=3.418		Neon ϵ/k=35.7 r_o=2.80		Helium ϵ/k=6.03 r_o=2.70	
	η_{exp}(a)	η_{calc}	η_{exp}(a)	η_{calc}	η_{exp}(a)	η_{calc}	η_{exp}(c)	η_{calc}	η_{exp}(c)	η_{calc}	η_{exp}(c)	η_{calc}
80					533	523	688	649	1198	1212	821	827
100	403	393	768	757	669	657	839	814	1435	1451	947	957
120	478	472	917	910	796	788	993	979	1646	1665	1068	1086
140	560	553	1061	1059	919	916	1146	1142	1841	1867	1182	1197
160	629	630	1202	1203	1038	1040	1298	1300	2026	2054	1290	1305
180	703	707	1341	1342	1154	1160	1447	1454	2204	2231	1395	1413
200	778	780	1476	1474	1268	1274	1594	1601	2376	2396	1496	1509
220	850	852	1604	1602	1379	1384	1739	1744	2544	2558	1595	1605
240	919	921	1728	1726	1486	1489	1878	1882	2708	2713	1692	1700
260	986	987	1845	1845	1589	1591	2014	2014	2867	2862	1789	1789
280	1053	1052	1958	1959	1688	1689	2145	2143	3021	3008	1888	1877
300	1116	1116	2071	2070	1785	1784	2270	2269	3173	3149	1987	1964
400		1405		2578		2219						
500		1661		3031		2607						
800		2312	4115(e)	4183		3595	4621(d)	4641	5918(e)	5945	3840(e)	3665
1000		2687	4720(e)	4853		4168	5302(d)	5391	6800(e)	6872	4455(e)	4237
1200		3034		5457		4681	5947(d)	6083				
1500		3498		6264		5380	6778(d)	6983				

(*a*) H. L. Johnston and K. E. McCloskey, *Journal of Physical Chemistry*, vol. 44, 1939, p. 1038.
(*b*) J. A. Bearden, *Physical Review*, vol. 56, 1939, p. 1023.
(*c*) H. L. Johnston and E. R. Grilly, *Journal of Physical Chemistry*, vol. 46, 1942, p. 948.
(*d*) V. Vasilesco, *Annales de Physik* (Paris), series 11, vol. 20, 1945, p. 292.
(*e*) M. Trautz and R. Zink, *Annalen der Physik*, vol. 7, 1930, p. 427.

TABLE 9 FORCE CONSTANTS BETWEEN LIKE MOLECULES

Gas	r_0 (Å) from Viscosity Data	ϵ/k (°K) from Viscosity Data	ϵ/k (°K) from Boiling Point	ϵ/k (°K) from Critical Temp.	r_0 (Å) from Critical Volume	Reference for Viscosity Data
Xe	4.051	230	228	192	4.04	i
C_2N_2	4.38	339	352	301		i
AsH_3	4.06	281	303			i
CH_2Cl_2	4.759	406	435			j
Kr	3.61	190	169	158	3.96	i
Cl_2	4.115	357	332	313	4.15	j
Br_2	3.859	400	461	431		k
COS	4.13	335	310	284		i
I_2	4.982	550	637	620		j
CCl_4	5.881	327	487	417	5.42	i
HgI_2	5.625	698	872			j
$SnBr_4$	6.666	465	660			j
CS_2	4.438	488	445	410		p
$HgBr_2$	5.414	530	827			j
CH_3Cl	3.375	855	346	312	4.29	j
$CHCl_3$	5.430	327	581	402	5.11	i
HCl	3.305	360	261	243	3.69	m
SO_2	4.290	252	366	323	4.15	n
$SnCl_4$	4.540	1550	538	444	588	j
CH ≡ CH	4.221	185	263	232	4.02	l
$CH_2 = CH_2$	4.232	205	235	212	4.19	i
C_2H_6	4.418	230	257	229	4.36	i
C_3H_8	5.061	254	321	278		i
$n\text{-}C_4H_{10}$	4.997	410	379	320		l
$i\text{-}C_4H_{10}$	5.341	313	366	305		l
$n\text{-}C_5H_{12}$	5.769	345	431	353	5.64	p
$n\text{-}C_6H_{14}$	5.909	413	475	381	5.97	p
$n\text{-}C_8H_{18}$	7.451	320	555	427	6.56	i
$n\text{-}C_9H_{20}$	8.448	240	589			i
cyclo-C_6H_{12}	6.093	324	491	416	5.65	p
C_6H_6	5.270	440	491	442	5.30	i
CH_3OH	3.585	507	470	385	4.08	p
C_2H_5OH	4.455	391	489	387	4.59	p

(*i*) Landolt-Börnstein, *Physikalisch-Chemische Tabellen.*
(*j*) H. Braune, and R. Linke, *Zeitschrift für physikalische Chemie*, vol. A148, 1930, p. 195.
(*k*) A. O. Rankine. Proceedings of the Royal Society of London, vol. 88, 1913, p. 582.
(*l*) T. Titani, Bulletin of the Chemical Society of Japan, vol. 5, 1930, p. 98.
(*m*) M. Trautz and A. Narath, *Annalen der Physik*, vol. 79, 1926, p. 637.
(*n*) M. Trautz and R. Zink, *Annalen der Physik*, vol. 7, 1930, p. 427.
(*p*) T. Titani, Bulletin of the Chemical Society of Japan, vol. 8, 1933, p. 255.

The force constants determined from viscosity seem unreasonable for CCl_4, $SnBr_4$, $SnCl_4$, CH_2Cl, CS_2, HgI_2, and $HgBr_2$. In the case of the tetrahalides, this is somewhat surprising because of their symmetric nature. The carbon disulphide discrepancy can be due to its cigar shape. The mercury halides are quite polar.

For example, the ϵ/k value for stannic chloride, which was calculated from viscosity data, is far greater than that estimated from the formulas in Equations [26] and [27]. This discrepancy might suggest that stannic-chloride molecules are associated in the vapor phase or might be polar. Joel Hildebrand suggests that the chlorine atoms might stand out from the central tin atom like the quills of a porcupine. As a result, there is a large interchange of energy between translation and rotation during collisions. Chapman and Cowling show that the viscosity for such "perfectly rough" spheres may be anomalously large by as much as 14 per cent.

TABLE 10 FORCE CONSTANTS BETWEEN UNLIKE MOLECULE

Gas Pair	Experimental D_{12} Measurement (cm^2 sec^{-1})	Temp. for D_{12} (°K.)	Arithmetic Mean r_{12} from Viscosity (Å)	Geometric Mean ϵ_{12}/k from Viscosity (°K.)	ϵ_{12}/k from D_{12} (°K.)	ϵ_{12}/k from Binary Viscosities (°K.)	Reference for D_{12} data
He - A	0.641	273.2	3.059	27.3	24.5	30.1	(a)
H_2 - O_2	0.697	273.2	3.201	61.4	58.2	59.8	(a)
H_2 - N_2	0.674	273.2	3.325	55.2	47.8	60.4	(a)
	0.743	288.2			46.1		(b)
	0.76	293.2			47.7		(c)
H_2 - CH_4	0.625	273.2	3.395	67.4	63.8	53.6	(a)
O_2 - N_2	0.181	273.2	3.557	102.	90.7	98.5	(a)
	0.22	293.2			67.7		(c)
O_2 - CO	0.185	273.2	3.512	112.	91.9	116.	(a)
CO - N_2	0.192	273.2	3.636	100.	68.2	104.	(a)
CO_2 - N_2O	0.096	273.2	3.938	204.	163.	190.	(a)
H_2 - CO	0.651	273.2	3.279	60.6	65.0		(a)
H_2 - CO_2	0.550	273.2	3.482	79.5	76.0		(a)
	0.619	288.2			63.8		(b)
	0.60	293.2			88.4		(c)
H_2 - N_2O	0.535	273.2	3.424	85.6	96.2		(a)
O_2 - CO_2	0.139	273.2	3.715	147.	115.		(a)
	0.16	293.2			110.		(c)
CO - CO_2	0.137	273.2	3.793	145.	120.		(a)
CO_2 - N_2	0.144	273.2	3.839	132.	93.3		(a)
	0.158	288.2			93.9		(b)
	0.16	293.2			100.		(c)
CO_2 - CH_4	0.153	273.2	3.909	161.	126.		(a)
H_2 - A	0.77	293.2	3.193	64.3	64.1		(c)
A - N_2	0.20	293.2	3.550	107.	83.8		(c)
A - O_2	0.20	293.2	3.426	119.	95.2		(c)
A - CO_2	0.14	293.2	3.707	154.	142.		(c)
He - Ne			2.75	14.7		12.7	
Ne - A			3.11	66.5		68.9	

(*a*) "Mathematical Theory of Non-Uniform Gases," by S. Chapman and T. G. Cowling, Cambridge University Press, Teddington, England, 1939.
(*b*) L. E. Boardman and N. E. Wild, Proceedings of the Royal Society of London, series A, vol. 162, 1937, p. 511.
(*c*) L. Waldman, *Naturwissenschaften*, vol. 32, 1944, p. 223.

It is not surprising that the force constants for the hydrocarbons do not behave properly. In order to fit their second virial coefficients, it is necessary to use a form for the intermolecular energy involving three adjustable constants rather than two (7). We are trying to evaluate the collision integrals for this three-constant model and hope that it will prove suitable for the hydrocarbons.

There are some substances for which our force constants could not be obtained from the experimental viscosity data. They are listed in Table 11, together with their Sutherland constant and the temperature index of their viscosity. For these substances there is no possible choice of ϵ/k and r_0 which would lead to the observed temperature dependence. Obviously, our simple model of the intermolecular potential (designed for spherical nonpolar molecules) does not apply in these cases. These molecules fall into the following classes:

(*a*) *Polar Molecules:* H_2O, NH_3, HBr, HCN, HI, $HgCl_2$. The energy of interaction of polar molecules is quite different from that of nonpolar molecules. Stockmayer (6) has considered the interaction of two polar spherical molecules. He finds that in addition to the interaction energy which we have assumed, Equation [1], there is a term proportional to the product of the dipole moments, inversely proportional to the cube of the separation, and dependent on the orientation of the molecules. With this Stockmayer potential it is possible to fit the second virial coefficients for simple polar molecules with high precision. In order to predict the transport properties for polar molecules, the collision integrals should be evaluated for this same potential. The work involved is stupendous, but sooner or later it will have to be done.

TABLE 11 VISCOSITY OF ANOMALOUS GASES

$$\eta \times 10^7 = c'T^s$$
$$\eta \times 10^7 = k_S T^{1/2}/[1 + (S/T)]$$

Gas	Temperature Range (°K.)	c'	s	k_S	S	(S/T) Sutherland Constant divided by Temperature in Middle of Range	Reference for Viscosity Data
H_2O	300 - 400	2.039	1.079	140.2	459.4	1.313	(a)
	500 - 600	1.227	1.164	235.8	1051.	1.911	
	600 - 700	1.598	1.123	244.4	1108.	1.705	
NH_3	300 - 400	1.203	1.181	202.7	740.7	2.116	(a)
	500 - 600	2.576	1.053	189.4	684.3	1.244	
	600 - 700	5.207	.9427	164.7	518.7	.7980	
HI	300 - 400	6.889	.9837	221.9	312.9	.8940	(b)
	400 - 500	10.42	.9152	229.4	334.4	.7431	
HBr	300 - 400	5.004	1.040	245.3	376.2	1.075	(a)
HCN	300 - 400	.7443	1.215	166.3	836.2	2.389	(a)
	500 - 600	1.131	1.144	185.4	999.1	1.817	
$HgCl_2$	500 - 600	1.521	1.180	351.6	1191.	2.165	(a)
	600 - 700	4.841	1.000	248.1	656.5	1.010	
	750 - 850	3.406	1.057	314.1	982.8	1.229	
Zn	850 - 920	1.384	1.237	757.1	2374.	2.682	(b)
	920 - 950	18.68	.8554	338.9	557.0	.5957	
Cd	750 - 850	5.390	1.048	475.5	1011.	1.264	(b)
	850 - 900	9.836	.9592	406.0	734.2	.8391	
Hg	500 - 600	7.488	1.039	486.1	640.1	1.164	(b)
	700 - 800	8.793	1.018	552.0	776.4	1.035	
	800 - 900	8.827	1.018	595.7	892.6	1.050	
n - C_7H_{16}	350 - 450	2.163	.9789	72.73	363.2	.9080	(b)
	450 - 550	.6715	1.172	133.1	1022.	2.044	
F_2	50 - 150	3.237	1.170	244.7	246.9	2.469	(c)
	200 - 300	13.52	.8793	170.7	139.3	.5572	

(a) H. Braune and R. Linke, *Zeitschrift für physikalische Chemie*, vol. A148, 1930, p. 195.
(b) "Physikalisch—Chemische Tabellen," by Landolt-Börnstein.
(c) E. Kanda, Bulletin of the Chemical Society of Japan, vol. 12, 1937, p. 463.

The energy of interaction between polar and nonpolar molecules is of the same form as the energy of interaction between two nonpolar molecules. It is a surprising fact that the effect of the permanent dipole moment of the polar molecule is negligible in attracting the nonpolar molecule (8). However, on this account we can treat such collisions as though they were between two nonpolar molecules.

(*b*) *Metal Vapors and Valence Unsaturated Molecules:* Hg, Cd, and Zn. Valence unsaturated molecules behave in a rather anomalous fashion. Sometimes their collisions follow one potential-energy curve and sometimes another. At large separations their van der Waal energy of attraction is perfectly normal. However, at shorter distances the energy of interaction depends very largely on the particular electronic state, which corresponds to the collision complex. According to quantum mechanics, there are well-defined a priori probabilities that a collision will result in a particular electronic state.

The collision between two hydrogen atoms should serve to clarify this complicated situation. At large separations, the van der Waal energy of attraction is perfectly normal. However, at shorter distances the energy of interaction depends upon the spin orientations of the atoms (and the electronic state is determined by the spin orientations). In an arbitrary collision between two hydrogen atoms there is a chance of one in four that the collision will correspond to a singlet electronic state, and a chance of three in four that the system will be in a triplet electronic state. The singlet corresponds to the normal H_2 molecule and has the force constants $\epsilon/k = 51{,}000$ deg K and $r_0 = 0.5$ Å. The triplet state corresponds to the lowest excited state of the hydrogen molecule—a state in which the molecules repel each other except at the largest separations. The triplet state has the force constants (14), $\epsilon/k = 3.8$ deg K and $r_0 = 3.5$ Å. Thus in collisions between hydrogen atoms, it is expected that one in four collisions will follow the potential curve corresponding to $\epsilon/k = 51{,}000$ deg K and $r_0 = 0.5$ Å, while the other three out of four collisions will follow the potential curve corresponding to $\epsilon/k = 3.8$ deg K and $r_0 = 3.5$ Å.

The metallic vapors Hg, Cd, and Zn, are not valence saturated, and it is to be expected that their collisions should be anomalous in the same sense as the hydrogen atoms. These metal-vapor atoms are initially in the $^1S_0$ state, but their valence electrons are easily promoted during the course of collisions.

Hildebrand, Wakeham, and Boyd (15) have determined the interaction potential between mercury atoms from a study of the experimental Menke distribution function for liquid mercury. They found that the mercury atoms are so "squishy" that it is necessary to use the inverse ninth rather than the inverse twelfth power to describe their energy of repulsion. This use of the smaller power might correspond to our view that collisions between mercury atoms are a statistical mixture of two sorts—

those with large ϵ/k and small r_0 (corresponding to the ground state of Hg_2) and those with small ϵ/k and large r_0 (corresponding to an excited state of Hg_2). If we try to fit Hildebrand, Wakeham, and Boyd's potential with an inverse twelfth power, we obtain the force constants, $\epsilon/k = 1522$ and $r_0 = 2.5$ Å. If we insert these force constants into Equation [29], we calculate values for the viscosity of mercury as shown in Table 12. There is a considerable discrepancy between the calculated and the observed values of the viscosity. It will be interesting to find out whether this discrepancy is due to the two types of collisions or just to the natural "squishiness" of these particular atoms.

TABLE 12 VISCOSITY OF MERCURY

T, (°K)	$\eta \times 10^7$ (calc)	$\eta \times 10^7$ (exptl)*
452	4945	4709
603	5943	5831
769	7166	7610
983	8552	8802

* Landolt-Börnstein, "Physikalische-Chemische Tabellen."

(*c*) *Cigar-Shaped Molecules:* *n*-Heptane. The transport properties are not very sensitive to the shape of the molecules. However, if the ratio of the length to the diameter becomes too great, all of the physical properties are affected. Thus the temperature dependence of the viscosity of *n*-Heptane is greater than would be expected for spherical molecules.

(*d*) *Fluorine.* We cannot guess why the temperature dependence of the viscosity of F_2 should be anomalous. Perhaps the experimental data should be checked. If they are substantiated, we would have to conclude that the forces between two fluorine molecules are of a different nature from those for any of the other halogens. This should have a bearing on fluorine chemistry.

The force constants between pairs of dissimilar molecules could very easily be calculated from the coefficient of diffusion as a function of temperature, if these data were available. The expression for the coefficient of diffusion is independent of the force constants for the individual components, and hence this particular transport property is exceedingly well adapted to the calculation of the ϵ_{12} and r_{12} for pairs of unlike molecules. The International Critical Tables give values of the diffusion constant for a number of pairs of gases at a single temperature. Using these figures and making the fairly reasonable assumption that the collision diameter r_{12} is given by

$$r_{12} = (r_1 + r_2)/2$$

(here r_1 and r_2 are the individual collision diameters), we have calculated the values of ϵ_{12}/k for these molecule pairs. These results are displayed in Table 10. It will be noticed that in many cases the values of ϵ_{12}/k can be fairly well approximated by the geometric mean of the ϵ_1/k and ϵ_2/k for the components involved. The values of ϵ_{12}/k, determined from diffusion coefficients, lead to values of the viscosity of mixtures which agree well with experimental data.

In Table 10 we have omitted the consideration of D_{12} for D_2 diffusing through H_2. The recent value of D_{12} given by Waldman (16) agrees perfectly with our expectation on the basis of the force constants already obtained from the viscosity of H_2. An older experimental value of D_{12} quoted by Chapman and Cowling was considerably in error.

Coefficient of Viscosity

In this and the following sections, the formulas for the various transport properties will be set forth, and their application will be discussed. The formulas for the transport coefficients are essentially those of Chapman and Cowling (10) and are written here for convenience in terms of the transport integrals which are given in Table 5.

The coefficient of viscosity for a single gas is given by the relation

$$\eta \times 10^7 = 266.93(MT)^{1/2}[r_0]^{-2}(V)/[W^{(2)}(2)] \quad [29]$$

where M is the molecular weight; T the temperature in degrees K; r_0 the low-energy collision diameter expressed in angstroms; and V and $W^{(2)}(2)$ are slowly varying functions of kT/ϵ given in Table 6. To obtain the intermolecular force constants Equation [29] is simply written for values of viscosities at two temperatures, the resulting two equations then being solved simultaneously for r_0 and ϵ. In Table 8(*a*) are shown the experimental data from which the force constants were determined along with the corresponding calculated values of the viscosity.

The temperature dependence of viscosity is often expressed in terms of a Sutherland constant, S

$$\eta \times 10^7 = k_s T^{1/2}/[1 + (S/T)] \quad [30]$$

Both k_S and S are supposed to be constants characteristic of the gas. Unfortunately, our relations show that this cannot be true over any large temperature range. If we require that at a particular temperature η and $d\eta/dT$ as determined from Equation [30] agree with that determined from Equation [29], S/T is obtained as a function of kT/ϵ tabulated in Table 13. This result is useful, since ϵ/k can be determined immediately from this table. The double values of $\epsilon/(kT)$ for a given value of S need cause no concern, since we usually know whether a gas is above or below the critical point, i.e., $\epsilon/kT_c = 0.75$.

Viscosity may also be expressed in terms of a temperature index, s

$$\eta \times 10^7 = c'T^s \quad [31]$$

where the exponent s, may be determined as a function of $\epsilon/(kT)$ in a method similar to that used for the Sutherland constant. Values of s so determined are shown in Table 13.

TABLE 13 TEMPERATURE DEPENDENCE OF SUTHERLAND'S CONSTANT AND THE TEMPERATURE EXPONENT, s

$\eta = k_S T^{1/2}/[1 + (S/T)]$
$\eta = c'T^s$

kT/ϵ	S/T	s
0.30	0.5538	0.8564
0.50	0.8786	0.9677
0.75	1.083	1.0200
1.00	1.012	1.0030
1.25	0.8660	0.9641
1.50	0.7443	0.9267
2.00	0.5466	0.8534
2.50	0.4331	0.8022
3	0.3669	0.7684
4	0.2829	0.7205
5	0.2453	0.6970
10	0.1857	0.6566
50	0.1697	0.6451
100	0.1681	0.6439
400	0.1680	0.6438

For the binary mixture, the formula for the first approximation to the viscosity already has become rather complicated

$$\eta_{12} \times 10^7 = \frac{R_1 + R_2 + R_3 + (E/H_1) + (E/H_2)}{(R_1/H_1) + (R_2/H_2) + (E/H_1H_2) + (R_4/E)} \quad [32]$$

in which

$$R_1 = (x_1/x_2)(2/3 + AM_1/M_2) \quad [33]$$

$$R_2 = (x_2/x_1)(2/3 + AM_2/M_1) \quad [34]$$

$$R_3 = 2[(2/3) - A] \quad [35]$$

$$R_4 = 2A(M_1 + M_2)^2/3M_1M_2 \quad [36]$$

$$H_i = 266.93(M_iT)^{1/2}(r_i)^{-2}/[W^{(2)}(2;\ kT/\epsilon_i)],\ (i = 1, 2) \quad [37]$$

$$E = 37.75[(M_1 + M_2)^3T/(M_1M_2)]^{1/2}(r_{12})^{-2}/[W^{(1)}(1; kT/\epsilon_{12})] \quad [38]$$

Here x_i is the mol-fraction of the ith component; M_i is the molecular weight of the ith component; the r_i and r_{12} are the low-velocity collision diameters measured in angstroms; A is a function of the collision integrals and is tabulated as a function of kT/ϵ in our previous paper (12). The H_i are simply the first approximations to the viscosity of the ith component.

Using the force constants between like molecules which were determined from viscosity data and those between dissimilar molecules which were determined from diffusion, we have calculated the viscosity of several binary mixtures.[4] The results of these calculations are shown in Table 14(a) along with experimental figures. It will be observed that the agreement is excellent in most cases. This is a nice illustration of the use of force constants obtained from one transport property in the calculation of another of the transport coefficients.

The viscosity of multicomponent gas mixtures has been worked out by C. F. Curtiss and J. O. Hirschfelder (11). For a mixture of f components, the generalized viscosity may be expressed as follows

$$\eta_{123\ldots f} \times 10^7 = \frac{-\begin{vmatrix} J_{11} & J_{12} & J_{13} & \cdots & J_{1f} & 1 \\ J_{12} & J_{22} & J_{23} & \cdots & J_{2f} & 1 \\ J_{13} & J_{23} & J_{33} & \cdots & J_{3f} & 1 \\ \cdot & \cdot & \cdot & \cdots & \cdot & \cdot \\ \cdot & \cdot & \cdot & \cdots & \cdot & \cdot \\ \cdot & \cdot & \cdot & \cdots & \cdot & \cdot \\ J_{1f} & J_{2f} & J_{3f} & \cdots & J_{ff} & 1 \\ 1 & 1 & 1 & \cdots & 1 & 0 \end{vmatrix}}{|J_{ij}|} \quad \ldots\ldots [39]$$

in which $|J_{ij}|$ is the fth-order determinant of the J_{ij}, the J_{ij} (for $i \neq j$) and J_{ii} being given by

$$J_{ij} = -A_{ij} + B_{ij} \quad [40]$$

$$J_{ii} = -A_{ii} + B_{ii} + \sum_{k=1}^{f}(x_k/x_i)(A_{ik} + B_{ik}M_k/M_i) \quad [41]$$

and the A_{ij} and B_{ij} are defined as

$$A_{ij} = (0.017663)T^{-1/2}[r_{ij}]^2[W^{(1)}(1;\ kT/\epsilon_{ij})] \times [M_iM_j/(M_i + M_j)^3]^{1/2} \quad [42]$$

$$B_{ij} = (0.0052988)T^{-1/2}[r_{ij}]^2W^{(2)}(2;\ kT/\epsilon_{ij})] \times [M_iM_j/(M_i + M_j)^3]^{1/2} \quad [43]$$

In Table 15 are shown some experimental figures for the viscosity of a helium-neon-argon mixture; along with these data are given the calculated results obtained by using Equation [39], letting $f = 3$. The force constants between like molecules which

[4] The diffusion data used to get the ϵ_{12}/k are those values tabulated in Chapman and Cowling (10). The experimental figures listed are from Landolt-Börnstein with the exception of the H_2 — N_2 data, which came from A. van Itterbeek, O. van Paemel, and J. van Lierde (17).

TABLE 14(a) VISCOSITY OF BINARY MIXTURES

Viscosity H_2 - CO_2						
T(°K)	%H_2	0.0	19.93	41.29	78.50	100.0
300	EX*	1493	1501	1506	1370	891
	CG*	1493	1507	1508	1372	889
	CD*	1493	1509	1512	1379	889
400	EX	1944	1945	1933	1713	1081
	CG	1920	1926	1913	1698	1065
	CD	1920	1928	1918	1703	1065
500	EX	2353	2358	2321	2026	1256
	CG	2301	2302	2275	1990	1228
	CD	2301	2303	2280	1998	1228
550	EX	55567	2542	2506	2173	1341
	CG	2479	2478	2445	2130	1308
	CD	2479	2479	2450	2137	1308

Viscosity H_2 - O_2						
	%H_2	0.0	18.35	39.45	60.30	78.08	100.0
		2057	2019	1925	1784	1494	889
		2064	2021	1934	1774	1524	889
		2064	2024	1939	1782	1531	889
		2568	2507	2381	2192	1858	1087
		2567	2506	2388	2178	1857	1065
		2567	2509	2394	2186	1865	1065
		3017	2950	2790	2556	2158	1259
		3015	2940	2795	2541	2158	1228
		3015	2943	2802	2551	2168	1228
		3220	3147	2978	2733	2288	1381
		3224	3140	2986	2714	2302	1308
		3224	3146	2993	2721	2313	1308

Viscosity CO_2 - N_2O						
	%CO_2	0.0	40.24	60.33	80.97	100.0
		1488	1494	1495	1490	1493
		1489	1497	1498	1496	1493
		1489	1523	1524	1513	1493
		1493?	1950	1950	1941	1944
		1936	1938	1934	1928	1920
		1936	1965	1961	1946	1920
		2355	2365	2365	2358	2353
		2338	2332	2325	2314	2301
		2338	2361	2354	2332	2301
		2555	2562	2564	2551	2556
		2525	2517	2508	2495	2479
		2525	2546	2537	2513	2479

Viscosity O_2 - CO						
	%O_2	0.0	23.37	42.01	77.53	100.0
		1776	1841	1900	1998	2057
		1779	1880	1946	2034	2064
		1779	1844	1897	1998	2064
		2183	2268	2343	2482	2568
		2210	2328	2407	2521	2567
		2210	2292	2358	2485	2567
		2548	2650	2741	2908	3017
		2593	2725	2817	2954	3015
		2593	2690	2768	2918	3015

Viscosity C_2H_4 - N_2						
	%C_2H_4	0.0	24.05	56.95	76.21	100.0
		1781	1574	1308	1169	1033
		1777	1562	1306	1176	1029
		2190	1956	1655	1491	1348
		2192	1946	1653	1501	1330
		2560	2292	1963	1786	1622
		2556	2284	1961	1792	1602
		2727	2453	2108	1921	1753
		2729	2444	2104	1927	1728

Viscosity H_2 - N_2O						
	%H_2	0.0	39.89	59.61	78.57	100.0
		1488	1481	1451	1348	891
		1489	1509	1483	1376	889
		1943	1907	1849	1684	1081
		1936	1932	1876	1710	1065
		2355	2292	2206	1990	1256
		2338	2311	2229	2009	1228
		2555	2477	2376	2137	1341
		2525	2489	2392	2150	1308

Viscosity N_2 - O_2						
T(°K)	%N_2	0.0	24.08	58.93	78.22	100.0
300	EX*	2057	1995	1894	1843	1781
	CG*	2064	1994	1894	1839	1777
	CD*	2064	2015	1921	1858	1777
400	EX	2568	2480	2345	2275	2190
	CG	2568	2475	2343	2272	2192
	CD	2568	2497	2372	2292	2192
500	EX	3017	2909	2741	2658	2560
	CG	3015	2901	2741	2654	2556
	CD	3015	2923	2768	2674	2556
550	EX	3220	3109	2932	2840	2727
	CG	3224	3100	2925	2833	2729
	CD	3224	3125	2956	2854	2729

Viscosity CO - N_2							
	%CO	0.0	18.46	39.70	65.68	83.71	100.0
		1781	1782	1781	1775	1774	1776
		1779	1826	1855	1852	1823	1777
		1779	1778	1780	1780	1780	1777
		2190	2186	2183	2191	2184	2183
		2210	2245	2279	2279	2252	2192
		2210	2196	2201	2205	2208	2192
		2560	2560	2558	2549	2551	2548
		2593	2617	2656	2661	2636	2556
		2593	2564	2573	2582	2588	2556
		2727	2721	2719	2722	2719	2714
		2771	2752	2834	2840	2814	2729
		2771	2737	2746	2757	2763	2729

Viscosity C_2H_4 - CO						
	%C_2H_4	0.0	26.32	43.54	80.62	100.0
		1776	1553	1402	1135	1033
		1779	1538	1399	1144	1029
		2183	1943	1763	1460	1342
		2210	1930	1768	1466	1330
		2548	2279	2098	1760	1622
		2593	2279	2097	1757	1602
		2714	2433	2240	1900	1753
		2771	2440	2249	1891	1728

Viscosity H_2 - C_3H_8						
	%H_2	0.0	37.04	78.82	92.25	100.0
		817	874	985	970	891
		819	892	995	980	889
		1070	1130	1233	1194	1081
		1074	1152	1241	1194	1065
		1308	1366	1459	1392	1256
		1309	1390	1462	1389	1228
		1422	1478	1566	1485	1347
		1418	1499	1566	1482	1308

Viscosity CO_2 C_3H_8						
	%CO_2	0.0	40.25	57.76	78.83	100.0
		817	1058	1174	1326	1493
		819	1033	1146	1304	1493
		1070	1383	1533	1730	1944
		1074	1345	1487	1685	1920
		1308	1670	1856	2093	2353
		1309	1627	1795	2026	2301
		1422	1815	2010	2267	2556
		1418	1759	1939	2186	2479

Viscosity N_2O - C_3H_8						
	%N_2O	0.0	20.16	58.29	79.82	100.0
		817	926	1167	1326	1488
		819	917	1145	1307	1489
		1070	1213	1525	1725	1943
		1074	1201	1494	1703	1936
		1308	1478	1854	2083	2355
		1309	1460	1811	2059	2338
		1422	1610	2012	2271	2556
		1418	1581	1959	2227	2525

* EX = experimental data; CG = calculated using a geometric mean ϵ/k; CD = calculated using an ϵ/k calculated from diffusion.

TABLE 14(*b*) VISCOSITY OF MOIST AIR

$\eta(10^{-7}$g/cm-sec)

Temp. °K	Per cent Moisture			
	0.0	0.5	1.0	5.0
100	702	701	700	688
150	1038	1035	1033	1016
200	1337	1335	1333	1315
273.16	1724	1722	1720	1704
300	1851	1849	1847	1832
400	2290	2289	2288	2276
500	2678	2678	2677	2671
600	3034	3034	3035	3033
800	3680	3680	3681	3687
1000	4257	4260	4265	4274
1200	4761	4765	4768	4786
1400	5251	5253	5257	5280
1600	5735	5739	5744	5770
2000	6680	6686	6690	6720
3000	8685	8689	8691	8730
5000	12070	12090	12100	12160

TABLE 14(*c*) FORCE CONSTANTS DETERMINED FROM VISCOSITY OF NH_3 MIXTURES

Gases	ϵ_{12}/k	r_{12}
$H_2 - NH_3$	99	3.094
$N_2 - NH_3$	138	3.527
$O_2 - NH_3$	133	3.453
$C_2H_4 - NH_3$	247	3.754

were used are those obtained from viscosity data; the force constants between unlike molecules which were used are those obtained by taking an arithmetic-mean collision diameter and a geometric-mean ϵ/k.

The methods presented here are well-suited to the prediction of transport properties for such industrially important mixtures as flue and fuel gases. In Table 16 we compare the experimentally observed values of the viscosity of flue and fuel gases with values calculated using Equation [39], together with the force constants given in Tables 8, 9, and 10. The agreement in more than half of the examples is excellent; however, in some of the other mixtures there is a considerable discrepancy. This might be explained on the basis of small errors in the experimental gas analysis. In any case we believe that our calculated values have an inherent accuracy of within 0.5 per cent. The fact that some of these mixtures contained as many as seven components caused no computational difficulties.

The viscosity of moist air is particularly useful for the determination of Reynolds numbers in aerodynamics. The values compiled in Table 14(*b*) were calculated by assuming that moist air may be treated as a mixture of two components, air and water vapor. The approximations in Equations [13] and [14] were used to get the interaction constants ϵ_{12}/k and r_{12}, in which the force constants for water were from the second virial coefficient tabulated by Stockmayer (6). The force constants for air are those in Table 8. The B_{ii} for water, which are defined in Equation [43], were taken directly from the experimental viscosity values of steam (18), making use of the simple relation

$$B_{ii} = 1/(2\eta_i)$$

Force constants between ammonia and several gases were obtained by fitting the experimental viscosity data (19) at two different temperatures. These values, shown in Table 14(*c*), were then used to calculate the viscosity of the binary mixtures in Table 14(*d*). Here again, the B_{ii} for ammonia were obtained

TABLE 14(*d*) VISCOSITY OF AMMONIA MIXTURES

Mixture	Temp.	%NH_3	$\eta_{12} \times 10^7$ Calc.	$\eta_{12} \times 10^7$ Expt. (a)
$N_2 - NH_3$	293	88.83	1095	1092
		71.47	1256	1254
		56.38	1386	1383
		29.20	1590	1585
		11.11	1698	1690
	373	88.83	1389	1398
		71.43	1566	1569
		56.38	1705	1710
		29.20	1922	1920
		11.11	2037	2031
	473	88.83	1770	1768
		71.43	1946	1946
		56.38	2085	2085
		29.20	2299	2296
		11.11	2415	2408
	523	88.83	1962	1930
		71.43	2132	2112
		56.38	2266	2250
		29.20	2475	2460
		11.11	2590	2572
$C_2H_4 - NH_3$	293	88.67	1000	1001
		69.61	1015	1022
		51.72	1023	1030
		29.93	1021	1027
		10.96	1014	1015
	373	88.67	1278	1294
		69.61	1288	1304
		51.72	1288	1303
		29.93	1279	1291
		10.96	1265	1269
	473	88.67	1640	1647
		69.61	1623	1639
		51.72	1605	1622
		29.93	1577	1595
		10.96	1551	1561
	523	88.67	1823	1809
		69.61	1788	1791
		51.72	1756	1764
		29.93	1717	1729
		10.96	1684	1689
$H_2 - NH_3$	293	90.05	1007	1004
		70.87	1049	1047
		51.77	1082	1080
		29.75	1068	1067
		10.82	1011	1011
	373	90.05	1288	1299
		70.87	1323	1333
		51.77	1344	1354
		29.75	1321	1329
		10.82	1198	1204
	473	90.05	1661	1660
		70.87	1679	1680
		51.77	1673	1676
		29.75	1609	1610
		10.82	1411	1432
	523	90.05	1852	1825
		70.87	1858	1837
		51.77	1835	1833
		29.75	1735	1737
		10.82	1514	
$O_2 - NH_3$	293	87.55	1145	1143
		70.79	1350	1350
		47.86	1609	1604
		29.86	1789	1783
		13.51	1931	1924
	373	87.55	1448	1459
		70.79	1681	1689
		47.86	1971	1972
		29.86	2174	2170
		13.51	2334	2326
	473	87.55	1838	1840
		70.79	2083	2085
		47.86	2391	2390
		29.86	2607	2604
		13.51	2782	2773

(*a*) Landolt-Börnstein, "Physikalisch-Chemische Tabellen."

from the average experimental values of viscosity (19, 20, 21). The individual force constants for the nonpolar component were those in Table 8.

TABLE 15 VISCOSITY OF TERNARY MIXTURE OF Ne-A-He

	Volume Percent			$\eta_{mix} \times 10^7$ g/cm-sec	
T °K	Ne	A	He	Calc	Expt*
193	55.76	26.70	17.54	2718	2740
	31.93	32.13	35.94	2562	2569
	21.66	58.51	19.83	2429	2411
	21.89	23.82	54.29	2500	2504
373	55.76	26.70	17.54	3205	3237
	31.93	32.13	35.94	3025	3044
	21.66	58.51	19.83	2895	2886
	21.89	23.82	54.29	2938	2957
473	55.76	26.70	17.54	3752	3790
	31.93	32.13	35.94	3551	3574
	21.66	58.51	19.83	3425	3415
	21.89	23.82	54.29	3449	3470

FORCE CONSTANTS USED

Like Molecules			Unlike Molecules		
Molecule	r_i (Å)	ϵ_i/k (°K)	Molecule Pair	Arithmetic Mean r_{ij}	Geometric Mean ϵ_{ij}/k
Ne	2.80	35.7	Ne - A	3.11	68
A	3.418	124.0	Ne - He	2.75	14
He	2.70	6.03	A - He	3.059	27

* M. Trautz and K. F. Kipphan, *Annalen der Physik*, vol. 2, 1929, p. 746.

In this report we do not consider quantum corrections, inasmuch as they are numerically small and negligible at any reasonable temperature ($T > 15$ deg K). The quantum corrections would be expected to be larger for hydrogen than for any heavier molecules. The magnitude of this correction may be seen from a comparison of the viscosity of H_2 and D_2. If there were no quantum corrections, η_{H_2} would equal $(M_H/M_D)^{1/2}\eta_{D_2}$. This would be true regardless of the form for the energy of interaction as long as classical mechanics applies, but quantum corrections would introduce deviations. From Table 17 it is seen that there is no appreciable deviation (nor quantum correction) down to

TABLE 17 VISCOSITY OF LIGHT AND HEAVY METHANE AND LIGHT AND HEAVY HYDROGEN

T(°K.)	$\sqrt{M_{H_2}/M_{D_2}}\,\eta_{D_2}$(exptl)	η_{H_2}(exptl) (a)	η_{H_2}(calc)
15	71	82	70
30	146	158	141
75	332	347	331
290	886	884	876
T(°K.)	$\sqrt{M_{CH_4}/M_{CD_4}}\,\eta_{CD_4}$(exptl)	η_{CH_4}(exptl) (b)	η_{CH_4}(calc)
90	384	376	353
200	828	785	780
225	922	874	868
250	1013	961	955
275	1101	1039	1037
300	1095	1111	1115

(a) A. van Itterbeek, and O. van Paemel, *Physica*, vol. 7, 1940, p. 265.
(b) A. van Itterbeek, *Physica*, vol. 9, 1940, p. 831.

TABLE 16 VISCOSITY OF MULTICOMPONENT MIXTURES INDUSTRIAL GASES

Composition (Volume %)							°K. Temp.	$\eta \times 10^7$ Exptl.	$\eta \times 10^7$ Calc.	Ref.
CO_2	O_2	CO	H_2	CH_4	N_2	Heavier Hydrocarbons				
8.6	2.3				89.1		293	1756	1761	2
13.3	3.9				82.8		293	1749	1765	2
6.2	10.7				83.1		293	1793	1789	2
10.4		28.5	1.6		59.5		293	1738	1798	2
10.80	2.00		2.20		85.00		300.5	1827	1792	1
							524.5	2715	2661	
							973	4117	4008	
							1279	4856	4753	
6.70	0.10	7.80	2.20		83.20		307.5	1842	1835	1
							519	2655	2653	
							975	4048	4019	
							1285	4808	4783	
6.40	3.00	0.30	0.70		89.60		314	1904	1856	1
							518	2706	2644	
							974.5	4113	4017	
							1287	4895	4777	
6.00	0.10	25.70	11.50		56.70		302	1823	1829	1
							526	2686	2696	
							976	4041	4042	
							1283	4777	4821	
10.6		29.8	3.9	0.3	55.4		293	1743	1794	2
8.9		30.7	3.3	0.4	56.7		293	1747	1797	2
8.7		32.8	1.5	0.2	56.8		293	1749	1802	2
3.70	0.30	27.10	9.50	1.60	57.80		300.5	1815	1816	1
							565.5	2819	2823	
							981	4045	4041	
							1282	4792	4803	
1.7	0.9	6.0	57.5	24.0	7.8	2.1	293	1262	1254	2
2.1	0.9	5.7	53.0	24.3	11.7	2.3	293	1304	1290	2
2.0	1.4	4.6	54.9	23.5	11.6	2.0	293	1310	1398	2
3.3	0.6	3.8	51.3	29.6	10.0	1.4	293	1332	1269	2
2.2	0.6	4.1	53.1	29.5	9.2	1.3	293	1306	1254	2
2.2	1.0	4.0	52.3	29.9	9.4	1.2	293	1307	1261	2
2.5	0.8	14.9	53.0	18.1	9.1	1.6	293	1355	1373	2
4.8	0.3	26.4	17.2	2.6	48.2	0.5	293	1714	1743	2
3.5	0.3	27.3	14.4	3.7	50.0	0.8	293	1712	1732	2
3.1	0.5	28.6	17.7	4.2	45.0	0.9	293	1715	1719	2

[1] Schmid, *Gas- und Wasserfach*, vol. 85, 1942, p. 92.
[2] F. Herning and L. Zipperer, *Gas- und Wasserfach*, vol. 79, 1936, pp. 49–54, 69–73.

15 deg C. Similarly, in the case of CH_4 and CD_4 where it is expected that $\eta_{CH_4} = (M_{CH_4}/M_{CD_4})^{1/2}\eta_{CD_4}$. Here, from the figures shown in Table 17, there is no appreciable quantum correction indicated by the experimental data down to 90 deg K. Only in the cases of H_2 and He is it expected that the transport properties would show a small quantum correction above 15 deg K. In these two cases it appears probable that a part of our difficulty in obtaining a suitable fit with the experimental viscosity data may arise from small quantum corrections. The conclusions have been substantiated by the theoretical work of Uehling and Uhlenbeck (22, 23, 24), and Massey and Mohr (25).

Coefficient of Diffusion

The first approximation for the coefficient of diffusion is given by the following equation

$$(D_{12})_1 = \frac{0.00092916T^{3/2}[(M_1 + M_2)/M_1M_2]^{1/2}}{p(r_{12})^2W^{(1)}(1; kT/\epsilon_{12})} \quad \ldots [44]$$

in which D_{12} is the coefficient of diffusion in $cm^2\ sec^{-1}$; p, the pressure in atmospheres; the M_i, molecular weights. Note that the first approximation to the diffusion coefficient is independent of composition. This is no longer true in the case of the second approximation

$$(D_{12})_2 = (D_{12})_1/(1 - \Delta) \quad \ldots [45]$$

Here Δ, a small quantity usually less than 0.03, is defined by

$$\Delta = 5(C - 1)^2(P_1x_1^2 + P_2x_2^2 + P_{12}x_1x_2)/(Q_1x_1^2 + Q_2x_2^2 + Q_{12}x_1x_2) \quad \ldots [46]$$

in which

$$P_1 = M_1^3[M_1 + M_2]^{-2}(2/3V_0)([D_{12}]_1/[\eta_1]_1)(273.16\ p/T) \quad \ldots [47]$$

$$P_2 = M_2^3[M_1 + M_2]^{-2}(2/3V_0)([D_{12}]_1/[\eta_2]_1)(273.16\ p/T) \quad \ldots [48]$$

$$P_{12} = [3(M_1 - M_2)^2 + 4M_1M_2A]/(M_1 + M_2)^2 \quad \ldots [49]$$

$$Q_1 = (P_1/M_1^2)(6M_2^2 + 5M_1^2 - 4M_1^2B + 8M_1M_2A) \quad \ldots [50]$$

$$Q_2 = (P_2/M_2^2)(6M_1^2 + 5M_2^2 - 4M_2^2B + 8M_1M_2A) \quad \ldots [51]$$

$$Q_{12} = \left\{ \begin{array}{l} 3(5 - 4B)(M_1 - M_2)^2/(M_1 + M_2)^2 \\ + 4AM_1M_2(11 - 4B)/(M_1 + M_2)^2 \\ + 2P_1P_2(M_1 + M_2)^4/M_1^2M_2^2 \end{array} \right\} \quad \ldots [52]$$

Here the x_i are mol-fractions of the ith component; the M_i are molecular weights; A, B, and C are functions of kT/ϵ_{12} given in Table 7; V_0 is the molar volume under standard conditions, i.e., 22414.6 cc.; and $[\eta_1]_1$ and $[\eta_2]_1$ are calculated first approximations to the viscosity of the pure component given by the formula

$$[\eta_i]_1 = 2.6693(10^{-5})(M_iT)^{1/2}/(r_i)^2/[W^{(2)}(2; kT/\epsilon_i)] \quad \ldots [53]$$

The possibility of getting good force constants between pairs of dissimilar molecules from Equation [44] has already been mentioned. This equation could be written for two temperatures, inserting two diffusion measurements, and the resulting equations solved simultaneously for r_{12} and ϵ_{12}/k.

In the case of self-diffusion

$$M_1 = M_2, \quad \epsilon_1 = \epsilon_2 = \epsilon_{12}, \quad r_1 = r_2 = r_{12}$$

and Equations [44] and [45] reduce to the particularly simple forms for the first approximation to the coefficient of self-diffusion

$$(D_{11})_1 = 0.0013140T^{3/2}/[pr_0^2W^{(1)}(1; kT/\epsilon)M^{1/2}] \quad \ldots [54]$$

and the second approximation is given by

$$(D_{11})_2 = (D_{11})_1/(1 - \Delta) \quad \ldots [55]$$

in which Δ is defined simply as

$$\Delta = 5(C - 1)^2/(11 - 4B + 8A) \quad \ldots [56]$$

and as before is a small correction factor.

The coefficients of self-diffusion may be calculated from our previously assigned values of the force constants without making any adjustments. The results are shown in Table 18, along with experimental values. Harteck and Schmidt determined the self-diffusion coefficient (SDK) for hydrogen by using ortho- and para-hydrogen. The self-diffusion coefficients for the other gases shown were determined using gases containing tracer isotopes. In all of these cases the agreement is very good between the experimental and calculated quantities. Additional experimental data would be very useful for purposes of comparison.

The available values for the coefficient of ordinary diffusion have been analyzed to give the force constants of Table 10 for the interaction between dissimilar molecules.

In a mixture containing f-components the concept of diffusion may be generalized (26). If U_i is the average velocity of molecules of the ith species relative to U, the mass average velocity of the gaseous mixture, then rigorously

$$U_i = (n^2/\rho n_i)\sum_{k=1}^{f} M_kd_{ik}\ \text{grad}\ x_j \quad \ldots [57]$$

where

$$n = \sum_{k=1}^{f} n_k = p/(RT) \quad \ldots [58]$$

is the total number of moles of gas in a cubic centimeter and ρ is the over-all density. The d_{ij} are not the usual diffusion constants for binary mixtures, D_{ij}, but the two are very closely related, in the general case by

$$d_{12} = -\frac{\rho n_1}{M_2}\left[\frac{\begin{vmatrix} 0 & A_{23} & A_{24} & \cdots \\ A_{32} & 0 & A_{34} & \cdots \\ A_{42} & A_{43} & 0 & \cdots \\ \cdots & \cdots & \cdots & \cdots \end{vmatrix} + \begin{vmatrix} A_{12} & A_{13} & A_{14} & \cdots \\ A_{32} & 0 & A_{34} & \cdots \\ A_{42} & A_{43} & 0 & \cdots \\ \cdots & \cdots & \cdots & \cdots \end{vmatrix}}{\begin{vmatrix} 0 & A_{12} & A_{13} & A_{14} & \cdots \\ A_{21} & 0 & A_{23} & A_{24} & \cdots \\ A_{31} & A_{32} & 0 & A_{34} & \cdots \\ A_{41} & A_{42} & A_{43} & 0 & \cdots \\ \cdots & \cdots & \cdots & \cdots & \cdots \end{vmatrix}}\right] \quad \ldots [59]$$

Here the coefficients in the determinant are

$$A_{ik} = (n_in_k/D_{ik}) + (n_kM_k/M_i)\cdot\sum_{s\neq i}^{f}(n_s/D_{is}) \quad \ldots [60]$$

The other d_{ij} may be obtained from the final form of the d_{12} by permuting the indexes or from Equation [59] by suitable modifications of the determinants in the numerator. This generalized formula may be obtained also from the work of Hellund and Uehling (27).

For the binary mixture

$$d_{12} = D_{12} \quad \ldots [61]$$

and for ternary mixtures

$$d_{12} = D_{12}\left[1 + \frac{n_3\left(\frac{M_3}{M_2}D_{13} - D_{12}\right)}{n_1D_{23} + n_2D_{13} + n_3D_{12}}\right] \quad \ldots [62]$$

TABLE 18 COEFFICIENT OF SELF-DIFFUSION

Gas	T °K.	P(atm)	D_{11} (cm²/sec) Calc	D_{11} (cm²/sec) Exptl	Reference for Exptl Values
Hydrogen	273	1	1.283	1.285 ± 0.0025	(a)
	85	1	0.167	0.172 ± 0.008	(a)
	20.4	1	0.01043	0.00816 ± 0.0002	(a)
Krypton	293	1	0.093	0.093 ± 0.0045	(b)
Xenon	293	1	0.055	0.054 ± 0.0022	(b)
Neon	293	1	0.491	0.473 ± 0.002	(c)
Argon	295	0.4211	0.422	0.423 ± 0.003	(d)
Nitrogen	293	1	0.198	0.200 ± 0.008	(e)
Methane	292	0.00811	26.38	26.32 ± 0.73	(f)
Hydrogen Chloride	295	1	0.127	0.1246	(g)

(a) P. Harteck and H. W. Schmidt, *Zeitschrift für physikalische Chemie*, vol. 21, 1933, p. 447.
(b) W. Groth and P. Harteck, *Zeitschrift Elektrochemie*, vol. 47, 1941, p. 167.
(c) W. Groth and E. Sussner, *Zeitschrift für physikalische Chemie*, vol. 193, 1944, p. 296.
(d) F. Hutchinson, *Physical Review*, vol. 72, 1947, p. 1256.
(e) E. B. Winn, *Physical Review*, vol. 74, 1948, p. 698.
(f) E. B. Winn and E. P. Ney, *Physical Review*, vol. 72, 1947, p. 77.
(g) H. Braune and F. Zehle, *Zeitschrift für physikalische Chemie*, vol. 49, 1941, p. 247.

Thermal-Diffusion Ratio

Since the second approximation to the thermal-diffusion ratio involves very complicated algebra, only the first approximation will be set forth here. It is

$$k_T = 5x_1x_2(C-1)(S_1x_1 - S_2x_2)/(Q_1x_1^2 + Q_2x_2^2 + Q_3x_1x_2) \quad [63]$$

in which

$$S_1 = \frac{M_1}{5}\left(\frac{r_1}{r_{12}}\right)^2\left[\frac{2(M_1+M_2)^3}{M_2}\right]^{1/}\left[\frac{W^{(2)}(2;\ kT/\epsilon_1)}{W^{(1)}(1;\ kT/\epsilon_{12})}\right] - 3M_2(M_2-M_1) - 4AM_1M_2 \quad [64]$$

$$S_2 = \frac{M_2}{5}\left(\frac{r_2}{r_{12}}\right)^2\left[\frac{2(M_1+M_2)^3}{M_1}\right]^{/2}\left[\frac{W^{(2)}(2;\ kT/\epsilon_2)}{W^{(1)}(1;\ kT/\epsilon_{12})}\right] - 3M_1(M_1-M_2) - 4AM_1M_2 \quad [65]$$

$$Q_1 = \frac{1}{5}\left(\frac{r_1}{r_{12}}\right)^2\left[\frac{2(M_1+M_2)}{M_2}\right]^{/2}\left[\frac{W^{(2)}(2;\ kT/\epsilon_1)}{W^{(1)}(1;\ kT/\epsilon_{12})}\right] \cdot [6M_2^2 + (5-4B)M_1^2 + 8AM_1M_2] \quad [66]$$

$$Q_2 = \frac{1}{5}\left(\frac{r_2}{r_{12}}\right)^2\left[\frac{2(M_1+M_2)}{M_1}\right]^{/2}\left[\frac{W^{(2)}(2;\ kT/\epsilon_2)}{W^{(1)}(1;\ kT/\epsilon_{12})}\right] \cdot [6M_1^2 + (5-4B)M_2^2 + 8AM_1M_2] \quad [67]$$

$$Q_3 = \left[\begin{array}{c} 3(M_1-M_2)^2(5-4B) + 4AM_1M_2(11-4B) \\ + \frac{4}{25}\left(\frac{r_1r_2}{r_{12}}\right)^2\left[\frac{(M_1+M_2)^3}{(M_1M_2)^{1/2}}\right] \end{array}\right]\left[\frac{W^{(2)}(2;\ kT/\epsilon_1)W^{(2)}(2;\ kT/\epsilon_2)}{W^{(1)}(1;\ kT/\epsilon_{12})}\right] \quad [68]$$

Here the M_i are the molecular weights of the ith species; the x_i are mol-fractions; the A, B, and C are functions of kT/ϵ_{12} previously tabulated; and the r_1, r_2, and r_{12} are low-velocity collision diameters in angstroms. When the thermal diffusion of isotopes is under consideration, Equation [63] may be used where the S's and Q's have the more simple form

$$S_1 = AM_1[(2/M_2)^{1/2} - 4M_2] - 3M_2(M_2-M_1) \quad [69]$$

$$S_2 = AM_2[(2/M_1)^{1/2} - 4M_1] - 3M_1(M_1-M_2) \quad [70]$$

$$Q_1 = A(2/M_2)^{1/2}[6M_2^2 + (5-4B)M_1^2 + 8AM_1M_2] \quad [71]$$

$$Q_2 = A(2/M_1)^{1/2}[6M_1^2 + (5-4B)M_2^2 + 8AM_1M_2] \quad [72]$$

$$Q_3 = 4A^2(M_1M_2)^{-1/2} + 3(M_1-M_2)^2(5-4B) + 4AM_1M_2(11-4B) \quad [73]$$

A graph of k_T versus composition for light and heavy methane calculated with the foregoing formula is shown in Fig. 6. The force constants for a mixture of isotopes are the same as those for the pure substance. It is interesting to note that these theoretical values predict the change in sign in the thermal-diffusion coefficient which has been found to occur at low temperatures. At very low temperatures the thermal diffusion is so small that no practical use can be made of this inversion.

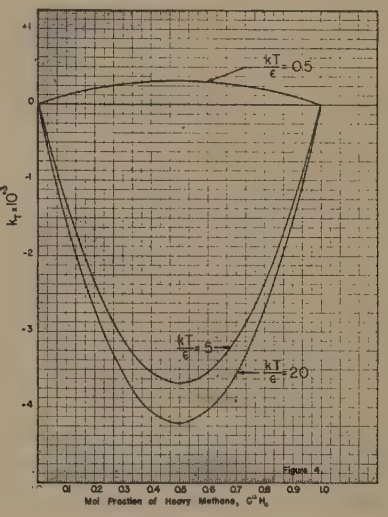

FIG. 6

Experimental data generally are reported as the ratio R_T of the thermal-diffusion ratio k_T, to the corresponding value for rigid spherical molecules. While the calculated and experimental k_T are functions of temperature for real molecules, k_T for rigid spheres is independent of temperature, and it is computed using the rigid-spheres quantities

$$A = 0.4,\ B = 0.6,\ C = 1.2,\ W^{(1)}(1) = 1/2,\ \text{and}\ W^{(2)}(2) = 1 \quad [74]$$

Table 19 shows some values of R_T(calc) and R_T(exptl). For those gas pairs for which diffusion data were available, ϵ_{12}/k obtained from diffusion (see Table 10) were used; otherwise, it was necessary to employ the geometric mean of the ϵ/k for the single components. For all of the gas pairs, r_{12} was taken to be the arithmetic mean of the r_0 for each of the two components. Force constants for ammonia were obtained from second-virial-coefficient data.

Since the concentration gradient which results from thermal diffusion is opposed by ordinary diffusion, a steady state is reached after a certain time interval. van Itterbeek, van Paemel, and van Lierde (28) have measured thermal diffusion in gas mixtures at low temperatures as per cent change in composition at the steady state $\Delta\gamma$, which may also be calculated from the following integral

$$\Delta\gamma = \int_{T_1}^{T_2} k_T\, d\ln T \quad [75]$$

TABLE 19 THERMAL DIFFUSION OF GASES

Gas Mixture	Concentration	T(°K)	R_T Calc.	R_T Expt.	Reference
He - Ne	53.8 % He	585.2	.71	.64	a
		233.2	.70	.64	
		117.2	.68	.58	
He - A	51.2 % He	585.2	.73	.66	a
		233.2	.71	.63	
		117.2	.63	.55	
He - Xe	53.6 % He	585.2	.75	.66	a
		233.2	.70	.66	
Ne - A	51.2 % Ne	585.2	.66	.57	a
		233.2	.52	.48	
		117.2	.27	.28	
Ne - Xe	54.2 % Ne	585.2	.66	.66	a
		233.2	.44	.46	
A - Xe	56.4 % A	585.2	.51	.45	a
		233.2	.15	.15	
$H_2 - D_2$		333	.63	.50	b
$Ne^{20} - Ne^{22}$		357	.62	.60	c
$A^{36} - A^{40}$		620	.65	.47	c
$C^{12}H_4 - C^{13}H_4$		274	.29	.49	b
$N^{14}H_3 - N^{15}H_3$		308	.08	.11	d
$CH_4 - H_2$		506	.68	.67	e
$O_2 - CO_2$		735	.61	.63	e
$CO - CO_2$		725	.60	.40	e
$H_2 - He$		284	.53	.41	b
$H_2 - CO_2$		596	.70	1.03	e

(a) K. E. Grew, Proceedings of the Royal Society of London, vol. 189, 1947, p. 402.
(b) B. F. Murphy, *Physical Review*, vol. 72, 1947, p. 836.
(c) L. G. Stier, *Physical Review*, vol. 62, 1942, p. 548.
(d) W. W. Watson and D. Woermley, *Physical Review*, vol. 63, 1943, p. 184.
(e) N. G. Schmahl and J. Schewe, *Zeitschrift Elecktrochemie*, vol. 46, 1940, p. 210.

TABLE 20 THERMAL DIFFUSION IN GAS MIXTURES

$\Delta\gamma$ = change in per cent H_2

Gas Mixture	Average Volume %H_2	T_1 °K	T_2 °K	$\Delta\gamma$ Expt.[a]	$\Delta\gamma$ Calc.
H_2 - Ne	35.6	290.4	90.2	6.9	7.1
	50.9	290.4	90.2	8.2	8.2
	66.7	290.4	90.2	7.7	7.9
H_2 - CO	39.7	293.3	90.2	5.6	5.9
	51.7	293.3	90.2	6.6	6.7
	73.7	293.3	90.2	5.7	6.4
H_2 - He	32.3	291.7	90.2	3.4	3.8
	50.5	291.7	90.2	4.6	4.2
	65.4	291.7	90.2	3.7	3.7
H_2 - N_2	40.9	292.1	64.4	7.6	8.1
	50.8	292.1	64.6	8.4	9.0
	78.0	292.1	64.4	6.3	8.1
H_2 - O_2	33.8	293.6	90.2	4.0	5.7
	48.2	293.6	90.2	5.5	7.1
	73.7	293.6	90.2	5.3	6.9

(a) A. van Itterbeek, O. van Paemel, and J. van Lierde, *Physica*, vol. 13, 1947, p. 231.

This integration was performed numerically, making use of Equation [63] for k_T, for the gases and temperatures in Table 20, where the experimental and calculated values of $\Delta\gamma$ may be compared.

Coefficient of Thermal Conductivity

For a single gas the coefficient of thermal conductivity λ, through the second approximation is given in terms of the viscosity η, and the specific heat at constant volume C_v, by the relation

$$\lambda = (H\eta/VM)[C_v + (9/4)R] \quad [76]$$

Here R is the usual gas constant per mole; M is the molecular weight; H and V are functions of kT/ϵ previously mentioned. The ratio H/V is very close to unity. The factor $[C_v + (9/4)R]$ depends upon the Eucken assumption that, during a collision, thermal equilibrium is established between the translational and internal degrees of freedom in the molecule. The experimental values of λ determined by Johnston and co-workers (29, 30) provide an opportunity to check the validity of this equation. Table 21 shows the comparison of the observed versus the calculated value of $(H/V) = (\lambda M/\eta)[C_v + (9/4)R]^{-1}$. The agreement is fairly good in the case of helium where there are no

TABLE 21 THERMAL CONDUCTIVITY

Gas	H/V	100°K.	200°K.	300°K.
He	Exptl[a]	0.9933	0.9897	0.9733
	Calcd	1.0042	1.0043	1.0045
CH_4	Exptl[a]	0.9676	1.0258	1.0675
	Calcd	1.0000	1.0002	1.0009
NO	Exptl[a]		0.9504	0.9974
	Calcd		1.0004	1.0013
CO_2	Exptl[a]		0.8788	0.9479
	Calcd		1.0001	1.0003
O_2	Exptl[a]	0.9529	1.0042	1.0320
	Calcd	1.0000	1.0005	1.0015
Air	Exptl[b]	0.9499	1.0022	1.0107
	Calcd	1.0001	1.0008	1.0019

(a) H. L. Johnston and E. R. Grilly, *Journal of Chemical Physics*, vol. 14, 1946, p. 233.
(b) W. J. Taylor and H. L. Johnson, *Journal of Chemical Physics*, vol. 14, 1946, p. 219.

internal degrees of freedom. In all other cases the discrepancies are large. This indicates that the Eucken assumption is not valid, and hence Equation [76] must be modified so as to take into account the difficulty of transferring energy from translation to rotation and vibration. The time lag in the specific heat is another indication of this difficulty. At very high temperatures, such as occur in combustions, the molecules behave more classically, and Equation [76] should apply.

Until the discrepancies in the Eucken assumption are settled, there seems little advantage in trying to apply the complicated Chapman-Enskog relationships for the heat conductivity of gaseous mixtures. Instead, we shall use Equation [76], using the viscosity and specific heat for the mixture to estimate the heat conductivity.

Unfortunately, accurate experimental measurements of heat conductivity are very difficult to obtain, so that there is no possibility of developing a more satisfactory empirical formulation at the present time.

Acknowledgment

The authors wish to express their appreciation to Dr. C. F. Curtiss for allowing them to set forth the generalized viscosity and diffusion equations in this paper, and for valuable assistance throughout the course of the work. The wide scope of the present report was made possible by the efforts of a computing group, under the direction of Ruth Shoemaker. In this connection we wish to thank Mary Nordling, Doris Jayne, Phyllis Rood, Phyllis Rhoades, Marjorie Leikvold, and Ted Mesmer.

The authors also wish to thank the Navy Bureau of Ordnance for its financial support under Contract NOrd 9938.

One of the authors, R. Byron Bird, desires to acknowledge the

financial help he has received from the Wisconsin Alumni Research Foundation.

BIBLIOGRAPHY

1 "Equation of State of Gases and Typical Phenomena," by J. E. Lennard-Jones, *Physica*, vol. 4, 1937, pp. 941–956.

"Statistical Mechanics," by R. H. Fowler, Cambridge University Press, 1936; chapt. 10 of book entitled, "Interatomic Forces," written by J. E. Lennard-Jones.

2 "The Evaluation of Gibbs' Phase-Integral for Imperfect Gases," by H. D. Ursell, Proceedings of the Cambridge Philosophical Society, vol. 23, 1927, pp. 685–697.

3 Reference (1).

4 Intermolecular Forces and the Properties of Gases," by J. O. Hirschfelder and W. E. Roseveare, *Journal of Physical Chemistry*, vol. 43, 1939, pp. 15–35.

5 "Thermodynamic Properties of Air," by C. F. Curtiss and J. O. Hirschfelder, CF-793, University of Wisconsin Naval Research Laboratory, April, 1948.

6 "Second Virial Coefficients of Polargases," by W. H. Stockmayer, *Journal of Chemical Physics*, vol. 9, 1941, pp. 398–402, 863–870.

7 "Second Virial Coefficients and the Forces Between Compl x Molecules," by J. O. Hirschfelder, F. T. McClure, and I. F. Weeks, *Journal of Chemical Physics*, vol. 10, 1942, pp. 201–211.

8 "The General Theory of Molecular Forces," by F. London, Trans. Faraday Society, vol. 33, 1937, pp. 8–26.

9 "Determination of Intermolecular Forces From the Joule-Thomson Coefficients," by J. O. Hirschfelder, R. B. Ewell, and J. R. Roebuck, *Journal of Chemical Physics*, vol. 6, 1938, pp. 205–218.

10 "Mathematical Theory of Non-Uniform Gases," by S. Chapman and T. G. Cowling, Cambridge University Press, Teddington, England, 1939.

11 "The Transport Properties of Multicomponent Systems of Gases," by C. F. Curtiss and J. O. Hirschfelder, *Journal of Chemical Physics*, vol. 17, June, 1949.

12 "The Transport Properties for Non-Polar Gases," by J. O. Hirschfelder, R. B. Bird, and E. L. Spotz, *Journal of Chemical Physics*, vol. 16, 1948, p. 968.

13 "Critical Phenomena in Gases," by J. E. Lennard-Jones and A. F. Devonshire, Proceedings of the Royal Society of London, series A, vol. 165, 1938, pp. 1–11; series A, vol. A163, 1937, pp. 53–70.

"Zero-Point Energy and Lattice Distances," by Jack Corner, Trans. Faraday Society, vol. 35, 1939, pp. 711–716.

14 "Rough Quantum Mechanical Calculation of J. O. Hirschelder," (unpublished).

15 "The Intermolecular Potential of Mercury," by J. H. Hildebrand, H. R. R. Wakeham, and R. N. Boyd, *Journal of Chemical Physics*, vol. 7, 1939, pp. 1094–1096.

16 "A New Measuring Method for Thermodiffusion and Diffusion Coefficients in Gases," by L. Waldmann, *Naturwissenschaften*, vol. 32, 1944, pp. 223–224.

17 "The Viscosity of Gas Mixtures," by A. van Itterbeek, O. van Paemel, and J. van Lierde, *Physica*, vol. 13, 1947, pp. 88–95.

18 "Thermodynamic Properties of Steam," by J. H. Keenan and F. G. Keyes, John Wiley & Sons, Inc., New York, N. Y., 1936.

19 "Physikalish—Chemische Tabellen," by Landolt-Börnstein.

20 "The Viscosity of Gases and Vapors and the Measurement of Viscosity With the Hoppler Viscometer," by R. Wobser and F. Muller, *Kolloid-Beihefte*, vol. 52, 1941, pp. 165–276.

21 "The Variation of the Viscosity of Gases With Temperature Over a Large Temperature Range," by A. B. Van Cleave and O. Maass, *Canadian Journal of Research*, vol. 13B, 1935, pp. 140–148.

22 "Transport Phenomena in Einstein-Bose and Fermi-Dirac Gases, I," by E. A. Uehling and G. E. Uhlenbeck, *Physical Review*, vol. 43, 1933, pp. 552–561.

23 "Transport Phenomena in Einstein-Bose and Fermi-Dirac Gases, II," by E. A. Uehling, *Physical Review*, vol. 46, 1934, pp. 917–929.

24(*a*) "Viscosity of Helium," by E. J. Hellund and E. A. Uehling, *Physical Review*, vol. 54, 1938, p. 479.

(*b*) "Transport Phenomena in Mixtures of Gases," by E. J. Hellund and E. A. Uehling, *Physical Review*, vol. 56, 1939, pp. 818–835.

25 "Free Paths and Transport Phenomena in Gases and the Quantum Theory of Collisions," by H. S. W. Massey and C. B. O. Mohr, Proceedings of the Royal Society of London, series A, vol. 141, 1933, pp. 434–453; series A, vol. 144, 1934, pp. 188–205.

26 "Theory of Propagation of Flames," by J. O. Hirschfelder and C. F. Curtiss, Part I," University of Wisconsin, CF 957; will be submitted to the *Journal of Chemical Physics* for publication.

27 Reference (24*b*).

28 "Measurements of the Thermal Diffusion in Gas Mixtures at Low Temperatures," by A. van Itterbeek, O. van Paemel, and J. van Lierde, *Physica*, vol. 13, 1947, pp. 231–239.

29 "The Thermal Conductivities of Eight Common Gases Between 80° and 380° K," by H. L. Johnston and E. R. Grilly, *Journal of Chemical Physics*, vol. 14, 1946, pp. 233–238.

30 "An Improved Hot-Wire Cell for Accurate Measurements of Thermal Conductivities of Gases Over a Wide Temperature Range. Results With Air Between 87° and 375° K," by W. J. Taylor and H. L. Johnston, *Journal of Chemical Physics*, vol. 14, 1946, pp. 219–233.

Experimental Determination of Heat Conductivity for Gases[1]

By F. G. KEYES,[2] CAMBRIDGE, MASS.

An examination of the available data for the heat conductivity of gases indicates that approximately 38 substances have been investigated, and 5 binary mixtures among the simpler gases. The most consistently accurate data appear to be available for helium, hydrogen, oxygen, nitrogen, carbon monoxide, carbon dioxide, and the essentially ternary mixture air. All the results are for atmospheric pressure or less, and the range of temperature extends from approximately —180 to 300 C in most cases.

The experimental method employed in the conductivity work cited has been almost entirely by the so-called "hot-wire" method perfected over the last 20 years. The method has been used to obtain the heat conductivity under pressure for liquid water, steam, nitrogen, and carbon dioxide. However, the hot-wire method does not appear to be the most suitable for the determination of heat conductivities under pressure, because of the difficulties of design as convection effects become enhanced with pressure.

A correlation of the low-pressure heat conductivities for the 7 gases referred to indicates that the data are reliable to approximately ±3 per cent. It is conceivable that the hot-wire method as at present developed is not capable of yielding results of higher accuracy than that indicated when the wire is used for both heater and thermometer. The most important of the reasons for this statement is connected with the temperature distribution along the wire and its distortion due to the Thomson effect when the comparatively large heating currents are flowing. Allowance for the Thomson effect has not been made so far as is known, but it could be taken into account, although accuracy in the measurement of the Thomson effect has only recently become promising.

The method employed in the present investigation is the very old one of containing the gas of interest in a cylindrical annulus fixed by concentric silver cylinders. In this method uniformity of the wall temperature of the inner heated cylinder can be secured, and the geometry of the system ascertained with precision. The numerous electrical leads from thermocouples and heater are controlled in temperature by a "heat station" having its own heater and thermocouples directly above the silver cell. In this way conduction along the leads can be controlled, and the gas above the cell kept at the same temperature as the mean temperature of the gas in the annulus. Electrical leads out of the stainless-steel pressure vessel in which the cell is contained have been insulated in two ways: in the first method by the use of Teflon disks between which the leads are contained under pressure; and by employing pressure-tight heater and thermocouple metal cases passing through the pressure vessel containing the cell, a necessary arrangement where slightly conducting fluids are to be measured, of which water is an example.

Measurements are being carried out on steam, liquid, and gaseous carbon dioxide, nitrogen, and mixtures of carbon dioxide and nitrogen to considerable pressures from 0 deg C to higher temperatures. At the present time temperatures higher than 400–450 C will not be exceeded. The results for steam are approximately in agreement with the values of Timroth and Vargaftig to 200 C. For nitrogen, our values extend to 150 atm and are in good agreement with Vargaftig's data which extend from 40 to 63 C and to a pressure of 87 atm.

---

[1] Abstract of a presentation of the experimental methods and results obtained to December 1, 1948.

[2] Department of Chemistry, Massachusetts Institute of Technology.

Contributed by the Research Committee on Properties of Gases and Gas Mixtures, the Applied Mechanics Division and the Heat Transfer Division, and Section M of the American Association for the Advancement of Science, and presented at the Annual Meeting, New York, N. Y., November 28–December 3, 1948, of THE AMERICAN SOCIETY OF MECHANICAL ENGINEERS.

NOTE: Statements and opinions advanced in papers are to be understood as individual expressions of their authors and not those of the Society. Paper No. 48—A-154.

Southwark Station Boiler Air-Flow Model Tests and Operation Results

By R. A. LANE[1] and E. L. MORRISON[2]

This paper discusses the engineering application of scale-model study of the combustion-air distribution for a proposed boiler installation. By obtaining an intimate mix of fuel and air, a more nearly uniform and nonreducing atmosphere results in the furnace to avoid the phenomenon of tube wastage. Following the operation of the prototype boilers, field tests were made for direct comparison with the model results. These comparisons, the actual combustion-gas analyses, and the boiler performance are reviewed.

Background and Objectives

DURING late 1941, and extending into 1942, a serious tube wastage or loss of metal from the face of furnace-wall tubes was experienced in many slag-tap pulverized-fuel-fired furnaces. This phenomenon had occurred previously, but to a minor degree, and perhaps had been too easily dismissed as caused by erosion from fuel impingement. It is believed that the severe accentuation of the phenomenon was the result of the sustained high loads which boilers were called on to carry during the great industrial activity brought on by the war.

Tube failures from this cause resulted in serious loss of boiler capacity during a critical period, and intensive study of the subject made possible the use of temporary expedients which reduced the wastage and decreased boiler outage while a more thorough investigation was being made.

The Bureau of Mines has investigated the problem very thoroughly and reported the circumstances under which loss of metal results and the chemistry involved in the attack in its reports presented before the Society in 1944.[3]

In the Philadelphia Electric Company's system, tube wastage was severe in two plants and of a somewhat milder nature in two boilers at its Chester Station. Test work on the Chester and some other boilers indicated that the loss of metal was experienced in areas where carbon monoxide was present in the furnace gases. Therefore it seemed obvious that an effort should be made to eliminate carbon monoxide by improvement of air distribution to the burners and gas flow in the furnace.

The company's new Southwark Station, then being designed, was to contain boilers very similar to those at Chester where loss of tube metal had been experienced. Since air-flow tests and furnace probing had disclosed that secondary-air distribution to the burners and within the burners was not entirely uniform, it was decided by the Philadelphia Electric Company and The Babcock and Wilcox Company to construct a $^1/_{10}$-scale model of the duct work, burners, and primary furnace, and to conduct tests on this model to determine (1) the flow pattern through the secondary-air duct; (2) the air distribution through the wind box and burners, with the thought of providing as uniform distribution of air as possible to all parts of the burner; (3) to determine probable gas flow within the furnace. In laying out the design of the secondary-air duct for the Southwark boilers, a strenuous effort was made to route the duct as directly as possible from the preheaters to the burners. By eliminating side offsets and reducing bends in the duct to a minimum, it was believed that the distribution of air as delivered to the burners would be more uniform and result in improved fuel-air mixture with more stable gas flow within the furnace. In order to check this hypothesis, the scale model was constructed by the Electric Company and test work was started in January, 1945.

Scope and Limit

Fig. 1 is a general view of the entire test setup. In the foreground are the fan with its motor drive, the 16-in. duct feeding the simulated air preheaters at the top of the model, and the smaller pipe which feeds the primary air to the coal pipes at the left. Uniformly perforated plates, having a resistance comparable to the actual air preheaters, were used in place of building model preheaters, so that the scale model started at the air outlet of the air preheaters. The primary and secondary-air control dampers are shown in the foreground and the location of the two measuring orifices are evident in the long runs of straight pipe leading to the model.

Fig. 2 shows the outline of the boiler in white, the secondary-air duct in transparent plastic with black metal banding, the incomplete burner-wind box construction, and at the base of the model, the primary furnace with the front wall tubes and rear slag-screen tubes clearly shown.

Fig. 3 shows the detail of three burners and wind boxes in various stages of construction. Fig. 4 is a close-up of the secondary-air dampers, the coal pipes, the primary-air supply header, and the simulated arrangement of the four coal pulverizers. Deviation from actual design was made on the pulverizers and the primary-air supply, as actual combustion could not be produced on the model. Dust boxes were provided in place of pulverizers and were equipped with air-injection connections to permit blowing fine-ground powders through the burners into the furnace.

Inasmuch as the model was constructed primarily of plywood and transparent plastic, it was of course necessary to limit the observations to such phenomena as could be tested without combustion. The secondary-air flow and the primary-air flow could be easily simulated. However, due to the absence of combustion and its effect on flow patterns, readings in the primary furnace proper are difficult to evaluate.

Determining the air distribution in the burner ports required the development of a special Pitot tube as the secondary-air ports

---

[1] Engineer, Mechanical Engineering Division, Philadelphia Electric Company, Philadelphia, Pa. Mem. ASME.

[2] Staff Engineering Department, The Babcock & Wilcox Company, New York, N. Y.

[3] "External Corrosion of Furnace-Wall Tubes—I History and Occurrence," by W. T. Reid, R. C. Corey, and B. J. Cross, Trans. ASME, vol. 67, 1945, pp. 279–288.

"External Corrosion of Furnace-Wall Tubes—II Significance of Sulphate Deposits and Sulphur Trioxide in Corrosion Mechanism," by R. C. Corey, B. J. Cross, and W. T. Reid, Trans. ASME, vol. 67, 1945, pp. 289–302.

Contributed by the Special Research Committee on Furnace Performance Factors and presented at the Annual Meeting, New York, N. Y., November 28–December 3, 1948, of The American Society of Mechanical Engineers.

Note: Statements and opinions advanced in papers are to be understood as individual expressions of their authors and not those of the Society. Paper No. 48—A-26.

FIG. 1 COMPLETE MODEL TEST SETUP

FIG. 2 PARTIALLY CONSTRUCTED SCALE MODEL OF DUCT, BURNERS, AND FURNACE

FIG. 3 DETAIL OF PARTIALLY CONSTRUCTED SCALE MODEL OF WIND BOX AND THREE BURNERS

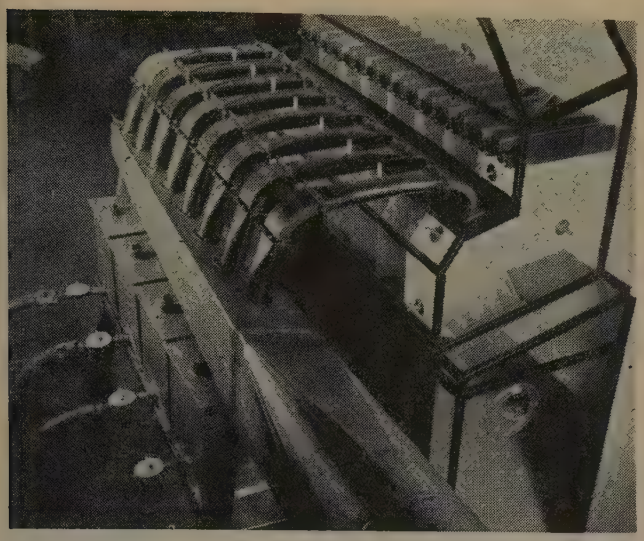

FIG. 4 COMPLETED SCALE MODEL OF BURNERS AND WIND BOX

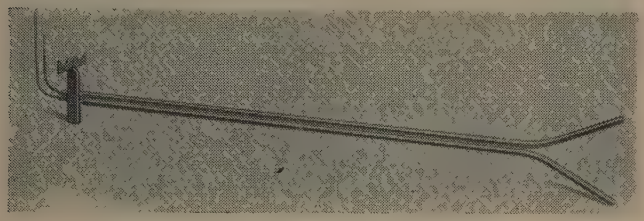

FIG. 5 ELEVEN-INCH PITOT TUBE

on the model were very small, being less than $^3/_{16}$ in. wide. Fig. 5 shows the 11-in. Pitot tube which was specially constructed to take the velocity readings in the burner ports. Of particular note are the small tubes at the left end of the instrument which are 0.040 in. OD × 0.025 in. ID, approximating the model scale on this portion of the instrument. It was necessary to increase the internal diameter of the extension tubes to speed up the response of the differential gage when shifting the Pitot tube from position to position in making a traverse. The shape of the burner ports where the Pitot-tube readings were taken suggested that the hole in the static tube should be at the same elevation as the impact tube. It was recognized that the streamlined leading end of the static tube could disturb the flow approaching the impact tube with the two tubes located immediately adjacent to each other. The relative position of the impact tube with respect to the static leg of the tube was carefully investigated and it was found that if the tubes were separated 4 diam they had no influence on each other. The U-shaped template near the measuring tip was the guide which rode on the underside of the furnace roof tubes at the burners and made it possible always to measure in the same relative position.

SCALE-MODEL AIR-FLOW CONSIDERATIONS

The total combustion air required at the burners on the actual boiler at a steam flow of 935,000 lb per hr is calculated to be 16,300 lb per min. The primary air at this rating, with four pulverizers operating, is 2100 lb per min. Therefore the secondary air equals 16,300 — 2100 or 14,200 lb per min (380,000 cfm at 600 F).

As the model was made at $^1/_{10}$ linear scale, the areas were in the ratio of $^1/_{100}$. Hence model equivalent of actual mass flow was $^1/_{100}$ of the latter requirement or 142 lb per min. This rate is referred to as "equivalent mass flow."

Since the design preheat-air temperature was 600 F, as against 80 F average model ambient temperature, a correction for weight per unit volume was necessary. The specific volume of air at 600 F is nearly double the specific volume at 80 F, hence by passing 283 lb per min through the model, velocities corresponding to the actual velocities were obtained. This rate is identified as "equivalent velocity flow."

Some authorities on model work hold that, in order to have hydraulic similitude between a model and its prototype, it is necessary to maintain the same Reynolds number. In order to accomplish this end on a $^1/_{10}$-scale model with the air at 80 F rather than 600 F, it would have been necessary to have an air flow approximately 6 times that of the mass-flow requirement. Unfortunately, the fan and fan drive were of insufficient size to deliver this air quantity, but under certain test conditions with six of the eight burners shut off, values of $3^1/_2$ times mass flow were attained.

TESTING METHODS AND CALCULATIONS

The several methods of testing employed were principally Pitot-tube measurements of air velocity in the secondary-air duct and burner ports, chemical smoke observations, telltale ribbons, and wet-paint panels in the primary furnace. The Pitot-tube readings were converted into values of velocity in feet per minute by formula. These velocity readings were then averaged in two directions and plotted as profiles from front to rear and from side to side of each burner. The curves plotted show per cent deviation above or below the average velocity.

In studying a new arrangement of wind-box approach, chemical smoke was employed to determine its merits. The chemical smoke employed was titanium tetrachloride, impregnated on cotton waste and blown out of the smoke pot by means of compressed air. This method of observation was particularly successful when the humidity was high enough to make adequate clouding. The smoke itself was employed in two ways. One method was to introduce chemical smoke in the model so as to fill the entire air stream under consideration. The other was to leave the air stream untouched and introduce the chemical smoke through a pencil-sized pipe or wand and explore different regions of the model with air flowing. With the use of a spotlight, it was possible to outline the smoke in the model by either the first or the second method. With the exception of the deposition of chemical which tended to dirty and disfigure the interior of the model, the chemical smoke and spotlight method of testing proved to be highly successful.

Telltale ribbons in the wind box or on a horizontal wire frame in the primary furnace proper which could be moved vertically from the top to the bottom of the furnace gave very good indications of the direction of air flow, the presence of voids, turbulent zones, or backwash, but of course did not indicate the actual velocity at the point of the ribbon.

Another method of testing was to introduce, through the simulated coal pulverizers, dust made of animal bone black or ferric oxide. The latter had the advantage of being yellow in color and more suitable for motion photography. Bone black was used in the majority of the tests involving the use of dust, as it was possible to obtain it in fineness comparable to the pulverized coal to be used in the actual burners. Static electricity of considerable magnitude created in the air and dust lines prohibited the use of pulverized coal or any combustible powder because of the explosion hazard. A sheet-metal panel was used for recording observations made with dust. This panel, cut to the exact size of the cross section of the primary furnace, was freshly coated on both sides with white enamel. The wet panel was placed in the furnace beneath the burner under test in such a position that the panel itself was directly below the center of the

burner. With the secondary and primary air flows established at the predetermined values, bone-black dust was admitted through the primary ports. This black dust, issuing from the burner ports, impinged upon and impregnated the white enamel surface in such a manner as to leave on the panel a positive outline of the air pattern issuing from the burners. It was possible then to examine the panels and photograph them for record (see Figs. 7 and 15).

A limited use was made of motion pictures using 16-mm film in both black and white and in color. Some of the exposures taken were with smoke introduced in the secondary-air duct, smoke wand in the primary furnace, telltale ribbons, ferric oxide in the primary furnace, and chemical smoke introduced through the burner ports into the primary furnace of the original and final designs.

Discussion of Original Design; Arrangement I

Fig. 6 is a sectional side view of the design of the burner and wind box originally constructed on the model. This view shows the coal piping A, distributor elbow B, riffle casting C, primary tips D, and burner ports E, as well as the outline of the wind box. Flow lines have been indicated on this sketch to show the air-flow

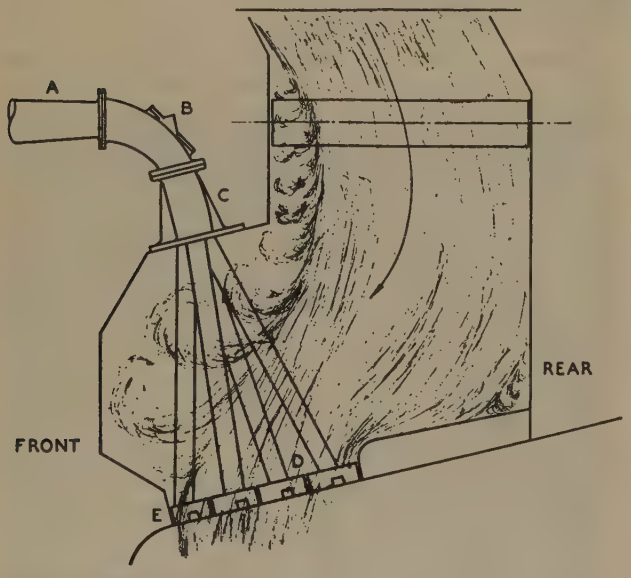

Fig. 6 Sectional Side View; Original Design of Burner and Wind Box

pattern as observed with the smoke wand. An item of particular interest to be noted here is the angle of discharge of the jets from the burner ports, as viewed from the side. The flow from the rear half of the burner ports was inclined slightly toward the front wall, rather than being normal to the burner roof tubes. It will be noted there were zones at the front of the wind box beginning at the wind-box dampers, and at the lower rear corner of the wind box, which were filled with turbulent eddies. Fig. 7 shows a wet paint panel taken with the original design which clearly indicates the path of the air stream as it leaves the burners and flows through the primary furnace.

A velocity traverse taken in the secondary-air duct at the preheater outlet is shown in Fig. 8, which indicates fairly uniform distribution from side to side of the duct. The distribution from top to bottom is definitely unbalanced, but, since the duct made several bends before reaching the burner wind box, it was not considered necessary to correct the top to bottom distribution at the preheater outlet. The velocity profiles taken in the ports

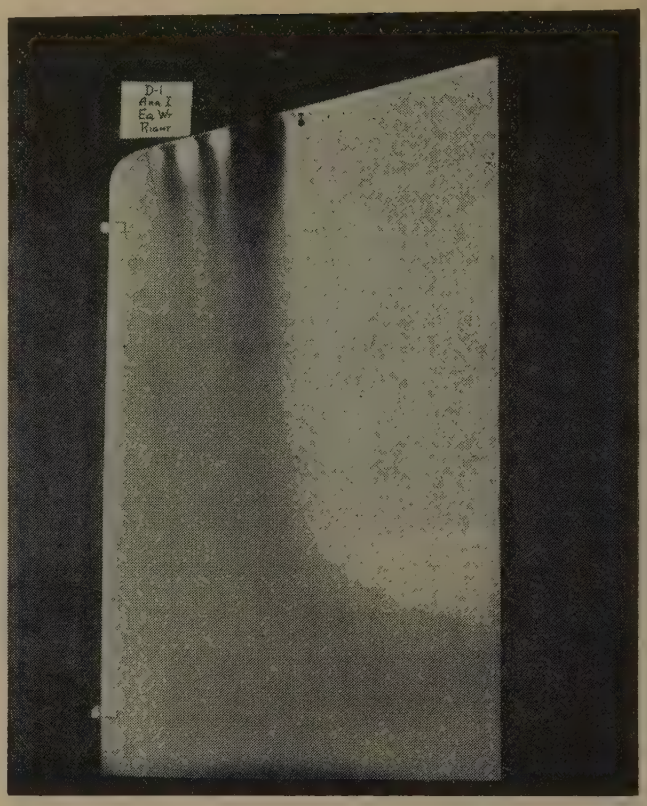

Fig. 7 Flow Pattern in Model of Primary Furnace With Original Wind Box Design

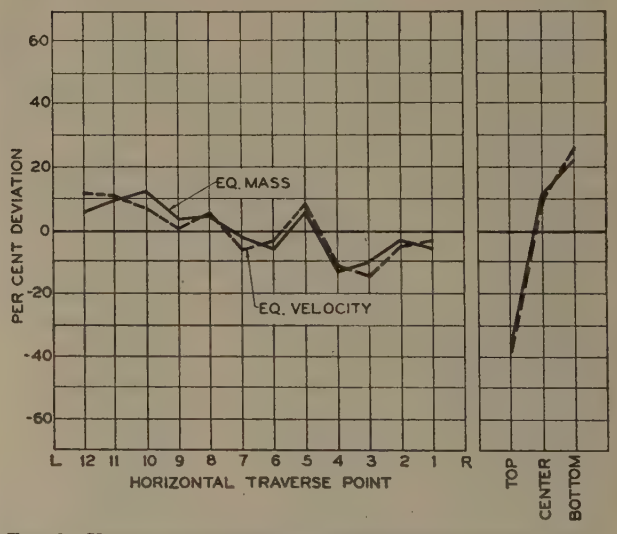

Fig. 8 Velocity Profiles on Model in Horizontal Duct Following Preheaters

of one burner, as shown in Fig. 9, indicate that the flow was already high at the rear of the ports, and the distribution practically identical for the two flows studied. The fact that the air distribution from side to side of the duct was reasonably uniform is further substantiated by the average velocities in each burner plotted in Fig. 10, for equivalent mass flow and equivalent velocity. It is also of interest to note that the distribution for these two flows remained essentially the same.

In order to establish what effect an unbalance of flow through the two preheaters would have, different-sized restrictor plates

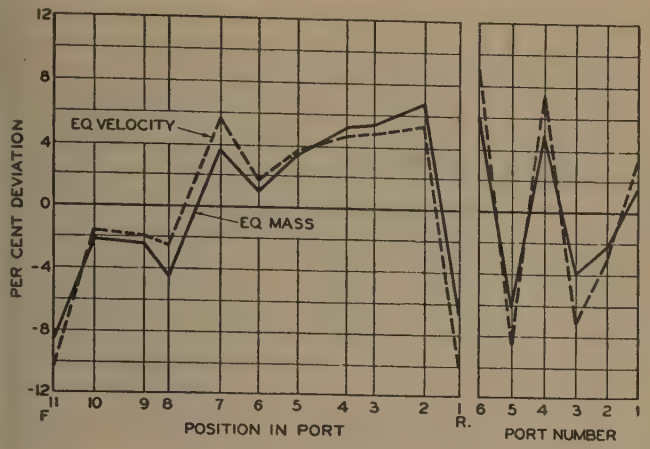

FIG. 9 VELOCITY PROFILES IN BURNER PORTS OF MODEL; ORIGINAL DESIGN

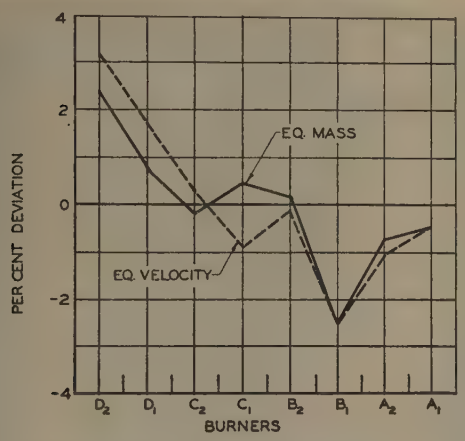

FIG. 10 AVERAGE BURNER VELOCITY-DISTRIBUTION CURVE FOR MODEL; ORIGINAL DESIGN

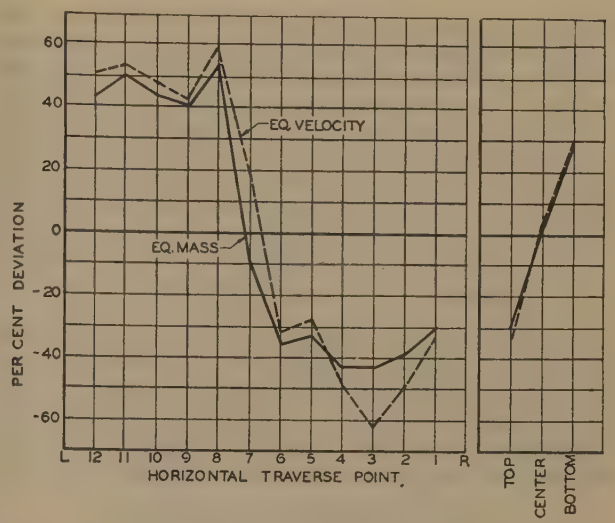

FIG. 11 VELOCITY PROFILES ON MODEL WITH UNBALANCED FLOW IN HORIZONTAL DUCT FOLLOWING PREHEATERS

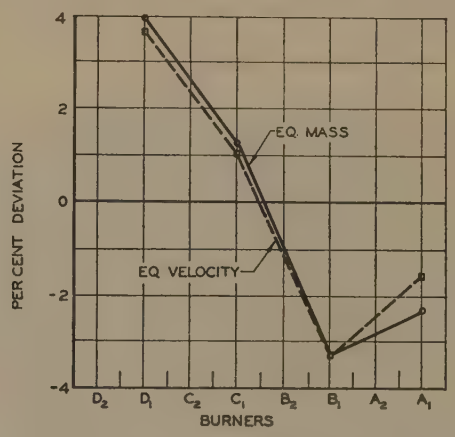

FIG. 12 AVERAGE BURNER VELOCITY-DISTRIBUTION CURVE FOR MODEL WITH UNBALANCED FLOW; ORIGINAL DESIGN

were installed in each of the simulated preheaters; the A-preheater plate, having 480 holes of $^{9}/_{32}$-in. diam, and the B, or left-hand preheater plate, having 312 holes of $^{1}/_{2}$-in. diam, resulting in 100 per cent increase in flow area through the B-preheater. The maldistribution from side to side leaving the preheaters is shown in Fig. 11 while the relatively uniform distribution from side to side at the burners is shown in Fig. 12.

From these data it is evident that the objective was to obtain a higher flow at the front of the burner ports and a jet which would issue in a direction normal to the furnace-roof tubes. As the traverses made both in the duct and in the burner ports show that the distribution remained identical for a range of flows, it seemed feasible to limit the velocity traverses to a single flow for establishing the distribution obtained with any design.

DISCUSSION OF INTERMEDIATE ARRANGEMENTS

In continuing the test work, decision was made to model all of the ideas developed concerning various designs in the wind box and air duct; thus with smoke-pattern observations and a velocity profile, evaluation of any baffle arrangement could be made. Each arrangement was designated as I, II, etc., tested as just outlined, and discarded if it did not show promise. Those which showed promise were tested more completely and often reappeared in some later arrangement as a modification. Outlining each of the forty-odd designs which were studied would be impractical.

One or two arrangements had considerable theoretical promise, but owing to the difficulty of their eventual operation, maintenance, or physical limitations, they had to be replaced with something of a more practical nature. For instance, considerable thought was given to building a false roof from the front of the wind box through the cluster of primary tips so that the high resistance, created by the convergence of the tips and the turbulent zones in that same physical area, would be eliminated.

Such a design was carefully modeled and investigated. The real difficulty with this design was the sharp offset through which the secondary air had to be deflected to pass through the burner ports. Various modifications in the form of resistance screens and baffles were tried with this wind-box design but failed to produce the distribution desired.

It became necessary to concentrate all of the modeling effort on the two end burners, namely, A-1 and D-2, as these were the only ones which could be torn down, modeled, and remodeled with any degree of ease. Also they were the only burners capable of complete observation from the side, which was of paramount importance in determining the merits of any new design. Pitot-tube measurements could be taken on any of the burners.

It will be recalled from the discussion heretofore of the original design, or arrangement I, that there was a marked tendency for a heavy downwash of the front-wall tubes. This condition suggested the design and testing of two distinct burner center-line

positions with respect to the front wall. Early in the test the D-2 burner was relocated toward the rear so that its center line was 1.5 in. model scale (15 in. actual size) further away from the front wall. There were advantages for this new position of the burner center line with respect to the front wall. However, it was impossible to determine from the model whether or not this change in position would influence slagging conditions on the front wall. The test work on the model continued, using different baffle arrangements for both positions of the burners and employing smooth curve baffles of many different radii and dissimilar loci, thus making similar arrangements for the two positions of the burner.

The original design of secondary-air dampers on a horizontal plane at the wind-box entrance prevented the extension of baffle arrangements from the wind box up into the secondary-air duct as far as seemed desirable. Consequently the secondary-air dampers were relocated to a position further up the duct, and with their axes normal to the face of the secondary-air duct.

Discussion of Final Arrangement

The final design was developed from the most promising features of many of the arrangements tested. A sectional side view of the final design is shown in Fig. 13. It will be noted that a

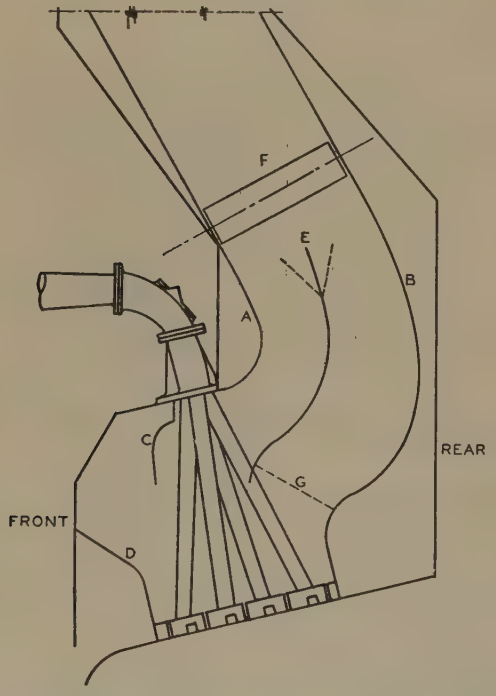

Fig. 13 Sectional Side View; Final Design of Burner and Wind Box

filler baffle A, was employed at the front end of the wind-box dampers to fill this pocket and eliminate the eddies formed in this zone. A curved rear baffle plate B, was installed tangent to the rear sloping wall of the secondary-air duct and formed a large radius, the lower extremity of which was tangent to the small radius at the rear of the burner ports. This curved baffle plate was found to give a smooth flow pattern which eliminated the ski-jump effect at the rear burner ports and resulted in a jet issuing normal to the furnace-roof tubes. A curved deflector baffle C, was installed in front of the primary tips just below the wind-box roof to eliminate eddies in this zone. Practical operating considerations requiring access and observation dictated the lower extremity of this deflector baffle, and the base baffle D, at

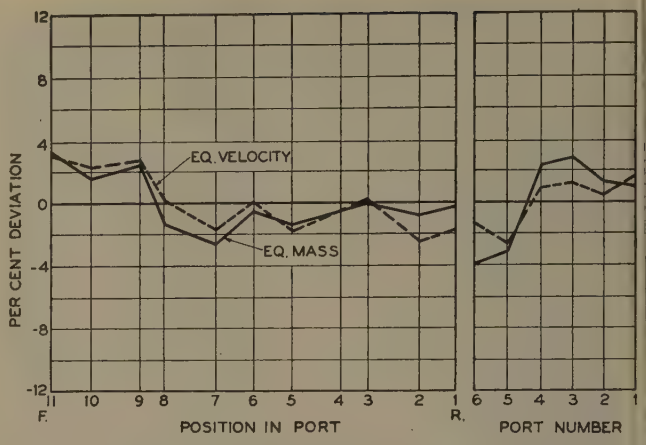

Fig. 14 Velocity Profiles in Burner Ports of Model; Final Design

Fig. 15 Flow Pattern in Model of Primary Furnace With Final Wind-Box Design; Contrast With Fig. 7

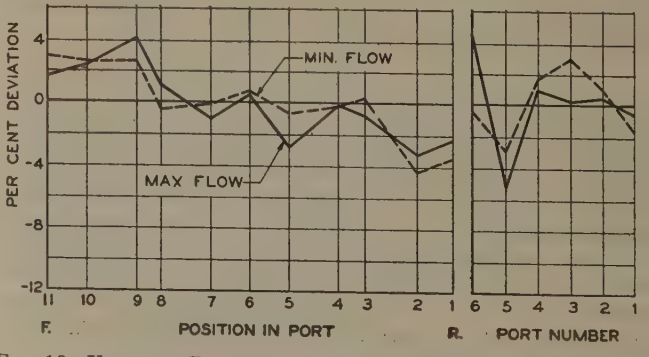

Fig. 16 Velocity Profiles in Burner Ports of Model With Maximum and Minimum Flows; Final Design

the front of the wind box. A curved vane E, was installed from a point just below the burner wind-box dampers F, through the rear row of primary tips to improve the front-to-rear velocity distribution at the burner ports. This result was not obtained completely with the vane alone, as the congestion of the primary tips at the outlet of the front channel resulted in high flows through the rear channel. Therefore it was necessary to balance this restriction. Resistance screens of various restriction were tested in the rear channel and a 65 per cent open screen G, was found to be the optimum size. The velocity profile at the burner ports, with the final design, as shown in Fig. 14, indicates that the distribution was uniform and slightly higher at the front of the ports, as contrasted with Fig. 9, the original arrangement, which showed less uniform distribution and higher velocity at the rear of the ports.

The jet pattern in the primary furnace is shown in Fig. 15 and indicates a direction of flow normal to the furnace-roof tubes as compared to Fig. 7. Velocity profiles in the burner ports on the final arrangement for the maximum and minimum flows are shown in Fig. 16. The similarity between the curves for these two flows substantiates further the earlier conclusion that the distribution did not vary with the quantity of flow for a given arrangement.

Comparison of Model With Actual Boiler

The burners, wind box, and secondary-air duct for the boilers were designed to duplicate this final arrangement on the model. Naturally, there was considerable interest in learning if the actual boiler showed the same flow characteristics that were observed on the model. Therefore a series of velocity readings in the burner ports were taken on the boiler in the same manner in which they were taken on the model. The results are similar to those obtained on the model as shown in Fig. 17. In Fig. 18 a summation is made of the average velocity per burner on the boiler and the model. The curves are both in good agreement one with the other. The end burners A-1 and D-2 show a slight reduction in air velocity.

A series of photographs taken during these tests are reproduced as follows: Fig. 19 shows the 20-ft-high scaffold erected in the primary furnace for the Pitot-tube traverses. Fig. 20 shows a close-up of the Pitot tube in the test position in the No. 3 port of the A-1 burner. Fig. 21 shows the chemical smoke issuing from the No. 1 port of A-2 burner.

Description of Steam-Generating Unit

These boilers are of the open-pass type, having a rated capacity of 850,000 lb of steam per hr with a 4-hr peak of 935,000 lb per hr.

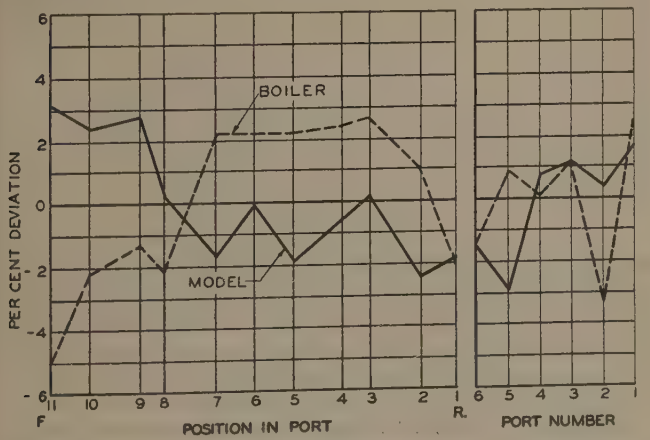

Fig. 17 Velocity Profiles in Burner Ports; Model Versus Boiler

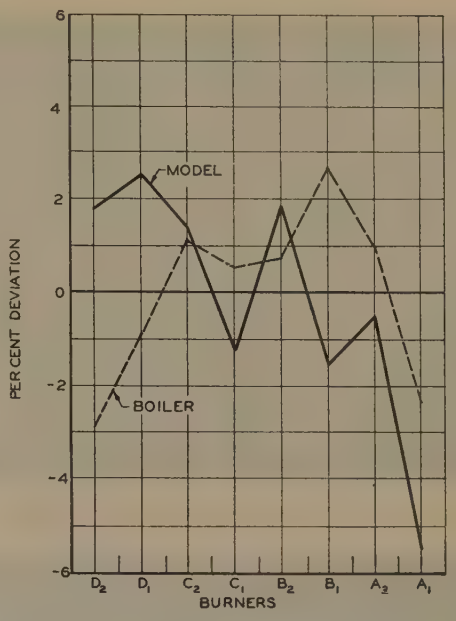

Fig. 18 Average Burner Velocity-Distribution Curves; Model Versus Boiler

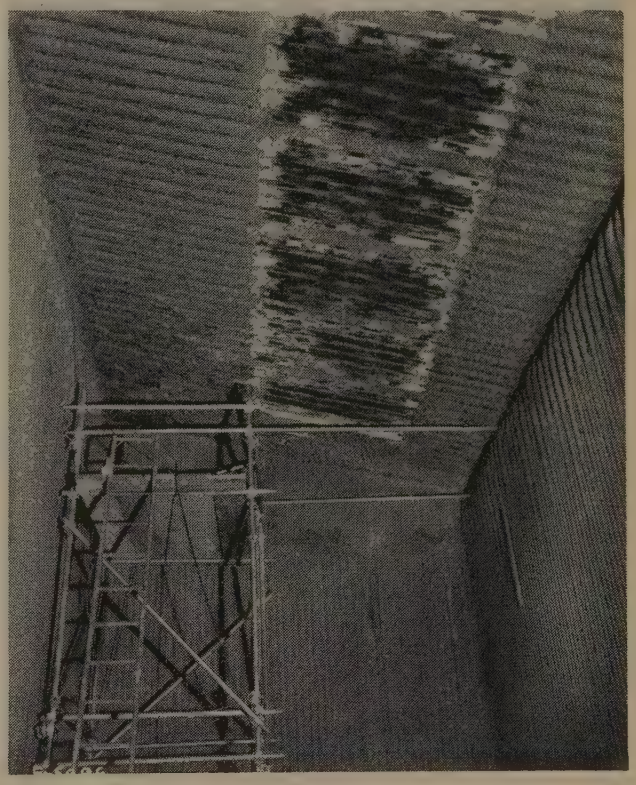

Fig. 19 Scaffold in Primary Furnace of Boiler

The design pressure and temperature conditions are 1075 psi and 900 F. Fig. 22 is a sectional side view of the boiler. Its salient features are as follows: The primary-furnace walls are of tube-to-tube construction, with full stud-and-chrome refractory covering on the furnace side. The primary furnace is of the continuous-slag-tap type. At the exit of the primary furnace, widely spaced tubes form a slag screen. The flow of gases is upward through the first open pass throug' spread tubes at the top of the first and

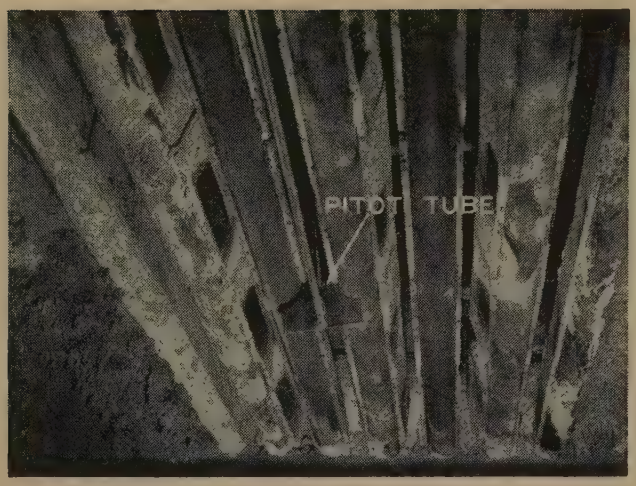

FIG. 20 PITOT TUBE IN BURNER PORTS OF BOILER

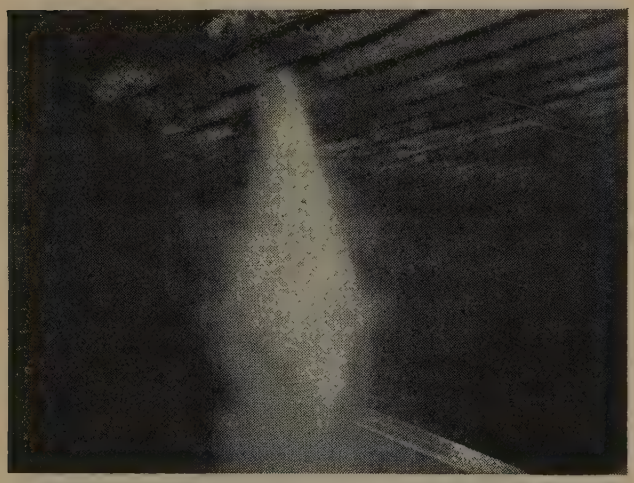

FIG. 21 CHEMICAL SMOKE ISSUING FROM BURNER PORT OF BOILER

second open passes; downward in the second open pass at the base of which is located the rear ash hopper. The last pass of the boiler contains a screen, secondary and primary superheaters, economizer, and above the boiler are located the two air preheaters and induced-draft fans. The combustion air is supplied by two forced-draft fans through the air preheaters into a single secondary-air duct which is routed across the top and down the front of the boiler into the wind boxes. The hot primary air is taken off each side near the center of the vertical run of the secondary-air duct and continues to the four pulverizers.

The secondary-air duct routing is of particular note both in over-all design and in the model changes in the wind-box region. The route is short, direct, and with a minimum number of bends. All turns are "easy" bends with a high aspect ratio and a low loss. The only offset in the entire run is at the wind box proper. Of particular note are the two sets of turning vanes which are located in the bends just ahead of and following the vertical run. These vanes were made of three turning leaves whose spacing, length, and radius of curvature, were determined by air-flow nomogram.

The segmental stiffening members were placed transversely in the turning vanes at the quarter points of the width of the duct. Model air-flow tests proved the location, type, and size of these vanes to be sound.

PERFORMANCE RECORD

At the time of writing this paper, the first two boilers had been in service approximately 12 months, August 1, 1947, to July 31, 1948, with total boiler service-hours of 16,461 and an availability factor of 95.3 per cent. In this period the average steam flow was 799,000 lb per hr, average preheated-air temperature 600 F, CO_2 14.5 to 15.5 per cent at the economizer outlet, and average exit-gas temperature 345 F. The coals burned during this period were from various sources. The average Btu content as-fired was 13,000 with a range of 12,300 to 13,600 per lb; moisture content averaged 4.4 per cent ranging from 1.9 to 7.1 per cent; the volatile matter averaged 28 per cent, ranging from 19.0 to 38.0 per cent; the ash averaged 10 per cent with a range of 9.1 to 10.6 per cent; and the sulphur content averaged 2.5 per cent with a range of 1 to 4 per cent.

OPERATING RESULTS AND OBSERVATIONS

The operating experience with these boilers showed that some coking occurred on the end burners, which may be attributable to the lower air velocity. In the early model tests it was noted that the velocity at the front and rear of the burner ports dropped sharply due, presumably, to the frictional drag of the adjacent surfaces. In order to attain a relatively flat velocity profile, it was thought advisable to lengthen the burner ports 0.6 in. (0.3 in. model size on each end). This was done to scale on the actual boilers and resulted in sufficient air-velocity reduction to increase the tendency to form coke. The explanation of this may be in the fact that the higher frictional resistance in the model was such that the design length of the increased opening was too great at prototype scale. With the partial closure of this increased opening, the operation is improved. The wide range of volatile matter in the coal being burned is another factor which makes the problem more complicated because of the increased tendencies of the higher-volatile coals to coke. With the coals being used some wear has been experienced in the coal directional ports. Investigation of this condition is being continued.

Probing of the furnace with a water-cooled tube for gas samples was done at the top of the first open pass. A uniform total air condition across the boiler is shown in Fig. 23. It was possible to reduce the average total air to as low as 108 per cent with no carbon monoxide present at the top of the first open pass.

Primary-furnace observations indicate that the ignition point is close to the burner ports. The flame issuing from the burner is essentially normal to the furnace-roof tubes, and of similar direction to the path observed on the model. Observations indicate the flame to be very luminous, free from smoke tails, and with well-defined boundaries over a wide range of loads, coal conditions, and with various numbers of burners in service. The flame appears to sweep smoothly in its course through the furnace with a noticeable lack of eddies or backwash along the walls. A colored motion-picture film taken in two different boilers at various locations, such as burner discharge, primary furnace, slag screen, top of open pass, and slag-tap hole, indicates very good combustion conditions in these boilers.

After several months of operation, the primary-furnace walls were covered with a smooth uniform thickness of slag having no well-defined or discernible pattern, nor is there any tangible evidence of tube wastage. Complete credit for the condition of the furnace walls cannot be attributed entirely to the performance of the burners, as due consideration must be given to the full stud and refractory wall construction. It will be recalled that two designs of burner center-line position were developed which are 15 in. different in the distance from the front wall of the furnace. Other than the change in burner center-line positions, the boilers are identical. It is impossible to say now that

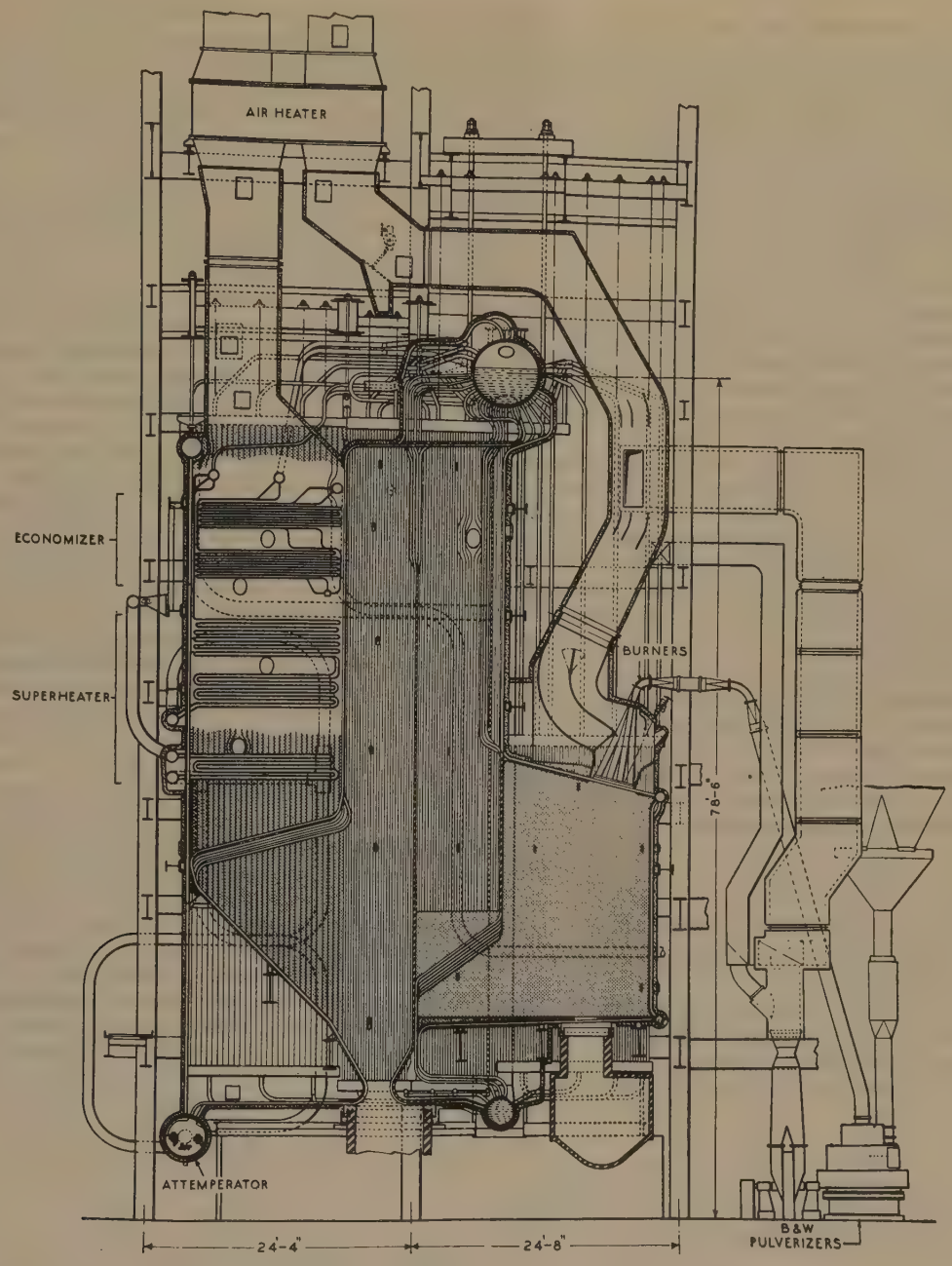

FIG. 22 SECTIONAL SIDE VIEW; SOUTHWARK STATION BOILER

there is any difference in the operating performance of these two designs; however, it must be recognized that the months of service on this equipment are insufficient to allow a conclusive statement at this time.

ACKNOWLEDGMENT

The authors thank the many people in both companies for their aid, advice, and assistance in the construction of the model, the model tests, the boiler tests, and the preparation of this paper.

Discussion

A. G. CHRISTIE.[4] This paper presents an interesting model

[4] Professor of Mechanical Engineering, Johns Hopkins University, Baltimore, Md. Past-President and Fellow ASME.

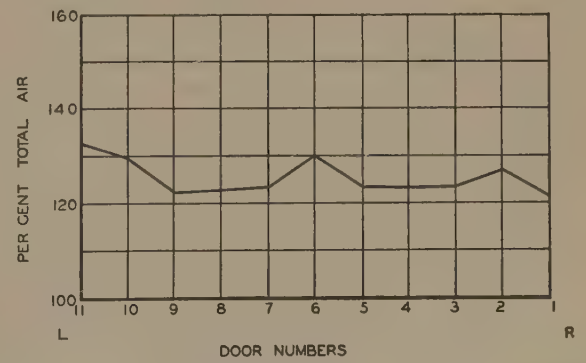

FIG. 23 TOTAL AIR-DISTRIBUTION CURVES ACROSS TOP OF FIRST OPEN PASS OF BOILER

study of gas and fuel distribution in a large furnace. Such a model presents difficulties both in operation and interpretation of results. One cannot duplicate in the model the increase in gas volume that occurs in the furnace nor the "chimney," and other effects of the high temperatures in the furnace. It is, therefore, gratifying to note that observations made on the flame and the slag deposits of the boiler itself in operation appear to confirm the conclusions of the model study. This will encourage model studies of other plant equipment.

These model tests emphasize the need of careful design of the ductwork into the wind box and of the contour of the wind box itself. The improvements in the model tests were principally due to changes in ducts and wind box to insure proper direction of the air to the burners. It is a reasonable deduction that the elimination of eddies in the improved ducts decreased in some measure the head losses of the preheated air and thus decreased the work of the forced-draft fan.

It has been said that tube wastage in earlier furnaces was due in some way to carbon monoxide. This gas formation appeared in eddies adjacent to the tube surfaces. A correction of the difficulty would appear to be the elimination of such eddies, and various schemes have been tried to effect this elimination. The authors note that there was a notable lack of eddies or backwash along the walls. It would be helpful if they would discuss the relative amount of eddying in the new boilers and in those boilers in which tube wastage occurred.

Turbulence is desirable to insure rapid and complete combustion of the pulverized fuel. Did the model indicate the same degree of turbulence as was seen in the actual boiler?

The writer saw some of the model tests and wishes to commend the authors upon the means used to show the flow effects at the burner nozzles and in the combustion chamber.

Authors' Closure

Professor Christie recognizes the problem of translating model observations and test results to full-size performance for this type of air-flow model work, where combustion and temperature effects cannot be duplicated.

An examination of the flame-propagation motion-picture films taken in the Southwark boilers clearly indicates a smooth progressive turbulent mass flow through the primary furnace with little, if any, recirculation of flow from the flame boundary. From the observations and results obtained in the Southwark boilers, it can be definitely stated that the modeling of ductwork, burners, and furnace proves much can be learned of the flow conditions that will be encountered on the actual boilers. It was possible to detect unsatisfactory flow conditions and to alter the model so as to obtain improved flow conditions which were reproduced on the actual boiler.

Carbon monoxide is not solely responsible for tube wastage but it is an indicator of a reducing atmosphere which must be present to establish the conditions necessary for wastage to occur. There is a marked improvement in the primary-furnace-wall appearance during combustion in these boilers as compared to other boilers on the system in which tube wastage had occurred. This is further borne out by subsequent inspections of the furnace-wall surfaces with the boilers out of service. The authors' opinion is that much of this improvement can be directly attributed to the smooth mass flow pattern of the boundaries of the flame and the absence of recirculating eddies or voids which contribute to a reducing atmosphere adjacent to the furnace walls. On the other boilers on the system in which tube wastage had occurred there was considerable recirculation along the furnace walls and flame eddies existed in the corners of the furnaces both at the junction of the side walls and the junction of the side walls with the furnace floor. The installation of baffles, vanes, and resistance screens in the ductwork and burners has improved the flow conditions and helped to reduce the eddies in these furnaces. These changes also completely directed the coal and air stream away from the walls of the primary furnace.

The model motion pictures, wet-paint panels, and visual observations made with chemical smoke and powder indicate close similarity of conditions in the furnace just below the burners with those observed on the actual boilers at this location with combustion taking place. Tests on the model with finely ground powder as a substitute for pulverized coal gave rapid mixing of the powder with the secondary air. Fig. 15 clearly indicates the density of the powder streams issuing from the model burners diminished uniformly until a completely homogeneous mixture of powder and air was attained at a point one quarter of the way down in the furnace where the powder was completely dispersed in the air stream resulting in a mixture of uniform density.

External Corrosion of Furnace-Wall Tubes—III Further Data on Sulphate Deposits and the Significance of Iron Sulphide Deposits

By R. C. COREY,[1] H. A. GRABOWSKI,[2] and B. J. CROSS[3]

Extended studies of the mechanism of external corrosion of furnace-wall tubes of high-capacity slag-tap furnaces, which were begun in 1942 by the Bureau of Mines in co-operation with the Combustion Engineering Company, have shown that liquid alkali-metal pyrosulphates can be formed under operating conditions from deposits of alkali-metal sulphates on the tubes. The rate of attack will be considerably higher than when the alkali-metal sulphates, or "enamel" deposits, do not form a liquid phase, which was described in a previous paper of this series. The phase boundaries for three compositions of alkali-metal sulphates in the system M_2SO_4–SO_3 have been established. The conditions for the thermal decomposition of coal ash, leading to the formation of the SO_3 necessary for the corrosion process, have been determined. Alkali-metal sulphate deposits on furnace tubes are believed to result from volatilization of alkalies in the coal, which condense as corresponding oxides on the tubes and then convert to sulphates by reaction with SO_3 in the furnace atmosphere. Furnace-wall-tube attack, associated with deposits consisting mainly of FeS, is believed to be related to the deposition of pyrites on the tubes. The pyrites, originating from coarse coal, or coal that is poorly distributed in the burners, with respect to size, adheres to previously formed deposits of alkali-metal sulphates, oxidizes relatively slowly to FeS and Fe_3O_4, and thereby produces sufficient SO_3 to react with the alkali-metal sulphates and the oxide on the metal. The net effect is to cause corrosion by the same processes that have been ascribed to corrosion by the alkali-metal-sulphate type of deposit. The relationship between the results obtained in the laboratory, and observations of furnaces before and after preventive measures have been applied, is described.

Introduction

INTERIM reports to the ASME in 1945,[4,5] showed that corrosion of the fire side of furnace-wall tubes in pulverized-coal-fired slag-tap furnaces is associated with two distinctly different types of deposits on the tubes.

Greatest frequency and severity of attack have occurred where the deposit on the tube was saltlike and quite soluble in water, in which it gave a strongly acid reaction. Previously, reference has been made to this type as enamel deposit[5] because of its glazed appearance, and has been investigated intensively since June, 1942, to determine its part in the corrosion process.

The other type of deposit found on furnace-wall tubes where attack occurred was rich in iron sulphide and magnetite, practically insoluble in water and strongly magnetic, and has been referred to as "iron sulphide" deposit.[5] However, since the frequency and severity of attack associated with this deposit were considerably less than in the case of the enamel type, less emphasis was placed on studies of its properties during the early part of this investigation.

The investigation has continued to the present time, and it is the purpose of this paper to report the results obtained since 1945, from extended studies of the enamel and the sulphide types of deposits. It is believed that definite conclusions now may be made regarding (*a*) the conditions necessary for the formation of, and corrosion by enamel deposits; and (*b*) the chemical and physical properties of iron sulphide deposits, and the mechanism of corrosion where such deposits occur.

Review of Problem and Previous Work

During 1941 a number of central stations and industrial plants reported thinning of the fire side of furnace-wall tubes of pulverized-coal-fired slag-tap steam generators operating at high pressures and steaming capacities. As the result of wartime demands, which required prolonged periods of operation at full load and reduced overhaul periods and maintenance, external corrosion became an acute problem. The extent of attack in some typical cases is shown in Fig. 1. Through co-operative efforts of the boiler manufacturers and the operating companies, attack was abated somewhat by temporary measures, such as supplying a blanket of air to the walls, and applying protective coatings to the tubes in the affected areas. These measures are a matter of record.[6]

Many theories were proposed to explain this type of corrosion, but there was no real progress made toward a plausible hypothesis until careful inquiry revealed the fact that thinning of wall tubes had been noted several years earlier, and had been attributed to "slag erosion," a vague theory which did not fit the facts. Nevertheless, this information made it possible to eliminate from further consideration a number of factors, factors based upon the assumption that external corrosion was a new phenomenon. The conclusion reached was that thinning of tubes had progressed slowly over a period of years and had gone practically unnoticed until accelerated attack, incurred by unusual operating schedules, caused excessive thinning, and even failure of wall tubes.

---

[1] Supervising Engineer, Combustion Research Section, Coal Branch, Bureau of Mines, Pittsburgh, Pa. Mem. ASME.

[2] Research Engineer, Combustion Engineering-Superheater, Inc., New York, N. Y.

[3] Manager, Research Department, Combustion Engineering-Superheater, Inc., New York, N. Y. Mem. ASME.

[4] "External Corrosion of Furnace Wall-Tubes—I History and Occurrence," by W. T. Reid, R. C. Corey, and B. J. Cross, Trans. ASME, vol. 67, 1945, pp. 279–288.

[5] "External Corrosion of Furnace Wall-Tubes—II Significance of Sulphate Deposits and Sulphur Trioxide in Corrosion Mechanism," by R. C. Corey, B. J. Cross, and W. T. Reid, ibid., pp. 289–302.

Contributed by the Committee on Furnace Performance Factors and the Fuel and Power Divisions, and presented at the Annual Meeting, New York, N. Y., November 28–December 3, 1948, of The American Society of Mechanical Engineers.

[6] "Boilers and Combustion, 1944," Publication M4, Edison Electric Institute, 1945.

Note: Statements and opinions advanced in papers are to be understood as individual expressions of their authors and not those of the Society. Paper No. 48—A-160.

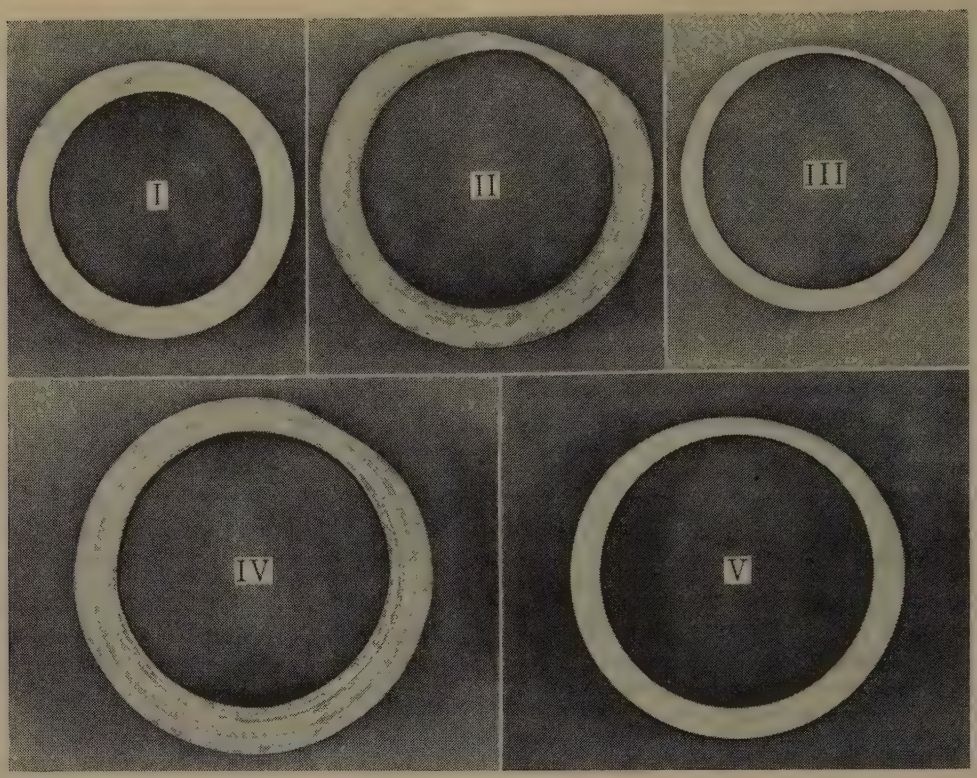

FIG. 1 TYPICAL CORRODED FURNACE-WALL TUBES FROM 700 TO 1400-PSI SLAG-TAP UNITS

Since the protective measures used to mitigate or arrest external corrosion were not entirely successful in each case they were used, it became obvious that before rational preventive measures could be applied, fundamental studies would be necessary to determine the cause and the mechanism of tube attack. The basic requirement for such an investigation is close liaison between the field and the laboratory, so that the data from each may be correlated. To this end, the Combustion Engineering-Superheater, Inc., and the Bureau of Mines began a co-operative investigation of the problem in June, 1942, which has continued to the present time.

The results of the first phase of the investigation, which dealt primarily with corrosion in the presence of enamel deposits, were presented at the 1944 Annual Meeting of the Society, and were subsequently published.[4,5] Examination of numerous furnaces in which corrosion was active, and studies of actual and synthetic-enamel deposits under controlled laboratory conditions, suggested that attack was the result of chemical reaction between (*a*) the normal oxide on the tubes, (*b*) the alkali-metal sulphates, comprising the enamel deposits on the tubes, and (*c*) the SO_3 in the atmosphere in contact with the deposits. The sequence of events proposed is shown in Fig. 2 and was described as follows:

Step A. Assuming a furnace with clean tubes is placed in operation, then normal oxidation of the steel will occur at tube-metal temperatures, which normally lie between 600 and 800 F, and the oxide formed thickens parabolically with time. In the absence of adverse conditions, a more or less limited thickness is approached.

Step B. A layer of alkali-metal sulphates, generally consisting of a solid solution of 3 mols K_2SO_4 and 1 mol of Na_2SO_4, which corresponds to the mineral "glaserite," forms on the surface of the oxide. This is believed to result from deposition on the tubes of alkali-metal oxides, which originate from the flame and from the molten slag on the hearth by volatilization, subsequent reaction with the SO_3 in the surrounding atmosphere forming alkali-metal sulphates. (For simplicity, K_2SO_4 is shown in Fig. 2 rather than the solid solution. The conclusions are the same in either case.)

Step C. As the layer of alkali-metal sulphate thickens, the surface temperature increases until ash particles begin to adhere to it. As the result of a porous structure, the initial deposit of ash has a relatively low thermal conductivity; therefore, as it thickens, the outside temperature increases gradually to the point where the ash begins to sinter, and ultimately to slag. During this process SO_3 is evolved as the result of reactions in the ash during the melting process.

Step D. Some of the SO_3 thus formed diffuses through the alkali-metal sulphates and reaction occurs at the oxide-sulphate interface, forming a complex alkali-metal ferric trisulphate

$$3\,K_2SO_4 + Fe_2O_3 + 3\,SO_3 \rightarrow 2\,K_3Fe(SO_4)_3$$

(enamel) (oxide on tube) (gas)

This process reduces the thickness of the oxide and the metal will oxidize further to renew the oxide layer. During this period the layer of slag thickens and reaches an equilibrium thickness, and the temperature at the surface decreases.

Step E. Deslagging increases the temperature of the deposit on the tube, causing a portion of it to exceed the decomposition temperature of the $K_3Fe(SO_4)_3$, releasing SO_3, part of which diffuses to the oxide-sulphate interface and reacts with excess K_2SO_4 and Fe_2O_3. Meanwhile, more alkali-metal-sulphate deposits on the tube until another layer of slag is formed, and the cycle is repeated.

There were insufficient data, however, to confirm certain of the postulates in the mechanism just described. For example, the sequence of events was based largely on the results of controlled experiments at 1000 F, a temperature considered for the pre-

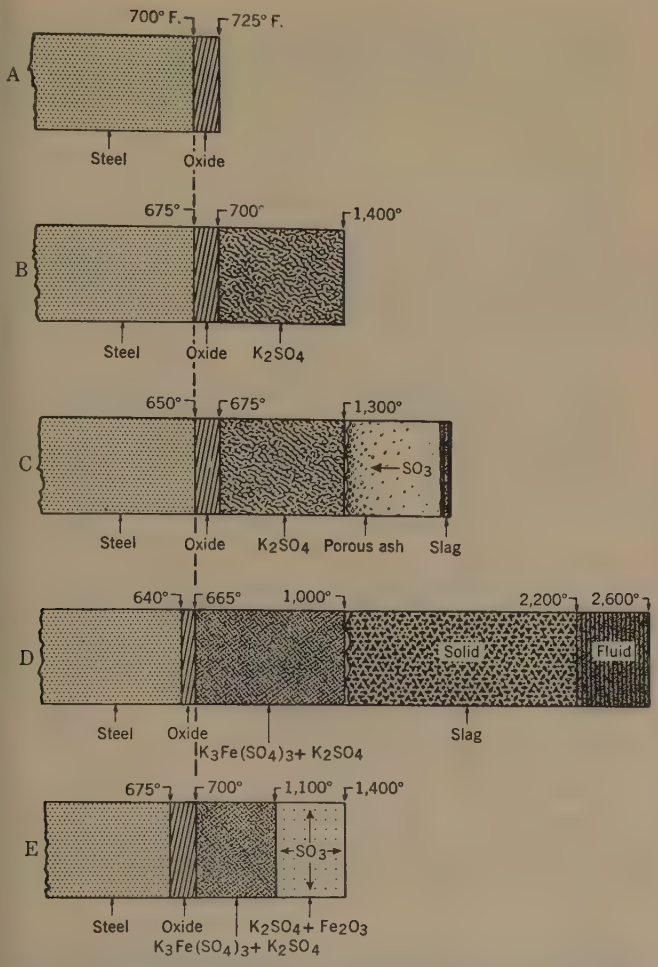

FIG. 2 MECHANISM OF CORROSION OF WALL TUBES BY SULPHATE DEPOSITS

liminary work to be close to the upper limit at which corrosion reactions would occur on furnace-wall tubes in high-pressure steam generators. However, since the metal temperature of the fire side of such tubes is known normally to be several hundred degrees lower than this, it was considered desirable to extend the data for enamel deposits down to about 500 F, thus covering the temperature range in which corrosion was likely to be most active.

Furthermore, although evidence was meager at the time the first reports were made to the Society that alkali-metal pyrosulphates were an active constituent in enamel deposits, they could not be dismissed entirely from consideration, since conditions for formation of pyrosulphates appeared to be favorable.

It is noted also that one of the steps in the mechanism of corrosion postulates that alkali-metal oxides, originating from the alkali metals in the flame, condense on the tubes and subsequently react with the SO_3 in the surrounding atmosphere to form the corresponding sulphates. This had not been demonstrated experimentally, although it was known that deposits of alkali-metal sulphates condense on relatively cool surfaces in glass furnaces, in which the primary source of sulphur is the sodium sulphate added to the charge.

Therefore, to obtain sufficient data to permit more general conclusions regarding the mechanism of corrosion by enamel deposits, and to determine the factors in corrosion by iron sulphide deposits, the investigation since 1945 has been concerned with the following main topics.

SCOPE OF INVESTIGATION

1 Determination of the temperature and concentration of SO_3 required to convert alkali-metal sulphates to solid and to liquid pyrosulphates, which are known to attack iron and steel rapidly.

2 Study of the reactions of Fe with alkali-metal sulphates and SO_3 over a range of temperatures and concentrations of SO_3. Included in this phase of the work is evaluation of the effect of small amounts of lithium, which has been found in enamel deposits from several furnaces.

3 Determination of the sulphur gases evolved from coal ash during heating below and in the slagging range.

4 Determination of the phases condensed on water-cooled surfaces from high-temperature gases containing small concentrations of alkali metals and SO_3.

5 Studies of the reactions of iron sulphide and iron disulphide (pyrites) as related to corrosion, where deposits are rich in iron sulphide.

Items 1 to 4, inclusive, represent extension of the work on enamel deposits since 1945, and item 5 relates to work on a phase of the problem that has not received attention previously.

All subsequent discussion of alkali-metal sulphates will refer to three compounds: namely, (*a*) the solid solution containing 3 mols of potassium per mol of sodium, (*b*) a synthetic mixture containing 80 per cent of (*a*) and 20 per cent of lithium potassium sulphate, by weight, and (*c*) pure potassium sulphate. The use of the first two substances is based upon the fact that analyses of numerous enamel deposits have shown the water-soluble portion to be either the solid solution $3\ K_2SO_4 \cdot Na_2SO_4$, corresponding to the mineral glaserite, or mixtures of glaserite with up to about 20 per cent of lithium potassium sulphate, $LiKSO_4$.[7] This compound gives rather strong x-ray diffraction lines at 3.94 and 3.09 angstroms.

It will be shown later that small amounts of lithium have an important influence on the reactions of alkali-metal sulphates with SO_3 and Fe_2O_3, which can be related to the distinctly different behavior in furnaces of enamels containing lithium. It should not be inferred that the K:Na ratio in the enamel deposits was invariably 3:1, but in a large number of samples the deviation from this ratio was sufficiently small to justify the selection of this particular composition for all the basic studies. Pure potassium sulphate never was found in enamel deposits, but was included for the purpose of comparison so that the effect of Na_2SO_4 could be ascertained. For simplicity of description, these materials will be hereafter referred to as glaserite, "synthetic enamel," and K_2SO_4.

EXTENDED STUDIES OF SULPHATE DEPOSITS

Formation of Pyrosulphates From Glaserite, Synthetic Enamel, and Potassium Sulphate. This investigation has shown that iron in contact with any one of the foregoing materials, and SO_3, will corrode more rapidly at a given temperature than when it is in contact with either one of these constituents, or in air, at that temperature. The reaction may be written

$$3\ M_2SO_4 + Fe_2O_3 + 3\ SO_3 \rightarrow 2\ M_3Fe\ (SO_4)_3 \quad [1]$$

(enamel) (oxide on tube) (gas)

where M is sodium or potassium, or both, and has been considered to be the basic reaction leading to corrosion of furnace tubes with enamel deposits. The physical appearance and chemical be-

[7] Twenty per cent by weight of $LiKSO_4$ is equivalent to approximately 1 per cent Li.

havior of some enamel deposits, which were described in detail in the earlier paper,[5] suggested that pyrosulphates might be an active constituent, although x-ray diffraction patterns did not show them to be present. Nevertheless, the possibility could not be eliminated that liquid pyrosulphates were present some time during the formation of enamel deposits, and that subsequently they either underwent thermal decomposition, or reacted with iron oxide according to the reaction

$$3\,M_2S_2O_7 + Fe_2O_3 \rightarrow 2\,M_3\,Fe\,(SO_4)_3 \ldots\ldots\ldots [2]$$
(liquid) (solid)

The product, alkali-metal ferric trisulphate, has been synthesized by Reactions [1] and [2] in two ways, namely, by a dry-reaction method, that is, where at no time did liquid phase occur, and by controlling conditions so that liquid pyrosulphate was clearly visible until the Fe_2O_3 had reacted with it. That the liquid phase was pyrosulphate was confirmed by withdrawing a sample and making an x-ray diffraction pattern. Thus absence of pyrosulphate in enamel deposits, particularly where the iron and aluminum content is high, is not conclusive evidence that it was not an intermediate product during the corrosion process, since it may have all reacted to form $M_3Fe(SO_4)_3$. Furthermore, the rate of attack of furnace tubes in a few cases has been so high as to suggest strongly that the liquid-phase Reaction, [2], was appreciable.

It was apparent, therefore, that the conditions necessary for the formation of pyrosulphates, by reaction of SO_3 with glaserite synthetic enamel and potassium sulphate, had to be determined, particularly to establish the phase boundaries of the liquid phase in each case. The apparatus for these studies is shown in Fig. 3. The procedure was to place a weighed quantity of the salt in the glazed-porcelain boat, which was suspended in the furnace and attached to the tared balance arm. The specimen was then heated to about 1050 F and when thermal equilibrium was reached, a gas containing an accurately determined amount of SO_3, 3-5 per cent oxygen and balance of nitrogen,[8] was passed upward through the tube at a slow rate. The nitrogen trap at the top of the tube prevented SO_3 from condensing in the cooler portions of the tube and on the suspension wire. After noting whether a change of weight had occurred, the temperature was lowered in 25-deg steps, holding it constant at each level for approximately 15 min and observing closely whether an increase of weight occurred, which would denote reaction of the salt with the SO_3 to form pyrosulphate.

At the first sign that reaction was occurring, the furnace was held constant at that temperature until the sample reached constant weight, and the total change was noted. Then the temperature was increased very slowly in 5-deg steps, until a loss of weight occurred. This temperature, within an error of ± 10 deg F, represented that at which the pyrosulphate had the same SO_3 vapor pressure as that of SO_3 in the surrounding gas. Observations of the charge in the boat at this temperature showed that it was liquid, and x-ray diffraction analysis of the product after quenching in air showed it to be the pyrosulphate of the corresponding sulphate. The patterns for K_2SO_4 and $K_2S_2O_7$ are shown in Fig. 4. Further confirmation was the fact that the total increase of weight corresponded to the stoichiometric amount of SO_3 required to form the pyrosulphate.

The concentration of SO_3 for these experiments was varied from approximately 0.05 to 1.0 per cent by volume, a range considered

[8] SO_3 was prepared by mixing SO_2, O_2, and N_2 in the desired ratios under pressure in a cylinder, and passing the mixture over a platinum catalyst at 750 F. Rather than determine the SO_3 in the final gas, the SO_2 was determined in the tank charge and corrections made for the volume contraction.

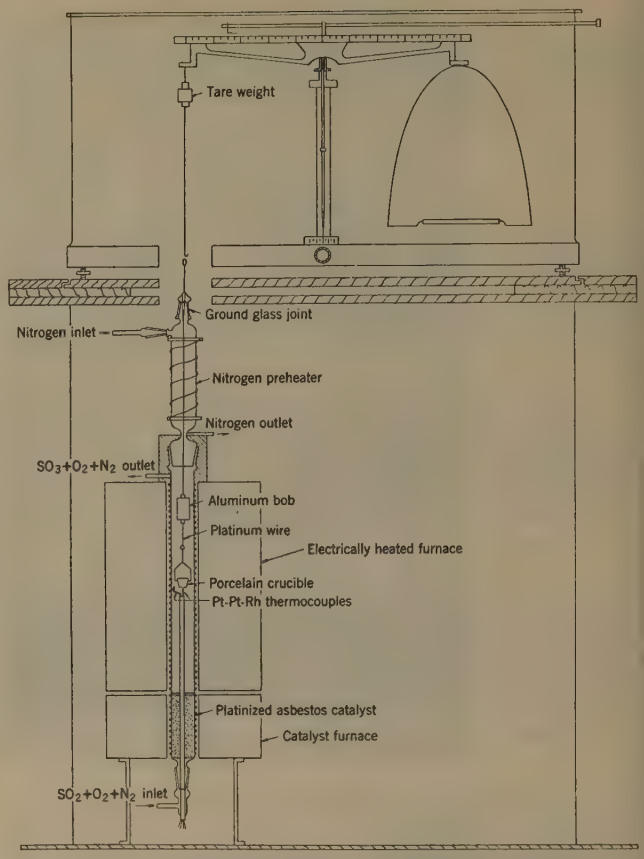

FIG. 3 APPARATUS FOR DETERMINING INSTANTANEOUS CHANGE IN WEIGHT OF SPECIMENS IN PLACE

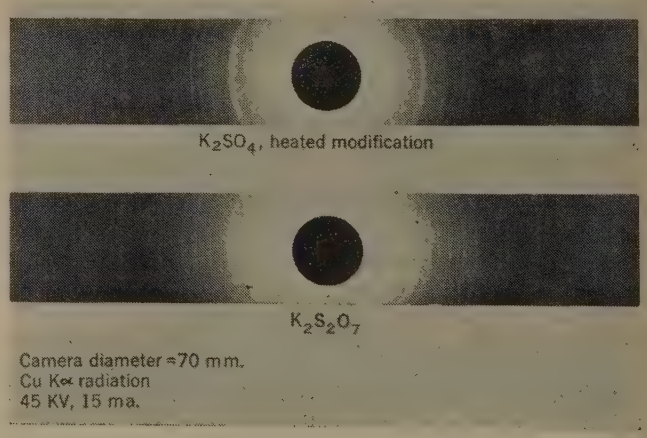

FIG. 4 DIFFRACTION PATTERNS OF K_2SO_4 AND $K_2S_2O_7$ RESULTING FROM REACTION AT 800 F IN 0.3 PER CENT SO_3

to cover adequately conditions likely to exist in a furnace. The temperature was varied from 400 to 1050 F, limits that were established by preliminary, semiquantitative tests with K_2SO_4.

It will be noted that the tests just described defined the boundary between solid glaserite, synthetic enamel, and potassium sulphate and the liquid phase of the corresponding pyrosulphate. It was not possible to determine accurately, however, the temperature at which the liquid phase solidified, that is, the melting point of these pyrosulphates. To obtain this information, quantities of the pyrosulphates were prepared and placed in the tubes shown in Fig. 5, which were evacuated and sealed. Then after heating the

tubes until the salt was melted completely, they were cooled slowly and the electromotive force (emf) of the thermocouple noted at regular intervals. From the cooling curve so obtained, an accurate value of the melting point was obtained. It should be mentioned that the free volume in the tubes was small enough to prevent decomposition of significant amounts of the pyrosulphate, which conceivably could lead to erroneous results due to the formation of the corresponding normal sulphates.

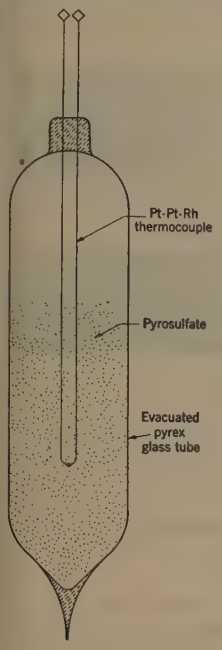

FIG. 5 APPARATUS FOR DETERMINING MELTING POINT OF ALKALI-METAL PYROSULPHATES

Having established the phase boundaries in these systems, they were plotted as shown in Fig. 6, in which the reciprocal of the absolute temperature is plotted against the logarithm of the concentration of SO_3 in the gas. The rather long extrapolation of line *ab* for the synthetic enamel was necessary because of the difficulties and uncertainties involved in working with concentrations of SO_3 less than 0.01 per cent. Thus there may be a small error in the slope of line *ab*, which would shift slightly the point of intersection of *ab* and *ac*, but this is not considered to be important either to the interpretation of the results or the conclusions therefrom.

For each case, the area *abc* shows the range of temperatures and concentrations of SO_3 in which liquid pyrosulphate can exist, line *ab* representing equilibrium between the solid, normal sulphate and liquid pyrosulphate, and the horizontal line *ac* representing the melting point of the pyrosulphate. The dashed line *ad*, the slope of which was estimated, represents equilibrium between solid normal sulphate and solid pyrosulphate, that is, the conditions under which pyrosulphate is formed in the absence of liquid phase.

Comparing the diagrams for K_2SO_4 and glaserite, two effects of Na_2SO_4 are noted, namely, the melting point of the salt is lowered and the point *a*, representing the minimum concentration for the formation of liquid pyrosulphate is shifted to the left. Therefore it appears that the chance of liquid pyrosulphate occurring in an enamel deposit increases as the Na_2SO_4 increases from 0-25 mol per cent. Although indications are that up to 50 mol per cent Na_2SO_4 will produce the same effects, it is emphasized that the conclusions from these data apply only to the range of composition that was investigated.

It may be seen from the diagrams for glaserite and synthetic enamel that the addition of sufficient $LiKSO_4$ to produce a mixture containing 1 per cent Li depressed the melting point of the glaserite about 100 deg F, and shifted the point *a* considerably. This is significant in view of the fact that quantitative spectrographic analyses of several enamel deposits showed Li to be present in amounts up to approximately 1 per cent, and x-ray diffraction analysis showed it to be combined as $LiKSO_4$, which explains the use of this particular salt to obtain a synthetic enamel.

The significant points in Fig. 6 are summarized in Table 1. The qualitative conclusions from these data, with regard to the behavior of enamel deposits in the composition range of 75 to 100 per cent K_2SO_4, corresponding to the majority of the deposits analyzed, are as follows: (*a*) Sodium and lithium tend to lower the melting point of the pyrosulphate formed by reaction with SO_3; and (*b*) the range of temperatures in which liquid phase can exist above the melting point of the pyrosulphate increases with the concentration of SO_3, in the gas that is in contact with the deposit.

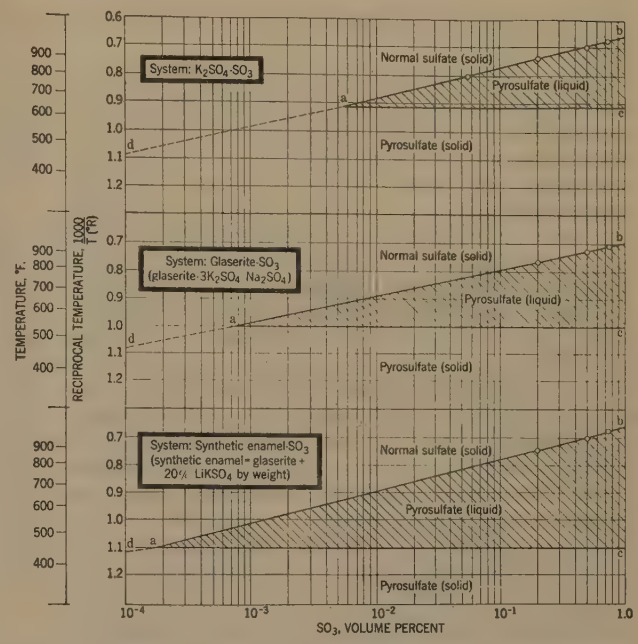

FIG. 6 TEMPERATURE-SO_3 BOUNDARIES FOR PYROSULPHATES FORMED BY REACTION OF ALKALI-METAL SULPHATES WITH SO_3

TABLE 1 BOUNDARY CONDITIONS FOR LIQUID PYROSULPHATES DERIVED FROM K_2SO_4, GLASERITE ($3K_2SO_4 \cdot Na_2SO_4$) AND SYNTHETIC ENAMEL (4:1 GLASERITE AND $LiKSO_4$)

Original salt		K_2SO_4	Glaserite	Synthetic
Melting point of corresponding pyrosulphate, deg F		635	535	450
Minimum concentration of SO_3 to form liquid pyrosulphate, per cent by volume		0.005	0.0007	0.0002
Approximate temperature range in which liquid pyrosulphate can exist above melting point when SO_3 by volume is as follows:				
0.01	F deg	40	140	225
0.05	F deg	130	230	310
0.10	F deg	205	270	370
0.30	F deg	290	340	460
0.50	F deg	335	375	518
1.00	F deg	445	455	605

Corrosion of Iron in Contact With Alkali-Metal Sulphates and SO_3. Although it is known that at any given temperature iron will corrode in liquid pyrosulphates at rates considerably higher than in air or low concentrations of SO_3, there was need of comparative corrosion data over a range of temperatures which might occur at the surface of furnace-wall tubes. Furthermore, it was thought that the results of corrosion experiments to obtain such data might reveal some specific effect of lithium that could be correlated with the observation that tube corrosion appeared to be more active where enamel deposits contained 0.5 to 1.0 per cent lithium.

Corrosion rates of iron were determined by embedding a cleaned and weighed specimen of iron wire[9] in a small quantity of glaserite or synthetic enamel contained in a porcelain boat, heating at constant temperature in a slow stream of gas containing SO_3 for a period of 168 hr, and pickling the specimens to remove corrosion products and determining the loss of weight. The volume ratio of salt to metal was kept relatively high to minimize the effect of changes in composition of the salt in contact with the metal, due to the products of corrosion. The experiments were

[9] All tests were made with the same batch of iron wire of thermocouple grade.

made in a horizontal modification of the furnace and catalyst shown in Fig. 3.

The rates of corrosion at 700 to 1000 F, in 100-deg steps, and in concentrations of SO_3 of 0.1 to 0.5 per cent are given in Fig. 7. It should be noted that small inconsistencies in the results are due to experimental factors, inherent in this type of corrosion testing, that were difficult to control. Nevertheless, the trends are clear-cut and reasonable.

Referring to Fig. 7, it was found that at 900 F and 0.1 per cent SO_3 neither the glaserite nor the synthetic salts melted, which is consistent with the phase diagram in Fig. 6. Accordingly, neither salt should melt at 1000 F, but the synthetic melted in contact with iron at that temperature, with a sharp increase in corrosion rate. Since glaserite did not melt under the same conditions, it is believed that the lithium in the synthetic has a specific effect, producing a complex iron compound that melts near 1000 F. The x-ray diffraction patterns of the synthetic enamel before use, its corresponding pyrosulphate, and the product from reaction with iron and SO_3 at 1000 F are shown in Fig. 8. Attention is called to the distinct difference of the latter pattern from the others, indicating the corrosion product to be a unique phase. It has been synthesized in the laboratory by placing mixtures of synthetic enamel and Fe_2O_3 in SO_3 at high temperatures, in an effort to determine its composition, but as yet the work is incomplete.

The data in Fig. 7 show also that over the range 0.1 to 0.5 per cent SO_3 the concentration of SO_3 in the gas appears to affect the rate of corrosion only in so far as it is sufficient to cause liquid pyrosulphate to form. Compare, for example, the rate of corrosion of iron in glaserite at 1000 F from 0.1 to 0.5 per cent SO_3, no liquid phase occurring. Up to 900 F there is no consistent trend that would indicate one liquid pyrosulphate to be more corrosive than the other.

Sulphur Trioxide From Thermal Decomposition of Coal Ash.

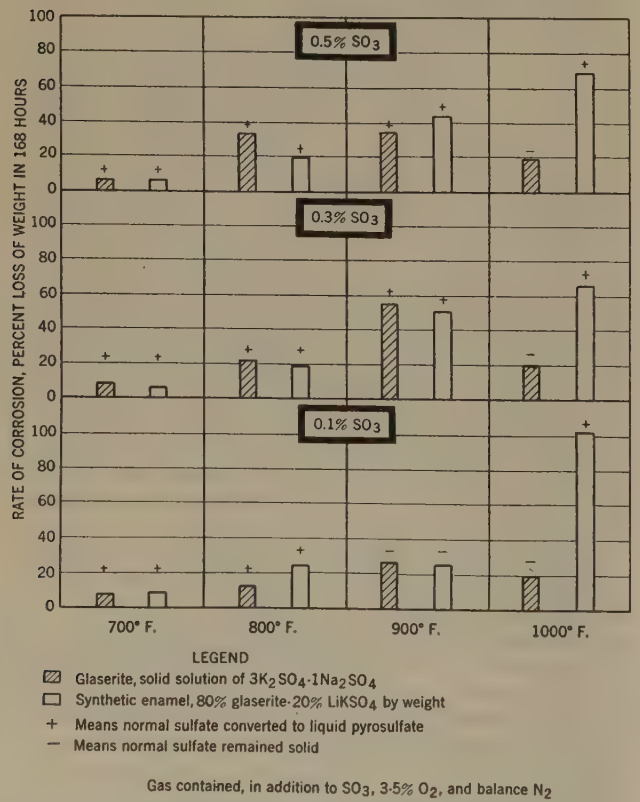

FIG. 7 RATE OF CORROSION OF IRON IN CONTACT WITH ALKALI-METAL SULPHATES AND SULPHUR TRIOXIDE

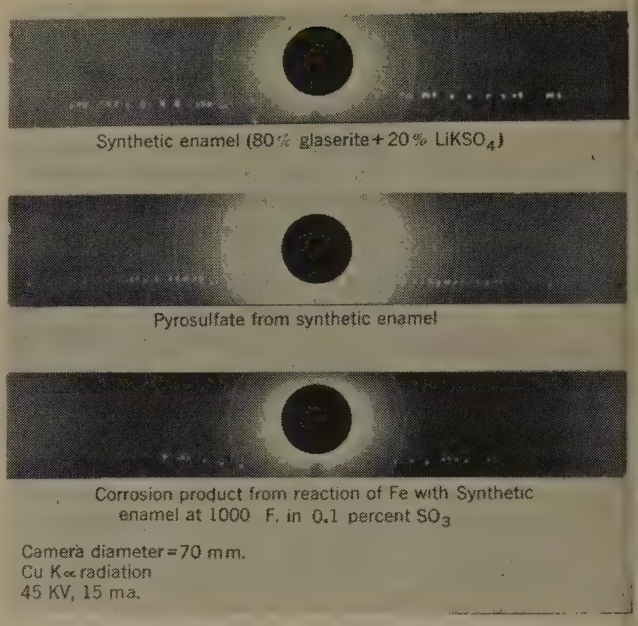

FIG. 8 X-RAY DIFFRACTION PATTERN OF SYNTHETIC ENAMEL, ITS PYROSULPHATE, AND PRODUCT AFTER REACTION WITH IRON

One of the basic premises in the proposed mechanism of corrosion of furnace-wall tubes is that the concentration of SO_3 in the gases in contact with the enamel deposit is sufficiently high for reaction to occur by either Equation [1], in which no liquid phase is formed, or Equation [2], in which liquid pyrosulphate is an intermediate product.

Analyses of gases from close to furnace walls, in areas where attack was active, showed the concentration of SO_3 to be negligible, but the concentration of SO_2 to be of the order of 0.1 per cent by volume.[4] Data for the dissociation equilibria of the reaction $SO_3 \rightleftarrows SO_2 + {}^1/_2\ O_2$, which are plotted in Fig. 9, show that under furnace conditions the ratio of SO_3 to SO_2 should be extremely low. For example, with low oxygen concentrations of 1 per cent or less, which are not unusual in areas where tube attack has occurred, the concentration of SO_3 becomes ${}^1/_{10}$ or less that of the SO_2 at temperatures as low as 1400 F. Consequently, at furnace temperatures of 2500–3000 F, quickly quenched samples of gas should show negligible amounts of SO_3.

Further to consider is the characteristic of wet-bottom furnaces that slag covers the tubes in affected areas completely and almost continuously during operation. Generally, the tubes are exposed directly to the furnace gases only during starting-up with a clean furnace, and during deslagging periods when the load is reduced or the walls are lanced.

These factors pointed to the probability that the SO_3 necessary for the corrosion reactions originates from the sintering and slagging of ash which adheres to the furnace tubes rather than from the SO_3 in the over-all furnace atmosphere. Due to the intimate contact of the ash with the tubes and the barrier formed by the overlying slag, which is shown schematically in Step C, Fig. 2, dilution of the SO_3 would be negligible, and the concentrations at the surface of the enamel deposits would be considerably higher than if the tubes were exposed only to the furnace gases. Some support of this thesis is found in the fact that although the furnace-wall tubes in dry-bottom furnaces frequently are coated with enamel deposits similar to those found at slag-tap furnaces, the rate of corrosion of such tubes occurs at a negligible rate. This is consistent with the fact that whatever ash accumulates on the tubes in dry-bottom units does not slag to any extent.

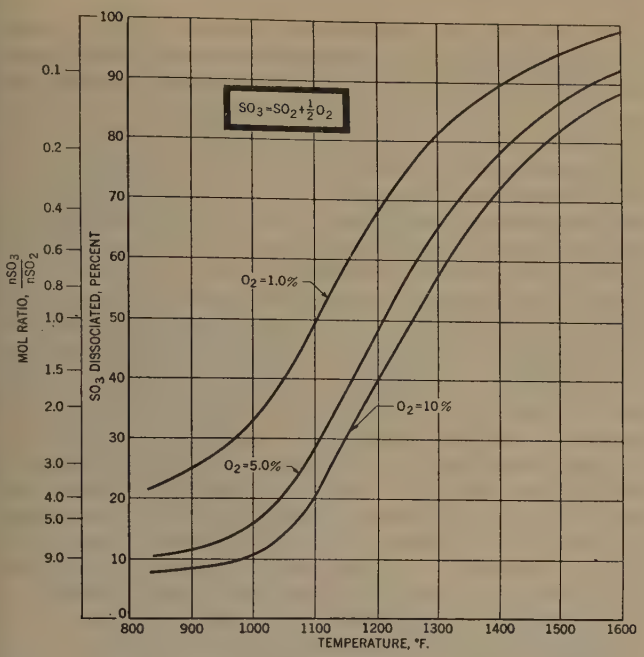

FIG. 9 THERMAL DISSOCIATION OF SO_3 AT VARIOUS CONCENTRATIONS OF O_2

To obtain data on the sulphur gases evolved from coal ash during heating, ashes selected to represent high and low sulphur were heated at various temperatures in a slow stream of nitrogen, and the gases evolved were analyzed for SO_2 and SO_3. The apparatus used for this work is shown in Fig. 10.

The ash samples were prepared by oxidizing at 1380 F high-volatile A Pennsylvania and high-volatile B Illinois coals. The ash analyses are given in Table 2.

A weighed sample of the ash was spread thinly in a porcelain boat and placed in the fused-silica furnace tube, which was heated previously to the desired temperature. Tank nitrogen containing about 0.2 per cent oxygen was passed through the tube at a rate of 150 cc per min, corresponding to a velocity of 18 cm per min. The exit gas passed to a fine-frit sintered-glass disk in a gas-absorption tube containing 50 ml of 0.2 N NaOH and 3 ml of benzyl alcohol. The SO_2 and SO_3 were determined by a modification of the method described by Johnstone,[10] in which the

[10] "The Corrosion of Power Plant Equipment by Flue Gases," by H. F. Johnstone, University of Illinois, Bulletin No. 41, 1931.

TABLE 2 ANALYSIS OF COAL ASH USED FOR HEATING TESTS

	High volatile-A (Penna)	High volatile-B (Illinois)
Chemical Analysis		
SiO_2	54.8	41.2
$Al_2O_3 + Fe_2O_3$	36.4	39.0
TiO_2	1.0	0.8
P_2O_5	0.3	0.1
CaO	3.9	9.4
MgO	1.0	0.4
Na_2O	0.6	0.6
K_2O	1.9	1.9
SO_3	2.2	9.0
Ash Fusibility		
IDT, deg F	2100	1960
ST, deg F	2270	2070
FT, deg F	2430	2290

solution first was titrated to pH 4.6 with 0.2 N HCl, a few ml of 3 per cent H_2O_2 added, and the solution finally titrated again to pH 4.6 with 0.2 N NaOH. The first titration minus the second gives the SO_3, and 2 times the second titration gives the SO_2. Check determinations, using metered quantities of a mixture of SO_2 and N_2, with two absorption bottles in series, gave absorption efficiencies of 98–99 per cent for the first bottle. To avoid excessive pressures in the heating-furnace tube, due to the high pressure drop across the sintered-glass gas-distributor tube, the end of the system was placed under a suction, regulated so that for the desired flow rate the pressure in the tube did not exceed 1 in. Hg.

Fig. 11 shows the cumulative weight of SO_2 and SO_3, expressed as percentage of total sulphur in the ash, given off during various periods of heating. For temperatures at and above the IDT of the ashes the sulphur is lost very quickly, as may be noted from the results at 2100 and 2300 F. However, in the sintering range, 1900 F, more of the available sulphur was lost in a given length of time from the Illinois ash, which had the lower IDT, than from the Pennsylvania ash. The significance of these results to the present problem is that the portion of the ash deposit on the tubes which does not fuse unless the slag sheet pulls away from the walls, can lose an appreciable percentage of its sulphur in a relatively short time at temperatures near the IDT.

It appears from Fig. 11 that the ratio of SO_3 to SO_2 is quite low and that the amount of SO_3 available for reaction with the enamel deposit might be insufficient unless the concentration of SO_2 were of the order of several per cent. The ratios shown correspond in magnitude to those for equilibrium at 1900 to 2300 F in low partial pressures of oxygen. It must be considered, however, that the temperature gradient through the slag to the enamel deposit is very steep, since there is no evidence that enamel deposits ever exceed about 1200 F in affected areas. Further, the concentration

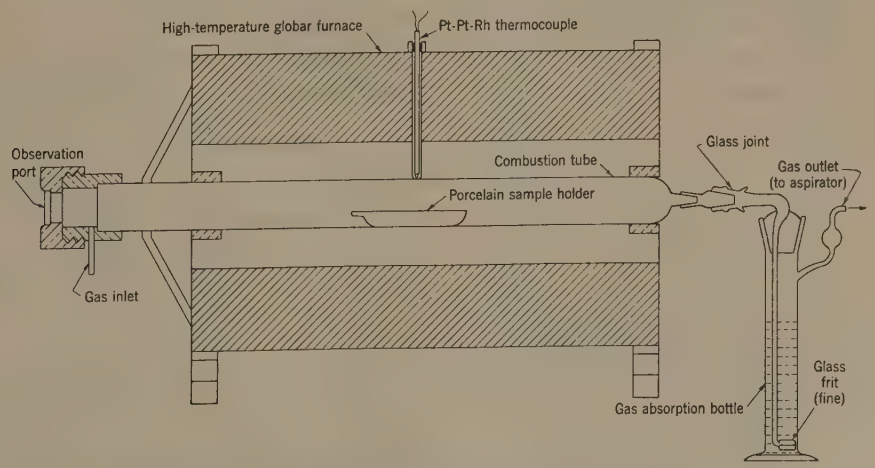

FIG. 10 APPARATUS FOR DETERMINING GASES EVOLVED DURING HEATING OF COAL ASH

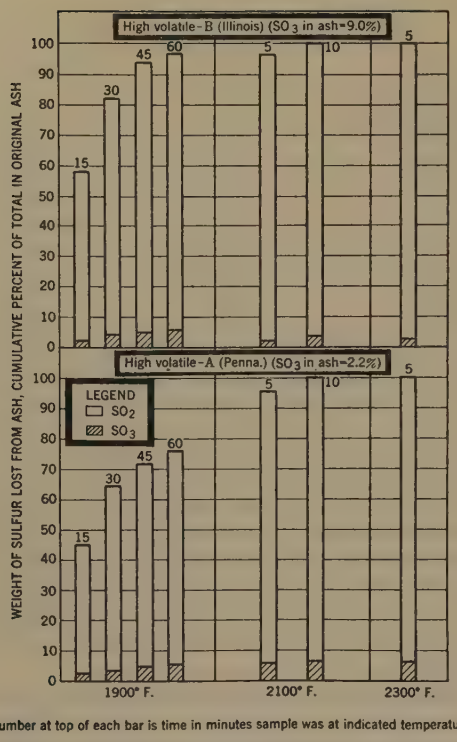

FIG. 11 EVOLUTION OF SO_2 AND SO_3 FROM COAL ASH HEATED TO VARIOUS TEMPERATURES IN ATMOSPHERE OF NITROGEN

of oxygen, due to infiltration between the tubes of air from the casing, may be appreciable at the surface of the enamel, or at the interface between the enamel and the ash adhering to it. These factors, low temperature and high concentration of oxygen, favor a higher ratio of SO_3 to SO_2, as may be seen from Fig. 9.

In general, therefore, although the sulphur is released from ash at temperatures where the ratio of SO_3 to SO_2 is extremely low, its passage through the ash toward the enamel is in the direction of lower temperature and higher concentration of oxygen, with continuous increase of the ratio.

Appreciable quantities of oxygen also may be available from decomposition of the coal ash, as the result of slagging reactions involved in the reduction of Fe_2O_3. Sherman[11] heated Central Illinois ash at various temperatures in a vacuum fusion system, and at 2400 F obtained the following amounts of oxygen, expressed as per cent of the weight of the ash: 0.6 in 5 min, 1.5 in 25 min, and 1.9 in 60 min.

It is conceivable, therefore, that where slag temperatures are high, due to flame impingement or other factors resulting in local high rates of heat release, sufficient oxygen and SO_2 are released from the ash to produce relatively high concentrations of SO_3 at the surface of the enamel.

Volatilization of Alkali Metals. Deposits rich in alkali-metal sulphates commonly occur on primary heating surfaces, such as boiler tubes, and secondary heating surfaces such as superheaters and air heaters of stoker-fired and pulverized-coal-fired furnaces. Barkley, Burdick, and Berk,[12] and Crossley,[13] made chemical analyses of numerous deposits from heat-absorbing surfaces of different types of units, one of the objectives being to evaluate the effect of such deposits on boiler availability and thermal efficiency. Alkali-metal sulphates were found to comprise a large percentage of these deposits. The first papers of this series[4,5] reported the results of chemical and x-ray diffraction analyses of a large number of external deposits from furnace-wall tubes of slag-tap units, up to 90 per cent of a solid solution of sodium and potassium sulphate being found in them.

Clearly, the source of the alkali metals is the coal, and any doubts in this respect should be dispelled by the significant fact that the mol ratio of potassium to sodium in the furnace-tube deposits corresponds in most cases exactly to that of the coal burned. Yet there is no evidence that the alkali metals are combined in the coal as sulphates. The question that naturally arises is "how do the alkali metals combine as sulphates on the heating surfaces?" A plausible assumption is that the alkalies condense on the tubes as alkali-metal oxides and react immediately with the SO_3 in the furnace gases, or with that evolved by the ash as described in the previous section. Since each of these compounds is

[11] Discussion of "The Horizontal Cyclone," by Grunert, Skog, and Wilcoxson, Trans. ASME, vol. 69, 1947, p. 632.

[12] "Test Data on Gas-Side Sulphate-Type Deposits on Tubes Beyond Boiler Furnace," by J. F. Barkley, L. R. Burdick, and A. A. Berk, Trans. ASME, vol. 70, 1948, pp. 81–89.

[13] "Deposits on the External Heating Surfaces of Boiler Systems," by H. E. Crossley, World Power Conference, Fuel Economy Section C2, paper No. 3, The Hague, 1947.

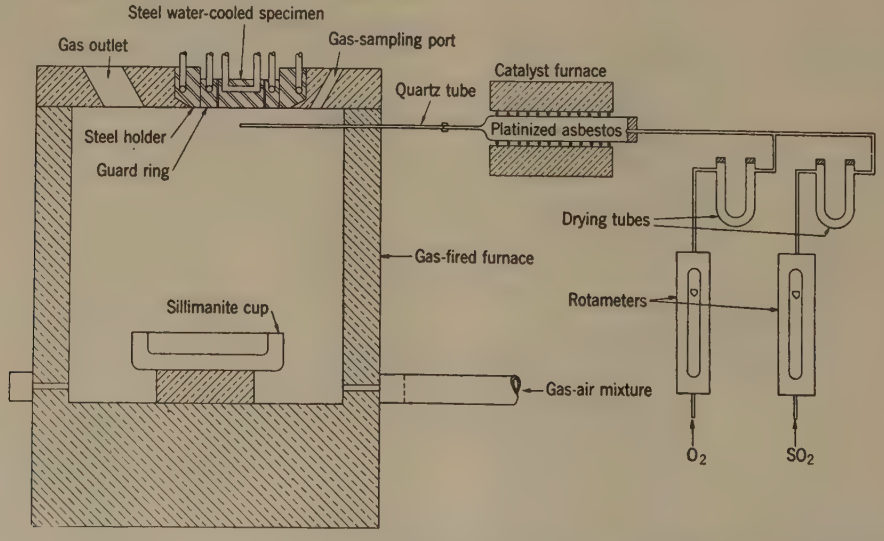

FIG. 12 APPARATUS FOR VOLATILIZING ALKALI-METAL SALTS IN A CONTROLLED ATMOSPHERE AND COLLECTING PRODUCTS ON WATER-COOLED SPECIMEN

relatively stable, as may be inferred from the fact that their vapor pressures at furnace temperatures are of a low order of magnitude, it is probable that extremely small concentrations of SO_3 will react with Na_2O and K_2O.

Some investigators have added solid materials containing alkali-metal sulphates directly to the flame in experimental furnaces, and observed the product formed on water-cooled surfaces. However, since there is a good chance that a certain amount of such materials is transported directly by the flame and deposited on the water-cooled surface unchanged, it seemed more appropriate to establish conditions so that only alkali-metal vapors reach the cold surface, since this is likely to be the situation in furnaces under actual operating conditions. Then, by supplying SO_3 to the furnace gases it becomes possible for the corresponding sulphates to form.

These conditions were established in this investigation with the apparatus shown in Fig. 12. Alkali-metal salts were heated above the melting point in the refractory cup by a natural gas-air flame, maintained slightly reducing. Sulphur trioxide, prepared by passing a mixture of SO_2 and O_2 over a platinum catalyst, was admitted to the furnace through a quartz tube, the end of which was located close to the water-cooled steel calorimeter. The calorimeter, fitted with guard rings to maintain a reasonably uniform temperature on the surface exposed to the furnace, was designed so that the metal temperature would be between 600 and 800 F with a furnace temperature of around 2500 F. This temperature range for the calorimeter was selected as representing furnace-wall tube temperatures in high-pressure steam generators.

For the first test, Na_2SO_4 was vaporized in the cup. In a short time the metal temperature began to fall, indicating deposition of solids on the surface. The test was concluded when the temperature reached 500 F, and an x-ray diffraction pattern made of the residue on the specimen showed that it was the heated modification of Na_2SO_4. Although the flame was colored yellow during the test, indicating that the vapor was dissociated to some extent, it could not be decided whether the deposit on the specimen was due to vaporization and condensation of Na_2SO_4 vapor, or sodium ions from the flame combined with O_2 and SO_3 at the metal surface and formed Na_2SO_4. It was clear, however, that a deposit could be produced on the specimen without transport of solid phase in the flame.

In the next test, Na_2CO_3 was vaporized without the addition of SO_3 to the atmosphere. The product on the specimen was found by x-ray diffraction to be anhydrous Na_2CO_3. Following this, Na_2CO_3 was vaporized with the addition of a slow stream of SO_3 to the furnace atmosphere. The x-ray diffraction pattern of the product, Fig. 13, showed it to be the phase $2\,Na_2SO_4 \cdot Na_2CO_3$, corresponding to the mineral "burkeite."

Thus although conversion to sulphate was not complete, due possibly to insufficient SO_3 in the furnace gases, it must be concluded that sulphates can form on water-cooled surfaces in contact with SO_3 and the vapor from Na_2SO_4 and Na_2CO_3 heated at 2500 F in a reducing atmosphere. Further work is needed to establish the limits of temperature and concentration of SO_3 and CO, in which this can occur, but the authors are confident that these tests simulated conditions in furnaces closely enough to conclude that deposits on furnace-wall tubes originate in the manner described.

In explanation of why such deposits are heaviest in areas where heat absorption is high, that is, where flame concentration is greatest, it is believed that it is in these zones of the furnace that the concentration of alkalies and sulphur is highest, and were it not for the fact that ash and slag quickly cover the walls, such deposits conceivably could become extremely thick. The deposits which occur on screen and superheater tubes, and on air-heater

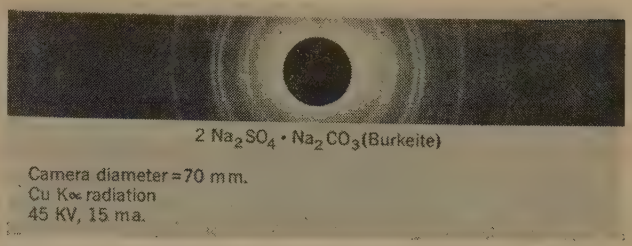

FIG. 13 X-RAY DIFFRACTION PATTERN OF CONDENSATION PRODUCT FROM VOLATILIZATION OF Na_2CO_3 IN ATMOSPHERE WITH LOW CONCENTRATION OF SO_3

elements, may originate in the same way, with the favorable factor that the concentration of SO_3 increases continuously with the attendant drop in temperature and contact with catalyzing surfaces during passage of the gases from the furnace.

Conclusions Regarding Corrosion of Furnace-Wall Tubes by Enamel Deposits. It is clear that the fundamental mechanism of external corrosion of furnace-wall tubes involves chemical reaction between (*a*) the normal oxide on the tube, (*b*) the sodium and potassium sulphates, comprising the enamel deposit on the tube, and (*c*) the SO_3 in the atmosphere in contact with the enamel deposit. The previous paper on this subject,[5] in which this theory first was proposed, considered only the "dry" reaction, that is, one in which the SO_2 reacted with solid oxide and solid enamel to form the solid compound $(KNa)_3Fe(SO_4)_3$. This reaction is given in Equation [1], and the sequence of events at the tube surface is shown schematically in Fig. 2 of this paper.

The results of the experiments which have been described show, in addition, that under certain conditions of temperature and concentration of SO_3, liquid pyrosulphates can form from reaction of the SO_3 directly with the sodium and potassium sulphates in the enamel, which can attack the oxide at a much higher rate than in the case of the dry reaction. Thus, as seen from Equation [2], there is direct attack of the oxide on the tube by the liquid pyrosulphate, with formation of the same compound, $(KNa)_3Fe(SO_4)_3$, as in the case of the dry reaction. Where the enamel has essentially the composition $3K_2SO_4 \cdot Na_2SO_4$, or glaserite, the liquid pyrosulphate can form at as low a temperature as 535 F if the concentration of SO_3 is 0.0007 per cent by volume or higher, and will persist over a range of temperatures well above this, depending upon the concentration of SO_3.

Where as little as 1 per cent lithium is present in the enamel deposit, which corresponds approximately to 20 per cent $LiKSO_4$, the melting point is depressed to 450 F, and the minimum concentration of SO_3 to form liquid phase becomes 0.0002 per cent by volume; the temperature range in which liquid phase can persist is higher for a given concentration of SO_3. Lithium has been found also to produce a complex compound with SO_3 and iron oxide which melts at about 1000 F, a factor which may account for the fact that in furnaces where lithium has been found in the enamel deposits, the deposits have a deep-red color and have a more fused appearance.

Indirectly, dew-point determinations on flue gases by electrical conductivity methods have shown that deposits of sodium and potassium sulphates undergo chemical reaction to produce compounds with relatively low melting points. For example, Flint[14] reports "dew points" in the temperature range between 350 and 650 F where sodium and potassium salts deposit on the apparatus, and attributes them to the formation and melting of bisulphates and pyrosulphates. However, he does not give corre-

[14] "The Investigation of the Dewpoint and Related Condensation Phenomena in Flue Gases," by D. Flint, *Journal of the Institute of Fuel*, vol. 21, 1948, pp. 248–253.

lations of these dew-point temperatures with the composition of the corresponding phases.

Regarding the relative rate of corrosion of iron in contact with SO_3 and glaserite and synthetic enamel, it has been shown that where liquid pyrosulphate forms, the rate of corrosion is considerably greater than when the sulphate does not melt. In the latter case, however, the rate of corrosion still is greater at a given temperature than if the metal were in contact with furnace gases only. From this it must be concluded that deposits containing alkali-metal sulphates in appreciable amounts, regardless of location in the furnace or on secondary heating surfaces, tend to corrode the steel with which it is in contact at a higher rate than normally would occur with clean surfaces. It should not be inferred from this that the presence of these deposits will lead to rapid destruction of such surfaces, but the danger exists that if conditions become favorable for the formation of liquid pyrosulphates, that is, a pseudo dew point, rapid attack will ensue.

The results of this investigation suggest that by far the largest source of SO_3 for these reactions is the ash deposit between the enamel and the slag. If this ash becomes heated to within a hundred degrees or so of the IDT, or higher, the sulphur compounds in the ash decompose at a rate that may result in high localized concentrations of SO_3 in direct contact with the enamel, and the consequent formation of liquid pyrosulphates.

It is obvious that a given amount of ash in contact with a tube can yield only as much SO_3 as is available from thermal decomposition of the sulphates, and it is probable that if a certain area of furnace wall retained the ash and equilibrium layer of slag laid down from the time the unit was placed in operation, attack of the metal would proceed only until the supply of SO_3 was exhausted.[15] However, observations of a number of slag-tap furnaces during operation show that over short or long intervals, depending on operating conditions, the walls deslag, and it is during these periods that the slag layer is restored and further attack may take place, that is, the sequence of events depicted in Fig. 2. This points to the possibility that the rate of attack in a given furnace is related to the frequency of deslagging, but to date, no reliable correlation in this respect is available.

With regard to the manner in which sodium and potassium sulphates are formed on furnace-wall tubes, it appears that during periods the walls are free of slag covering, the alkalies vaporized by the flame condense as oxides on the relatively cool tube surfaces, particularly in areas where flame concentration is greatest, and reaction with SO_3 from the furnace gases converts the oxides to sulphates. Subsequent reactions with the higher concentrations of SO_3 from thermal decomposition of the sulphates in the ash then may lead either to solid or liquid pyrosulphates.

Without exception, the worst cases of external corrosion that have been observed have had the following characteristics:

(*a*) A relatively thin covering of dense glassy slag that was frequently bonded quite firmly to the wall and removed with difficulty.

(*b*) A thin dark to reddish-brown layer of sintered ash, which generally came off with the slag, but occasionally remained attached to the enamel deposit on the tubes.

(*c*) A saltlike deposit that was thin, glazed, and reddish-colored on the portion of the tube most severely corroded, but becoming less glazed, thicker, and brownish to greenish white around the sides of the tube. This deposit always was strongly acid and quite soluble in water.

The most characteristic signs of amelioration of attack in areas where corrosion previously was severe have been found to be as follows:

(*a*) A thicker layer of slag that was easily detached, or fell from the wall during the cooling of the furnace.

(*b*) A soft deposit of light to dark-tan ash on the tubes, and a porous layer of ash on the concave side of the slag which showed little or no signs of having been heated in the sintering range.

(*c*) An enamel deposit on the tube that appeared less glazed and greenish to brownish-white, indicating the presence of less iron.

In general, it appears that if the gases along the walls are diluted with sufficient air, particularly during starting up, heavy deposits of the enamel type will not form on the tubes. Further, by preventing localized high rates of input to the walls, to the point that the ash deposited on the enamel (Fig. 2, Step C) does not sinter appreciably, the chances are lessened for the formation of liquid pyrosulphates.

That enamel deposits can exist on furnace-wall tubes without causing appreciable corrosion is exemplified by pulverized-coal-fired dry-bottom furnaces, where rather thick deposits have been found on tubes in the burner zones. These deposits have similar chemical and physical characteristics to those from slag-tap furnaces, but generally do not appear to have been fused, or to contain appreciable amounts of pyrosulphate. It is obvious that because the tubes are for the most part exposed directly to the furnace gases, the SO_3 concentration does not become high enough to produce liquid pyrosulphate; nevertheless, it is high enough to react with alkali-metal oxides to yield sulphates. However, it should not be inferred that dry-bottom units are immune from attack, since if conditions inside area *abc* of Fig. 6 should be attained, attack may ensue.

The success that has been had in reducing the rate of corrosion in slag-tap units by admitting a portion of the secondary air to the casing around the lower portions of a furnace, so that air could infiltrate between the tubes, may be attributed to two things, i.e., the temperature of the ash in contact with the enamel was reduced, resulting in less decomposition, and the air diluted whatever SO_3 was present. Numerous examinations of furnaces after extended operation with an air belt showed corrosion to be arrested, the ash and slag to be more easily detached from the wall, the ash to be softer and more porous, and the enamel to be less fused and lighter in color.

Air-belting was a temporary, but effective expedient initiated by the boiler manufacturer's engineers to arrest attack until more effective measures could be devised. Were it not for the fact that fly ash and other debris filled the space between the tube, preventing uniform distribution of the air to the affected wall areas, it seems certain that complete arrest of attack might be obtained. Other considerations, however, made it more desirable to change burner design to secure more uniform distribution of heat in the furnace, to provide a blanket of secondary air along the walls, and to prevent flame impingement on wall areas where attack tended to be active. There has been considerable promise along these lines, but it is as yet too early to evaluate completely the advantages of various burner arrangements. Frequent and extensive field inspections were started some time ago to accumulate as much data as possible on the effectiveness of burner design, but sustained operation, with only short and infrequent outages during the past few years, has made it virtually impossible to plan a rational schedule of inspections. For example, it is desirable to gage tubes in suspected areas at least twice a year, and to record carefully the condition of the slag, ash, and tubes.

Experience has shown that close adherence to the boiler manufacturer's recommendation is absolutely essential to the success of any preventive measure. Trouble may be expected wherever

[15] The flowing layer of slag, which is replaced continuously during operation, liberates practically all of its sulphur to the furnace; this sulphur cannot penetrate the stationary layer of solid slag shown in Fig. 2, step D.

sustained loads are carried in excess of the design capacity, ash and slag are permitted to accumulate in a manner to cause abnormal flame conditions, improper or insufficient attention is given to burner damper settings, and the excess air is carried too low. Lack of attention to these factors can, and does lead to tube damage that might not ordinarily be experienced.

Considerable attention has been paid to another method for preventing attack, that of applying protective metallic coatings to the tubes in affected areas. The laboratory and the field work on this phase of the problem is nearly completed, and will be reported in the next and last paper of this series.

Significance of Iron-Sulphide Deposits to Corrosion of Furnace-Wall Tubes

In a few cases, severe tube corrosion has been found where, after the slag was detached from the walls, the tubes were covered with a dull, black, brittle, adherent scale beneath which little or none of the enamel type of deposit was evident, except around the sides of tubes. Usually these deposits were quite thick, $^5/_{32}$ to $^3/_{16}$ in. not being unusual. The analyses of a few typical samples of these deposits are given in Table 3.

TABLE 3 ANALYSES OF TYPICAL IRON SULPHIDE DEPOSITS FROM FURNACE-WALL TUBES

Sample	SiO_2	Fe_2O_3	Al_2O_3	CaO	MgO	Sulphur as SO_3	Sulphur as S	Equivalent FeS	Carbon
A	2.1	79.0	2.7	1.5	0.3	3.36	23.7	65.5	0.5
B	4.8	68.0	4.7	2.9	0.4	2.47	21.2	58.4	2.0
C	2.5	85.6	3.3	0.1	0.2	0.2	26.3	72.3	6.8
D	2.5	81.8	3.7	0.2	0.0	0.1	32.3	88.8	1.0

Note: All samples were strongly magnetic, brittle, iridescent blue or black in appearance, and very slightly soluble in water.

The x-ray diffraction patterns of each were the same as that shown in Fig. 14, in which comparison is made with a standard pattern of FeS to show the predominance of this phase. The diffraction lines of Fe_3O_4 also are present.

At first, the observation that there was very little of the enamel-type deposit beneath the iron sulphide deposit where the metal was most corroded, suggested that attack was caused by an entirely different mechanism from that described for enamel deposits. The disturbing feature of these cases, however, was that enamel deposits never were entirely absent, there often being a paper-thin skin of fused enamel on the corroded area, which gradually thickened toward the side of the tube.

Early in the investigation it was proposed that enamel had been present originally in these areas, but that carbon monoxide in the furnace atmosphere reduced the sodium and potassium sulphates to the corresponding sulphides, which then reacted with the steel to form iron sulphide. As the laboratory experimental work progressed, and correlations were made with a considerable amount of field data that had been obtained from frequent inspections of furnaces, three cogent objections to this theory became apparent:

1 The amount of iron in these deposits far exceeded the amount that could be accounted for by the measured loss of metal.

2 Assuming for simplicity that the original enamel consisted entirely of K_2SO_4, then the product of the foregoing reaction would have to be a complex potassium iron sulphide, which would produce a characteristic x-ray diffraction pattern and a strongly alkaline reaction in water. None of the sulphide deposits examined to date ever has had the slightest evidence of these characteristics. The assumption that the alkali metal subsequently is volatilized, leaving only iron sulphide, is convenient but improbable because of the relatively low temperatures involved.

3 The appreciable amounts of carbon in the deposits suggested strongly that it originated from the coal, and therefore that incompletely burned coal deposited on the walls, carrying with it pyrites, FeS_2, which oxidized on the walls relatively slowly to FeS. In at least one case, which came to the authors' attention, severe tube attack occurred during a period when the riffle distributors in the coal-feed pipes had become badly eroded and poor distribution of the coal from the burners resulted. The black deposits on the walls, at the time the poor condition of the riffles was discovered, were exceptionally thick and contained a relatively high percentage of carbon.

Therefore, as a working hypothesis on which to base the experimental work, it was decided that pyrites from the coal adheres to the tubes, a condition that can arise from poor distribution of the coal stream leaving the burners or from excessive coarse coal, and oxidizes slowly to FeS according to

$$FeS_2 + O_2 \longrightarrow FeS + SO_2 \quad [3]$$

If the oxidation proceeds further, Fe_3O_4 may be formed according to

$$3\,FeS + 5\,O_2 \longrightarrow Fe_3O_4 + 3\,SO_2 \quad [4]$$

These reactions could account for the presence of FeS and Fe_3O_4 in the deposits and for a comparatively large source of SO_2, which could cause corrosion by reacting directly with the metal, or by oxidizing to SO_3 and reacting directly with the metal, or with enamel deposit on the tube to form pyrosulphates.

The extent that pyrites decomposed was determined in a range of temperatures of the order that conceivably could exist in a deposit in contact with a furnace tube. Pyrites of reagent grade, containing 95.3 per cent FeS_2, was crushed to pass a 100-mesh screen, weighed into a porcelain boat, and placed in the furnace shown in Fig. 10. Two series of tests were run, one with a slow stream of tank nitrogen passing over the sample, and the other with a mixture consisting of 12 per cent CO and 88 per cent tank nitrogen. Since the tank nitrogen contained a few tenths per cent of oxygen, the conditions for the tests with nitrogen only were slightly oxidizing.

The temperature was controlled from a shielded chromel-alumel thermocouple in contact with the boat. Although the indicated temperature probably did not represent the sample temperature any closer than ±25 deg F, it was considered sufficiently precise for the purpose.

Since FeS comprises the largest percentage of the deposits, similar tests were made with reagent grade FeS for the purpose of comparing its behavior with pyrites. The results of these tests are given in Table 4.

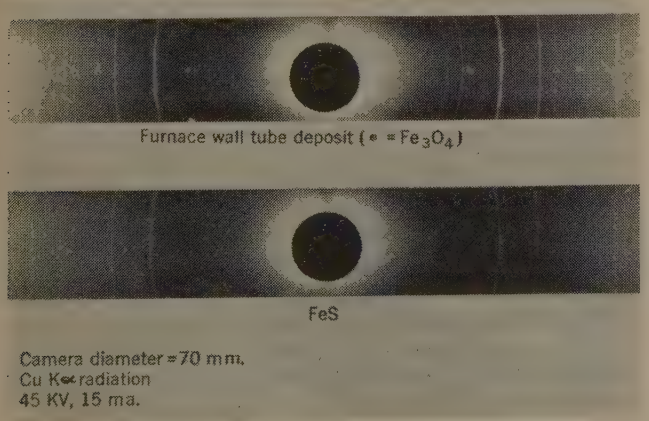

Fig. 14 X-Ray Diffraction Patterns of Typical Iron-Sulphide-Type Deposit and FeS

TABLE 4 CHANGE OF WEIGHT OF FeS_2 AND FeS WHEN HEATED 1 HR IN MILDLY OXIDIZING, AND STRONGLY REDUCING ATMOSPHERES

(Ox. = Tank N_2 containing 0.2 per cent O_2; Red. = 12 per cent CO, 88 per cent N_2)

Temperature, deg F	Change of weight, per cent — FeS_2 (pyrites) Ox.	FeS_2 (pyrites) Red.	FeS Ox.	FeS Red.
1000	—16.7	—14.4	+1.9	+3.4
1200	—25.6	—23.4	+0.5	+3.1
1400	—30.0	—30.0	+0.7	+2.5

NOTE: + indicates a net increase of weight.

The product from the tests with pyrites was shown by x-ray-diffraction analysis to be FeS and a small amount of Fe_3O_4. The FeS was virtually unchanged, faint lines of Fe_3O_4 appearing as the result of slight oxidation by the oxygen in the nitrogen.

These data show that pyrites readily loses an atom of sulphur at relatively low temperatures, and that the extent of the decomposition at a given temperature is not affected appreciably by the atmosphere.

The primary reaction probably is

$$FeS_2 \longrightarrow FeS + S \quad [5]$$

and when conversion to FeS is complete, the residual oxygen in the nitrogen oxidizes it as follows

$$3\ FeS + 5\ O_2 \longrightarrow Fe_3O_4 + 3\ SO_2 \quad [6]$$

It is apparent that the latter reaction takes place relatively slowly, as shown by the results with FeS, slight oxidation to Fe_3O_4 occurring and producing a net increase in weight of the samples.

The free sulphur from the primary reaction, Equation [5], may combine directly with the tube metal and form FeS at a relatively high rate, that is, at temperatures of 700 to 800 F the rate of attack would be much higher than that of normal oxidation in this temperature range. Although it is unlikely that free sulphur ever reaches a furnace tube, since a certain amount of oxygen always will be available to oxidize it, corrosion tests were made in evacuated tubes containing an iron-wire specimen embedded completely in FeS_2, and in FeS for comparison. Conducting the test in this manner insured contact of the metal only with sulphur vapor from decomposition of the sulphides. The results are given in Table 5.

TABLE 5 RATE OF CORROSION OF IRON IN FeS_2 AND FeS IN EVACUATED TUBES

Iron in	Per cent loss of weight in 168 hr — 700 F	850 F	1000 F
FeS_2	6.2	20.2	100.0
FeS	nil	nil	0.5

It is to be noted that the rate of corrosion in the pyrites increased rapidly with temperature, being of the order of magnitude at 700 F, the nominal temperature of a furnace tube in a high-pressure boiler, of the rate of corrosion in molten pyrosulphate, as seen in Fig. 7. The results with FeS were to be expected since the sulphur vapor pressure of this compound is very low in the range of temperatures studied.

On the basis of these experiments, and observations in the field where tube corrosion has been associated with iron sulphide deposits, it is believed that the deposition of pyrites on enamel deposits may lead to rapid attack of furnace tubes. It is thought that the mechanism of corrosion does not differ from that in the case of enamel deposits, except that the pyrites is a richer source of SO_2 and SO_3 than coal ash, with the probability that liquid pyrosulphates are formed more rapidly. This may account for the fact that frequently the enamel is very thin under iron sulphide, liquid pyrosulphate having formed and flowed from the areas where the metal temperature was highest.

This does not dismiss the possibility that deposits of pyrites, in the absence of enamel deposits, can cause corrosion by supplying local high concentrations of SO_2 and SO_3 to the surface of the tubes. The probability of this occurring, however, appears to be negligible since SO_2 and SO_3, even in high concentrations, do not corrode steel appreciably faster than air, at temperatures normally to be expected at the surface of a furnace tube, that is, 700 to 800 F.

Summary and Conclusion

In summary, the sequence of events proposed for furnace-tube corrosion in the presence of sulphide deposits is as follows:

Sodium and potassium sulphates deposit on the tubes as indicated by Step B, Fig. 2.

Unburned coal, containing relatively large amounts of pyrites adhere to the enamel and forms a thick deposit.

The pyrites oxidizes slowly to FeS and Fe_3O_4, the sulphur evolved combining with oxygen to form SO_2 and SO_3.

Subsequent reaction of these gases with enamel then causes corrosion by the dry or "wet" reactions described in the first part of this paper.

It is recognized by the authors that the evidence is indirect and the deductions therefrom are inferential. However, considering the practical difficulties, or even the impossibility, of securing representative samples of deposit, in situ, during the operation of a furnace, the method of approach is considered to be justified and the hypothesis proposed for the mechanism of attack to be reasonable. Considerable weight was given to the fact that in two cases where severe corrosion occurred in furnace areas rich in iron sulfide deposits, mill adjustments and coal-distributor-pipe repairs improved conditions considerably, that is, to the extent that subsequent gaging of tubes in previously affected wall areas showed considerable reduction in the rate of thinning, and the characteristic sulphide deposits no longer were found.

In conclusion, corrosion of furnace tubes, where pyrites deposits occur may, under certain conditions, lead to relatively high rates of attack. Such attack can be minimized (*a*) by close attention to coal fineness to prevent excessive amounts of coarse coal reaching the furnace, (*b*) maintenance of distributors in the coal feed pipes to the burners, and (*c*) avoidance, in so far as possible, of flame impingement on the furnace walls.

Discussion

W. T. REID.[16] The continuation of this study has yielded valuable information on the reaction of alkalies and iron oxide with sulphur trioxide on the wall tubes of modern boiler furnaces. Originally started to explain the action whereby furnace-wall tubes were being severely corroded during normal service, this investigation has disclosed a basic mechanism whereby superheater elements or, indeed, any part of the heat-receiving surfaces of a boiler could be damaged. Particularly, the explanation of the quantitative effect of sulphur trioxide on the ability to form an objectionable deposit was a necessary step in the over-all understanding of the problem.

Although external corrosion of wall tubes seems no longer to be occurring at the rates observed during 1942–1944, yet instances are still occurring where superheaters and other higher-temperature elements are being corroded at an excessive rate. These data will be most helpful in the future, as the increase in steam temperature and the trend toward reheat poses new problems in materials and maintenance for designers and operators alike.

It is particularly interesting that the earlier conclusions re-

[16] Supervisor, Fuels Research, Battelle Memorial Institute, Columbus, Ohio. Mem. ASME.

garding the mechanism of corrosion, as proposed by this same group of investigators, has been confirmed. The actuality of the mechanism in 1945 was predicated on the availability of sulphur trioxide at the surface of the wall tube. However, without knowledge of the actual concentration of sulphur trioxide required to permit the formation of corrosion products, it was not possible then to state exactly that the mechanism was correct. Rather, the explanation was based largely upon the elimination of other possible factors. With the data available in this paper, however, the conditions required to produce "enamel" deposits can be specified exactly; they are shown to be within the range in which sulphur trioxide can be present to form enamel. The tests made in the gas-fired furnace in which sodium sulphate was transported in one case, and formed from sodium carbonate in the other, seem convincing enough that the alkali metals can be condensed from the gas phase on relatively cool surfaces in boiler furnaces.

Although it is understood that this report will be the last in this series and that the investigation is to be terminated, it is expected that many problems will require solution in the future regarding deposits on heat-receiving surfaces. These data will be of inestimable assistance in such investigations.

Authors' Closure

Mr. Reid's comments are appreciated, especially so in view of his close connection with the experimental work conducted by the Bureau of Mines.

Reports of tube corrosion of the type described in these papers have been infrequent during the past few years, which may be the result of better maintenance and less forcing of steam generators above design ratings since the end of the war. Also to be considered are significant improvements in new units with regard to the distribution of heat and the coal-air streams in the furnace. However, field experiments with protective metallic coatings, applied to furnace tubes, still are in progress, and it is hoped that sufficient quantitative data will be obtained during the next year to submit in the final paper of this series.

Methods and Instrumentation for Furnace Heat-Absorption Studies: Temperature and Composition of Gases at Furnace Outlet

By PAUL COHEN,[1] R. C. COREY,[2] AND J. W. MYERS,[3] PITTSBURGH, PA.

As part of the general program of investigations by the ASME Special Research Committee on Furnace Performance Factors, the Combustion Research Section of the Bureau of Mines is making a series of determinations of furnace heat absorption of representative pulverized-coal-fired boiler furnaces. During the course of these studies, modifications have been made in the test technique to improve the precision of furnace testing. Automatic recording instruments have been employed, which permit more detailed sampling and examination of furnace-outlet gases than heretofore, without an appreciable increase in the time or work required. Improved designs of radiation shields have been developed for high-velocity thermocouples with accuracy comparable to the B&W multiple-shield high-velocity thermocouple, but which may be employed conveniently in pulverized-coal-fired furnaces. Detailed descriptions are presented of the distribution of gas composition and temperature at the outlet of a 640,000-lb per hr horizontally fired boiler furnace. Based upon this knowledge, the sampling characteristics of the gases at the furnace outlet for furnace heat-absorption measurements have been examined, and a procedure is suggested for the rational selection of simplified sampling schedules. The methods of calculating furnace heat absorption from the temperature and gas-composition data are examined critically with special emphasis on the effect of weighting with respect to mass velocity. Suggestions are presented whereby the significance of mass velocity for furnace heat-absorption calculations may be determined from the temperature and gas-composition data.

Introduction

THE ASME Special Research Committee on Furnace Performance Factors was organized in 1941, to collect and rationalize data on commercially important furnaces as an aid to design and operation. The committee laid out a broad program of investigation of the many factors affecting furnace performance, an essential part of which was the accurate measurement of the heat absorption in furnaces by the determination of the temperature and composition of the gases leaving the furnace. At the request of the committee, the Combustion Research Section of the Bureau of Mines assumed responsibility for this phase of the committee's work. So far two units have been studied, and a complete report on the first has been presented to the Society.[4]

Because of the importance in this work of testing techniques and instrumentation, the Special Research Committee established a Subcommittee on Instrumentation, which in 1946, recommended methods for measurements related to the work of the committee, including the measurement of the temperature of the gases leaving the furnace. The primary objective was to devise accurate procedures that were convenient for use under plant operating conditions. In conjunction with the plant tests, considerable attention has been devoted to this end, and enough progress has been made to justify a separate report on this phase of the committee's activity.

In the subsequent discussion it is assumed that the enthalpy of the gas is defined completely in terms of a single temperature measured by a particular instrument. Although this assumption is not generally correct, as shown by the discussion of Mayorcas, Pritchard, and Thring,[5] it does hold for the conditions met so far in the work of the committee. However, the possible consequence of the failure of the enthalpy of a gas to be defined by an indicated temperature must always be borne in mind, so that where temperature measurements are not permissible, other procedures may be substituted.

General Considerations

Outline of Procedure of Furnace Heat-Absorption Measurements. The heat absorption in a boiler furnace is defined as the heat transferred by convection to the furnace-wall tubes, not including the screen, and the heat transferred by radiation to the furnace-wall tubes, including the screen. It is obtained as the difference between the heat available in the furnace (the low heat value of the fuel fired, corrected for unburned combustible, plus the sensible heat in the air used for combustion) and the sensible heat in the furnace-outlet gases and the refuse, and the heat transferred from the furnace casing. With but slight modifications, the test procedure is that of Method (*b*) of the ASME Test Code for Stationary Steam-Generating Units. The most significant difference between furnace and boiler testing, aside from the conditions under which the temperature and composition of the gases must be determined, is that the heat available in the preheated air is an important factor in the furnace heat balance, whereas, it does not enter into the over-all boiler heat balance. The accurate determination of this quantity, which usually amounts to 5 to 10 per cent of the total heat available in the furnace, presents some difficulties. It may be determined most

---

[1] Fuel Engineer, Combustion Research Section, Bureau of Mines. Mem. ASME.

[2] Supervising Engineer, Combustion Research Section, Bureau of Mines. Mem. ASME.

[3] Fuel Engineer, Combustion Research Section, Bureau of Mines.

Contributed by the Research Committee on Furnace Performance Factors and the Fuels and Power Divisions, and presented at the Annual Meeting, New York, N. Y., November 28–December 3, 1948, of THE AMERICAN SOCIETY OF MECHANICAL ENGINEERS.

NOTE: Statements and opinions advanced in papers are to be understood as individual expressions of their authors and not those of the Society. Paper No. 48—A-161.

[4] "An Investigation of the Variation in Heat Absorption in a Pulverized-Coal-Fired, Water-Cooled, Steam-Boiler Furnace. II. Furnace Heat Absorption as Shown by the Temperature, Composition, and Flow of Gases Leaving the Furnace," by W. T. Reid, Paul Cohen, and R. C. Corey, Trans. ASME, vol. 70, 1948, pp. 569–585.

[5] "Problems of Gas Temperature Measurement Above 1500° C," by R. Mayorcas, W. Pritchard, and M. W. Thring, presented at the Third Symposium on Combustion and Flame and Explosion Phenomena, The University of Wisconsin, Madison, Wis., Sept. 7–11, 1948.

conveniently from a heat balance on the air heater, and this procedure is currently being followed. Simultaneous determinations of the velocity and temperature of air in the primary and secondary-air ducts in a recent series of furnace tests will permit comparison of the two methods and evaluation of the simplified procedure.

The other quantities in the furnace heat balance are calculated by standard procedures. The basic data for the temperature and composition of the gases, obtained by means of specialized techniques appropriate for furnace testing, are used to calculate the sensible heat in the furnace-outlet gases. The quantities of the individual gas components are calculated from the test data, and their heat contents are then obtained from the tables of Heck.[6]

The distribution of the residue (ash-pit refuse and fly ash) is determined by standard means, and from the analysis and distribution of the residue the combustible loss is determined. The sensible heat in the refuse and fly ash is similarly calculated. The heat loss from the furnace casing is generally taken as one half that of the entire unit, as determined from the ABMA Standard Radiation Loss Chart. The value so obtained is probably too high, and, if possible, a more direct estimate of this quantity should be made from observed casing temperatures and appropriate radiation and convection heat-transfer coefficients.

Sampling Procedures. In addition to the chosen techniques of measurement, sampling procedures also are decisive in fixing the limits of precision of furnace testing. For the coal fired and the fly ash, standard procedures are available and should be followed. For sampling the furnace-outlet gas, there exists only the recommendation of the ASME Test Code for Stationary Steam-Generating Units that the cross section of the gas passage be divided into equal areas, preferably of not less than 18 sq ft each, and that a sample be taken from, and the velocity of the gas be measured at, the center of each area, and a weighted average calculated therefrom. Because of limited access to most boiler furnaces, it is frequently difficult to do this, and compromises must be made. In a recent series of tests, the Test Code procedure was found to be quite adequate; indeed, a smaller number of samples would have been satisfactory. If this sampling procedure is followed in preliminary tests, the sampling characteristics of the furnace-outlet gases can be determined, and a logical choice of the number and location of sampling points can be made. This process is illustrated in a later section of this report.

Temperature Measurements

Apparatus, Review. The accurate measurement of the temperature of gases in boiler furnaces presents special difficulties. These arise from the high temperatures at which measurements must be made and the high rate of heat transfer that may exist between the measuring instrument and the flame and the water-cooled surfaces of the furnace. Considerable attention has been given to this problem, both theoretical and experimental. Mullikin[7] and Mullikin and Osborn[8] have discussed the theory of this problem and the application thereto of the high-velocity thermocouple, which has become the basic instrument for measuring the temperature of furnace gases.

The single-shield high-velocity thermocouple (SHVT), shown in Fig. 1(*a*), consists of a thermocouple, generally of platinum-rhodium platinum, mounted at the end of a water-cooled holder or probe and surrounded by a cylindrical ceramic shield through which the gas is aspirated past the thermocouple at high velocity. The manner by which this arrangement decreases the error of temperature measurement will be apparent from simplified considerations of the heat-transfer balance of a bare thermocouple immersed in a stream of gases in a water-cooled furnace, where the walls are colder than the gas, and radiation from the gas to the thermocouple is negligible.

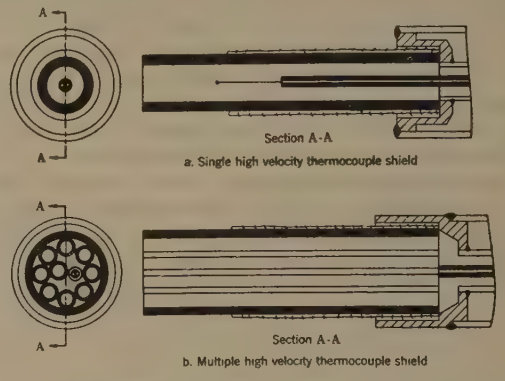

Fig. 1 High-Velocity Thermocouple Shields, Conventional Types

Heat is transferred by convection from the gas, at absolute temperature T_g, to the thermocouple at absolute temperature T_t, at a rate equal to $h_c A(T_g - T_t)$, where h_c is the coefficient of convection heat transfer, and A is the surface area of the thermocouple. Heat is lost by radiation from the thermocouple to the surroundings at a rate equal to $\epsilon\sigma A(T_t^4 - T_w^4)$, where T_w is the effective absolute temperature for radiation of the surroundings, σ is the radiation constant, and ϵ the emissivity of the thermocouple surface, and by conduction along the thermocouple leads. Since the loss of heat by conduction can be reduced to a negligible amount by proper design of the couple component parts, it is neglected in this discussion. Therefore the heat received by the thermocouple by convection at its equilibrium temperature is equal to the heat lost by radiation and

$$\epsilon\sigma(T_t^4 - T_w^4) = h_c(T_g - T_t)$$

Thus the greater the difference between T_t and T_w and the lower the value of h_c, the greater will be the value of $T_g - T_t$, which is the error of temperature measurement of the gas. The shielded high-velocity thermocouple is designed to decrease both sources of error of the bare thermocouple. Thus by aspirating the gas past the thermocouple at high velocity, h_c is considerably increased, and, simultaneously, the shield is heated by the gas, bringing its temperature closer to that of the thermocouple and gas, decreasing the term $T_t^4 - T_w^4$, which determines the radiation heat transfer.

Experience has demonstrated that single-shield high-velocity thermocouples of the type shown in Fig. 1(*a*) are seriously in error when used under extreme conditions, such as in boiler furnaces, and numerous modifications of this device have been made, consisting mainly of increasing the effective number of radiation shields between the thermocouple and the environment. Of these, the multiple-shield high-velocity thermocouple of Mullikin[8] Fig. 1(*b*) (B&W MHVT) has gained widest acceptance in this country as a reference standard for the calibration of simpler

[6] "The New Specific Heats," by R. C. H. Heck, *Mechanical Engineering*, vol. 62, 1940, pp. 9–12.

[7] "Gas Temperature Measurement and the High-Velocity Thermocouple," by H. F. Mullikin; Temperature—Its Measurement and Control in Science and Industry, Reinhold Publishing Company, New York, N. Y., 1941, pp. 775–804.

[8] "Accuracy Tests of the High-Velocity Thermocouple," by H. F. Mullikin and W. J. Osborn; Temperature—Its Measurement and Control in Science and Industry, Reinhold Publishing Company, New York, N. Y., 1941, pp. 805–829.

instruments of the type shown in Fig. 1(*a*). As shown in Fig. 1(*b*), the shield of the multiple-shield high-velocity thermocouple consists of a number of porcelain tubes inserted into a larger external cylindrical ceramic tube. The furnace gas is aspirated through all of the tubes and the spaces between the tubes; the thermocouple may be inserted into one of the tubes or a space between the tubes. There exist a multiplicity of surfaces heated by the gas between the thermocouple and the external environment.

Comparison tests between the indications of this multiple-shield high-velocity thermocouple (B&W MHVT) and true gas temperatures were made by Mullikin and Osborn,[8] in a laboratory setup, and the differences were found to be negligible for the conditions of the comparison. In addition, comparisons between the indicated temperatures of a modification of the single-shield high-velocity thermocouple shown in Fig. 1(*a*), B&W SHVT (the modification consists in enclosing the thermocouple in a protection tube for work in dirty gases) and the B&W MHVT have been published.[9] These corrections, based on field studies, in addition to the laboratory work of Mullikin and Osborn,[8] are used to correct data taken more conveniently with the B&W SHVT.

It is the opinion of some workers in the field that the errors of simple high-velocity thermocouples, such as that shown in Fig. 1(*a*), are unique to each condition of measurement. Thus for each furnace heat-absorption test, an instrument with low inherent error should be used, such as the B&W MHVT, or extensive calibrations with such an instrument should be made during each test. Since either procedure involves use of the MHVT, the work required would be considerably increased, because the B&W MHVT can be used for only very short intervals in dirty gases, such as those of pulverized-coal-fired furnaces. Therefore the possibilities were considered of designing shields with improved accuracy, compared to the SHVT of Fig. 1(*a*), without appreciable loss of convenience in operation. Two designs were developed, constructed, and tested during a series of furnace heat-absorption tests on a pulverized-coal-fired dry-bottom steam generator rated at 640,000 lb of steam per hr and 900 F total steam temperature. The results of these tests are presented in a later section of this report.

Apparatus—Current Types. The main elements of the temperature-measuring system now being used are: (*a*) Water-cooled thermocouple holder, (*b*) refractory thermocouple shield, (*c*) thermocouple, lead wire, and insulators, (*d*) flue-gas connections and measuring system, and exhauster, (*e*) recording potentiometer, and (*f*) equipment for calibrating the thermocouple. These elements will be described in detail.

[9] "Improved Application of Coal-Burning Equipment: Designing Coal-Burning Equipment to Eliminate Trouble Spots," by W. H. Rowand, ASME Paper No. A-46-81, bound at back of vol. 69, Trans. ASME, 1947, fig. 2, p. 9.

Elements of Temperature-Measuring System

(*a*) *Water-Cooled Thermocouple Holder.* Fig. 2 is an assembly drawing and shows most of the details of the water-cooled holder. The three outer tubes may be plain carbon steel but preferably should be of corrosion-resistant materials. The inner tube is 18-8 stainless and has three thin fins welded to it, 2 in. from the front end, to center it in the $^3/_4$-in. tube. The $1^1/_8$-in. tube has sets of 120-deg spacers at 2-ft intervals along its length to center it in the outer tube. The tip is copper and the fittings are brass. The back opening of the suction-connection fitting is large enough to pass the fins on the $^1/_4$-in. tube. This permits the $^1/_4$-in. tube to be removed from the back end of the holder, eliminating the necessity of dragging the thermocouple lead wire through the dirty gas tube, and accounts for the special design of the packing gland on the $^1/_4$-in. tube. The thermocouple spool is bakelite.

These holders have been built to a maximum length of 15 ft. For assembly, the $1^1/_2$-in. tube should be cut to length desired; the $1^1/_8$-in. tube $^5/_8$ in. longer than the $1^1/_2$-in. tube; the $^3/_4$-in. tube $8^1/_2$ in. longer than the $1^1/_2$-in. tube; and the $^1/_4$-in. tube not less than $11^1/_2$ in. longer than the $1^1/_2$-in. tube. The tubes are cut to proper size, and $^5/_8$-in. water holes are cut in the $1^1/_2$-in. and $1^1/_8$-in. tubes. The ends of all tubes are cleaned; the $1^1/_2$-in. and $1^1/_8$-in. tubes are sweated to the water-connection fitting. The copper tip is silver-soldered to the $^3/_4$-in. tube; the $^3/_4$-in. tube is then inserted into the tube assembly, and the $1^1/_2$-in. tube is silver-soldered to the tip. The suction-connection fitting is then sweated on the $^3/_4$-in. tube.

The water-connection fittings can be adapted to suit available equipment. The water pressure should not be less than 60 psig for long holders (15 ft) at temperatures up to 2300 F. For higher temperatures a pressure of 100 psig is advisable. In any case, it always should be possible to place the bare hand on the holder at the outlet end.

(*b*) *Radiation Shields.* The two new designs of radiation shield just mentioned are shown in Fig. 3. Each is 4 in. long and $1^1/_8$ in. OD, and consists of a central cylindrical bore, in which the thermocouple is located, and an outer section containing a multiplicity of symmetrically arranged holes, which form an addi-

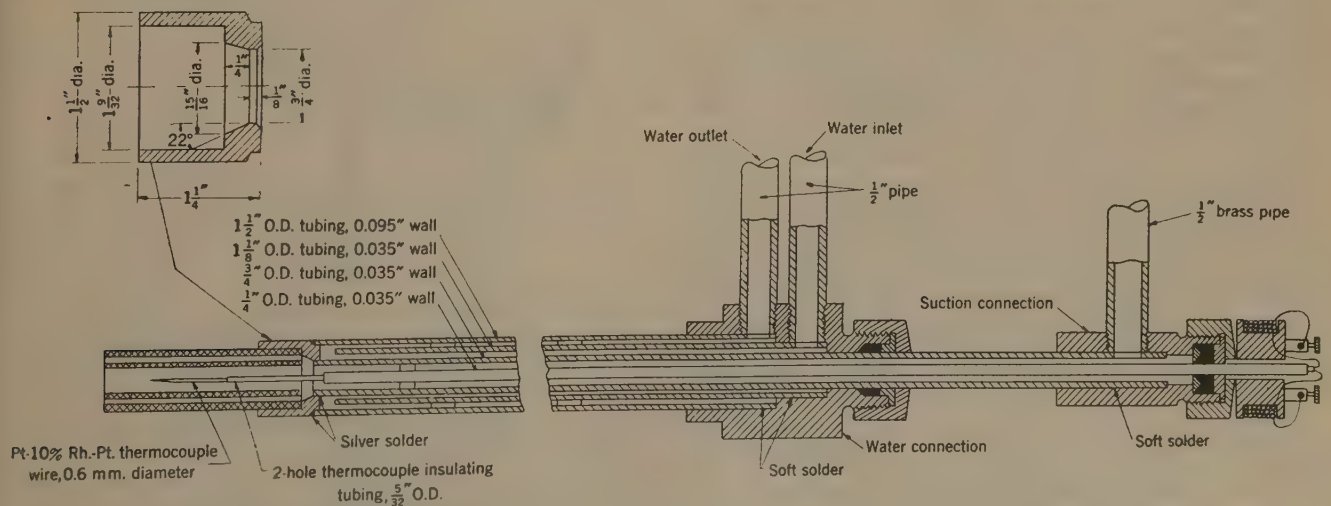

Fig. 2 Assembly Drawing of Water-Cooled High-Velocity Thermocouple Probe

tional gas-heated surface to provide a second shield. The outer section of type G contains eight cylindrical holes, whereas that of type E contains four kidney-shaped holes. To obtain enough holes of adequate diameter, the over-all diameter of these shields is considerably greater than the SHVT, but not much greater than the B&W MHVT. These shields are made by the McDanel Refractory Porcelain Co., Beaver Falls, Pa., as extrusions from special dies, and their unit cost is comparable to that of the single-shield type. The shields were originally made in both an alumina-base and a zirconia-base refractory body. Experience has demonstrated no superiority of one over the other, and current supplies are being made of the alumina body (304), which fires to a more consistent size and shape than does the zirconia body.

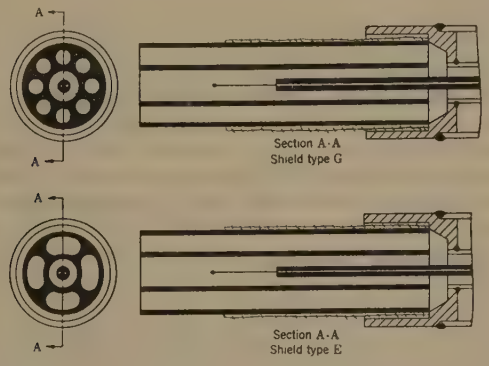

FIG. 3 HIGH-VELOCITY THERMOCOUPLE SHIELDS, BUREAU OF MINES, TYPES E AND G

Before use, a 2-in. × 4-in. strip of nichrome gauze, No. 24 wire, 16 mesh, is wrapped around the base of the shield and fastened with a loop of No. 20 gage nichrome V wire to provide a flexible cushion between the shield and the copper tip. The wrapped end of the shield is covered with a stiff paste of Norton RA-1148 refractory cement, so that the gauze is well covered. The paste may be allowed to dry, or the shields can be used immediately. The gauze end of the shield is forced into the copper tip of the holder, and the open spaces between shield and tip are sealed with more refractory cement.

In a series of 11 furnace tests, about 350 measurements at temperatures up to 2450 F were made with 85 type E shields, the ash of the pulverized coal having an initial deformation temperature on the oxidizing basis of 2230 F. Although shields of the type in Fig. 1(*a*), were not used in these tests, and there is no exact basis for comparison, it is the opinion of the authors that the new shields gave little more trouble than previous experience indicates would have been obtained with the single shield.

(*c*) *Thermocouple, Lead Wire, and Insulators.* The thermocouple, consisting of 0.6-mm-diam Pt, 10 per cent Rh, and Pt wires, should be at least 4 ft long.[10] One inch of bare wire is exposed at the hot junction, which is located 1 in. back from the front end of the shield. The ends of the thermocouple and the binding posts at the end of the holder are connected with bare compensating lead wires, consisting of a positive lead of No. 20 gage thermocouple-grade copper wire and a negative lead of No. 20 gage copper-alloy wire. The latter may now be obtained from the Wheelco Instrument Company, for lengths under 1000 ft, or from the Driver-Harris Company, for lengths over 1000 ft.

The thermocouples and lead wire are joined by butt welding in the oxy-gas flame without flux, which will require some practice. The assembly of thermocouples and lead wires is strung through 24-in. lengths of $^{5}/_{32}$-in-OD double 0.040-in-bore thermocouple insulating tubing. The insulators and wire are then threaded through the $^{1}/_{4}$-in-OD 18-8 thermocouple-protection tube. Excess lead wire at the end is insulated with lengths of spaghetti, and after the thermocouple protection tube is placed in the holder, is wound around the spool, taped in place, and the ends connected to the binding posts on the spool. Connection between the binding posts and the potentiometer is made with standard compensating lead wire.

(*d*) *Gas Connections, Gas-Measuring System, and Exhauster.* Because of the large flow cross section of shields E and G, the rate of flow of gas required is considerably greater than with conventional shields. For this reason the gas tube in the water-cooled holder is $^{3}/_{4}$ in. OD, and all gas connections must be of large cross section and capable of withstanding 15 in. Hg vacuum without leakage or collapse. Compressed-air hose, or steam hose, is recommended for connecting the water-cooled holder and the exhauster. All connections are made with $^{3}/_{4}$-in. iron-pipe-thread steam-hose couplings.

The gas-measuring system shown in Fig. 4 comprises a dial thermometer to measure the temperature of the gas, a $^{1}/_{2}$-in. orifice, and static pressure and differential manometers. The assembly is readily constructed from available pipe fittings. Moisture traps are provided on the manometer connections and may prove of value for work in gas-fired furnaces.

If it is known, or at all probable that the thermocouple holder

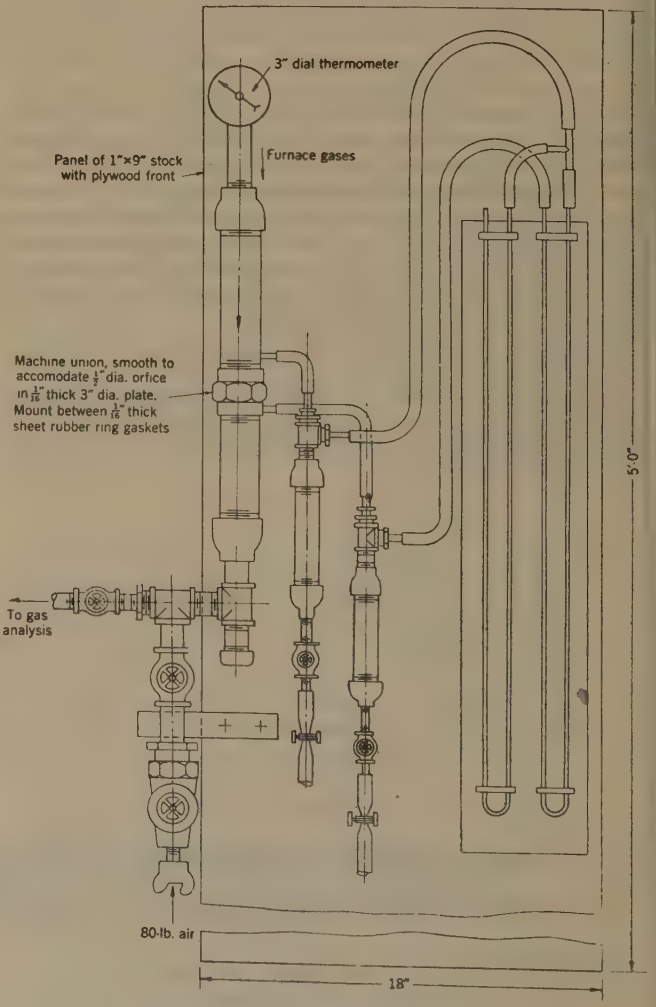

FIG. 4 GAS-MEASURING SYSTEM

[10] The reader is referred to the discussion of this paper for further details on the length of thermocouples.

will be depressed below the horizontal when immersed in the furnace, the gas flow should be adjusted to an appreciable rate before the holder is inserted in the furnace. This precaution is necessary to prevent condensed water in the gas tube from flowing down on the hot shield and cracking it.

Gas is aspirated through the system by means of a Schütte-Koerting steam-jet exhauster $1^1/_2$-in. size, operated with compressed air. The air pressure should be not less than 80 psig; 100 psig is preferable. Because of the operating characteristics of the exhauster, best control of gas-flow rate is obtained by operating the exhauster close to its maximum capacity, and controlling the rate of flow of gas by means of the throttling valve shown in Fig. 4.

(*e*) *Recording.* Every effort should be made to record temperatures automatically with a high-speed electronic recorder at high chart speeds (strip chart) or with a 1-hr clock (radial chart). With such equipment, the inevitable fluctuations of the temperature of the gas, illustrated in Fig. 5, are recorded, and a good average value of the indicated temperature of the gas can be obtained from observations lasting less than 1 min. Recent experience has shown that this procedure represents a convenient method for obtaining a useful average of the temperature of the gas at a given point in the furnace.

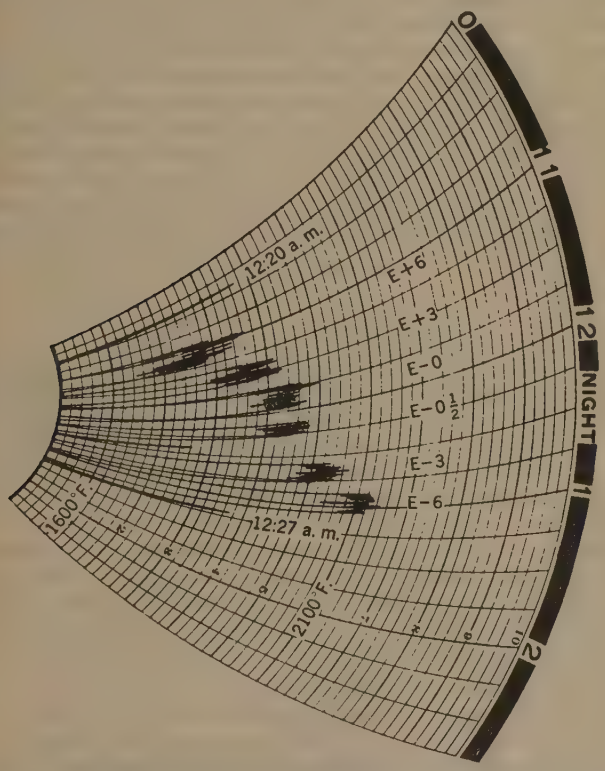

FIG. 5 TYPICAL RECORD OF GAS TEMPERATURES AT FURNACE OUTLET BY HIGH-SPEED ELECTRONIC TEMPERATURE RECORDER

(*f*) *Checking of Thermocouples.* The Subcommittee on Instrumentation of the Special Research Committee on Furnace Performance Factors in its report of 1946, wrote: "Because of the possibility of contamination of the platinum thermocouple by alloying with elements from the slag or by the action of hot gases, it is a wise precaution to check the accuracy of the thermocouple at frequent intervals. This can be done in the field by the use of a simple electrically heated immersion furnace, which is readily made up from an alundum tube, wound with resistance wire of the nichrome type, one end being closed by a plug of refractory material. The resistance should be such that a temperature of 1800 F can be obtained with an applied voltage of 110 volts. A continuously variable transformer is desirable for control of the temperature.

"The following detailed procedure for conducting the immersion test is recommended: The thermocouple being tested and its porcelain insulators shall be withdrawn from the water-cooled holder for a distance of at least one foot. An uncontaminated reference couple of the same composition and wire size, and fitted with identical porcelain insulators, at least one foot long, shall be tightly wired at three points to the service couple in such a manner that the hot junctions of the two thermocouples are as close together as possible, but not touching. This assembly shall be inserted in the immersion furnace, and accurately centered in the tube at several depths of immersion, taking comparative readings of the two thermocouples when stable conditions are reached at each point of immersion. The thermocouples may be tested with or without exposure of bare wire at the hot junction, depending upon how the service thermocouple is used in the high-velocity holder, but both thermocouples must have the same exposure. A suitable plug of refractory material shall be used to close the insertion end of the furnace tube, while the calibration test is being run.

"If the wires of the service thermocouple are not contaminated, its readings will check the reference couple at all depths of immersion in the calibrating furnace. If local nonhomogeniety is present, the amount of error will vary progressively for increased depth of immersion until final agreement may be reached, when the entire contaminated portion is within the furnace and at the temperature of the hot junction.

"For ideal calibration, there should be an accurate reproduction of temperature gradient in the wires inserted into the immersion furnace corresponding to that which exists in the service thermocouple, and if exacting accuracy is called for, it may be found advisable to adjust the resistor windings of the furnace tube. Readings observed at $4^1/_2$ in. immersion length, however, may be considered as showing the nominal error of the service couple at the temperature indicated by the reference couple.

"Although such a checking furnace can be carried only to about 1900 deg F, it serves to check for gross errors, and the observed trend of calibration may be extrapolated with reasonable validity to higher temperature ranges in which the couple was used. For greater accuracy, calibration can be made at higher actual temperatures in a furnace wound with platinum-wire resistors."

Calibration checks should be made daily, or at more frequent intervals, depending on the severity of service. If the ash on the wire is molten, contamination will be relatively rapid, even though combustion is complete and the atmosphere is oxidizing. To restore the thermocouple to its original calibration the contaminated portion of the wire is cut off and a new junction is welded.

Comparison of Thermocouple Shields. Although the relationship of the temperature indicated by a particular high-velocity thermocouple to the true gas temperature cannot be stated with absolute certainty, a knowledge of the relative relationship between different types of high-velocity thermocouples can serve to establish the errors, relative to the best type, and the probable magnitude of the error of the best instrument. As previously stated, the B&W MHVT has been taken as a standard for such comparisons.

Comparisons have been made in a 640,000-lb per hr pulverized-coal-fired dry-bottom boiler furnace between shields E, G, and the B&W MHVT at various mass velocities, against a B&W MHVT at high mass velocity as a standard. These comparisons

are made by inserting the two holders, suitably clamped together into the furnace so that the shields are parallel, and separated, by only a few inches. The location and relative position of the shields are so chosen that they are symmetrically exposed to radiation from the flame and to the cooled walls. Each couple is connected to a separate high-speed recorder, or the couples are connected differentially to a single high-speed recorder. The mass velocity in the standard is adjusted to the desired value, about 15,000 psf-hr which is maintained constant throughout the test. The mass velocity of the couple being tested is started at a similar high rate and reduced by increments to about 5000 psf-hr. The temperatures of the two couples, or the differential temperature, are recorded continuously. The pressure drop through the couple holders is watched carefully for indications of plugging of the shields, and as needed, the holders are withdrawn from the furnace, and the shields cleaned or replaced. It will be noted that this procedure eliminates the effects of fluctuations of furnace conditions on the comparisons, except for variations in the performance of the two couples with gross changes in furnace conditions.

The results of such comparisons are plotted in the manner shown in Fig. 6. In this type of correlation, the difference between the temperature indicated by the comparison couple at the stated high mass velocity and the temperature indicated by the couple being tested, at the various mass velocities, is plotted against the mass velocity in the shield of the test couple. Curve *a* in Fig. 6 is a plot of the B &W MHVT against itself and shows how the indicated temperature may be expected to vary with changes in mass velocity for essentially constant conditions of gas-temperature and radiation environment. Curves *b* and *c* in Fig. 6 are similar plots for Types E and G shields, respectively, with the B &W MHVT at high mass velocity as standard; to convert them to comparisons against themselves, the values of the difference at 15,000 psf-hr mass velocity must be subtracted from the ordinates.

These results show that the optimum mass velocity is approximately the same for each of the three types of shields, about 10,000 psf per hr. Further, at or above the optimum mass velocity, Type E shield indicates a temperature 30 deg F lower, and Type G shield a temperature 40 deg F lower than the B&W MHVT for the conditions of comparison used here. The temperature of the gases being sampled during these comparisons was approximately 2000 F, and the location was about 5 ft in front of the furnace-outlet screen at the elevation of the mid-plane of the furnace outlet, and about midway between the side walls. Although, as previously stated, the errors of high-velocity thermocouples must vary with the conditions of application, it is felt that the differences just noted will apply, with little error, to the average conditions of measurement of the temperature of the gases leaving the particular furnace in which the comparisons were made.

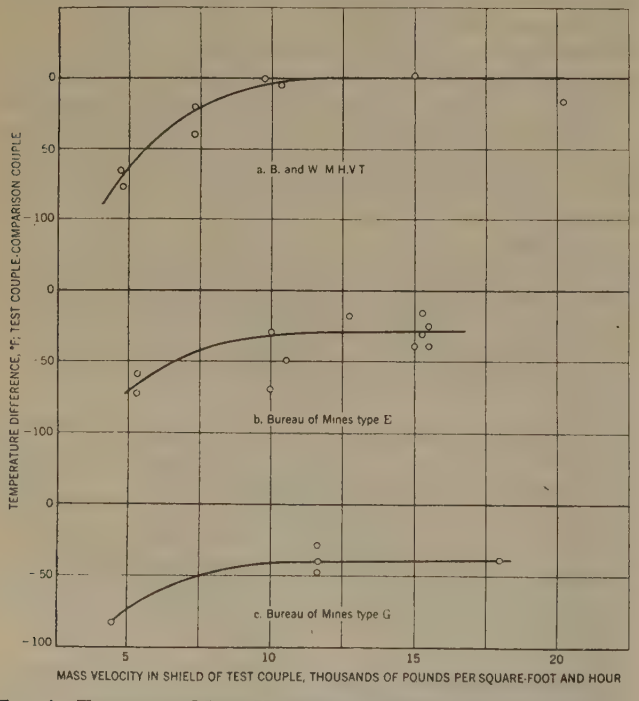

FIG. 6 EFFECT OF MASS VELOCITY IN SHIELD ON TEMPERATURE INDICATED BY VARIOUS HIGH-VELOCITY THERMOCOUPLES (Comparison with B&W MHVT, operated at a mass velocity of 15,000 psf per hr. Gas temperature 2000 F.)

The differences shown in Fig. 6, between the B&W MHVT and shields E and G are, respectively, 40 deg and 50 deg F less than the corresponding difference reported for the single-shield high-velocity thermocouple.[8] Thus for the test on this particular unit, the necessary corrections are not only smaller than with the single-shield thermocouple, but since the uncertainty in the correction must vary with its magnitude, they are probably of a higher order of accuracy than that for the single shield.

No new insight has been gained concerning the relationship between true gas temperature and that indicated by the B&W MHVT. Although the B&W MHVT yields the highest temperatures, the relationship between indicated temperature and mass velocity is the same as that for the other two shields. Only carefully designed laboratory experiments under conditions closely simulating those of boiler furnaces will permit a determination of the absolute error of the B &W MHVT, and therefore those of the other shields. If an opinion may be ventured at this point, it is that this error would not be greater than the difference between the B &W MHVT and the Type E shield, in other words, less than 30 deg F for the conditions of the comparisons cited here.

Gas Sampling and Analysis

The sampling and analysis of gases at the furnace outlet present no problems markedly different from those encountered with similar measurements at other locations in the boiler. Except for the fact that the sampling tubes must be cooled adequately, both to protect the sampler and to quench the sample, and higher velocities of sampling must be used to decrease the time lag of sampling, familiar techniques and apparatus may be used. Under certain circumstances, modifications of technique are permissible which greatly decrease the time required for complete furnace testing, and increase the convenience with which such determinations can be made. These modified techniques have been tested thoroughly, and their description is included here for the benefit of possible users.

The modified gas-sampling and analysis system is designed to be incorporated with the temperature-measuring system previously described. In pulverized-coal-fired furnaces, because of the rapid accumulation of ash in the shields, simultaneous temperature measurement and gas sampling require rapid sampling and, unless a large sample collection-and-storage system is set up and personnel and equipment are available to analyze the many samples required, an automatic gas analyzer will be needed. Of the available automatic gas analyzers, the Bailey oxygen recorder has been found to meet these requirements within the range of conditions of gas composition for which it is applicable. However, the sample must contain no combustible gas, since oxygen recorders of this type determine the oxygen by burning it with a standard fuel, for which the heat of combustion per unit quantity of oxygen burned is fixed. In the presence of other combustibles, the meter indications are in error.

The basic method for determining the composition of the gases in the furnace is still the collection of gas samples and analysis of these samples with an Orsat apparatus. The function of an oxygen recorder, when one can be used, is to increase the number of samples which can be analyzed conveniently for one of the gas components, and thereby increase the representativeness of the average value of this component calculated. It is necessary, however, to correlate the oxygen content of the gases with the other constituents, by means of regular though less frequent complete Orsat analyses of gases simultaneously analyzed by the recorder. This procedure also serves to maintain a continuous calibration of the recorder. When the check samples are being taken, the rate of flow of gas through the high-velocity thermocouple is reduced to minimize plugging of the shields.

The elements of the gas-sampling and analysis system are (*a*) the gas-sampling train and constant-rate gas sampler, (*b*) the oxygen recorder, and (*c*) the apparatus for complete gas analysis. The latter equipment is standard; the others will be described in detail.

(*a*) *Gas-Sampling Train and Constant-Rate Gas Sampler.* Fig. 7 shows complete details of a gas-sampling train, including a Bailey oxygen meter. Referring to Fig. 7, the gas sample may be obtained either through the thermocouple holder, the gas then entering the system at valve 3, or from other samplers at various points on the furnace, depending upon the setting of valves 3, 4, and 5. When gas composition and temperatures are determined simultaneously, it is necessary for the Bailey oxygen meter to pump against the relatively high vacuum produced by the exhauster; however, with the large pipe and hose used, and with clean shields, the vacuum can be held under 14 in. Hg at the pump. This is the critical value for this particular instrument; if the vacuum exceeds this figure, the pump will not supply sufficient gas for analysis.

The piping from valves 3, 4, and 5 to the analyzer must be installed according to the instrument manufacturer's instructions. Compressed air for blowing out all the sample lines is supplied by means of valve 14. This should be done at least once each day and more often if the lines appear to be getting dirty. It is necessary to close valve 10 to the pump and shut off the water to the top of the inductor when blowing out the lines. The double-valve arrangement, 14 and 12, with the bleed valve 13 between, is for the purpose of preventing leakage of high-pressure air into the system. When compressed air is not being used, valves 12 and 14 are kept closed, and valve 13 is kept open to the atmosphere.

The vacuum at the Bailey meter pump can be controlled by valve 7. The calibration of the instrument may vary with the vacuum at the pump, owing to changes in solubility of CO_2 with partial pressure. Therefore a constant vacuum should be maintained when possible; in recent tests this was 10 in. Hg, as required by the high exhaust rates used.

The Orsat samples are taken from the system through valve 8. Although the oxygen meter discharges part of the gas at pressures above atmospheric, this gas is not used for analysis because it has been washed in the pump. In order to obtain raw gas before it passes through the pump, it is necessary to sample against the vacuum produced by the high-velocity thermocouple exhauster and the meter pump. This is accomplished by the apparatus shown on the left side in Fig. 7.

The sampling rate for the Orsat is controlled by the screw clamp 29 on the tubing between the two bottles. To maintain the pressure low enough to draw the sample, both the top of the lower brine bottle and the line passing over the upper brine bottle are connected through bubbler 21 to the auxiliary exhauster 22. The inner tube of the bubbler is large in diameter so that flow can occur in either direction without drawing the liquid out of the bottle. All the flexible lines are of heavy rubber to prevent collapse at the high vacuum.

The sample is collected as follows: The brine is forced up into the tube above the stationary bottle close to the tee in the sample line, and after closing cock 16, the movable bottle is suspended on the spring sufficiently lower than the stationary bottle to draw the sample at the desired rate (it will usually be necessary to adjust clamp 29 at the beginning of a series of tests to secure the required rate of flow). With cocks 16, 19, and 20 closed, valve 8 is opened to connect the system to the sample line. Valve 23 is opened to supply air to exhauster 22, and cock 20 is then opened.

The air to the exhauster is adjusted until a definite flow in the correct direction has been established, as indicated by the bubbler. With steady flow established, cock 16 is opened to collect the sample. Care must be exercised to prevent backflow of air during

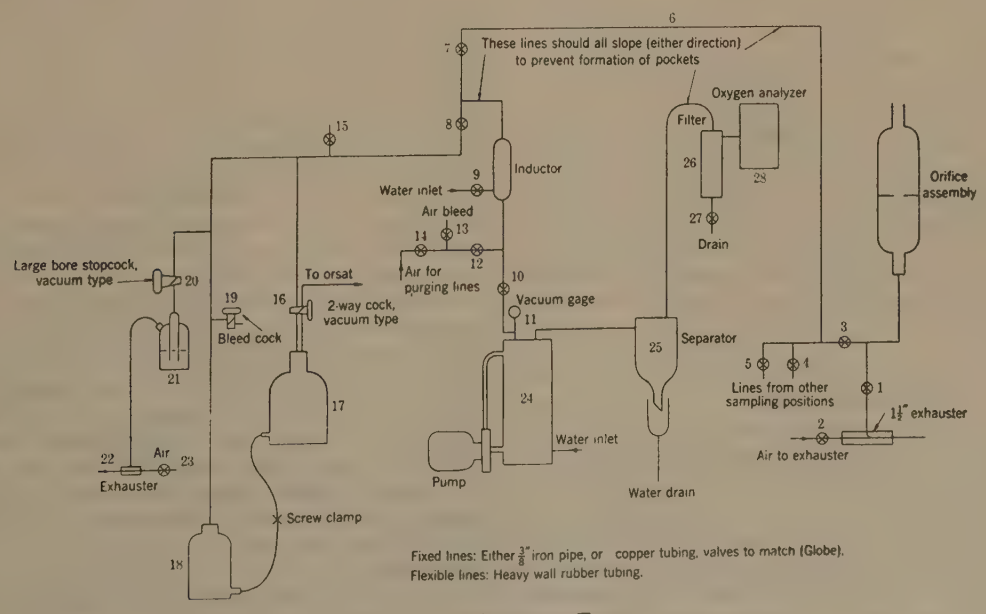

FIG. 7 GAS-SAMPLING TRAIN

the sampling period. Should this happen, it will be necessary to wait until the air has been purged from the line before sampling can be started. This probably will take about 15 to 30 sec, and is indicated when the oxygen recorder returns to a normal reading. When the required amount of sample has been collected (about twice the volume usually needed for sampling) cock 16 is closed, valve 8 is closed, and cock 20 is closed. The lower brine bottle is elevated to place the sample under pressure. The air supply to the exhauster is shut off at valve 23, and bleed cock 19 is opened to restore the system to atmospheric pressure. The sample is transferred to the Orsat in the usual way through the other side of 2-way cock 16.

(*b*) *Bailey Oxygen Meter, Operation, and Calibration.* The instrument operates on the principle of burning oxygen with a special liquid fuel on a platinum filament. The combustion results in an increase of the temperature, and consequently an increase of the resistance of the filament. This change of resistance upsets the balance of a bridge circuit, of which the filament forms one arm, and balance is restored by the rotation of a slide wire controlled by an amplifier fed from the bridge output. The slide wire is connected to a cam which operates the pen of the instrument.

For testing service, a 1-hr clock is substituted for the 24-hr chart drive with which the instrument ordinarily is equipped. For continued operation with dirty gas, the gas must be washed. This is accomplished in the inductor and in the pump used to pull the sample, and the gas is filtered before it enters the instrument; excess gas is bled to the atmosphere by a pair of relief valves in the analyzer. In the washing process, CO_2 is absorbed in an amount proportional to its partial pressure, and therefore a constant percentage of the CO_2 in the raw gas is removed. Under one set of representative conditions, the figure was 15 per cent. For the conditions expected in a recent test, the average increase in oxygen content, resulting from the removal of CO_2 from the sample, was 0.1 per cent. Therefore the instrument was calibrated to include this change in gas composition when analyzing washed gas. The instrument is most conveniently calibrated with standard gas mixtures; but to facilitate field checking, changes were made in the bridge circuit, which, in conjunction with spot analyses of flue gas, permitted the use of air as a standard gas in trimming the instrument to indicate the oxygen content of the raw gas. To guard against errors due to changes in calibration, the instrument is checked at frequent intervals as an integral part of the test procedure, so that daily calibration curves are obtained. In a recent series of tests of 2 weeks' duration, it was not found necessary to readjust the instrument.

The oxygen-recorder chart shown in Fig. 8 is typical. A daily calibration curve is shown in Fig. 9(*a*), and the relationship between the oxygen content of the raw gas and the CO_2 is given in Fig. 9(*b*), from the same analyses. Thus from the average indications of the instrument, the average oxygen content of the raw gas is obtained from Fig. 9(*a*), and thereafter the average CO_2 content from Fig. 9(*b*). The nitrogen content is obtained by difference. It should be noted that calibration data in Fig. 9(*b*) apply only to a specific set of test conditions and cannot be considered to be typical.

Typical Results of Temperature and Gas Composition Determinations

Temperature of Furnace-Outlet Gases. The quality of the data obtained with the new technique is best illustrated by typical results obtained in a recent series of furnace tests. Fig. 10 is a drawing of the furnace outlet, approximately 19 ft high × 31 ft wide. Thirty sampling positions were used, in 6 columns designated A, B, C, D, E, and F, corresponding to access doors located in the front wall, each column having 5 sampling points designated +6, +3, 0, —3, and —6, which are the approximate

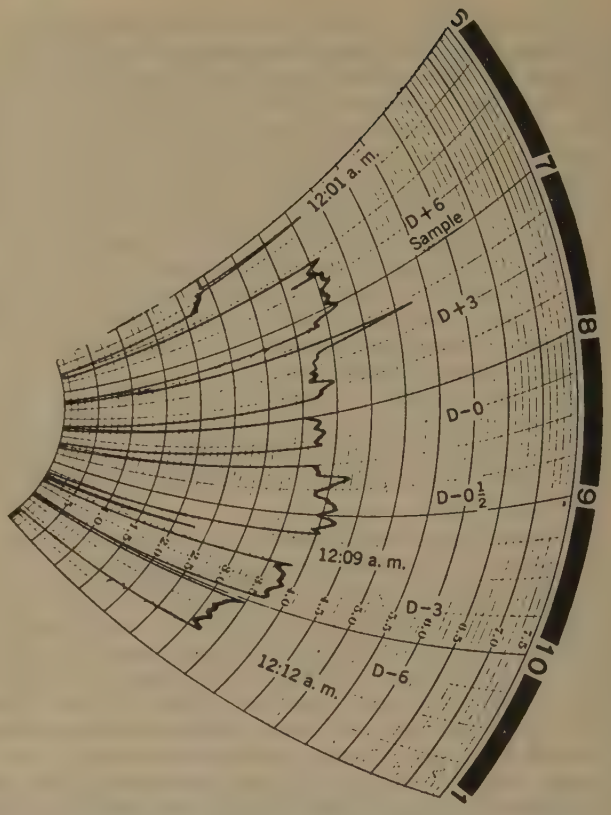

Fig. 8 Typical Record of Oxygen Analysis of Gas at Furnace Outlet by Bailey Oxygen Recorder

vertical distances in feet from the horizontal mid-line of the furnace outlet. At each sampling point plotted to scale there is given the average of approximately a ½ to 1-min temperature record on the high-speed recorder. Lines of constant average temperature have been drawn on the plot. There are no wild points; and the isotherms, though quite complex, conform excellently with the data and with each other.

The turbulence and mixing characteristics of pulverized-coal firing, even under steady operating conditions for the furnace as a whole, cause the temperature, composition, and velocity of the gas at any point in the furnace to vary with time. On the other hand, it can be assumed that over a reasonable time interval the properties of the gas at any point in the furnace, particularly at the furnace outlet, will have well-defined average values, which are representative of the operating conditions. As shown in Fig. 5, the changes of gas temperature with time are quite rapid and extensive. The method of recording used permits determination of the average of the temperature values at a point over an interval of about ½ to 1 min. Although it is not to be assumed that the rapid fluctuations shown in Fig. 5 are the only variations of the temperature at a point with time and that the average for the short period of observation will coincide exactly with the true average for a test period of 2 to 3 hr, it is evident that much of the possible error of measurement of the average temperature at a point at the furnace outlet is eliminated by recording the temperatures over a definite interval of time. Further, if the residual errors were still great, the probability would also be great that the values plotted in Fig. 10 would be subjected to chance variations of considerable magnitude, and it is hardly conceivable that the regularity inherent in Fig. 10 would be obtained.

Finally, even if the data plotted in Fig. 10 are partly the result of chance variations of the averages of the periods of ob-

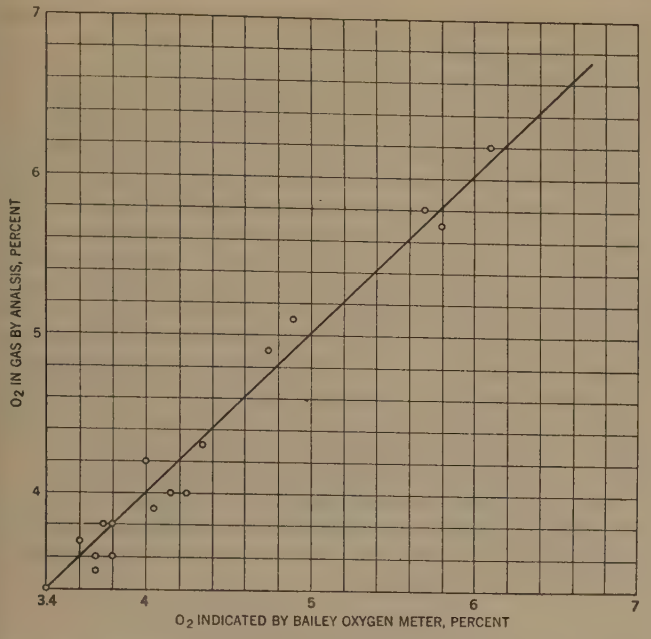

FIG. 9(a) TYPICAL DAILY CALIBRATION CHART OF BAILEY OXYGEN RECORDER

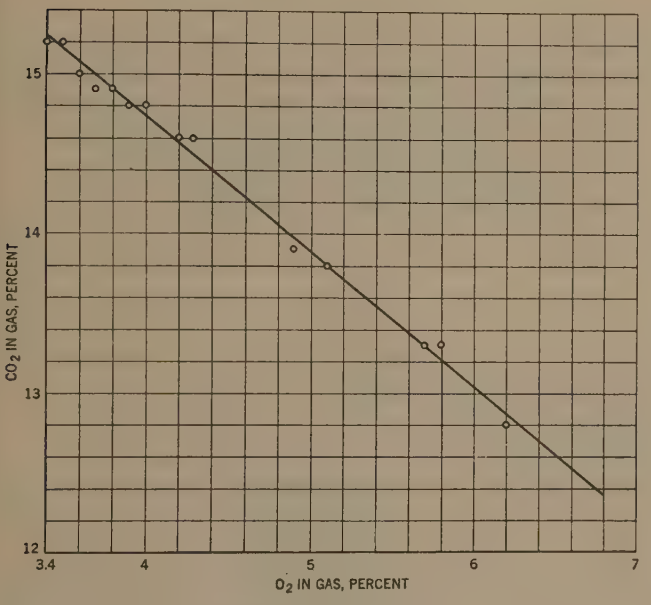

FIG. 9(b) RELATION BETWEEN CO_2 AND O_2 IN A GIVEN FURNACE-OUTLET GAS, DERIVED FROM CALIBRATION ANALYSES

servation for the test points from the averages for the entire test period, variations above the mean for any point are equally as probable as variations below the mean, and the average of a considerable number of such observations would have a considerably lower standard deviation from the true average than that of an observation at a single point from the average at that point. In this light, then, Fig. 10 is presented as a representation of the distribution of the time-average temperature over the furnace outlet, subject to unknown, but presumably small, errors.

From these data, also, one can obtain an idea of the sampling characteristics for temperature measurements, as determined by the distribution of the average temperature at various points at the furnace outlet. Thus symmetrically disposed rows of

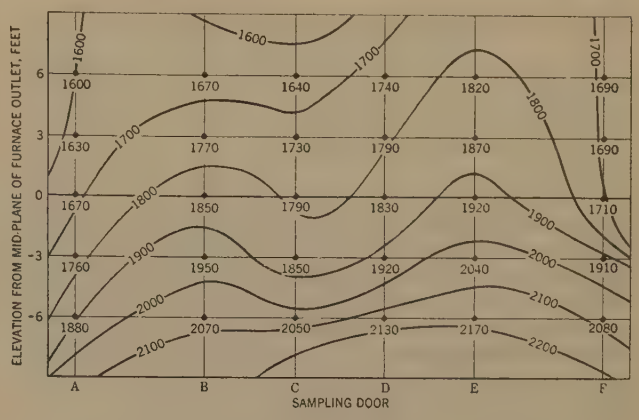

FIG. 10 DISTRIBUTION OF TEMPERATURE AT FURNACE OUTLET

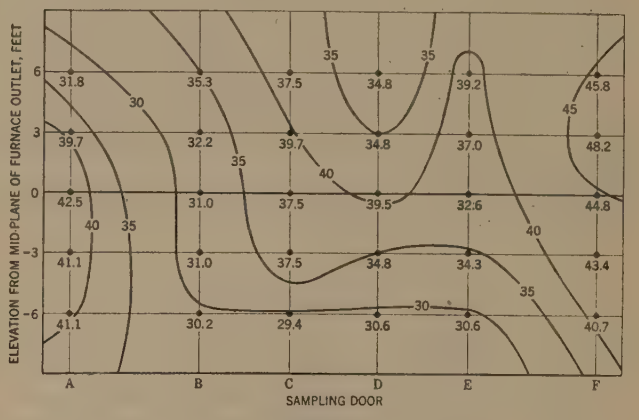

FIG. 11 DISTRIBUTION OF PERCENTAGE OF EXCESS AIR AT FURNACE OUTLET

samples give the numerically averaged temperatures for the combined gas at the furnace outlet shown in Table 1.

TABLE 1 NUMERICALLY AVERAGED TEMPERATURES FOR COMBINED GAS AT FURNACE OUTLET

No. of rows of samples	Location of rows	Numerical average temp, deg F
1	0	1795
2	+3, —3	1826
3	+6, 0, —6	1851
5	+6, +3, 0, —3, —6	1841

For this particular furnace, a simpler sampling procedure, using only +6, 0, —6 positions, appears to be adequate to determine the average temperature for the whole furnace outlet for the test period. In general, such a procedure can be justified only as a result of the type of analysis given here.

Composition of Furnace-Outlet Gases. The distribution of gas composition over the furnace outlet in the test just cited is shown in Fig. 11. The excess air at the 30 sampling points is shown, and lines of constant excess air have been drawn. Some systematic relationship between the temperature and composition plots can be seen; but the range of variation of excess air is quite low. The sampling characteristics, as determined by the distribution over the furnace outlet, are again best illustrated by comparing the numerical averages of excess air for various combinations of symmetrically arranged rows of samples. These are given in Table 2.

In this particular case, although this is probably fortuitous, a single row of six samples, at the mid-line of the outlet, gives the same results as the 30 samples. The deviations, in general, are so small that a considerably restricted sampling scheme for gas

TABLE 2 NUMERICALLY AVERAGED EXCESS AIR FOR COMBINED GAS AT FURNACE OUTLET

No. of rows of samples	Location of rows	Numerical average excess air, per cent
1	0	37.0
2	+3, —3	37.8
3	+6, 0, —6	36.4
5	+6, +3, 0, —3, —6	37.0

composition would be permissible. Aside from the uniformity of distribution of the average composition at a point which Fig. 11 may be taken to represent, it is hardly conceivable that any great fluctuations of gas composition with time, *not already averaged by the recording instrument*, could exist, for the reasons cited in connection with the analysis of the temperature measurement.

Methods of Calculating Sensible-Heat Content of Gases Leaving Furnace

Most of the uncertainty of measurements of furnace heat absorption by the method of losses resides in the determination of the sensible-heat content of the furnace-outlet gases. Having devoted considerable effort toward obtaining representative and accurate data, it is pertinent to examine the methods of calculation of the heat content of the gases from the temperature and gas-composition data for significant avoidable errors which may be inherent in them.

The most accurate method of calculation that is at all practical is described in the following equations

$$\left(\frac{\overline{H_G}}{W_G}\right) = \frac{\int_A \left(\frac{H_G}{W_G}\right)_i M_i\, dA_i}{\int_A M_i\, dA_i} \quad [1]$$

$$\left(\frac{\overline{W_f}}{W_G}\right) = \frac{\int_A \left(\frac{W_f}{W_G}\right)_i M_i\, dA_i}{\int_A M_i\, dA_i} \quad [2]$$

$$\frac{H_G}{W_f} = \frac{\left(\frac{\overline{H_G}}{W_G}\right)}{\left(\frac{\overline{W_f}}{W_G}\right)} \quad [3]$$

$$H_G = \left(\frac{\overline{H_G}}{W_f}\right) W_f \quad [4]$$

$$W_G = \frac{W_f}{\left(\frac{\overline{W_f}}{W_G}\right)} \quad [5]$$

where H_G, W_f, W_G = hourly quantities, respectively, for the heat content of the gases leaving the furnace, the mass of fuel fired, and the mass of gas leaving the furnace

$\left(\frac{H_G}{W_G}\right)_i$ = heat content per pound of gas at section i of furnace outlet, Btu per lb, average for test period

$\left(\frac{W_f}{W_G}\right)_i$ = mass of fuel burned to form gas at section i of furnace outlet, lb per lb; average for test period

$\left(\frac{\overline{H_G}}{W_G}\right), \left(\frac{\overline{H_G}}{W_f}\right), \left(\frac{\overline{W_f}}{W_G}\right)$ = average values, respectively, of heat content per pound of gas, heat content of gas formed per pound of fuel fired, and pounds of fuel burned to form a pound of gas, all for conditions of gas at furnace outlet

M_i = mass velocity out of furnace at section i, psf-hr; average for test period

dA_i = area of ith section of furnace outlet, sq ft

The integral is taken over the whole furnace outlet area, A.

$(H_G/W_G)_i$ and $(W_f/W_G)_i$ are calculated from the average values for the test period of the temperature and composition of the gas at the ith section of the furnace outlet. As shown previously, with little error in the final results, these terms may be calculated from the corresponding average temperature and gas composition for the periods of observation. These calculations require that the average relative mass velocities of the gas out of the furnace for the test period (or as in the foregoing, for the period of observation) be known. That the form of the equations is correct is readily seen if it is assumed that the mass velocities are absolute values. In each case the equations become simple integrals of the desired quantity over the area of the furnace outlet. Although this method of calculation has been used in a number of cases, it is cumbersome and is readily simplified.

For the usual conditions of temperature and composition of the gas at a furnace outlet, the relationship between the heat content per pound of gas, and pounds of gas per pound of fuel is expressed by the following equations

$$\left(\frac{H_G}{W_G}\right)_i = (a + bt_i) f(X_i) \quad [6]$$

$$\left(\frac{W_G}{W_f}\right)_i = c + dX_i \quad [7]$$

where a and b are constants independent of the fuel fired, c and d are constants for a particular fuel, t_i and X_i are the temperature and excess air for the gas at the ith section of the furnace outlet, and $f(X_i)$ is a function of the excess air at the ith section, which for a given fuel, varies with X_i between narrow limits.

If these substitutions are made in Equations [1] and [2], the results may be expressed with no significant error by

$$\left(\frac{\overline{H_G}}{W_G}\right) = (a + b\bar{t}) f(\overline{X}) \quad [8]$$

$$\frac{1}{\left(\frac{\overline{W_f}}{W_G}\right)} = c + d\overline{X} \quad [9]$$

where

$$\bar{t} = \frac{\int_A t_i M_i\, dA_i}{\int_A M_i\, dA_i} \quad [10]$$

$$\overline{X} = \frac{\int_A X_i M_i\, dA_i}{\int_A M_i\, dA_i} \quad [11]$$

The limitations imposed are that the excess air should not vary over the furnace outlet by more than 20 per cent excess air, and that there be no combustible gas in the furnace-outlet gases. The significant point in these equations is that the heat content and quantity of the furnace-outlet gas may be calculated from the mean values of the temperature and excess air for the gas, suitably weighted for the mass velocity out of the furnace. Also, the mean percentage of any of the furnace-gas components similarly obtained may be substituted for the mean excess air.

Owing to the difficulty of making the necessary measurements, and the frequent lack of suitable access to the furnace, mass-velocity data are rarely obtained in large boiler furnaces. Calculations are then based on area averages of the observed temperature and gas composition, or, if the sampling points are rea-

sonably well distributed, on simple numerical averages of these quantities. Because of these circumstances it is essential to determine (*a*) what errors may arise because of neglect of weighting for mass velocity, and (*b*) if any indications can be found from the temperature and gas-composition data, that weighting for mass velocity will be significant in any given case. The pertinent factors with respect to the furnace outlet are the spread of temperature and gas composition, the ratio of maximum to minimum mass velocity, and the nature of the relationship between the three variables.

Examination of the data used for illustration in this paper indicated that for that particular furnace there readily could be a 30-deg F difference in the mean temperatures calculated with and without weighting for mass velocity. In most cases, however, the difference may be expected to be less. In a previous investigation,[4] in which mass-velocity data were obtained, the difference between weighted and unweighted mean temperatures was about 10 deg F, consistent with the relatively low temperature spread at the outlet for that particular furnace. In general, then, errors in the mean temperature varying from 0–30 deg F, and possibly higher in rare cases, may occur if the effect of mass velocity is not considered.

In any particular case, the simplest procedure is to carry out the calculations of the mean temperature and gas composition with and without an assumed mass-velocity distribution. The choice of the latter will depend on the availability of velocity-distribution data for similar circumstances, visual observations, or personal judgment. The decision as to whether or not velocity data shall be taken, or if some allowance for variations in the velocity of the gases should be made in the calculations, will depend on the purpose of the tests. These errors of calculation will have little effect on the correlation of the performance of a given unit with the operating variables, because the effects are not large, and will not vary much with changes in operating conditions. However, if the test data are to be used for the purpose of comparing units of widely different geometry and different firing methods, the errors of calculation may be significant and should be given consideration. It is in this second set of circumstances that the whole question becomes pertinent to the work of the committee.

The value of velocity-distribution data for other aspects of furnace design and operation is well appreciated and in most instances is the strongest incentive for velocity measurements. Instruments suitable for furnace work have been described,[4] and these are not difficult to construct. They are Pitot tubes of the double-impact type, which are inherently sensitive to direction, for it is necessary to determine at each point selected for study, the velocity head in the direction of flow. From the data and the geometry of the furnace outlet, the mass velocity out of the furnace can be calculated. Absolute calibration is not required, since relative values of gas velocity are sufficient for weighting purposes.

Summary and Conclusions

Although the test procedure is far more complex and the experimental apparatus is on a much larger physical scale, the basic considerations of furnace heat-absorption measurements are similar to those of simple laboratory determinations of the properties of materials. These are as follows: (*a*) The accuracy of the individual measurements; (*b*) the precision of the results, primarily as determined by the sampling characteristics of the material being studied; (*c*) the convenience of the experimental procedure; and (*d*) the relationship of the experimental results to the information desired. The foregoing description of the instrumentation and methods of analysis employed in recent furnace heat-absorption studies demonstrates that significant advances in the art of furnace heat-absorption measurements have been made along each of these lines.

The accuracy of the most critical of the measurements for furnace heat-absorption determinations, that of the temperature of the gas, has been improved with the development of the Type E shield. Although this instrument still requires calibration, the difference between its indications and that of the B&W MHVT, amounting to about 30 deg F at 2000 F, is sufficiently small so that little error is introduced in the calibrating process. Because it is as convenient to use in dirty gas as the single shield, it should become preferred equipment for temperature measurements in pulverized-coal-fired furnaces.

The problem of obtaining representative measurements of the rapidly fluctuating temperature of the gas at the furnace outlet has largely been solved by the use of high-speed recording potentiometers. With such equipment the average temperature of the gas at a given point, over an interval of $^1/_2$ min to 1 min, is readily obtained. Plots of these short-time average values yield smooth and consistent distribution patterns for the temperature of the gas at the furnace outlet, and it is believed that these plots are representative of average conditions for the whole test period.

The use of an automatic oxygen analyzer permits the convenient and simultaneous determination of the temperature and the oxygen content of the gas. A limited number of complete gas analyses serve both to calibrate the oxygen meter and to relate the oxygen content of the gas to that of the other gas components.

An accurate specification of the number of points for sampling the gas at the furnace outlet requires, as in other sampling problems, a priori knowledge of the distribution of the property being sampled, in this case the temperature of the gas. In the absence of such knowledge, the sampling specifications of the ASME Test Code for Stationary Steam-Generating Units provide a conservative estimate of the number of sampling points. As data are accumulated for a given unit, the number of sampling points may be reduced if the test results do not deviate too widely from the mean.

The calculation of the heat content of the furnace-outlet gas from the temperature and composition data involves the additional factor of the distribution of the mass velocity of the gases out of the furnace. Since it is always difficult, and in some cases impossible, to obtain the necessary data, typical cases where the velocity data were taken have been examined for the effect of weighting with respect to mass velocity on the calculated heat content of the gases. It has been estimated that the error in the calculated mean temperature of the gas will be in the range of 0 to ± 30 deg F, and, in general, will be significant only for the comparison of units of different geometry and firing methods.

No experimental data are available for the precision of a single furnace heat-absorption determination. The accuracy is also unknown, but should be readily determined by tests in some recently installed units which have practically no steam-generating surface other than the furnace, where comparisons could be made with independent determinations of the heat absorption in the furnace. As in all test procedures, evaluation of the method must be based upon an analysis of the results of a multiplicity of tests made under identical conditions. Because of the amount of work required per test, and the ever-present desire to cover the widest possible range of operating variables in each series of tests, this has not yet been done. By making these tests in a unit of the type described, both the precision and the accuracy could be determined simultaneously. Such tests are strongly recommended.

Central-station steam-generator design has been subject to continuous development, which has brought about the present high level of performance. There is, however, yet room for im-

provement to increase availability, and to increase flexibility with regard to the coal burned. Essential to this continued development is the steady accumulation of accurate performance data particularly for the furnace. The development of the test method that has been described is one of many contributions to the continued development of steam-generating equipment now being made by boiler manufacturers, steam-plant operators, and this Society through its Special Research Committee on Furnace Performance Factors, with which the Bureau of Mines is working in close co-operation.

Acknowledgments

The authors gratefully acknowledge, with appreciation and thanks, the contributions to this investigation made by the following:

Dr. A. C. Fieldner, chief, Fuels and Explosives Division, and Dr. R. L. Brown, chief, Coal Branch, Bureau of Mines, who authorized the work and made many helpful suggestions.

The engineers and assistants of the Combustion Research Section: J. Jonakin, C. H. Schwartz, J. J. Pfeiffer, H. Perry, E. G. Graf, G. R. Kollar, and J. P. Stein, who assembled the test equipment and assisted in the conduct of the tests.

The officials and engineers of the Louisville Gas & Electric Company: A. G. Rosenbaum, superintendent of steam power; Fred Tetzel, assistant superintendent of steam power; J. D. Brecher, plant engineer, Paddy's Run Station, who gave unstinted and able assistance in the arrangements for the tests.

The Bailey Meter Company for the loan of a Bailey oxygen recorder.

Fred Ely, Research and Development Division, Babcock & Wilcox Company, for the loan of a high-speed recording potentiometer.

Discussion

F. G. Ely.[11] It is gratifying to note the advances made in furnace-testing techniques which the authors have presented very clearly and comprehensively in this paper. In particular, the use of the fast-action temperature recorder with simultaneous analysis of gas composition, as well as the measurement of gas velocity over the thermocouple junction, effectively reduce uncertainties in measurement and correlation of the traverse data and shorten the time required for a survey of the furnace outlet.

In a large well-proportioned furnace, it may be expected that gas mass-flow distribution would have no extreme unbalance, and the assumption of uniform distribution or a moderate adjustment based upon visual estimation, would not involve serious consequences in final calculation of the furnace heat balance. The authors appropriately have reserved opinion on this for changes in furnace geometry. It is not difficult to imagine furnace arrangements of practical and acceptable design in which the upset in gas-mass flow is as significant as that of temperature alone, and it is urged that further ingenuity and effort be applied to the development and use of an instrument that will provide at least a relative measurement of gas velocity and direction.

For use of the high-velocity thermocouple in high-temperature zones of a furnace there is a possibility of error in temperature readings caused by heating of the splice between noble and base-metal wires if the aspirated gas is not cooled sufficiently in passage through the water-cooled holder. When used for traverses where the furnace-gas temperature exceeds 2400 F, it is advisable to retain not less than a 4-ft length of noble metal before attachment of the copper-alloy lead wires.

[11] Research Engineer, Research and Development Department, The Babcock & Wilcox Company, Alliance, Ohio. Mem. ASME.

R. B. Engdahl[12] and H. E. Carlton.[13] Through the courtesy of the authors, the writers were fortunate to be able to obtain a sample of the Type E aspirating-thermocouple shield shown in Fig. 3 of the paper. The shield seemed desirable for application in an oil-fired locomotive firebox where the comparative transparency of the flame and the large proportion of clean water-cooled surface combined to introduce an unknown but probably considerable error in measurement of flame and gas temperature.

However, in making temperature traverses, the shield was moved across high-temperature gradients, and it was found that the internal thermal stresses under these conditions were too severe to permit more than a few readings before the shield broke and was carried away. The readings which were obtained indicated that at a flame temperature of approximately 2500 F, the average temperature across the 8-ft width of the firebox, when being operated at low rate, was approximately 80 deg F higher than when measured with a simple single cylindrical shield. This was in a region immediately in front of the burner and in a shallow refractory firebox, hence the intense radiation of the initial flame plus the hot refractory compensated considerably for the radiation to the comparatively cold firebox walls above the refractory pan.

At a slightly higher rate of operation but in a position near the flue sheet of the boiler, where the gases leave the firebox and enter the boiler flues, the average temperature using a Type E shield was about 2300 F, which was approximately 260 deg F higher than the average temperature attained with the single shield.

Despite the decidedly improved accuracy with the Type E shield, unfortunately it could not be used in this service because of the failure resulting from frequent thermal shock. Heat release of the order of 120,000 Btu per cu ft per hr resulted in intense mixing and high-temperature gradients. It has been found since that a single quartz shield is definitely superior to even the simple porcelain shield, and the latter is distinctly better than the Type E shield when the shield is subjected to thermal shock.

W. T. Reid.[14] The authors have given a very realistic appraisal of various methods of shielding high-velocity thermocouples. Based upon designs chosen principally for mechanical strength, ease of installation, and freedom from clogging with ash, these shields, nevertheless, approach the performance of the MHVT construction which the authors consider most accurate. Missing, however, is an analysis of the conditions existing in each type of shield. Perhaps consideration of the flow process within the various openings in different shields might disclose useful design parameters.

High rates of mass flow are important in high-velocity thermocouples for two reasons, i.e., (1) to transfer heat to the "thermocouple" to compensate for radiation and conduction losses; and (2) to transfer heat to the "shield" to minimize radiation losses from the thermocouple. The MHVT shield has the advantage of several layers of low-conductivity material, where each layer assists in maintaining at gas temperature the surface "seen" by the thermocouple. The other shields now proposed by the authors are intended to duplicate this same condition. It is evident that any procedure which will result either in rapid transfer of heat to the internal surfaces of the shield or in minimizing heat transfer through the shield will be desirable.

The data shown in Fig. 6 of the paper indicate that the Type E shield with kidney-shaped holes is somewhat preferable to the

[12] Supervisor, Battelle Memorial Institute, Columbus, Ohio. Mem. ASME.

[13] Research Engineer, Battelle Memorial Institute.

[14] Supervisor, Fuels Research, Battelle Memorial Institute, Columbus, Ohio. Mem. ASME.

Type G shield with a larger number of smaller circular holes. The difference is not great, but it may be significant. A further distinction is the apparent ability of the Type G shield to reach thermal equilibrium at lower mass velocity than the Type E shield, although perhaps not so low as the MHVT. Unfortunately, these data are too few to assure that this is a fact.

It would be very helpful in the future for designing an ultimate high-velocity thermocouple to have an exact analysis of the heat transfer in these shields. If the mass velocity were constant for each hole in the shield, then the Reynolds number and the film coefficient would be less as the diameter of the hole decreased, and the amount of heat transferred would be smaller. Contrariwise, the use of a large number of small holes would decrease the cross section of the refractory, and the thermal conduction through the shield itself would be less. These effects, then, are opposite. If the relative magnitude of each could be evaluated, the optimum size and number of holes, and perhaps their arrangement, could be stated with certainty instead of being speculative as at present.

Perhaps such an analysis is beyond the scope of this paper, but it is hoped that the authors will consider it for future developments on instrumentation for furnace-performance testing.

R. I. Wheater.[15] In the comparison of thermocouple shields, the authors have determined the relationship between temperatures obtained by the Type E and Type G shields and temperatures obtained by the B&W MHVT, using the B&W MHVT as a standard. These comparison tests were made at various mass velocities through the shields and curves were drawn depicting the comparisons. Fig. 6 of the paper shows three curves (*a*, *b*, and *c*), curve *a* being a plot of the B&W MHVT against itself, showing how mass velocity affects the indicated temperature under essentially constant conditions of gas temperature and radiation environment. Curves *b* and *c* are similar plots for the Types E and G shields, respectively, at various mass velocities. In each case the difference between the indicated temperature of the B&W MHVT at 15,000 lb psf–hr is plotted at various mass velocities.

However, while agreeing with the methods, instrumentation, and so forth, of these comparison tests, the writer does not agree with the authors' statement in the test that these results show the optimum mass velocity to be approximately the same for all three shields and that this optimum velocity is about 10,000 lb per sq ft per hr. The optimum velocity chosen depends upon the characteristic of the curves drawn through the various points. While the characteristics of these various shields might be exactly as depicted by the curves, the writer does not feel that the data obtained, by themselves, substantiates the curves drawn. Particularly in the case of curve *b* in Fig. 6, a straight line could be drawn through the data taken on the Type E shield instead of the curve *b*, and this line would then indicate that 15,000 psf per hr was not a sufficiently high mass velocity to create a stabilized indicated temperature for this shield.

In other words, it seems that the data could be represented in another manner which would indicate an entirely different characteristic of the Type E shield and also indicate that 15,000 psf per hr mass velocity is not high enough for this particular shield to reach its maximum indicated temperature. It seems that these data indicate that more comparison data are required, over a wider range of mass velocities, in order to assure that the true correction factors have been obtained for these shields, and also to verify the minimum mass velocity required in order to reach the flat part of the correction curve, or maximum indicated temperature for the particular shield.

[15] Service Department, Foster Wheeler Corporation, New York, N. Y.

This is not to say that the authors' curves are necessarily incorrect, but rather it is felt that their knowledge of the characteristics of MHVT shields influenced them in drawing the curves. Perhaps more comparison data would be advantageous in order to prove the characteristics of the curves and the optimum mass velocity to use with the respective shield.

Authors' Closure

The authors wish to thank the discussers for their significant contributions to the paper.

Mr. Ely agrees with the authors that in most cases the distribution of the mass flow out of the furnace will have little effect on the final calculations of the furnace heat balance, but he believes that furnace arrangements of practical and acceptable design are imaginable in which the distribution may be significant. For use in such cases, he urges the development of a suitable device for measuring the relative velocity and the direction of the gases leaving the furnace, to provide weighting factors for the observed gas temperatures.

The conventional water-cooled Pitot tube has some practical limitations, particularly where flame pulsations cause widely fluctuating readings, and make it difficult to locate the direction of the principal velocity vector. The Bureau of Mines has had some success with a type of direction-finding Pitot tube, in which two double Pitot tubes are mounted on perpendicular axes, in the same plane, at the end of a water-cooled probe. This is shown in Fig. 12 of this closure. Each Pitot tube is connected to a differential manometer, and when the axis of one tube is parallel to the velocity vector a maximum reading will be produced, while the reading of the other will be zero. Since the fluctuations in the latter are the smaller, location of the flow direction becomes relatively simple, and the angle with respect to any arbitrary plane is shown on the scale by the plumb-bob pointer.

This instrument has been used successfully in a gas-fired furnace at temperatures up to 2600 F, and, with slight modification of the water-cooling arrangement, could be adapted for use at higher temperatures.

Mr. Ely properly calls attention to the temperature errors that may be produced by excessive heating in the probe of the junction between the noble-metal thermocouple wire and the base-metal compensating leads, over which the aspirated furnace gas passes. He agrees with the recommendation in the paper that the noble-metal leads should be at least 4 ft long. However, since the manuscript was completed, the factors affecting the temperature of this junction have been studied and compared with some test data, and it is now recommended that the noble-metal leads extend the full length of the probe, and that the junction with the compensating leads be made at the external terminal block. For economy, 0.4-mm Pt-Rh Pt, wire may be used for all but the first 2 or 3 ft from the thermocouple junction, which should be 0.6-mm wire.

For the conditions of the shield comparison cited in the paper, the temperature error from this source amounted to about 5 deg F for a mass velocity through the shield of 15,000 lb per hr and ft^2, and consequently the results given in Fig. 6 of the paper are not affected.

Mr. Wheater is correct in asserting that more comparison data are required to establish fully the relationship of the various types of thermocouple shields. However, it should be mentioned that in drawing curves *b* and *c* of Fig. 6, which show the effect of mass velocity on the indicated temperature of Type E and Type G shields, respectively, the authors were guided not by the characteristic of curve *a* for the B&W MHVT, but by other data taken with Types E and G shields alone. Referring the indicated temperatures of these shields to the value simultaneously determined with B&W MHVT, was intended to eliminate the effects

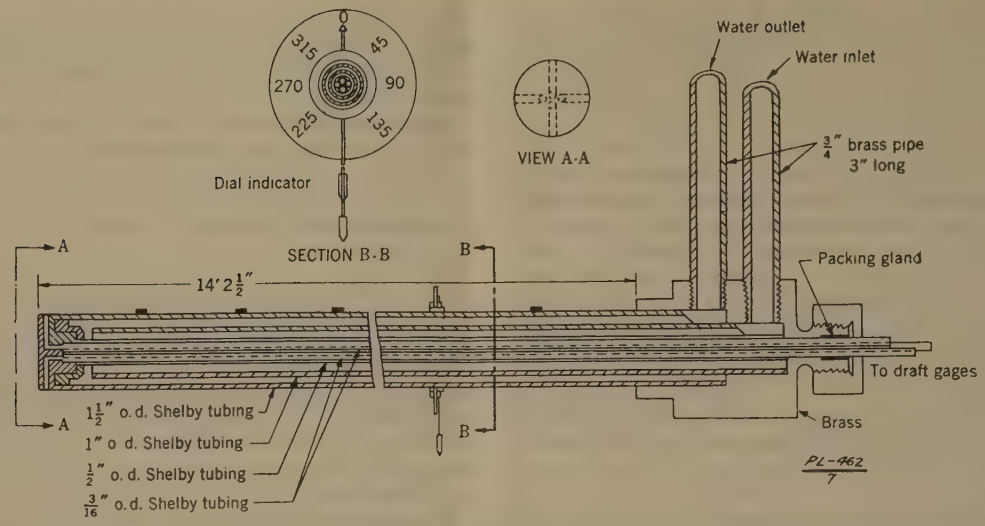

FIG. 12 DOUBLE-IMPACT PITOT TUBE FOR DETERMINING DIRECTION AND VELOCITY OF FURNACE GASES

of unavoidable variations in flame conditions during comparison. Additional work on direct comparison of shields under widely different conditions is required, and will be done as opportunities arise. Other methods of comparison also will be tried.

The observations described in the discussion of Messrs. Engdahl and Carlton demonstrate that an instrument of high inherent error, such as the single-shield high-velocity thermocouple, is extremely sensitive to the conditions under which it is used. For accurate work such instruments require calibration against a multiple-shield unit under the conditions of use. The more perfect the performance of a shield, the lower will be its error for a given location in the furnace, and the less the error will vary for changes in conditions of application. Thus it is essential that instruments of poor performance receive detailed calibration in place, whereas instruments of high performance such as the Type E and Type G shields need only spot checks in representative locations, or can be corrected on the basis of simple correlations. In oil or gas-fired furnaces, the B&W MHVT should be the preferred instrument. In pulverized-coal-fired furnaces, where plugging of the openings in the shield is a problem, Types E and G shields should be used, subject to one or two comparisons in place against the B&W MHVT.

The breakage of shields in regions of high thermal gradients mentioned by Messrs. Engdahl and Carlton has also been experienced by the authors. It can be minimized to some extent by operating the shield at very high flow rates, and is always reduced as experience is acquired in manipulating the probes in a particular application. Unfortunately, Messrs. Engdahl and Carlton did not have a large enough supply of Type E shields to give the design an extended trial in their particular application. They point out that a single shield made of fused quartz gave the best service, but of course was subject to the greatest error. For accurate work, which was not necessary for the purposes of their investigation, a more complicated shield would be required. The best line would appear to be to attempt to develop bodies for the Type E shield which would have greater spalling resistance, and there is some hope of accomplishing this. In pulverized-coal-fired furnaces, it has been found that the single shield, of whatever composition, plugs nearly as rapidly as the Type E shield.

As suggested by Mr. Reid, analysis of the heat transfer in the various shields would appear to be very helpful for developing an optimum design from the thermal standpoint. Practically, this line of attack is not fruitful for two reasons, i.e., (1) the analysis is extremely difficult for all but the simplest physical designs, and (2) considerations of utility in pulverized-coal-fired furnaces are decisive in fixing dimensions of apertures. Analyses of this type have been made by several investigators, notably Moffat,[16] and Schack.[17] However, owing to the assumptions necessary for the analysis, and uncertainties in the values of the various parameters, the results are only semiquantitative, and although useful as a guide for development, are not decisive.

Development work continues on practically all of the instrumentation described in this paper. As more experience is gained through application of the techniques to a wider variety of furnaces, changes undoubtedly will be necessary. It is hoped that ultimately a standard test procedure will evolve from these studies, to take its place with other power test procedures, and meet the needs of the industry for accurate furnace-performance data.

[16] "Errors in High-Temperature Probes," by E. Marston Moffat, presented at the Annual Meeting, New York, N. Y., November 28–December 3, 1948, of THE AMERICAN SOCIETY OF MECHANICAL ENGINEERS. Paper No. 48—A-52.

[17] "The Theory and Application of the Suction Pyrometer," by A. Schack, Institute of Fuel, Symposium on Gas Temperature Measurement, *Journal of the Institute of Fuel*, vol. 12, 1939, pp. S-30–S-38.

Modern Control Dynamics and Stability Criteria as Applied to Gyroscopic Speed Detectors With Hydraulic Drive[1]

By RENE FEISS, WINTERTHUR, SWITZERLAND

A gyroscopic speed detector is described and its application to the speed control of a steam or gas turbine is discussed. A frequency-response method of analysis of regulatory systems, involving the use of Nyquist's criteria, is presented and applied to the analysis of the stability of the turbine-speed regulatory system. The results obtained are compared with results from the classical approach, involving the solution of the characteristic equation of motion of the system.

Nomenclature

The following nomenclature is used in the paper:

J_x = moment of inertia about the x-axis of the gyro rotor
n_e = angular velocity of rotation of gyro rotor
n_p = angular velocity of rotation of plane of gyro rotor ring
M = torque produced by gyro
θ = angle between axis of gyro plane rotation n_p and axis of rotor rotation n_e
M_f = equivalent mass applied to collar of gyro, referred to rectangular motion of collar
β = angle of turning of gyro gimbal ring
ϕ = speed deviation of machine group
y_{max} = maximum travel of gyro collar
y = departure of collar position from equilibrium position
ω = angular velocity of machine group
ω_{max} = maximum angular velocity of machine group
$\Delta\omega$ = departure from equilibrium angular velocity for machine group
s = static force on gyro collar
k = coefficient of friction for push rod connected to gyro
δ_1 = degree of nonuniformity of detector
ψ = relative deviation of machine group speed
η = relative deviation of detector
T_f = fall time of detector
T_b = characteristic response time of detector
M_1 = reduced mass of the detector = $\dfrac{M_f\, y_{max}}{S}$
z = instantaneous distance of servomotor piston from new position of equilibrium
z_{max} = full travel of servomotor piston from no load to full load
T_s = traversing time of servomotor
μ = relative servomotor deviation = z/z_{max}
P = instantaneous pressure in steam chest in excess of new equilibrium pressure
P_{max} = pressure in steam chest at maximum load
Q = relative pressure deviation = P/P_{max}
T_e = filling time of chest
M_0 = coefficient of resisting torque of power consumer
H_0 = constant of proportionality between chest pressure and turbine driving torque
T_a = machine starting time
λ = change in generator load
Ψ_e = harmonic input disturbance
A_1 = amplitude of input disturbance
γ = frequency of input disturbance
δ = damping factor
Ψ_a = harmonic output disturbance
A_2 = amplitude of output disturbance
α = phase shift of transmission for a system
$A = \dfrac{A_2}{A_1}$ = attenuation of transmission for a system
p = imaginary frequency = $i\gamma$
$F(\ )$ = transfer function of a system
a_n = general coefficient for characteristic equation
D = Hurwitz determinant
Ψ = Response function for a system for harmonic disturbances = $\dfrac{\Psi_a}{\Psi_e} = F(i\gamma)$

Description of Speed Detector

The purpose of a speed detector in a speed-regulating system is to measure the speed of the regulated machine and to transmit the measured value to the device controlling the flow of energy into the machine.

The most widely used and perhaps simplest speed-measuring device is one which utilizes centrifugal force. It may function either by measuring the displacement of weights (as in a pendulum or flyball governor) or by measuring fluid pressure (for example, as produced by a centrifugal pump). A further possibility is measurement of speed by electrical means, based on measurement of frequency, current, or voltage. The possibility of using the moment of a gyroscope as a means of measuring speed has been little used until now. A speed detector of this type, which is by no means simple in construction, is the subject of this paper.

The theoretical considerations for this device may be reviewed briefly with the aid of Fig. 1. Let J_z be the moment of inertia about the x-axis of a symmetrical weighted ring supported at its center of gravity by a Cardan suspension; n_e be the angular velocity with which the weighted ring rotates; and n_p the angular velocity of rotation of the plane of the ring. The torque equation for the rotating disk is

$$M = J_z n_p n_e \quad \ldots\ldots\ldots\ldots\ldots\ldots [1]$$

[1] This paper was translated from the German by A. M. Hopkin and presented by him under the sponsorship of the Industrial Instruments and Regulators Division at the Semi-Annual Meeting, Chicago, Ill., June 16–19, 1947, of The American Society of Mechanical Engineers. It was brought to the attention of the Division by Edmund D. Haigler who visited the author, Dr. René Feiss, late in 1945. Dr. Feiss is now head of the Diesel Engine Department of the Swiss Locomotive & Machine Works, Winterthur, Switzerland. His latest work has been on high-pressure supercharging of locomotive Diesel engines operating on the Franco-Ethiopian Railroad over an 8000-ft altitude range.

However, this relation is valid only for the so-called "fast" gyroscope, in which n_e is large compared with n_p. For the "slow" gyroscope the following holds

$$M = [J_x + (J_x - J_y)(n_p/n_e)\cos\theta]n_p n_e \ldots\ldots [1a]$$

In the practical case where $\theta \approx \pi/2$ and $n_p/n_e < 0.05$ Equation [2] becomes essentially the same as Equation [1].

The idea of using a gyroscope as a speed detector is not new. About 10 years ago, for example, Vocca (1)[2] of Naples made a device similar to that shown in Fig. 1. Vocca used a synchronous

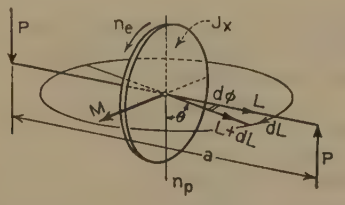

FIG. 1 RATIOS OF FORCES IN A PRECESSING SYMMETRICAL GYRO SUPPORTED AT ITS CENTER OF GRAVITY

(Centrifugal moment $M = P \cdot a$; moment of inertia of the mass of the gyro J_x, torsion vector B, vector of inherent speed of rotation N_e, vector of precession velocity N_p.)

electric motor to drive the rotor. Since machine builders have a disinclination, not altogether unfounded, toward the use of electrical apparatus where absolute reliability of operation must be guaranteed, the author used a hydraulic rather than an electrical drive.

Gyroscopes used for navigation purposes in aircraft have a pneumatic drive for the rotor. By evacuation of the gyro housing a sufficient pressure difference can be maintained. The incoming air is directed by a nozzle to impinge on a set of vanes or blades on the gyro rotor, causing it to rotate.

Since oil under pressure is usually used in heavy machinery for lubrication, it was convenient to use it to drive the gyro rotor. Such a device is shown in Fig. 2, while Fig. 3 shows the vectors of Fig. 1 for easier understanding.

The rotor S, which has angular velocity n_e, is free to rotate about the x-axis[3] and is carried in the gimbal ring P, which rotates at the so-called "precession velocity" n_p, which is the rotational speed of the prime mover. The rotational moment M set up by the precession of the gyro is absorbed by the springs F, causing the gimbal ring P to turn through the angle β. As a result of the spring characteristic, this turning is proportional to the angular velocity n_p of the prime mover. A thrust rod R and a lever U carry the displacement to the detector collar V, by which it is transmitted to the controlling device. The rotor S carries on its periphery two-sided Pelton buckets, on which two opposing jets of oil impinge. If the oil pressure at the two nozzles, W_1 and W_2 is the same, the speed of the rotor n_e, is zero. It increases with an increase of difference of pressure between the two nozzles. Therefore it is sufficient to vary the pressure at one nozzle in order to change the speed n_e and thus to cause a shift in the operating range of the detector. The same result could be obtained by deflecting one jet, with equal pressures at the two nozzles. The presence of two opposing oil streams is particularly noticeable upon lowering of speed, as the effect of rotor inertia is greatly reduced, so that acceleration and deceleration times equal one another.

The gyroscope construction, together with its transmitting

[2] Numbers in parentheses refer to the Bibliography at the end of the paper.

[3] It lies in the gimbal ring P, which is in turn rotatable about the y-axis.

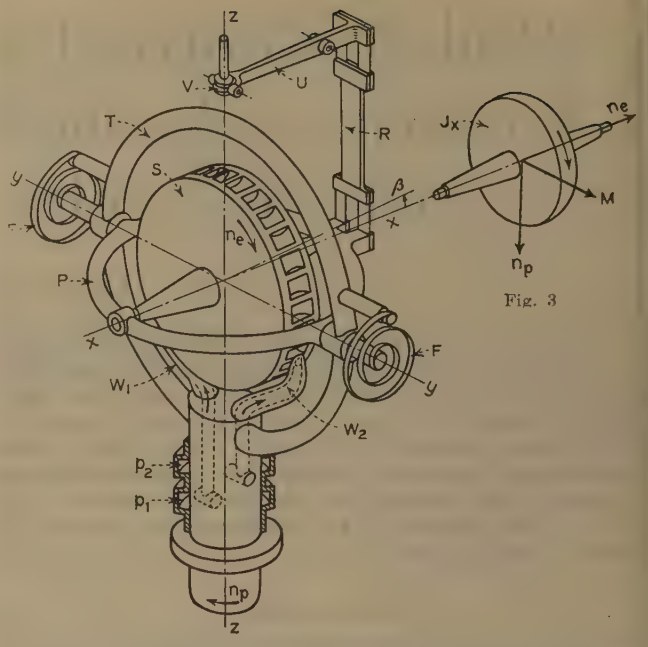

FIG. 2 (*left*) DIAGRAM SHOWING CONSTRUCTION OF A GYRO SPEED DETECTOR WITH HYDRAULIC DRIVE

(Weighted ring or fly ring S, with double row of Pelton wheel vanes; Cardan type supporting member in form of gimbal ring P and carrier ring T; centrifugal moment M taken up by two springs F; pipe leads W_1 and W_2 for oil under pressure P_1 or P_2; transmitting mechanism consisting of push rod R with laminated universal joints; speed-detector collar V, and connecting or coupling lever U.)

FIG. 3 (*right*) FLY RING S OF GYRO SPEED DETECTOR IN FIG. 2, WITH VECTORS TAKEN FROM FIG. 1

mechanism, is shown in Figs. 4 and 5. The notation is the same as in Fig. 2.

Tests have shown that the speed of the gyro rotor can be controlled very easily by the two jets of oil. The nozzles must be accurately finished if the jet under high pressure P_1 or P_2 is not to break up before reaching the rotor buckets. The upper speed limit n_e is fixed by this condition. Since n_e will vary only in the case of a change in operating range, the effect of temperature is negligible. In Fig. 6 is shown a portion of the speed-detector characteristic, obtained experimentally with the gyro speed detector shown in Figs. 4 and 5. This shows a section of the operating region covering a range of speed variation of 1 to 3.5. In contrast to other speed detectors, the range of this device can be extended almost indefinitely without affecting its stability.

ESTABLISHING DYNAMIC EQUATION FOR REGULATOR

The static stability of the speed detector is determined by the extent of increase of its stroke or movement as speed increases, but the dynamic stability of the detector can be investigated only in conjunction with an actual control circuit.

Therefore we shall assume that a gyro J, is functioning as the speed detector for a turbogenerator unit (see Fig. 7), whose steam or gas turbine A drives an electric generator B whose load is the network H. The controlling motion of the gyro collar V, is transmitted to the steam or gas valve C, by means of a pilot valve D, and a servomotor E. This valve gear is known under the name of Brown and Farcot (2). Between the valve C and the nozzle ring of the turbine is the volume G whose capacitance effect on the regulating process must be considered (3).

In general, each individual regulator has its own characteristic control circuit. If the regulator circuit is not closed, we speak of it as a controller. In the case of automatic regulators, the regulator together with the machine to be controlled form the regulatory

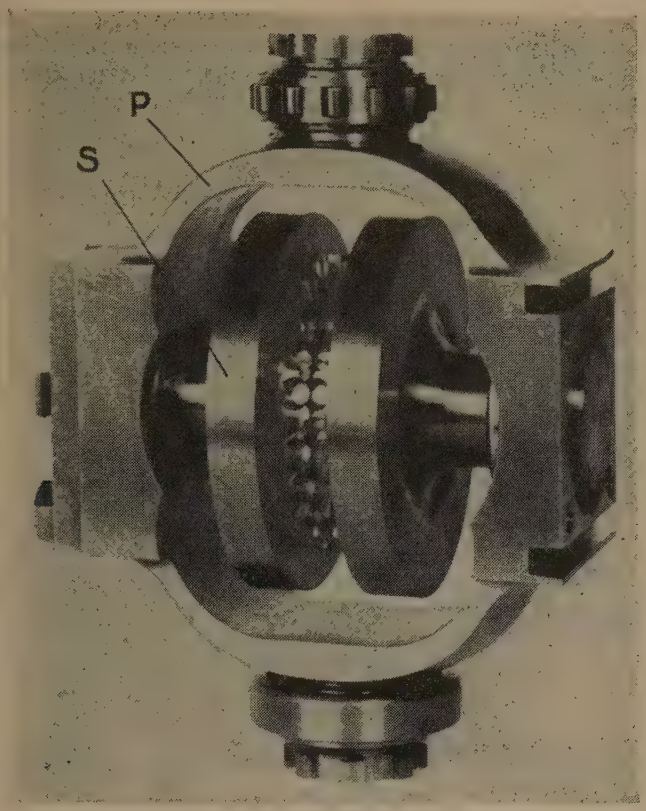

FIG. 4 COMPLETE GYRO SPEED DETECTOR
(Fly ring *S* of detector with its double row of Pelton vanes carried in bearings in gimbal ring *P*.)

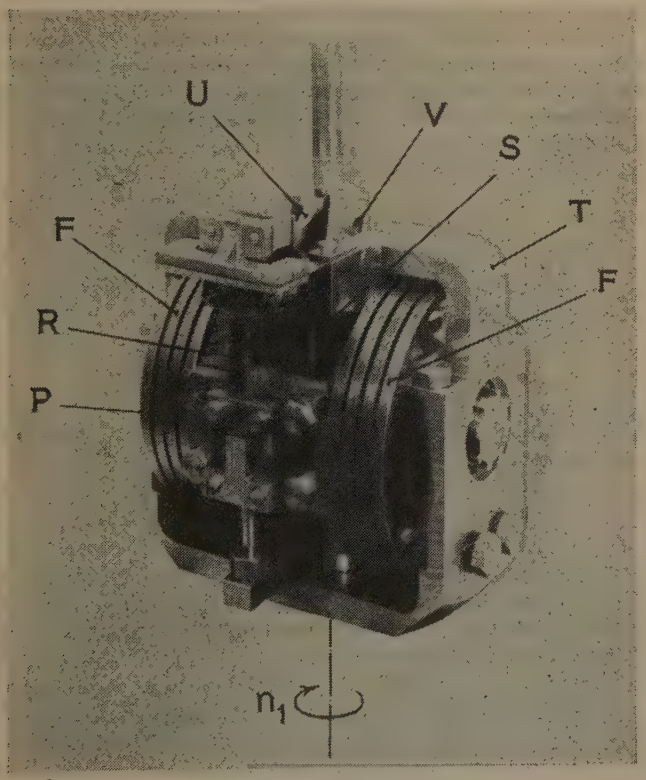

FIG. 5 ASSEMBLED GYRO SPEED DETECTOR WITH VISIBLE ADJUSTING MECHANISM
(Markings are the same as in Fig. 2.)

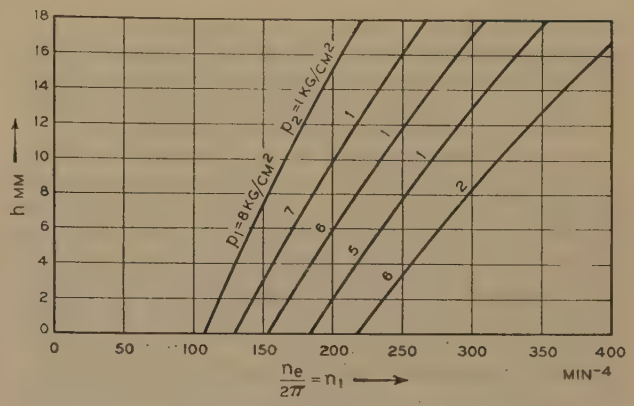

FIG. 6 EXTRACT FROM CHARACTERISTIC OF GYRO SPEED DETECTOR SHOWN IN FIGS. 4 AND 5

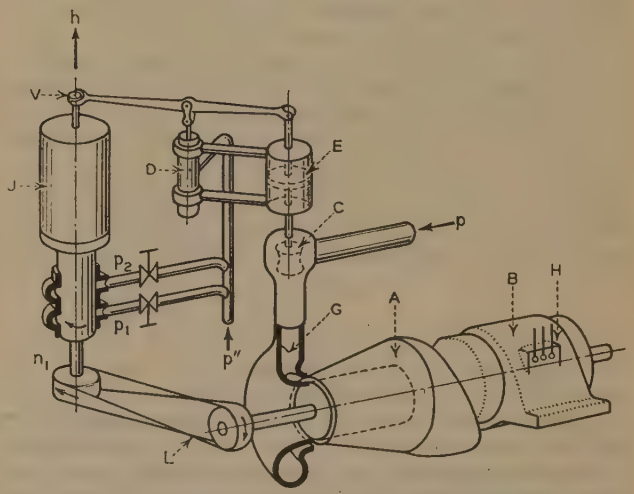

FIG. 7 REGULATING OR CONTROLLING SYSTEM
(Including gyro speed detector *J*, governor piston *D*, servomotor *E*, valve *C*, gas space *G*, turbine *A*, generator *B*, network *H*, and drive *L* for gyro speed detector.)

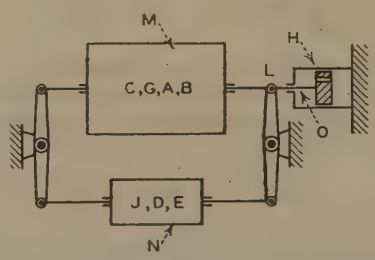

FIG. 8 DIAGRAM OF REGULATING OR CONTROLLING CIRCUIT SHOWN IN FIG. 7
(Regulating path *M*, regulating organs *N*, external load *H*, connecting or coupling rods *O*, and coupling joint *L*.)

circuit which we have shown schematically in Fig. 8, based upon the system shown in Fig. 7. Here *H* is the external load which in practical operation, may cause a change in the steady-state condition if its magnitude varies.

In Fig. 7, *C*, *G*, *A*, and *B* comprise the machine group *M* which must be in equilibrium with the external load *H*. The actual components *J*, *D*, and *E* from Fig. 7 are therefore designated as the regulator *N*. The particular speed ϕ, of the point *L* corresponds to the rotating speed of the machine group *A*, *B*. This system is analogous to that of the well-known feedback amplifier used in high-frequency work. Accordingly, we can apply all theorems used in that technique, since the differential equations

for electric oscillating circuits are of the same form as those for mechanical oscillating systems (4). In the following we shall derive the equations of motion of the speed detector, and assume the equations of the remaining regulatory members to be known, since they appear in the literature (2, 3).

The Speed Detector Equation. Since the detector is driven by a machine, which because of its inertia is not subject to sudden speed changes, the gyro will not be subject to sudden changes and so will not be forced to make any sudden nutational movements. The friction due to bearings and universal joints is reduced to a minimum through the use of ball and roller bearings and laminated-spring universal joints. Therefore the sensitivity of the device is as high as possible, and the detector is able to meet every requirement likely to be made on it as a regulating device. Furthermore, since the gyro is symmetrical, is supported at its center of gravity, and has its torque absorbed by a spring, it is stable over the entire speed range. Only a small angle β is used for the controlling range so $\theta \approx \pi/2$ at all times, and we may assume the gyro characteristic to be linear.

Let us consider a mass M_f as being applied to the collar of the gyro, this being the equivalent mass referred to the rectilinear motion of the collar. In other words, when the collar is moved, it requires the same operating force as the gyro rotor and transmission mechanism, including the mass of the operating gear on the governor-piston side. Then the kinematic equation for the gyro speed detector is similar to that for a centrifugal detector, except that here the characteristic is linear rather than quadratic

$$M_f \frac{d^2y}{dt^2} = S\left(\frac{\Delta\omega}{\omega} - \frac{y}{y_{max}}\frac{d\omega}{dt}\frac{y_{max}}{\omega}\right) - k\frac{dy}{dt} \quad \ldots\ldots [2]$$

In this equation y_{max} is the maximum collar travel, ω is the angular velocity of the machine group, with ω_{max} as its maximum value, y and $\Delta\omega$ the momentary deviation measured from the new state of equilibrium, S is the static force on the collar which can be calculated from Equation [1] as the reaction force of the spring at standstill, K the coefficient of friction arising from the movement of the control push rod activated by the gyro and

$$\frac{d\omega}{dt}\frac{y_{max}}{\omega} = \delta_1 = (\omega_{max} - \omega_{min})$$

is the degree of nonuniformity of the detector.

We shall now write Equation [2] with the introduction of dimensionless quantities as used in other publications (2, 3, 5)

$$\frac{T_f^2}{2}\frac{d^2\eta}{dt^2} + T_b\frac{d\eta}{dt} + \delta_1 = \psi \quad \ldots\ldots [2a]$$

in which $\Delta\omega/\omega = \psi$ is the relative deviation; y/y_{max} is the relative detector deviation; $T_f = (2M_f\, y_{max}/S)^{1/2}$ the fall time of the detector; and $T_b = ky_{max}/S$ the characteristic response time for the detector, both with the rods included.

For our stability investigation, we will write Equation [2] as follows

$$M_1\ddot{y}/y_{max} + T_b\dot{y}/y_{max} + \delta_1 y/y_{max} = \frac{\Delta\omega}{\omega_{max}} \quad \ldots\ldots [2b]$$

This is the equation of motion for the reduced mass of the detector under the influence of the reduced spring characteristic and laminar friction. Upon substitution of numerical values suitable for a turbine of 6000 kw, Equation [2b] becomes

$$9.13 \times 10^{-6}\ddot{y} + 2.56 \times 10^{-3}\dot{y} + 5 \times 10^{-2}y = 3.182 \times 10^{-5}\Delta\omega$$

Power Gear With Rigid Follow-Up. With $z/z_{max} = \mu$ the relative servomotor deviation, z the instantaneous distance of the servomotor piston from the new position of equilibrium, z_{max} the full travel of the piston from no load to full load, and T_s the traversing time of the servomotor, we obtain the equation of motion of the driving force in dimensionless form

$$T_s\frac{d\mu}{dt} + \mu = \eta \quad \ldots\ldots [3a]$$

For our stability study this is equivalent to

$$\left(T_s\frac{y_{max}}{z_{max}}\right)\frac{dz}{dt} + \frac{y_{max}}{z_{max}}z = y \quad \ldots\ldots [3b]$$

If $T_s = 1$ sec, $z_{max} = 0.04\, M_1$, Equation [3b] becomes

$$0.25\dot{z} + 0.25z = y \quad \ldots\ldots [3c]$$

where

$$\dot{z} = \frac{dz}{dt}$$

Capacity Between Valve and Turbine. With $P/P_{max} = Q$ as the relative pressure deviation, P as the instantaneous pressure in excess of that corresponding to the new state of equilibrium, P_{max} as the pressure in the chest corresponding to maximum load, and T_c as the filling time, we have

$$T_c\frac{dQ}{dt} + Q = -\mu \quad \ldots\ldots [4a]$$

This may be written as

$$T_c\frac{z_{max}}{P_{max}}\frac{dP}{dt} + \frac{z_{max}}{P_{max}}P = -z \quad \ldots\ldots [4b]$$

If $T_c = 0.25$ sec, $P_{max} = 300$ psi, this becomes

$$0.05 \times 10^{-6}\dot{P} + 0.2 \times 10^{-6}P = -z \quad \ldots\ldots [4c]$$

The Machine Group. Let H_0 be the constant of proportionality between the chest pressure and turbine driving torque, M_0 the coefficient of resisting torque of the power consumer, increasing with speed of revolution n_p, λ the portion of external generator load which is suddenly removed, T_a the machine starting time. Then the machine equation is

$$T_a\frac{d\phi}{dt} + M_0\phi = H_0Q - \lambda \quad \ldots\ldots [5a]$$

A convenient form for our study, but without the external disturbing quantity λ, is

$$T_a\frac{P_{max}}{\omega_{max}}\frac{d\overline{\Delta\omega}}{dt} + M_0\frac{P_{max}}{\omega_{max}}\overline{\Delta\omega} = PH_0 \quad \ldots\ldots [5b]$$

If $T_a = 10$ sec, $M_0 = 1$, $H_0 = 1$, $\omega = 314$ sec^{-1}, then Equation [5b] becomes

$$0.637 \times 10^{-4}\frac{d\overline{\Delta\omega}}{dt} + 0.0637 \times 10^{-4}\overline{\Delta\omega} = P \quad \ldots\ldots [5c]$$

The Complete Regulator Circuit. The four simultaneous differential Equations [2a], [3a], [4a], and [5a], or the equations derived from them, determine the behavior of the individual system quantities upon a variation in generator load. Since in practice it is necessary to make certain guarantees in regard to speed variations following sudden load changes, we are especially interested in the differential equation for the relative deviation of ϕ for the system. Upon step-by-step elimination of all other variables we obtain the desired equation

$$C_0\phi^{(5)} + C_1\phi^{(4)} + C_2\phi^{(3)} + C_3\phi^{(2)} + C_4\phi^{(1)} + C_5\phi = f(t) \quad \ldots [6a]$$

For a study of system stability, the right-hand side of this equation, which denotes the external disturbance, can be set equal to zero, and we obtain a linear differential equation of fifth order with constant coefficients $C_0, C_1, \ldots . C_5$ of the form

$$C_0\phi^{(5)} + C_1\phi^{(4)} + C_2\phi^{(3)} + C_3\phi^{(2)} + C_4\phi^{(1)} + C_5\phi = 0 \ldots . [6b]$$

Methods for Investigating Dynamic Stability of Regulator Circuits

In order to understand the following we must review the basic ideas of general oscillation theory, since every regulatory circuit may be represented in terms capable of representing an oscillatory condition. Let $z = x + iy$ be a number in the complex (or Gaussian) plane, which may be written in polar coordinates as

$$z = Re^{i\alpha} = R \cos \alpha + iR \sin \alpha$$

If we substitute for α the quantity γt, in which t signifies time, z for increasing t becomes a circle of radius R with the center at the origin. Therefore z can be regarded as a rotating vector having an angular velocity γ. Either the real or the imaginary parts of z represent a harmonic oscillation, but we will assume that the instantaneous value is always represented by the real part, that is, the projection of the vector on the real axis.

If $p = \delta + i\gamma$ is a complex number, then

$$z = Re^{pt} = Re^{\delta t}(\cos \gamma t + i \sin \gamma t)$$

represents a similar point circling about the origin, whose distance $Re^{\delta t}$ from the origin changes exponentially with time. If δ is negative, the amplitude progressively decreases, and the oscillation is damped. But if δ is positive, the amplitude progressively increases and the oscillation builds up. In this connection p denotes the complex frequency of oscillation. If $\delta = 0$, we obtain a harmonic or undamped oscillation, and finally, if $R = 1$, we speak of a constant amplitude, or unit vector.

From the standpoint of oscillatory theory, each of the simultaneous differential equations formulated at the outset describes the motion of a regulatory system component under the influence of a disturbing function, for example, that resulting from a forced oscillation, and hence the equation permits one to find the form of the output disturbance.

A system component is said to be linear if its output oscillations remain proportional at all frequencies to the oscillatory input disturbance. If, for example, the input disturbance is a harmonic oscillation equal to the real part of the vector Ψ_e, which is

$$\Re_e A_1 \epsilon^{i\gamma t} = A_1 \cos \gamma t$$

the output will also be harmonic as expressed by the real part of the vector Ψ_a

$$\Re_e A_2 \epsilon^{i(\gamma t + \alpha)} = A_2 \cos (\gamma t + \alpha)$$

This output vector rotates at the same frequency as the input, but has a different magnitude and phase. The ratio of these two vectors is given by $\Psi = A\epsilon^{i\alpha}$, which also has the character of a vector, and which we will designate as the "transfer function." It is dependent upon frequency. If we plot the transfer function on the complex plane for purely imaginary frequencies $p = i\gamma$ with $i\gamma$ increasing from 0 to ∞, we obtain a locus which we may designate as the frequency curve. This curve of course can also be obtained experimentally by means of measurements on the original or on a mechanical or electrical model (11, 12).

If we know the transfer function of each component of the regulatory system, then we can find the transfer function of the complete system by multiplication of individual transfer functions. This is possible since the individual members are unilaterally coupled together so that the output of one is the input to the next. The ratio of the disturbance input on the first member to the resulting oscillations of the last element in the system yields the "open-loop" frequency curve if the imaginary frequency $i\gamma$ is varied from 0 to ∞. The term open loop is used because the regulatory circuit must be a closed loop in practical operation in order that regulation may be effected properly. It is clearly immaterial at what point the circuit is opened, so long as the point lies between two members of the circuit. In order to signify that the transfer function is dependent on frequency, we will denote it as $AF(i\gamma)$ or, in general, as $AF(p)$, where A denotes the amplitude ratio (gain or attenuation), and F the phase displacement.

If we close the opened loop again to obtain a closed-loop system by coupling the last element to the first, the significance is that the output oscillation becomes the input disturbance for the system, since the output and input must be identical for any motion to take place in the system. In other words, in any closed circuit, $AF(i\gamma)$ for the open loop (the open-loop transfer function) must equal unity. This condition is fulfilled only for certain frequencies, that is, for the roots of the equation

$$AF(i\gamma) = 1 \ldots . [7]$$

We call these frequencies the characteristic frequencies or characteristic modes of oscillation of the system. Without external driving forces a system can oscillate only at its own characteristic frequencies.

In general, the characteristic frequencies are complex. If all of the characteristic frequencies have negative real parts, then only damped oscillations as mentioned previously will occur, and any disturbances will ultimately die out and disappear. We call such a system stable. However, if any one of the characteristic frequencies has a positive real part, then the oscillation at that frequency will build up in amplitude. Such a disturbance will not die out but will tend to increase and hence the system will be unstable. Characteristic frequencies which possess only imaginary values mark the boundary between stable and unstable response, and in our investigation will be considered unstable.

Method of Small Oscillations. The classical method used in mechanics for determining the stability of oscillating phenomena, known as the "method of small oscillations," has been described in many publications, particularly regarding its application to the regulation or governing of prime movers. It is also to be found in most textbooks dealing with the theory of oscillation. The permissible magnitude of these small oscillations depends on how closely the equations of motion represent the actual motions, that is, on the limits within which the actual motions permit the assumption of linear relationships. In general, the Equation [6b] has the form

$$C_0\phi^{(n)} + C_1\phi^{(n-1)} + \ldots . + C_{n-1}\phi^{(1)} + C_n\phi = 0 \ldots . [8]$$

The assumption of an exponential solution of the form gives the characteristic equation

$$p^n + a_1p^{n-1} + \ldots . + a_{n-1}p + a_n = 0 \ldots . [9]$$

The existence of a stable state of equilibrium is dependent upon the condition that none of the n-roots $p_1 \ldots . p_n$ of Equation [9] has positive real parts. Hurwitz (8) states this condition in his criterion: All coefficients a_1 to a_n either must be positive or zero and furthermore all the following determinants must be greater than zero, that is,

$$D_1 = \begin{vmatrix} a_1 & a_3 \\ 1 & a_2 \end{vmatrix} > 0;\ D_2 = \begin{vmatrix} a_1 & a_3 & a_5 \\ 1 & a_2 & a_4 \\ 0 & a_1 & a_3 \end{vmatrix} > 0;\ D_3 = \begin{vmatrix} a_1 & a_3 & a_5 & a_7 \\ 1 & a_2 & a_4 & a_6 \\ 0 & a_1 & a_3 & a_5 \\ 0 & 1 & a_2 & a_4 \end{vmatrix} > 0; \ldots$$

Hurwitz criterion is really an expression determining limits of stability. Its application is difficult as soon as the order of the characteristic equation passes beyond the third degree. Hence literature on the subject so simplifies the dynamic equations for the individual components of the regulating circuit that the equation for the complete regulatory circuit is not higher than third order. However, seldom has investigation been conducted to see if such simplification is permissible.

Method of Self-Excited Oscillations. This method is treated in the basic work of Nyquist. If a disturbance is introduced into a circuit which is capable of oscillating, it passes through the circuit and eventually returns to the starting point. If the disturbance is an oscillation of sinusoidal form with unit amplitude and frequency γ, the vector representing the disturbance after a single passage through the circuit will exhibit the same frequency γ, but will differ from the original vector in magnitude and phase. The factor $AF(i\gamma)$ mentioned before represents this variation. In practice, the disturbing function will contain components of various frequencies, and each component in passing through the circuit will experience a definite change characteristic of its own frequency.

If we let the disturbance be represented by a converging Fourier integral of the form

$$f(t) = \frac{1}{2\pi} \int_{-\infty}^{\infty} \epsilon^{i\gamma t} d\gamma \int_{-\infty}^{\infty} f(t) \epsilon^{-i\gamma t} dt \quad \ldots\ldots [10]$$

and permit it to pass through the regulating circuit n-times, its magnitude is given by the series

$$f_n(t) = f(t) + AF(i\gamma)f(t) + [AF(i\gamma)]^2 f(t) + \ldots + [AF(i\gamma)]^n f(t) \ldots\ldots [11]$$

As already mentioned, $AF(i\gamma)$ represents the change in magnitude and phase caused by the disturbance passing once through the system. Integration of this series produces the desired magnitude of the disturbance at the output.

In order to evaluate the stability, we are now interested in the magnitude $f_n(t)$ after a very long time, when the disturbance $f(t)$ has disappeared, that is, when $f(t) \longrightarrow 0$ and $t \longrightarrow \infty$. If the limit value

$$\lim_{n \to \infty} f_n(t) = \infty$$

the system is undamped and can continue to oscillate in the absence of the disturbance. If this is not the case, the system is stable.

Let us represent the disturbing vector in the complex plane as a unit vector lying along the real axis. Then the loci of the apex of the output vectors for all frequencies after a single passage through the system, interrupted at any desired point, will describe a curved path which we will call the frequency curve. At the point where the loop is broken, the open ends must be terminated in the proper impedances so that the components react as if the system were closed. The open-loop regulatory circuit therefore can be regarded as one member of a train of an infinite number of similar circuits in which the disturbance can pass in only one direction.

Nyquist shows that when the locus of this transfer vector $AF(i\gamma)$ for all frequencies from $-\infty$ to $+\infty$ encloses the point (1, $i0$), the apex of the original disturbance vector, then the Series [10] is divergent. It converges to a finite value or to zero if the point (1, $i0$) lies on the outside.

If we turn back to the original stability considerations and denote the plane in which we plot the frequency curve as the J-plane and that in which the characteristic modes are plotted as the p-plane, it can be shown that the frequency curve is the conformal representation of the imaginary axis of the p-plane on the J-plane. It can further be shown that all characteristic modes of the system will with proper transformation fall at the point $(1 + i0)$ since, according to definition, they are the roots of Equation [7]. If we make use of this information, and remember the condition that the roots have no positive real parts, that is, they must always lie to the left of the imaginary axis on the p-plane, then we can put Nyquist's criterion into the following form: (If one passes along the frequency curve in the sense of increasing frequency $i\gamma$, a regulator is stable if the point (1, $i0$) on the J-plane always lies to the left of the curve.)

If we now make a conformal plot on the J-plane for the p-plane lines $i\gamma = \text{const}$, and $\delta = \text{const}$, we obtain two sets of curves perpendicular to one another. In accordance with the character of conformal transformation, we obtain a grid in which one family of curves forms the orthogonal trajectories of the other. Since, to maintain continuous oscillations with a closed-loop regulator circuit, Equation [7], $\Psi = \Psi_a/\Psi_e$ must be satisfied, we shall in accordance with the procedure of Profos (10) replace γ in Ψ with $\gamma_s + i\delta_s$, whereby the Ψ-curve is transferred to pass through the point (1, $i0$) so

$$\Psi^* = \epsilon^{-\delta_s t} \Psi = \epsilon^{-\delta_s t} \frac{\Psi_a}{\Psi_e} = 1$$

The characteristic values so obtained yield the characteristic frequencies γ_s, and the characteristic damping δ_s of the system, and can be taken from the grid already mentioned. Now if a uniformly spaced γ scale be marked off on the frequency curve on the J-plane, then the curvilinear square system can be sketched in accordance with known methods, or even by eye. From the position of the (1, $i0$) point on this grid, one can at the same time read both γ_s and δ_s directly (see Fig. 11).

From the values for δ_s and γ_s from the curves of the grid which go through the point (1, $i0$), an approximate calculation of the performance of the regulatory process can be made. Actually, all frequencies from $-\infty$ to $+\infty$ contribute to the regulation process. However, the principal contribution is made by the frequencies in the neighborhood of the real axis.

The exact calculation of the regulating process, as a consequence of a change of external load, for example, through a unit impulse ϵ^{pt}/p, based upon the frequency curve $F(p)$, is found by La Place's inversion integral (16, 17, 18, 19, 20, 21)

$$\phi(t) = \int_{-i\infty + c}^{i\infty + c} \frac{F(p)}{p} \epsilon^{pt} dp \quad \ldots\ldots [12]$$

This integral can be found graphically from the frequency locus and a harmonic analysis of the input disturbance. In actual practice, this probably will be the easiest method.

The application of Nyquist's stability criterion to the regulating or governing of prime movers has been described by the author in a detailed work (11, 12), and its practical value demonstrated by examples (13, 14).

In contrast to the Hurwitz criterion, the criterion of Nyquist does not require that the equation of motion of the regulatory circuit be found. The degree of the characteristic equation in no way affects the practical usefulness and clarity of the results. It can even be applied when the behavior of one or all of the members is not given in differential form, but is in the form of a

plotted curve. The necessary condition is that the system be linear and capable of being represented by a differential equation with constant coefficients. Therefore this method should be the best to use in practice, especially since the frequency curve of a regulator can be determined experimentally.

For completeness, reference must be made to a work by Luthi (15), who delineated conformally the boundary of the region of the p-plane, in which all the roots of the characteristic equation must be situated, in order that a definite minimum damping be obtained. This refers to the area symmetrical to the negative real axis whose boundary points can be found by means of oblique angled vector diagrams. Since this variation of Nyquist's criterion is not as elegant as the other, we shall not consider it further.

Investigation of Dynamic Stability of Regulatory Circuit Based Upon Frequency Curve

In the following we will investigate the stability of the previously described regulator circuit on the basis of Nyquist's criterion with an explanation of its practical application.

Analysis of the Regulatory Circuit. We shall draw a simplified schematic diagram for the regulator circuit in which we shall disregard all elements which do not affect the regulator stability; for example, high-pressure or overspeed protective devices. In the remaining schematic we will then distinguish between oscillating elements and coupling elements. We shall denote as an oscillating element that portion of the regulating system which has a given function assigned and which produces individually or mutually a mass, friction, or spring force.

In the present case we can distinguish the following oscillating elements: The speed detector J, the driving gear DE, the steam chest G, and the turbine AB. The coupling elements are those connections between the individual oscillating elements; for oscillatory technique they are for the most part without significance. Coupling elements should transmit the regulating impulse in only one direction in order to avoid a disturbing reaction. We shall denote such a connection as a unilateral coupling. In the present regulating system, for example, the valve C has no reaction which affects the servomotor piston E. In practice it has been shown repeatedly that reciprocal coupling between individual oscillating elements can make the regulation ineffective (22). If this fact, which is too little considered, be borne in mind in the designing stage, one can easily survey the behavior and frequently find a remedy for instability by eliminating the secondary effects of reciprocal coupling.

Formulation of Equations of Motion. The equations of motion of each separate oscillating component as previously described can be formulated as shown in the classical literature. In this manner Equations [2a], [3a], [4a], and [5a] were obtained. In order that the coupling relations not be lost, we have converted the dimensionless equations to a form involving dimensions (see Equations [2b], [3b], [4b], and [5b]), so that the relations between the individual components can be deduced. For our investigation of dynamic stability, we shall transform these equations into those for small harmonic oscillations (y, z, P, $\overline{\Delta\omega}$), whose frequency γ is that of the whole circuit concerned. As an example, we have for the speed detector

$$y = a \sin \gamma t; \quad \dot{y} = \gamma a \sin\left(\gamma t + \frac{\pi}{2}\right); \quad \ddot{y} = -\gamma^2 a \sin \gamma t = -\gamma^2 y$$

By substituting these values into Equation [2b] we obtain an equation involving vectors to replace the scalar equation. The scalars y, $\dot{y}$, and $\ddot{y}$ are now replaced by vectors which we also call y, $\dot{y}$, and $\ddot{y}$. These vectors are displaced from one another by $\pi/2$. The "multiplication" of a vector with the operator i represents a rotation of $\pi/2$, and that with i^2 a rotation of π. For example, $\dot{y} = i\gamma y$ and $\ddot{y} = i^2\gamma^2 y$. Equation [2b] then becomes the vector equation

$$M_1 i^2\gamma^2 \frac{y}{y_{max}} + T_b i\gamma \frac{y}{y_{max}} + \delta_1 \frac{y}{y_{max}} = \frac{\overline{\Delta\omega}}{\omega_{max}}$$

In this equation M_1, γ, T_b, δ_1, are scalars, y and $\overline{\Delta\omega}$ are vectors, and i is the operator just described. In this manner the following system of vector equations is derived from Equations [2c] to [5c]

$$-0.913 \times 10^{-6}\gamma^2 y + 2.56 \times 10^{-3} i\gamma y + 5 \times 10^{-2} y = 3.182 \times 10^{-5}\overline{\Delta\omega} \quad [2d]$$

$$0.25 i\gamma z + 0.25 z = y \quad [3d]$$

$$0.5 \times 10^{-6} i\gamma P + 0.2 \times 10^{-6} P = z \quad [4d]$$

$$0.367 \times 10^{-4} i\gamma \overline{\Delta\omega} + 0.0637 \overline{\Delta\omega} = P \quad [5d]$$

Selection of Disturbing Frequencies. The selection of disturbing frequencies (some 6 to 10 in number) is, if necessary, to be made in such a way that the curve, to which reference is made later,[4] is clearly defined in the region of the positive real axis. The probable resonance frequencies of the regulatory circuit will be known to the expert. For a given type of machine, these frequencies do not vary greatly, and therefore one needs to use only a small frequency range. In place of the frequency of the disturbance γ, one might use the period of the disturbing oscillation $T = 2\pi/\gamma$, and this has usually been done in practice. For steam turbines of average size, for example, this period varies between 1 and 10 sec, and similar values hold for medium and large-size Diesel engines and generators.

In order to obtain as comprehensive a picture as possible of the locus of the transfer vectors, we will select for the case under consideration a very broad frequency band from

$$\gamma = 200\pi/\text{sec} \text{ to } \gamma = 0.002\pi/\text{sec}, \text{ or from } T = 0.01 \text{ sec to } T = 1000 \text{ sec}$$

Determination of Transfer Function. If one chooses a single oscillatory component from the regulatory circuit (for example, the gyro speed detector) and applies to its input speed n_p, a disturbance in the form of a superimposed oscillation of constant amplitude and frequency γ, there will appear at the output an oscillation displaced in phase and different in magnitude. The quotient of these two will be termed the transfer ratio or the transfer function. If in the previous example we consider a disturbing frequency of $\gamma = 1.257$/sec, corresponding to an oscillation period of 5 sec, then the phase-shift angle α_1 is found to be

$$\text{Tan } \alpha_1 = \frac{\text{friction force}}{\text{spring force minus inertia force}} = \frac{2.56 \times 10^{-3}\gamma}{0.05 - 9.13 \times 10^{-5}\gamma^2} = 0.0642$$

therefore

$$\alpha_1 = 3°40'$$

The amplitude of the oscillation at the output end is

$$y = y_0 \frac{(\text{spring force} - \text{inertia force}) \text{ at } \gamma = 0}{(\text{spring force} - \text{inertia force}) \text{ at } \gamma = \gamma_1} \times \cos \alpha_1$$

where y_0 is the steady-state displacement of the speed detector corresponding to a speed variation $\overline{\Delta\omega_0} = \delta_1\omega_{max}$ and therefore

[4] Section entitled, "Tracing Frequency Curve of Regulating Circuit."

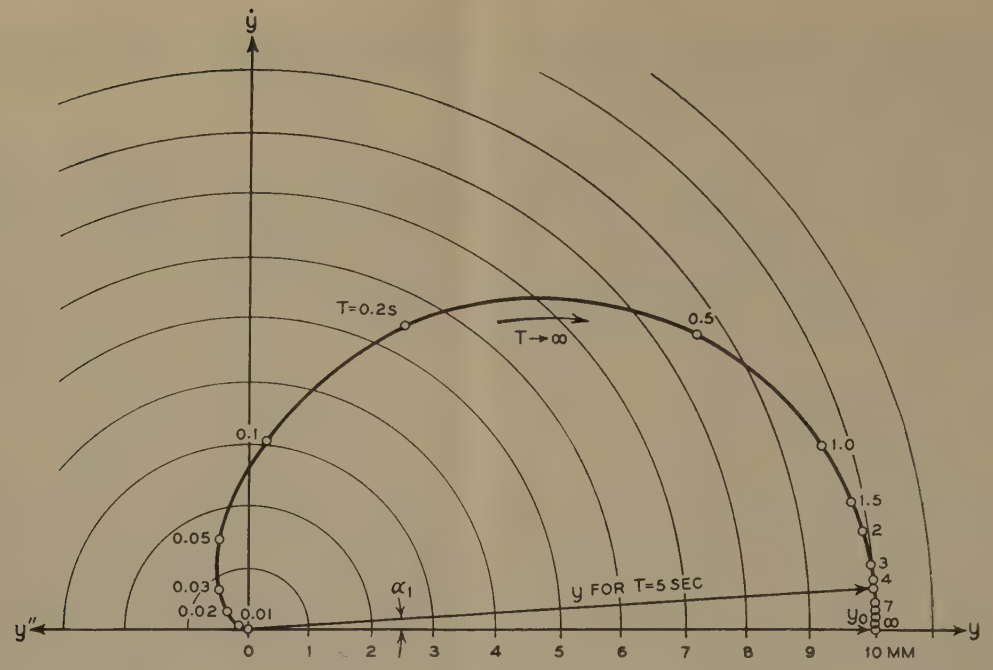

FIG. 9 PATH OF OUTPUT VECTOR y WHEN GYRO SPEED DETECTOR IS ACTED UPON BY INPUT OR DISTURBANCE VECTOR y_0 WITH DISTURBANCE OSCILLATION DURATION T

FIG. 10 CURVE OF FREQUENCY PATH Ψ OF INTERRUPTED REGULATING OR CONTROLLING CIRCUIT, AS IN FIG. 7, IN LOGARITHMIC SCALE

($\Delta\omega/\Delta\omega_0$) is transmission factor; α total phase displacement between input and output.)

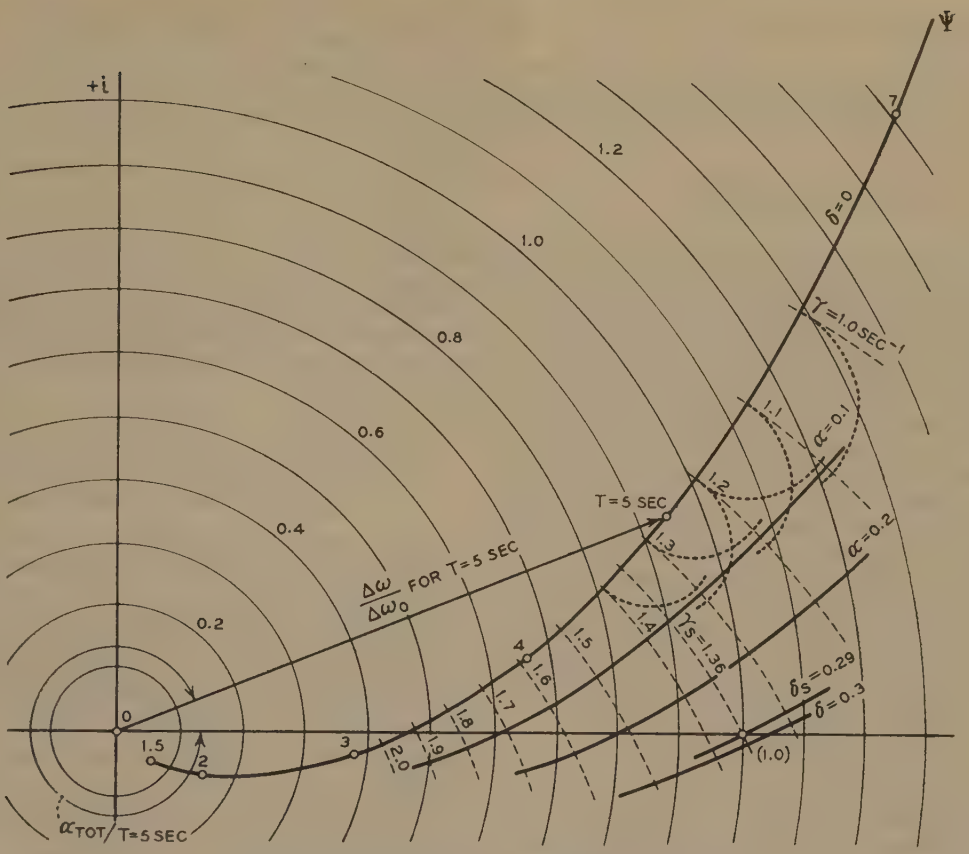

FIG. 11 EXTRACT FROM PATH OF FREQUENCY CURVE
(Construction of γ-δ network marked in for finding inherent damping and frequency of uninterrupted, or closed, regulating or controlling circuit. Descriptions are the same as in Fig. 10.)

corresponding to an indefinitely long period. In the foregoing case it is

$$y = 0.01 \times 0.997 = 0.00997 \text{ m} \ldots \text{or} \ldots 9.97 \text{ mm}$$

Fig. 9 shows the results of calculations for the speed detector for periods from 0.01 sec to 1000 sec. The value for $T = 5$ is particularly emphasized.

As we will see later on, if the period of the resonant frequency of the regulatory circuit is approximately 5 sec, then the reduction of output amplitude of the speed detector, about 3 per cent of its steady-state value, is negligible. The effect of friction from external gear, however, produces a phase shift (3°40′) which cannot be disregarded completely.

In the same way we can compute the transfer function for other oscillating components of the regulator as follows:
From Equation [3*d*]

$$\text{Tan } \alpha_2 = T_s\gamma \quad \text{and} \quad z = y \frac{z_{\max}}{y_{\max}} \cos \alpha_2$$

From Equation [4*d*]

$$\text{Tan } \alpha_3 = T_\epsilon\gamma \quad \text{and} \quad P = z \frac{P_{\max}}{z_{\max}} \cos \alpha_3$$

From Equation [5*d*]

$$\text{Tan } \alpha_4 = T_\theta\gamma \quad \text{and} \quad \overline{\Delta\omega} = P \frac{\omega_{\max}}{P_{\max}} \cos \alpha_4 = P \frac{\overline{\Delta\omega_0}}{\delta_1 P_{\max}} \cos \alpha_4$$

Tracing Frequency Curve of Regulating Circuit. Tracing the frequency curve of the regulating circuit for various disturbing frequencies by means of vector combination of the individual component transfer functions found under the foregoing section, for each frequency there is a phase-shift angle and an amplitude ratio. For the example previously given these are

$$\alpha_{\text{total}} = \alpha_1 + \alpha_2 + \alpha_3 + \alpha_4$$

$$A = |\Psi| = \frac{\overline{\Delta\omega}}{\overline{\Delta\omega_0}} = \frac{1}{\delta_1} \cos \alpha_1 \cos \alpha_2 \cos \alpha_3 \cos \alpha_4$$

If we allow the input disturbing vector for the open-loop regulatory circuit to coincide with the real positive axis of the complex plane, and give it unit amplitude, the apex of the output vector will describe a locus which is a function of frequency. We will call this the frequency curve for the open-loop regulatory circuit.

In Fig. 10 the curve for the foregoing example is shown on a logarithmic scale. The point for the frequency whose period is $T = 5$ sec is particularly emphasized.

With this curve we are now in a position to apply Nyquist's criterion to determine the dynamic behavior of the regulator. The criterion of Nyquist states that the circuit is stable if the frequency path in the complex plane for all frequencies from $-\infty$ to $+\infty$ does not cut or enclose the unit point (1, *i*0) on the real axis. Expressed otherwise this is: If one moves along the frequency curve of the open-loop regulatory circuit in the direction of increasing frequency γ or decreasing period T, then the regulatory circuit is stable only if the unity point on the positive real axis is always to the left of the curve.

On this basis it follows from Fig. 10 that the given regulator

is stable, since the point (1, $i0$) lies outside of the region enclosed by the frequency curve.

Estimating Resonant Frequency and Damping of Regulator. After we obtain the frequency curve Ψ for the open-loop regulatory circuit, we can see that to maintain oscillations the following must hold

$$\Psi^* = \epsilon^{-\delta t}\,\Psi = \epsilon^{-\delta t\frac{\Psi_a}{\Psi_e}} = 1$$

This relationship can be obtained by the introduction of complex disturbing frequencies. Only in the case of sustained harmonic oscillations is the point (1, $i0$) on the curve Ψ for purely real frequencies. The desired resonant frequency is then determined by the foregoing condition for the existence of a resonant value being fulfilled for the case where $\gamma_0 = \gamma_s$, and δ has a finite value. Since the curves for $\gamma_0 = \text{const}$ and $\delta = \text{const}$ form a system of orthogonal trajectories, we can find the values for $\gamma_0 = \gamma_s$, and $\delta = \delta_s$ by mapping the grid of $\gamma = \text{const}$ and $\delta = \text{const}$ from the open-loop frequency curve.

Unfortunately, the analytical determination of the grid is difficult, so we shall have to use a method of graphical approximation. In Fig. 11 is shown the grid for our example, the frequency curve no longer being plotted to a logarithmic scale. The construction of the $\gamma - \delta$ grid is also shown for the disturbing frequencies $\gamma = 1.1$, 1.2, and 1.3 per sec. The numerical values $\gamma_s = 1.36$ per sec and $\delta_s = 0.23$ for the closed-loop regulatory circuit are only approximate, but we can see that the damping is sufficiently large to insure a rapid decay to steady state in event of a sudden change of generator load.

In order to check this value we can use the classical methods for solution of the equation of motion. If we neglect the mass and friction of the speed detector, then by elimination of all variables except $\overline{\Delta\omega}$ from the differential Equations [2*d*] to [5*d*], we obtain as the simplified equation of motion of the regulating circuit

$$\overline{\Delta\omega}^{(3)} + 5.1\overline{\Delta\omega}^{(2)} + 4.5\overline{\Delta\omega}^{(1)} + 8.3925\overline{\Delta\omega} = 0 \ldots\ldots [8a]$$

The characteristic equation for this is

$$p^3 + 5.1p^2 + 4.5p + 8.3925 = 0$$

For this third-degree equation, the Cardan formula yields three roots, namely, $p_1 = -4.515$, and $p_{2,3} = -0.292 \pm i\,1.3316$. We see that the $p_{2,3}$ agrees very well with the graphically obtained roots $p_{2,3} = -0.29 \pm i\,1.36$. Small differences are to be expected of course, since the effect of friction in the speed detector was not considered in determining $p_{2,3}$.

A complete discussion on the effect of individual oscillating elements on the regulator stability has already been given in an earlier publication (13), so that further discussion of this problem is unnecessary at this point.

Summary and Conclusions

An investigation of the stability of a regulatory system has been demonstrated for the hydraulically driven gyro speed detector. A general section of this report gives a survey of the newer regulator dynamics which have already been adopted extensively in actual practice. The frequency-curve method, based on the Nyquist criterion, has proved practical because of its simplicity. In contrast to the classical method based on the Hurwitz criterion, the method demonstrated here has the advantage of showing in a very simple manner the effect of each individual element on the stability behavior of the complete regulatory system. The estimation of the characteristic damping of the regulating circuit gives us an additional advantage, enabling us to draw conclusions concerning the duration of oscillations following a change in load. Since the frequency curve is generally the complete equivalent of the usually unknown equations of motion, and since the frequency curve can be determined experimentally, it permits the calculation of regulator operation for any disturbance.

Therefore it is possible by the foregoing method to find the open-loop frequency curve for the complete regulating system from the frequency curves for the individual members. It is suggested at this point that the frequency curves be generally used by manufacturers for characterizing the regulatory apparatus obtainable through trade channels, in exactly the same manner as is done in amplifier technique, and more or less in the form shown in Fig. 9.

BIBLIOGRAPHY

1 "The Employment of a Gyro for Controlling Speed," by O. Vocca, *Werft, Reederei und Hafen*, vol. 15, 1934, pp. 53–55.

2 "Governing Prime Movers," by M. Tolle, Berlin, Germany, 1921.

3 "The Effect of Steam Spaces on the Governing of Steam Turbines," by F. Weiss, *Schweizerische Bauzeitung*, vol. 108, 1936, pp. 137–139.

4 "Mechanical Oscillations," by J. P. Den Hartog, Julius Springer, Berlin, Germany, 1936, pp. 35 et seq.

5 "Notes on the Governing of Turbines," by A. Stodola, *Schweizerische Bauzeitung*, vol. 22, 1893, pp. 113–117, 121–122, 126–128, 134–135; vol. 23, 1894, pp. 108–112 and 115–117.

6 "Encyclopedia of Mathematical Science," by R. von Mises, vol. 4, part Ia, p. 254.

7 "The Theory of Oscillations," by W. Hort, Berlin, Germany, 1922, p. 266.

8 "Notes on the Conditions Under Which an Equation Can Only Have Roots With Negative Real Parts," by A. Hurwitz, *Mathematical Annals*, 1895, p. 273.

9 "Regeneration Theory," by H. Nyquist, *Bell System Technical Journal*, 1932, pp. 126, et seq.

10 "The Treatment of Regulating or Governing Problems by Means of the Frequency Curve of the Regulating Circuit," by P. Profos, Diss. Eidgenössische Technische Hochschule, Zurich, Switzerland, 1943.

11 "An Investigation of the Stability of Regulating by Means of the Vector Diagram," by R. Feiss, Diss. Eidgenössische Technische Hochschule, Zurich, Switzerland, 1939.

12 "The Regeneration Theory and the Stability of Regulation," by R. Feiss, *Schweizerische Bauzeitung*, vol. 115, 1940, pp. 97–99.

13 "The Determination of Regulatory Stability by Means of the Vector Diagram," by R. Feiss, *Zeitschrift des Vereines deutscher Ingenieure*, vol. 84, 1940, pp. 819–824.

14 "A New Method of Determining the Stability of Regulation," by R. Feiss, *Schweizerische Bauzeitung*, vol. 118, 1941, pp. 61–65.

15 "Regulator Oscillations and Oblique-Angled Vector Diagrams," by A. Luthi, *Schweizerische Bauzeitung*, vol. 119, 1942, pp. 171–174.

16 "Notes on the Dynamics of Automatic Amplifying Regulators," by K. Küpfmüller, *Elektrische Nachrichtentechnik*, vol. 5, 1928, p. 18.

17 "Electrical Compensation and Operational Calculus," by J. R. Carson, Jr., Julius Springer, Berlin, Germany, 1929, p. 14.

18 "Operational Calculus," by K. W. Wagner, Barth Publishing Company, Leipzig, Germany, 1940.

19 "Solution by the Laplace Transformation for Compensating Linear Networks Applied to Automatic Regulation," by E. Grunwald, *Archiv. fur Elektrotechnik*, vol. 35, 1941, p. 379.

20 "The Delineation of Regulating Operations," by H. Tischner, *Zeitschrift für Hochfrequenz und Elektroakustik*, vol. 5, 1941, pp. 145–148.

21 "Rules for Regulating Operations," by E. Gork, *Wissenchaftliche Veröffentlichungen* from Siemens' Works, vol. 2, Oct. 31, 1941, pp. 109–144.

22 "Theoretical Control Investigation Into the Automatic Governing of Heating Systems," by M. Lang, *Zeit. Wärme*, vol. 60, 1937, pp. 8–13 and 23–26.

Mechanical Vibration of Piping Induced by Gas-Pressure Pulsations

By R. C. BAIRD[1] and I. C. BECHTOLD,[2] LOS ANGELES, CALIF.

The generation and nature of gas-pressure pulses from reciprocating compressor action are described, together with the propagation of such pulses through pipe lines. The means whereby pulse energy is converted to mechanical vibration is discussed by the aid of analogous mechanical, acoustical, and electrical oscillatory systems. The economic importance of minimizing vibration in compressor and compressor-dependent installations is indicated.

Introduction

INDUSTRY employs many kinds of compressors in diverse ways for the general purpose of transmitting gases from place to place. Practically all compressors and their associated piping will show evidence of certain dynamic forces which are the result of the reciprocating action of the compressor pistons. One of the most important of these is the presence of pulsative flow in the gas phase of the system. Accompanying these more or less rapid periodic variations in flow rate are corresponding periodic changes in pressure of the compressed fluid known as pressure pulses. Some of the energy contained in such pulses, which are propagated through pipes with approximately the speed of sound, may be converted to physical vibration of piping, associated equipment, and supporting structures, depending upon the amplitudes and frequencies of the sinusoidal components making up the pulse wave shape. This conversion is due to the presence of mechanically resonant components in the piping and associated structures sympathetic to frequencies present in the pressure pulses. Depending upon the complexity of the pulse wave shape and the extent and diversity of the piping network with its associated equipment, there is an extremely high probability of occurrence of similar pulse and mechanical resonance frequencies in a typical compressor installation. Thus very few compressor plants have been constructed, even when prior planning was involved toward minimizing pulsation, in which no vibration due to this cause resulted. In many cases such pulsation-induced vibration has been the limiting factor in the operation of petroleum-gas systems even to the extent of preventing design operating conditions to be reached.

Over a period of years, reliable theoretical formulas, confirmed and tempered by empirical evidence, have been developed for the sizing of pipes and supports for static stress conditions. These have been in the main quite reliable in the over-all sizing picture. However, in more cases than many design engineers like to admit, a system designed and built from the singular viewpoint of static forces may show a predilection to operate dangerously stresswise when subjected to dynamic forces. In such instances, gas piping, for example, can lend itself to such a degree of vibrational indulgence that at certain points in its structure the instantaneous stresses present may and often do produce fractures. The resulting hazard and economic loss sometimes may be considerable. It may be argued that the original rule-of-thumb type of design data have been derived based upon an allowance for routine vibrational stresses. That may well be, but the fact remains that vibrationally produced fractures still do occur. Furthermore, if the design engineer is familiar with the probable amounts of vibrational stresses to be expected for a given piping arrangement, a considerable original cost saving might be effected by a more judicious oversizing of the system components.

The main objectives of this paper are to describe the generation and nature of gas pipe-line pressure pulsations, the means whereby they can produce mechanical vibration in pipes and associated structures, and the manner in which pulsations are propagated through a pipe line. No attempt will be made to show how they may be minimized or eliminated.[3,4]

Sources of Pipe Vibration

The usual sources of energy for vibration of pipes and associated structures are as follows:

1 Outside energy sources operating to produce vibration of a mechanical self-excited type. The humming of telephone wires in a wind is an example of this type.

2 Direct mechanical coupling to vibrating engines or supporting structures.

3 Pulse energy of gas flowing inside a pipe.

Sources 1 and 2 are often of major consideration in the vibrational problem. Source 3, nevertheless, is in many cases the most important factor and, at the same time, may be the least understood.

There are three principal ways in which pressure pulses can be produced and superimposed upon the mean static pressure of a gas-flow system. These may be listed in order of importance as follows:

1 Compressor action in pressurizing the system for producing and maintaining gas flow.

2 Acoustical resonance effects of chambers and pipe lengths involved in the flow path.

3 Pressure variations produced by the Bourdon-tube principle because of mechanical vibration of the piping.

Method 3 is of rare importance in gas-flow problems because of the compressibility of the gas and normal rigidity of piping which precludes anything but vanishingly small percentage change in volume by mechanically produced vibration.

Method 2 can be of considerable importance and actually often prevents the accurate measurement of the pulsation wave shape produced by compressor action because of its masking influence. As a matter of fact, when using reciprocating compressors, it is practically impossible to segregate the effects of compressor valve

---

[1] Senior Research Engineer, The Fluor Corporation, Ltd.

[2] Director of Research and Development, The Fluor Corporation, Ltd.

Contributed by the Petroleum Division and presented at the Semi-Annual Meeting, San Francisco, Calif., June 27–30, 1949, of The American Society of Mechanical Engineers.

Note: Statements and opinions advanced in papers are to be understood as individual expressions of their authors and not those of the Society. Paper No. 49—SA-27.

[3] "Pulsation Phenomena in Gas Compression Systems," by I. C. Bechtold, *Engineering and Science Monthly*, California Institute of Technology, October, 1947, p. 6.

[4] "The Effects and Corrections of Gas Pulsation Problems," by F. M. Stephens, *Oil and Gas Journal*, vol. 45, Sept. 14, 1946, pp. 78, 79, and 102.

action and piping resonance. In the case of rotary compressors, the latter could more readily be estimated or obtained experimentally, but since the use of the reciprocating compressor is far more common, the attention of this paper will be directed toward analyzing its effect in producing pulsative flow.

The resonance effects of piping and manifolding chambers can often produce economic loss in that they may alter the effective static-pressure conditions at the juncture of compressor valve and piping so that a real and undesirable increase in engine fuel consumption or horsepower requirement becomes necessary. This is a standing-wave condition whereby the reflected pressure wave or pulsation produces an increase in the average pressure at the outlet of compressor cylinders at approximately the time that the valve opens to disgorge another compressed "slug" of gas into the line. As might be expected, the resulting erratic valve action may also be recognized by an increase in the rate of wear with consequent rise in valve-replacement costs.

Pulsation

In the discussion to follow, pulsation will be defined as the maximum differential pressure in pounds per square inch from peak to trough of the pressure variation. This definition is illustrated by means of Fig. 1, which, it will be noticed, looks much like the situation in the electrical analogy where an alternating current is superimposed upon a direct-current flow. Indeed, in the electrical analogy a gas compressor may be regarded as a direct-current generator producing a voltage carrying an appreciable "ripple" of complex wave form. Pulse amplitudes which are 10 per cent of the average line pressure are often obtained in practice and may be sometimes considerably greater than this. As a general rule, pulse amplitudes which are greater with respect to the average system pressure are usually found in the lower-pressure systems due probably to larger ratio of compressor cylinder displacement to line size normally encountered there.

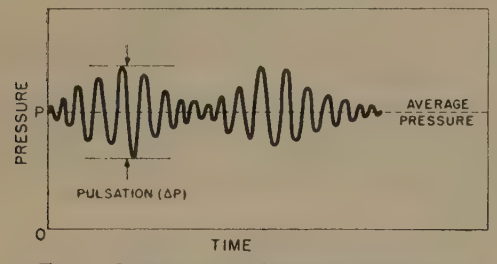

Fig. 1 Definition of Pressure Pulsation
(This is shown as the maximum pressure differential between adjacent peaks and troughs. Pulsation expressed in per cent = $[\Delta P/P] \times 100$.)

A reciprocating compressor with even angular piston spacing produces a fundamental pulsation rate which can be computed by the following relationships

(a) For an even number of cylinders

$$f_p = \frac{SN}{60} \quad \ldots\ldots [1]$$

(b) For an odd number of cylinders

$$f_p = \frac{SNA}{60} \quad \ldots\ldots [2]$$

where

f_p = pulse frequency, cycles per sec (cps)
S = drive-shaft speed, rpm
N = number of cylinders
A = action of compressor; 1 for single and 2 for double-acting

A fundamental pulsation rate f_p, does not necessarily mean that much energy is contained in the fundamental sine-wave component of this frequency in the Fourier analysis of the pulse wave shape. On the contrary, it has been found that oftentimes the second and even the third harmonic contain most of the pulse energy. However, because of acoustical and/or mechanical reaction on the pressure pulse by shock forces due to the sudden ejection or stoppage of the gas slug from the compressor cylinder, there usually results an alteration of the original wave shape by addition of spurious perturbations not harmonicallly related, to the extent that the resultant wave cannot be subjected to a Fourier analysis for determination of its sinusoidal components. This fact has been confirmed by studies of actual pulsation traces and therefore it is difficult to tell accurately what percentage of the total pulse energy is contained in the fundamental pulse frequency f_p.

The net pulse wave shape resulting from compressor action may be quite complex, as illustrated by the actual pulsation traces reproduced in Fig. 2, depending on such factors as valve action, size and shape of suction "bottle," acoustical and mechanical reaction of associated piping, etc. The two traces in Fig. 2 were chosen to illustrate the general increase in wave-shape complexity when going to higher reciprocating rates. Note that the chart recording speed for the 300-rpm trace is greater than for the 68.5-rpm one, thus resulting in an apparent equivalence in f_p for the two traces. The increase in complexity is probably due to erratic valve action at the higher speeds resulting in high-frequency additions to an otherwise smooth wave. However, as long as all the compressor cylinders operating are connected to the same drive shaft so that their relative action in time is fixed, the fundamental pulse frequency will remain unchanged.

Interaction Between Fixed Pulse Patterns of Several Compressors

In many installations several compressors pump into the same discharge header. Under such conditions, there will be a reaction between the fixed pulse patterns of the individual units due to nonsynchronous crankshaft speeds in which, theoretically, peak pulses equal to the algebraic sum of the individual compressor peak pulses may obtain aperiodically. Similarly, there may be short intervals of time in which pulsations are entirely absent because of relative compressor crankshaft phasing resulting in algebraic cancellation of their individual pulsation patterns.

For an example of an actual pipe-line instance of this kind involving manifold compressor units, refer to Fig. 3. There in Fig. 3(a) the fundamental pulse frequency of each of the two 300-rpm compressors can be seen along with the slower "beat" produced by the nonsynchronous compressor engines. "Hunting" of the engines adds greatly to the resulting complexity of wave shape. The beat or slow interaction frequency is observed here to be heterogeneous in period due to this effect. Figs. 3(b) and (c) show the general increase in "beat-frequency" complexity when a larger number of compressors are manifolded together. The beating together of frequencies of slightly different periods is analogous to the heterodyning of radio waves in which two high-frequency alternating electrical currents, each being far out of the range of audibility, can beat together to produce an audiofrequency current which can be used to convey intelligence. Or as illustrated in Fig. 4, electrical sine waves (from separate audio oscillators) representing sinusoidal pressure fluctuations, are combined or manifolded, to use pipe-line terminology, to produce beat-frequencies which adding to the primary components result in very complex fluctuations as shown.

(A) LOW SPEED 68.5 RPM COOPER BESSEMER TYPE 19 TWIN TANDEM AT 500 PSI.

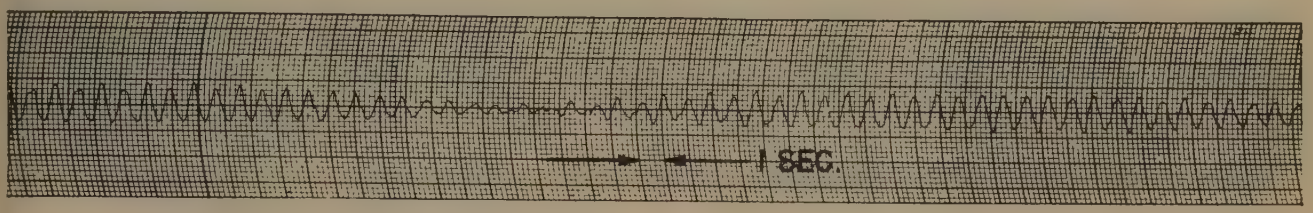

(B) HIGH SPEED (305 RPM). I-R TYPE LVG-8 AT 830 PSI.

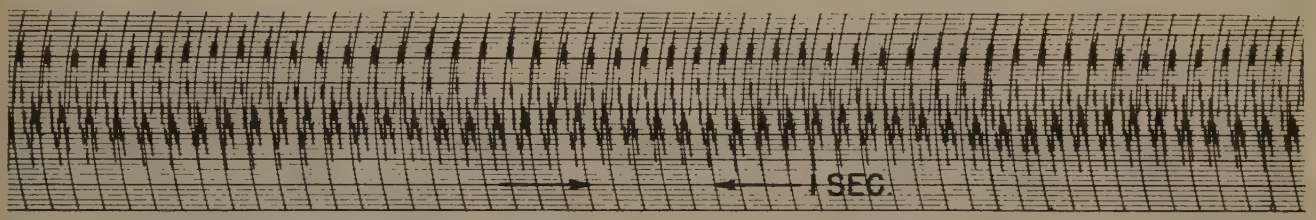

FIG. 2 ACTUAL GAS-DISCHARGE PULSATION TRACES OF INDIVIDUAL RECIPROCATING COMPRESSORS, SHOWING CHANGE OF PULSE WAVE-SHAPE COMPLEXITY WITH COMPRESSOR SPEED

(A) TWO I-R TYPE XVG-8 COMPRESSORS. 300 AND 310 RPM (HUNTING) AND 450 PSI.

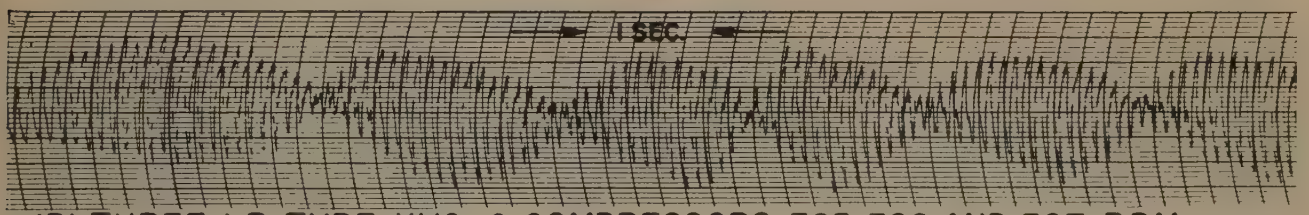

(B) THREE I-R TYPE KVG-6 COMPRESSORS. 325, 329 AND 327 RPM AND 1710 PSI.

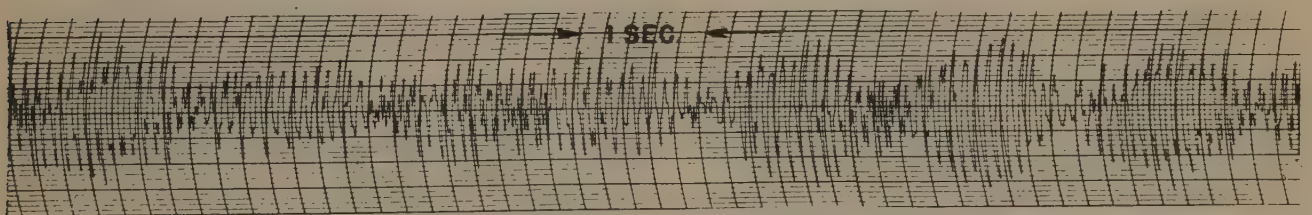

(C) SIX I-R COMPRESSORS: THREE KVG-6 325, 329 AND 327 RPM; THREE LVG-8 303, 305 AND 298 RPM; 1690 PSI.

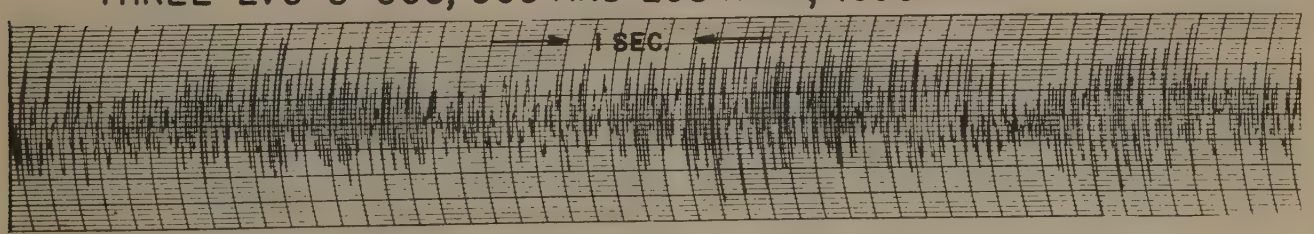

FIG. 3 ACTUAL GAS-DISCHARGE PULSATION TRACES OF MANIFOLDED RECIPROCATING COMPRESSORS

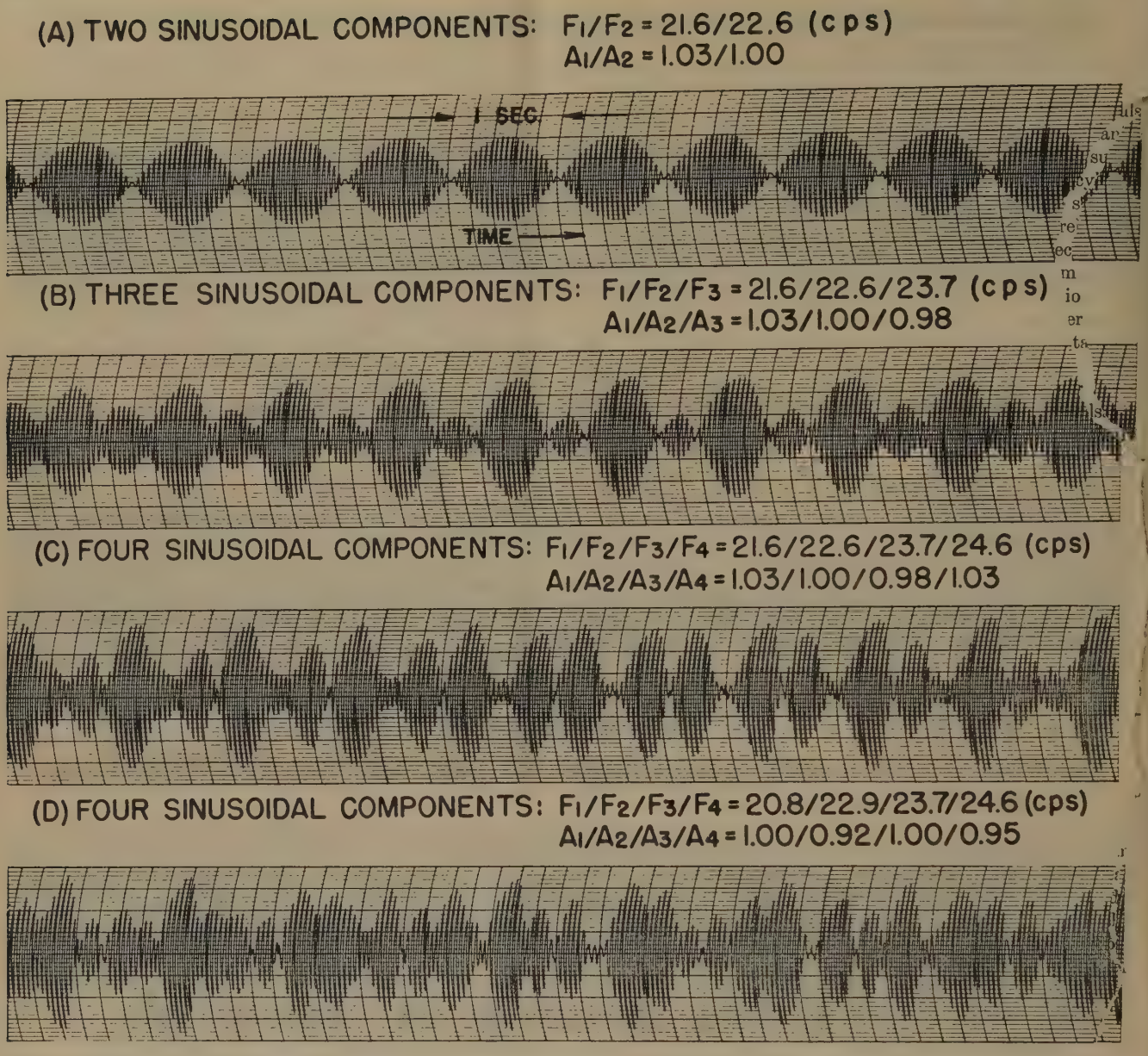

FIG. 4 COMBINATION OF SINUSOIDAL ELECTRICAL WAVES FROM SEPARATE OSCILLATORS, SHOWING RESULTANT BEAT FREQUENCIES
(These traces represent manifolding of similar numbers of reciprocating compressors having nonsynchronous speeds.)

Fig. 4(*a*), (*b*), and (*c*) represent different operating conditions of our "synthetic compressor station" in which two engines are operating, then three, and finally four. Note the increase in complexity as more "compressors" are added. Fig. 4(*d*), compared with Fig. 4(*c*), illustrates the sensitivity of the beat-frequency wave shape to slight differences in engine speeds. This effect may be incomparably augmented by hunting of the compressor engines due to inadequate speed-governor control. Compare these patterns and their trend in wave complexity with Fig. 3.

PROPERTIES OF VIBRATIONAL SYSTEMS

To understand the phenomenon of mechanical vibration produced by pressure pulses in a pipe, a few remarks on the properties of vibrational systems are necessary.[5] As is well known, a close dynamical analogy exists between mechanical, acoustical, and electrical systems. Each of these systems contains three elements which have their counterparts in those of the other two systems. These three elements which may be used to describe the reaction of the three systems to dynamically exciting energy are as follows:

1 The change-resistant element or the unit which stores kinetic energy.

2 The change-producing element or the unit which stores potential energy.

3 The dissipative element or the one which more or less slowly dissipates energy fed into the system in the form of heat and/or radiated energy.

The three elements for any one of the systems, mechanical, acoustical, or electrical, may be arranged so as to allow one or more degrees of freedom, that is, the complexity of the resultant circuit may require several equations to describe completely its

[5] "Elements of Acoustical Engineering," by H. F. Olson, D. Van Nostrand Company, Inc., New York, N. Y., 1942, chapt. 4.

dynamic characteristics, the number of equations required denoting the total possible number of degrees of freedom.

For this discussion we shall limit ourselves to simple oscillatory circuits of one degree of freedom. "*Mechanically*," such a circuit may comprise a weight suspended by a spring from a fixed point; "*acoustically*," a cavity side branch connected by means of a tube to a conduit passing sound energy; and "*electrically*," an inductance in parallel with a condenser, the combination then connected in series with one lead of an electrical line. The three circuits are illustrated in Fig. 5.

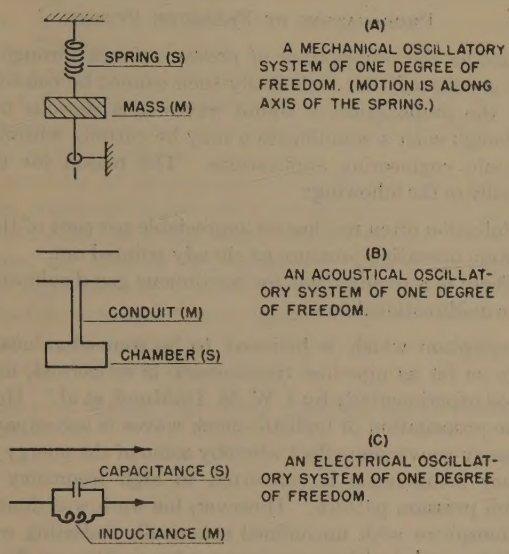

FIG. 5 ANALOGOUS MECHANICAL, ACOUSTICAL, AND ELECTRICAL SYSTEMS OF ONE DEGREE OF FREEDOM
(For simplicity the dissipative elements are not shown.)

Each of these circuits has a natural oscillatory frequency which is called its resonant frequency and which varies as the reciprocal of the square root of the product of the magnitudes of its "kinetic" and "potential" elements, the dissipative element limiting the maximum amplitude of the oscillation. Thus if the weight suspended by the spring is given an initial displacement from its rest position, it will oscillate up and down at a definite rate practically independent of the amplitude. Blowing across the mouth of a bottle will produce a tone of pitch nearly independent of the exciting energy. Alternating current of a frequency resonant to that of an "LC" series-parallel circuit connected in the line will be prevented effectively from flowing onward, due to electrical resonance. The latter may be recognized as the "wave trap" of early radio days.

MAGNITUDE OF VIBRATION STRESSES

Thus any collection of mechanical, acoustical, or electrical elements can be analyzed, the number of natural periods of resonance being a function of the total number of degrees of freedom it possesses. A piece of pipe, for example, fastened tightly at its ends, has its mass, compliance, and resistance distributed throughout its length, and thus with many degrees of freedom, can be excited at different frequencies depending upon where along the length the exciting energy is applied. With many vibrational frequencies possible, however, the one normally easiest to excite is the fundamental in which the center of the pipe moves up and down as a whole. From the stress standpoint, nevertheless, although such a vibration may look bad, actually in many cases the more unobtrusive higher-frequency vibrations may be the ones producing the most dangerous stresses. This may be seen easily as follows, assuming the motion of an elementary element of mass (Δm) to be sinusoidal and its position therefore capable of being expressed as

$$s = A \sin \omega t \quad [3]$$

where

s = displacement from rest position
t = time
A = the peak amplitude of displacement
ω = $2\pi f$ where f is frequency of vibration

The velocity of the mass is

$$\frac{ds}{dt} = \omega A \cos \omega t \quad [4]$$

and its acceleration is

$$\frac{d^2s}{dt^2} = -\omega^2 A \sin \omega t \quad [5]$$

The force associated with this acceleration is

$$F = -(\Delta m)\, \omega^2 A \sin \omega t. \quad [6]$$

and is directed toward the rest position of the element.

It is apparent, therefore, that vibrational stresses are a function of the square of the frequency, as compared with the first power of the amplitude Thus a structure vibrating at a high frequency but with a very small amplitude actually may be producing stresses far greater than one having low frequency and large-amplitude oscillations.

PETROLEUM-INDUSTRY STRUCTURES

In the case of the large pressure vessels, piping, and structures employed in the petroleum industry, fundamental resonant frequencies are often too low to be excited by the fundamental pulse energy f_p, of high-pressure gas flow. Hence higher harmonics of the fundamental and/or spurious high frequencies present are usually the ones which, pursuant to Equation [6], may produce high mechanical stresses. Further, as one goes to the heavier pressure vessels usually associated with higher pressures, the dissipative element tends to become less proportionally than the other two, thus allowing larger peak vibrational amplitudes to develop.[6] At the same time, the "potential" storing or stiffness element may increase more rapidly than the "kinetic" or mass element so that the fundamental frequency of vibration increases. This increase in f then results in increased stress forces in accordance with Equation [6]. However, although f_p may be too high to excite fundamental vibration in large units such as gas cleaners, accumulators, open section cooling coils, heat exchangers, building structures, structure and vessel foundations, and long pipe lines, vibration in this mode may yet result from pulsative flow. In such instances, because of the high ratio of mass to compliance and/or damping coefficient, dangerous stresses may develop even at sub-f_p frequencies. This phenomenon may come about because the fundamental resonant frequency is an exact submultiple of f_p. However, by far the most important reason is the presence of sympathetic beat frequencies as already described and illustrated, from manifolded nonsynchronized compressors. This vibration-producing mechanism is subtle in production but sometimes devastating in effect, and can manifest itself suddenly after a period of satisfactory operation (from a vibrational standpoint) due to a particular relationship in compressor speeds giving the requisite beat frequency.

CHANGES IN VELOCITY-HEAD LOSS

The chief method, as already pointed out, by which pulse energy can be converted to vibrational energy of the pipe carrying the flowing gas itself is through changes in the velocity-head

[6] "Vibration Analysis," by N. O. Myklestad, McGraw-Hill Book Company, Inc., New York, N. Y., 1944, sect. IV-3, p. 102.

loss in accordance with the pulsation wave shape. Supposing that there is constant smooth flow through the pipe in Fig. 6,

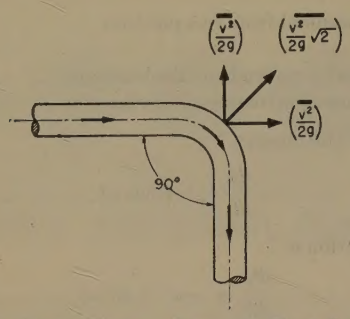

FIG. 6 VECTOR COMPONENTS OF VELOCITY-HEAD LOSS OF FLOWING GAS IN A 90-DEG DIRECTIONAL CHANGE IN PIPING

there will be a velocity-head loss producing static forces equal to

$$\left(\frac{\overline{v^2}}{2g}\right) ft$$

of the flowing gas in each of two directions shown. The vector sum of these two forces is also shown and in this case equals

$$\left(\frac{\overline{v^2}}{2g}\sqrt{2}\right)$$

Now, as long as this head-loss force is constant (no pulsation), the pipe will not vibrate even though loosely supported. Under pulsative flow conditions, on the other hand, the velocity-head force

$$\left(\frac{\overline{v^2}}{2g}\sqrt{2}\right)$$

will vary correspondingly, thereby setting up a pulsating force acting directly on the pipe, which will set the latter into vibration if it contains frequencies near to the natural frequency of vibration of the pipe itself.[6] The resultant vibrational amplitude and consequent internal stresses produced will depend, as before, upon the pipe damping coefficient and the closeness of the exciting frequencies to the natural (or a harmonic) frequency of the pipe structure.

OTHER CAUSES OF VIBRATION

Two other means whereby pulsative flow can result in vibration are (1) viscous drag exerted by pipe walls on the gas stream, and (2) the Bourdon-tube effect. Type (I) is known simply as pipe-friction pressure loss and varies as the instantaneous gas velocity, which in turn is controlled by the pressure pulse propagating through the section of the pipe in question. This effect gives rise to a varying force directed axially along the section of the pipe where it is produced. The Bourdon-tube effect can perhaps be best realized in long stretches of relatively unsupported pipe where the sag due to gravity results in imparting to it a noncircular cross section. It should be noted that this mechanism, as contrasted with the other two already described, can be effective at very low rates of gas flow whereas the others become ineffective under this condition. However, it is believed that the vibration-producing mechanism chiefly responsible in vibration problems is the pulsation-controlled velocity-head loss. It is thought, therefore, that if techniques for measuring the relative effects of the three methods could be developed, vibration induced by the velocity-head effect would be found to far outweigh that due to the others.

To summarize the foregoing with regard to the manner in which pulsation energy results in mechanical vibration, some of the pulsation energy is converted to periodic physical force because of interaction between the gas and the pipe through which it is flowing. These periodic physical forces, which usually have a complex wave shape, often will contain component frequencies which lie close or are resonant to the mechanically resonant frequencies of the pipe and/or associated structures. The force stimulation necessary for mechanical vibration is thereby achieved.

PROPAGATION OF PRESSURE PULSES

Regarding the propagation of pressure pulses through a pipe line, it is believed that technically such cannot be considered as simply the propagation of sound waves in a gaseous medium, even though such a simplification may be entirely within reason for certain engineering applications. The reason for this lies principally in the following:

1 Pulsation often reaches an appreciable per cent of the average system operating pressure as already pointed out.

2 There is a requirement for continuous gas displacement or positive unidirectional flow.

A conception which is believed to be somewhat nearer the truth in so far as pipe-line transmission is concerned, has been indicated experimentally by J. W. M. DuMond, et al.[7] He shows that the propagation of ballistic shock waves is accompanied by a frequency-conversion effect whereby some of the energy of low-frequency components is converted to high frequency in the pulsation pressure pattern. However, his work was done in the free atmosphere with unconfined spherically radiating waves, a case which coupled with no requirement for positive net flow of the conducting medium is obviously somewhat different from pulsative flow conditions in a pipe line.

There is evidence that a basic change in pulse wave form with distance of travel is present in pipe lines. This is based on observation of the variation in effectiveness with distance of pulsation-removing devices downstream from the compressor. Perhaps the chief counteracting effect of a pipe line to the conversion of pulse energy to higher-frequency components would lie in increased frictional forces exerted by the pipe wall tending to damp out the high-frequency components in the pulse. This implies that frequency conversion of pipe-line pulsation would not be carried to the degree theoretically indicated and experimentally substantiated by DuMond for unconfined ballistic shock waves.

Discussion

J. W. M. DUMOND.[8] During the war, I was engaged on a piece of war research to develop a training device for soldiers and for gunnery equipment whose object was to indicate the errors of fire of projectiles shooting at air-borne targets. The device which, I am happy to say, has been eminently successful and is now in extensive use by the armed forces, utilizes ballistic shock waves to actuate it. In order to carry out the development it was necessary to make extended theoretical and experimental studies of the nature, wave forms, and laws of propagation of ballistic shock waves in free air.

In wartime, technical people are frequently called upon to do things quite out of their habitual chosen fields. I am an atomic

[7] "A Determination of the Wave Forms and Laws of Propagation and Dissipation of Ballistic Shock Waves," by J. W. M. DuMond, E. R. Cohen, W. K. H. Panofsky, and E. Deeds, *Journal of The Acoustical Society of America*, vol. 18, 1946, p. 97.

[8] Norman Bridge Laboratory of Physics, California Institute of Technology, Pasadena, Calif.

and nuclear physicist, and not a mechanical engineer or an acoustician. It is unlikely that I will ever do further work on ballistic shock waves or mechanical shock waves of any other kind. I greatly appreciate, nevertheless, the recognition which the present paper gives to our shock-wave studies.

These shock-wave studies, as well as the pipe-line phenomena discussed in the paper, seem to illustrate very nicely a general type of mechanics which has long been recognized but whose analysis is so difficult that very little progress has been made on it up until now. I refer to so-called nonlinear mechanics. Actually, nearly all of the real cases of vibrations, be they mechanical, electrical, or acoustic, must be treated rigorously by nonlinear methods. The ear, for example, is a nonlinear receiving element, just as is a radio tube or a loud-speaker system. The familiar treatment of a vibration problem by means of linear differential equations is a sort of easy limiting case, which actually is never realized exactly in practice.

The equation of propagation of acoustical and mechanical vibration, whatever the boundary conditions may be (pipe or free air) becomes always nonlinear for large amplitudes. Under such conditions, the velocity of propagation is slightly different for different amplitudes so that different parts in one and the same wave form are propagated with slightly different velocity. Thus the wave form changes as the propagation progresses. Lord Rayleigh has discussed this in his book.[9]

[9] "Theory of Sound," by Lord Rayleigh, Dover Publications, vol. 2, pp. 33–41.

In the case of air, this occurs is such a way that those parts of the wave form in which the pressure is rising with time tend to become steeper, and those parts in which the pressure is falling with time become less steep as the propagation progresses. Eventually, the steepening regions would become rigorously vertical if it were not for dissipative effects which enter to prevent such a nonphysical state of affairs. In spite of this, however, the rising regions of pressure become astonishingly steep, and they are then called shock waves.

It has been shown by R. Becker[10] and many others that very weird effects, involving enormous pressures and temperatures, can be generated by this nonlinear propagation of high-amplitude waves. This is almost a virgin field for applied studies, both on the theoretical and experimental side. I think it is safe to predict that nonlinear mechanics is a field which will be of increasing importance for mechanical engineers, and, in fact, for the entire engineering profession.

In our mathematics department, Prof. H. F. Bohnenblust has initiated mathematical studies in the line of nonlinear mechanics. I believe that research and study along this line should be given a great deal of encouragement because of its very important applications. Extensive studies of shock waves in pipes have been made at Princeton, N. J.

[10] "Stosswelle und Detonationen," by R. Becker, *Zeitschrift für Physik*, vol. 8, 1921, pp. 321–347.